Outage probability formulas for cellular networks : contributions for MIMO, CoMP and time reversal features

Dorra Ben Cheikh Ben Cheikh Battikh

ParisTech
INSTITUT DES SCIENCES ET TECHNOLOGIES
PARIS INSTITUTE OF TECHNOLOGY

TELECOM ParisTech

2012-ENST-0031

EDITE - ED 130

Doctorat ParisTech

T H È S E

pour obtenir le grade de docteur délivré par

TELECOM ParisTech

Spécialité Informatique et Réseaux

présentée et soutenue publiquement par

Dorra BEN CHEIKH BATTIKH

le 6 juillet 2012

Outage Probability Formulas for Cellular Networks: Contributions for MIMO, CoMP and Time Reversal Features

Formules de probabilités de coupure pour les réseaux cellulaires: contributions pour les fonctionnalités MIMO, CoMP et de retournement temporel

Directeur de thèse: **Philippe GODLEWSKI**
Co-encadrement de la thèse: **Marceau COUPECHOUX**

Devant le jury composé de :

Mohamed-Slim ALOUINI, KAUST	Rapporteur
Jean-Marie GORCE, INSA de Lyon/INRIA	Rapporteur
Mérouane DEBBAH, Supélec	Examinateur
Walid HACHEM, Télécom ParisTech/CNRS	Examinateur
Mylène PISCHELLA, CNAM	Examinatrice
Jean-Marc KELIF, Orange Labs	Examinateur

TELECOM ParisTech
École de l'Institut Mines-Télécom - membre de ParisTech

THÈSE

Abstract

The implementation of cellular systems have aroused issues related to the design of cellular networks termed to as *network dimensioning*. It includes the coverage estimation and the traffic analysis. Simple models and methods are required to reduce the time consumption of these two analysis. At the same time, the growing demand for higher data rates constrained by the scarcity of frequency spectrum, and the requirements in terms of power consumption reduction make the telecommunication community think about new transmission techniques moving from the classical single antenna systems to multiple antenna systems and even the newly envisaged cooperative systems. In this thesis, we provide analytical models to assess the performance of these different cellular network evolutions in terms of outage probabilities.

In a first study, we consider multicellular single input single output (SISO) systems. First, we propose two accurate methods to study the joint impact of path-loss, shadowing and fast fading. This system has so far been studied either considering the only impact of path-loss and Rayleigh fading, or considering the same channel model as in our case but providing very complex outage probability expressions. Then, we provide an outage probability expression in a wideband communication context implementing the Time Reversal (TR) transmission technique considering the impact of fast fading.

In a second study, we focus on multiple antenna systems. We study the performance of a Multiple Input Multiple Output (MIMO) system implementing a transmit and a receive diversity schemes namely the Alamouti code and the Maximum Ratio Combining (MRC). In the literature, these two schemes have been studied either in a single cell context or considering only path-loss and fast fading effects.

Then, we consider a multiuser multicellular system using the Zero Forcing Beamforming (ZFBF). So far, ZFBF has been studied in an isolated cell with multiuser communication. Here, we provide an analytical expression of the outage probability of the ZFBF in a multicellular context considering path-loss, constant shadowing and Rayleigh fading.

Multicell cooperation (or CoMP for Coordinated Multi-Point) has been proposed to mitigate inter-cell interference, increasing hence data rates without additional spectrum requirement. We propose a study of the performance of a multiple antenna cooperative system using the Maximum Ratio Transmission (MRT) scheme considering path-loss, very slowly varying shadowing and Rayleigh fast fading. In particular we highlight the influence of the number of cooperating base stations and transmit antennas.

For a traffic analysis purpose, we finally consider a dynamic system. It takes as input the previously obtained analytical expressions of the Signal to Interference Ratio (SIR) distributions in SISO, Multiple Input Single Output (MISO) and MIMO communication contexts as well as a traffic model of service demand. We provide analytical expressions for the mean user throughput and the cell capacity.

Résumé

L'*étude de dimensionnement* d'un réseau cellulaire est une phase de conception qui doit permettre de déterminer les performances d'un système dans une configuration donnée. Elle inclut l'étude de couverture et l'analyse de trafic. De complexes simulations sont possibles pour connaître les paramètres de performances d'un réseau mais seules les études analytiques fournissent des résultats rapides. Par ailleurs, pour faire face à la demande de hauts débits, à la rareté du spectre fréquentiel et à l'impossibilité d'émettre à de plus fortes puissances, de nouvelles techniques de transmissions sont apparues. Nous sommes ainsi passés d'un système classique à une seule antenne à des systèmes à multiple antennes et même à des scénarios de coopération entre stations de base. Dans cette thèse, nous proposons des modèles analytiques pour l'étude des performances, notamment en termes de probabilités de coupure, de ces évolutions des réseaux cellulaires.

Dans une première phase, nous considérons des systèmes multicellulaires à une antenne émettrice et une antenne réceptrice (SISO). Nous proposons deux méthodes d'étude de l'impact conjoint de l'affaiblissement de parcours, de l'effet de masque et des évanouissements rapides. Nous étudions, par la suite, un système à large bande utilisant le retournement temporel comme technique de transmission.

Dans une deuxième phase, nous considérons des systèmes multicellulaires à antennes multiple à l'émission ou à la réception (MISO/MIMO) implémentant les schémas de diversité Alamouti et de combinaison par rapport maximal (MRC). Ensuite, nous considérons un système multicellulaire multi-utilisateurs à précodage de forçage à zéro (ZFBF). Les systèmes de coopération multi-point (CoMP) ont été introduits pour réduire l'interférence intercellulaire et permettre ainsi d'atteindre de plus hauts débits. Nous proposons ici une étude de ces systèmes avec des stations de base à plusieurs antennes utilisant la technique de transmission par rapport maximal (MRT) en considérant l'affaiblissement de parcours, un effet de masque constant et des évanouissements rapides. En particulier, nous mettons en évidence l'effet du nombre de stations qui coopèrent et du nombre d'antennes.

Enfin, dans le cadre d'une étude de trafic, nous considérons un système dynamique. Cette étude prend comme entrées les distributions analytiques des rapports signaux à interférence (SIR) des systèmes SISO, MISO et MIMO obtenues auparavant ainsi qu'un modèle de trafic des demandes de service. Nous proposons des expressions analytiques du débit moyen par utilisateur et de la capacité de la cellule.

Contents

List of Figures

List of Tables

List of Acronyms

AoA	Angle of Arrival
AoD	Angle of Deprature
AWGN	Additive White Gaussian Noise
BF	Beamforming
BLAST	Bell Laboratories Layered Space-Time
BS	Base Station
BW	Bandwidth
CB/S	Coordinated Beamforming/Scheduling
CDF	Cumulative Distribution Function
CDMA	Code Division Multiple Access
CLCF	Central Limit Theorem for Causal Functions
CLCFM	Central Limit Theorem for Causal Functions Method
CoMP	Coordinated Multi-Point
CQI	Channel Quality Indicator
CSI	Channel State Information
CSIR	Channel State Information at Receiver
CSIT	Channel State Information at Transmitter
DAS	Distributed Antenna System
DAST	Diagonal Algebraic Space-Time Block Code

DoA	Direction of Arrival
DPC	Dirty Paper Coding
DSB	Double Sideband
D-TxAA	Double Transmit Antenna Array
EDGE	Enhanced Data Rates for GSM Evolution
EGC	Equal Gain Combining
FCC	Federal Communications Commission
FDD	Frequency Division Duplex
FDMA	Frequency Division Multiple Access
FM	Fluid Model
FWBM	Fenton-Wilkinson Based Method
GMSK	Gaussian Minimum Shift Keying
GPRS	General Packet Radio Service
GSM	Global System for Mobile Communications
HSPA	High Speed Packet Access
ICI	Inter-Cell Interference
IEEE	Institute of Electrical and Electronics Engineers
IMT	International Mobile Telecommunications
IC	Interference Cancellation
ISI	Inter-Symbol Interference
ITU	International Telecommunication Union
JP	Joint Processing
LOS	Line of Sight
LTE	Long Term Evolution
LTE-A	Long Term Evolution Advanced

MCP	Multicell Processing
MCS	Modulation and Coding Scheme
MIMO	Multiple Inputs Multiple Outputs
MISO	Multiple Inputs Single Output
ML	Maximum Likelihood
MMSE	Minimum Mean Squared Error
MRC	Maximum Ratio Combining
MRT	Maximum Ratio Transmission
MS	Mobile Station
MU	Multi-User
NLOS	Non-Line of Sight
NTT	Nippon Telegraph and Telephone
OC	Optimum Combining
OFDM	Orthogonal Frequency Division Multiplex
OFDMA	Orthogonal Frequency Division Multiple Access
OSTBC	Orthogonal Space Time Block Code
PAM	Pulse Amplitude Modulation
PCI	Precoding Control Indication
PDC	Personal Digital Cellular
PDF	Probability Density Function
PS	Processor Sharing
PSK	Phase Shift Keying
QAM	Quadratic Amplitude Modulation
QPSK	Quadratic Phase Shift Keying
QoS	Quality of Service

RV	Random Variable
SC	Selection Combining
SC-FDMA	Single Carrier Frequency Division Multiple Access
SDMA	Space Division Multiple Access
SIMO	Single Input Multiple Outputs
SINR	Signal to Interference plus Noise Ratio
SIR	Signal to Interference Ratio
SISO	Single Input Single Output
SNR	Signal to Noise Ratio
STBC	Space Time Block Coding
STC	Space Time Coding
STTD	Space Time Transmit Diversity
SU	Single User
SVD	Singular Value Decomposition
TDD	Time Division Duplex
TDMA	Time Division Multiple Access
TM	Transmission Mode
TR	Time Reversal
TSTD	Time Switched Transmit Diversity
TTI	Transmit Time Interval
TxAA	Transmit Antenna Array
UE	User Equipment
UMTS	Universal Mobile Telecommunications Systems
UWB	Ultra-Wideband
WB	Wideband

W-CDMA Wideband CDMA

WiMAX Worldwide Interoperability for Microwave Access

WSSUS Wide Sense Stationary Uncorrelated Scattering

ZF Zero Forcing

ZFBF Zero Forcing Beamforming

3GPP 3rd Generation Partnership Project

Résumé des travaux de la thèse

Introduction

Depuis l'invention des réseaux cellulaires, les systèmes de télécommunication n'ont cessé d'évoluer. De la seconde génération (2G) à la troisième (3G), nous sommes passés d'un acheminement des communications par circuit à une transmission par paquets, plus adaptée aux services de données nouvellement proposés avec la 3G. Depuis, les demandes en termes de débit n'ont cessé d'augmenter sans pour autant que l'exigence d'un certain niveau de qualité de service, notamment en termes de couverture ne soit reniée. Le 3GPP, organisme en charge de définir les spécifications de la 3G et des futurs standards, prévoit d'intégrer certaines techniques dans la normalisation de la quatrième génération (4G) pour satisfaire cette demande accrue de hauts débits et de qualité de service, tout en assurant une utilisation optimale du spectre fréquentiel. Parmi ces techniques, nous pouvons citer la transmission et la réception multi-antennaires (MIMO), la coordination multi-point (CoMP) et les relais.

Dans cette thèse, nous proposons une étude analytique des performances en termes de probabilité de coupure des systèmes multi-cellulaires utilisant ces différentes techniques, en se focalisant sur MIMO et CoMP. Nous étudions également une nouvelle technique qui n'est pas encore normalisée, le retournement temporel.

Bibliographie

La probabilité de coupure sur la qualité radio est définie comme la probabilité que le rapport signal à interférence plus bruit (SINR) à l'entrée de la chaîne de réception soit inférieur à une valeur seuil, γ_{th}. En faisant varier le seuil considéré, nous obtenons la fonction de répartition (CDF) du SINR. La probabilité de coupure est donnée par:

$$P_{out}(\gamma_{th}) = Pr[SINR < \gamma_{th}]. \tag{1}$$

La problématique d'exprimer la probabilité de coupure dans un réseau cellulaire a été largement étudiée dans la littérature. Dans [3, 4, 5, 6, 7, 8], les auteurs proposent des expressions de probabilités de coupure pour des systèmes à une antenne émettrice et une antenne réceptrice (SISO) en considérant différents modèles de canaux. Dans une première

approche, seuls les effets de l'affaiblissement de parcours et de masque sont pris en compte. Dans une seconde, seuls les évanouissements rapides sont considérés. Dans plusieurs cas, les auteurs ont recours à des hypothèses statistiques simplificatrices.

La probabilité de coupure des systèmes à plusieurs antennes réceptrices et/ou plusieurs antennes émettrices (MIMO) a aussi été examinée par la littérature. Dans [9], des expressions de probabilité de coupure ont été obtenues pour différents schémas de diversité de réception comme la combinaison par rapport maximal (MRC), la combinaison par gain égal (EGC) et la combinaison par sélection (SC) en considérant des évanouissements rapides avec distribution de Rayleigh. Dans [10], la probabilité de coupure du lien montant d'un système cellulaire MIMO utilisant la technique de transmission par rapport maximal (MRT pour *Maximum Ratio Transmission*) comme technique de diversité en transmission a été proposée pour un modèle de canal intégrant l'affaiblissement de parcours, l'effet de masque et les évanouissements rapides de Rayleigh. Dans [11], les auteurs donnent des expressions analytiques de la probabilité de coupure pour des systèmes multi-cellulaires utilisant le MRT combiné à deux techniques de diversité en réception, à savoir le MRC et la technique d'annulation d'interférence pour un canal à évanouissements de Rayleigh.

Les performances des systèmes de coopération entre stations de base (BS) ont été récemment explorées dans la perspective d'une intégration à la norme. Très peu d'analyses analytiques ont cependant été menées pour l'obtention d'expressions de probabilités de coupure dans ce contexte. Parmi les études existantes, nous pouvons citer [12] qui calcule cette probabilité dans le cas d'une coopération non cohérente pour un canal de Rayleigh. En coopération cohérente, [13] propose une approximation de la probabilité de coupure d'un système MIMO coopératif implémentant MRT et MRC comme techniques de transmission et de réception. Il suppose que l'utilisateur servi est au centre du cercle formé par les cellules qui coopèrent et que l'effet de masque suit une loi de Gamma. La loi communément utilisée pour ce type d'effet est la loi log-normale. Les résultats analytiques proposés manquent également de précision puisqu'il y a une différence non négligeable avec les simulations.

Cette thèse s'inscrit donc dans la continuité de ces études. En effet, nous proposons ici des expressions de la probabilité de coupure pour des systèmes multi-cellulaires en considérant différentes techniques et stratégies de transmission et en faisant l'hypothèse de différents modèles de canaux.

Les études proposées sont essentiellement dites *statiques*, c'est-à-dire que nous considérons un utilisateur fixe pour lequel nous évaluons la qualité du canal ou une distribution uniforme d'utilisateurs dans la cellule. Dans la dernière partie de cette thèse cependant, nous nous intéressons au cas où les utilisateurs entrent dans la cellule, téléchargent un fichier puis en ressortent. On parle donc, dans cette thèse, d'un système *dynamique* avec un trafic aléatoire dont l'étude analytique se fonde sur la théorie des files d'attente.

Dans ce domaine également, plusieurs travaux ont été menés. Dans [14], Bonald et Poutrière ont conduit une étude de trafic dans le contexte d'une cellule isolée puis d'un réseau cellulaire en considérant l'affaiblissement de parcours. Les auteurs ont pris l'hypothèse d'un trafic uniforme où l'arrivée des flux suit une loi de Poisson. Ils ont égale-

ment utilisé des critères de contrôle d'admission tel que un nombre maximal d'utilisateurs actifs ou un débit moyen minimal par utilisateur. Des expressions du débit moyen par utilisateur et de la capacité cellulaire ont été proposées. Il a été montré que considérer un ordonnancement opportuniste qui tient compte de la variation temporelle du canal ne permet pas d'avoir une nette amélioration des performances par rapport à un simple ordonnancement équitable. Ce qui va à l'encontre de ce qu'on peut observer avec un modèle supposant un trafic permanent des utilisateurs. Une dégradation considérable des performances due à l'interférence multi-cellulaire a aussi été constatée. Dans [15], Borst propose une étude de performances de l'ordonnancement proportionnellement équitable (*proportional fair*) dans un système dynamique. Supposant l'existence de K classes caractérisées par des taux d'arrivée différents, il a été démontré que dans le cas où les fluctuations des débits atteignables par les utilisateurs sont statistiquement identiques, ce système peut être évalué en utilisant le modèle du processeur partagé ou *processor sharing* (PS) multi-classes. Les performances du système ont été étudiées en terme de délais moyen de transfert et du nombre moyen d'utilisateurs actifs.

Dans cette thèse, nous considérons un système multi-cellulaire, un ordonnancement équitable en temps de transmission et un trafic uniforme dans la cellule caractérisé par un volume moyen de données demandées. Nous prenons en entrées les distributions des SINR obtenues dans la première partie de la thèse pour les systèmes SISO, MISO et MIMO afin d'obtenir des expressions analytiques du débit moyen par utilisateur et de la capacité de la cellule.

Contributions de la thèse

Dans cette partie, nous présentons un résumé des principaux résultats obtenus dans cette thèse, où nous proposons deux types d'études : une série d'études statiques et une étude dynamique. Pour les premières, nous étudions les performances de différents systèmes multi-cellulaires en termes de probabilité de coupure ou, de manière équivalente, de fonction de répartition du SINR. L'étude dynamique en fin de thèse illustre une possible application des résultats précédemment obtenus à une étude de trafic.

Probabilité de coupure des systèmes SISO multi-cellulaires

Après les chapitres d'introduction, nous étudions les performances d'un réseau cellulaire SISO en considérant l'affaiblissement de parcours, l'effet de masque et les évanouissements rapides de Rayleigh. Nous proposons deux méthodes de calcul de la probabilité de coupure d'une station mobile localisée à une certaine distance de sa BS serveuse. La première méthode, fondée sur l'approche Fenton-Wilkinsom [16], donne une approximation de la somme de variables aléatoires log-normales par une variable log-normale et de l'évanouissement rapide dans le terme de l'interférence par sa moyenne. Nous appelons cette méthode FWBM. La seconde est fondée sur la forme causale du théorème Central Limite [17]. Elle permet de

faire l'approximation d'une somme de variables aléatoires positives par une distribution de Gamma. Nous appelons cette méthode CLCFM. Chaque méthode permet d'établir une formule simple, facile à calculer de la probabilité de coupure. Nous comparons les formules obtenues aux résultats obtenus par simulations. Nous nous sommes également fondés sur le modèle fluide [18] pour exprimer la probabilité de coupure uniquement en fonction de la distance entre le mobile considéré et sa BS serveuse.

En figure 1, nous comparons les probabilités de coupure obtenues par simulations, FWBM et CLCFM pour une distance séparant le mobile de sa BS de $r = 0.2$ Km et pour des valeurs d'écart-type de l'effet de masque variant de $\sigma = 3$ à 8 dB. Il est clair que plus σ est grand plus les erreurs des approximations sont importantes. Pour $\sigma = 3$ dB, les deux méthodes permettent d'obtenir des résultats très précis mais ce n'est clairement pas le cas pour la méthode CLCFM pour $\sigma = 8$ dB.

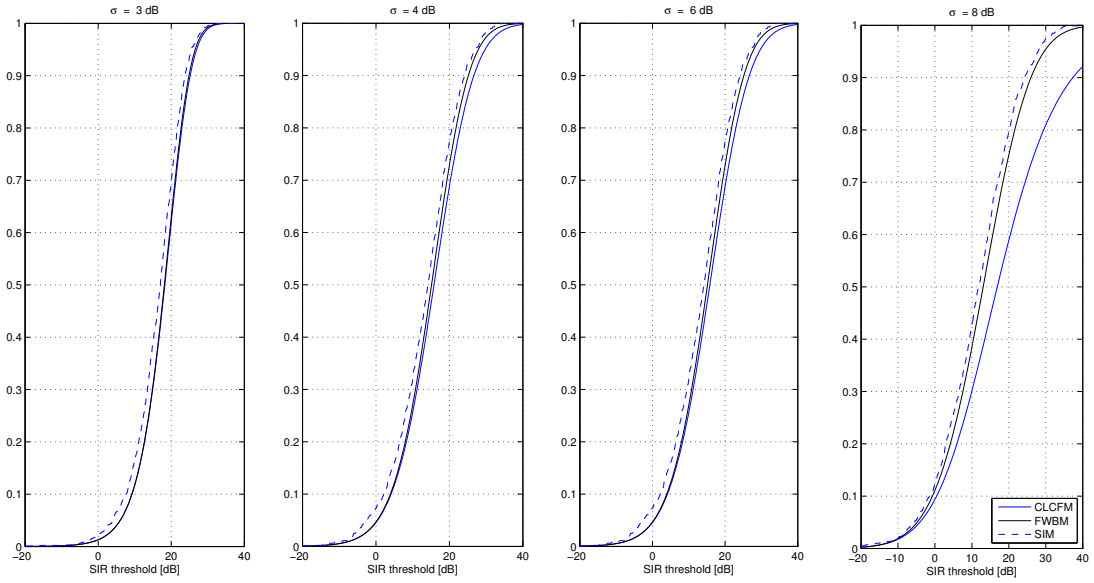

Figure 1: Comparaison des méthodes FWBM, CLCFM et avec les résultats issus de simulations. Influence de l'écart-type de l'effet de masque σ [dB] ($r = 0.2$ Km and $\eta = 3.0$).

En figure 2, nous étudions l'influence de la distance entre le mobile et la BS pour $\sigma = 4$ dB. Cette distance a une très faible influence sur la précision des méthodes proposées, toutes les expressions analytiques obtenues sont valides.

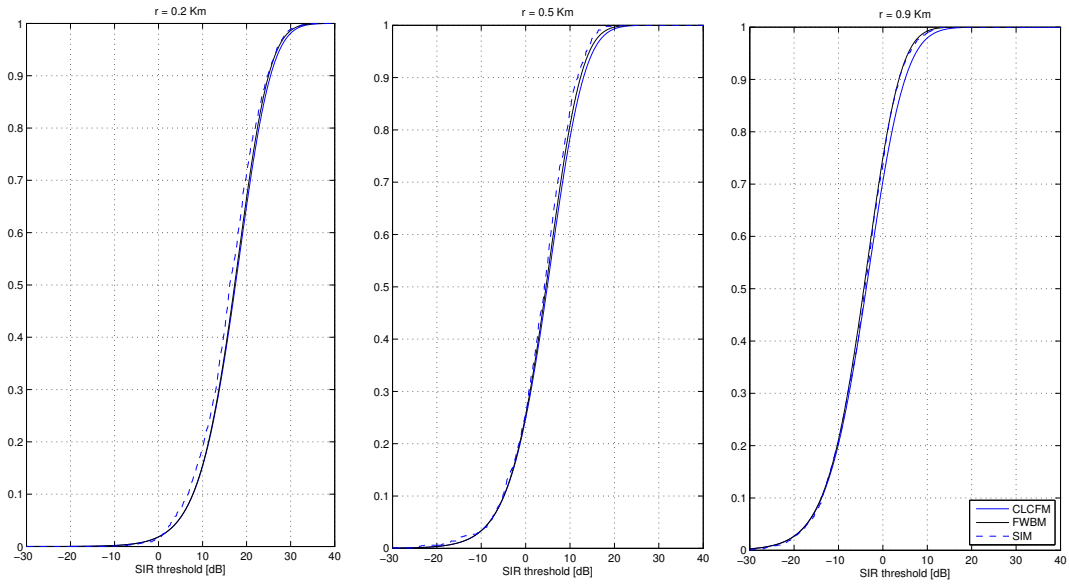

Figure 2: Comparaison des méthodes FWBM, CLCFM et avec les résultats issus de simulations. Influence de la distance r [Km] à la BS serveuse ($\sigma = 4$ dB and $\eta = 3.0$).

Probabilité d'un système multi-cellulaire avec retournement temporel

Dans ce chapitre, nous avons considéré une communication large bande dans un système multi-cellulaire où les stations de base sont équipées d'une seule antenne de transmission et utilisent le retournement temporel comme technique de réduction d'interférence.

Le retournement temporel (RT) est une technique qui utilise la réponse impulsionnelle du canal, retourné temporellement, comme pré-filtre au niveau du transmetteur. Elle permet une focalisation temporelle et spatiale de l'énergie :

- la focalisation temporelle consiste en une focalisation de l'énergie dans un pic prédominant avec de faibles lobes secondaires ;

- la focalisation spatiale résulte en un pic de puissance dans la position cible et qui s'évanouie rapidement en s'éloignant de cette cible.

Grâce à ses propriétés de focalisation, le retournement temporel permet une détection plus fiable et moins complexe au niveau du récepteur.

En appliquant le retournement temporel à un canal sélectif en fréquence avec évanouissement de Rayleigh dans un réseau cellulaire, nous avons proposé une expression de la distri-

bution du SIR défini par :

$$\gamma = \frac{X}{Y+Z}, \tag{2}$$

où X est la puissance du signal utile, Y la puissance de l'interférence co-canal et Z la puissance de l'interférence inter-symbole (ISI). Etant donné que X et Z sont deux variables aléatoires corrélées, il est très difficile de proposer une expression de la distribution du SINR sans avoir recours à une approximation. Sachant que le RT permet de réduire considérablement la puissance de l'ISI, nous prenons l'hypothèse de la négliger dans notre étude analytique. Cette hypothèse a été validée en comparant notre expression analytique de la probabilité de coupure avec les résultats de simulations qui prennent en compte l'ISI. La figure 3 illustre des résultats de comparaison obtenus.

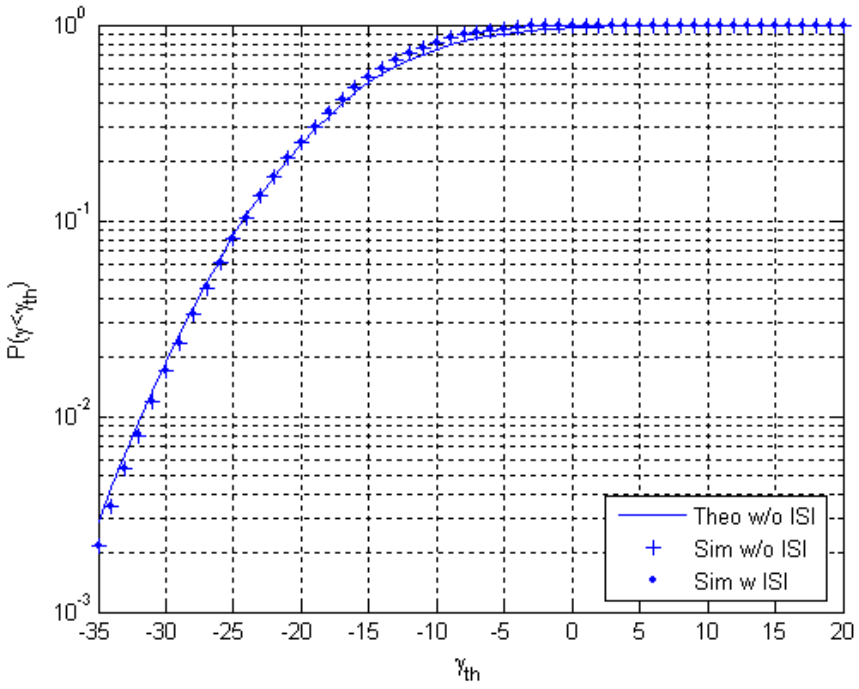

Figure 3: Comparaison entre résultats de simulations et expressions analytiques de la probabilité de coupure avec et sans ISI en utilisant le RT pour 18 BSs interférentes.

Performance du schéma Alamouti dans un réseau cellulaire

Dans ce chapitre, nous étudions les performances du schéma Alamouti, d'abord dans un système multi-cellulaire 2×1 puis combiné avec le MRC dans un système $2 \times N$. Nous exprimons les probabilités de coupure de ces systèmes en prenant différentes hypothèses :

- Puissances égales des interféreurs (EP) / puissances inégales (UEP).
- Effet de masque constant / effet de masque aléatoire.
- Avec et sans approximation utilisant le modèle fluide.

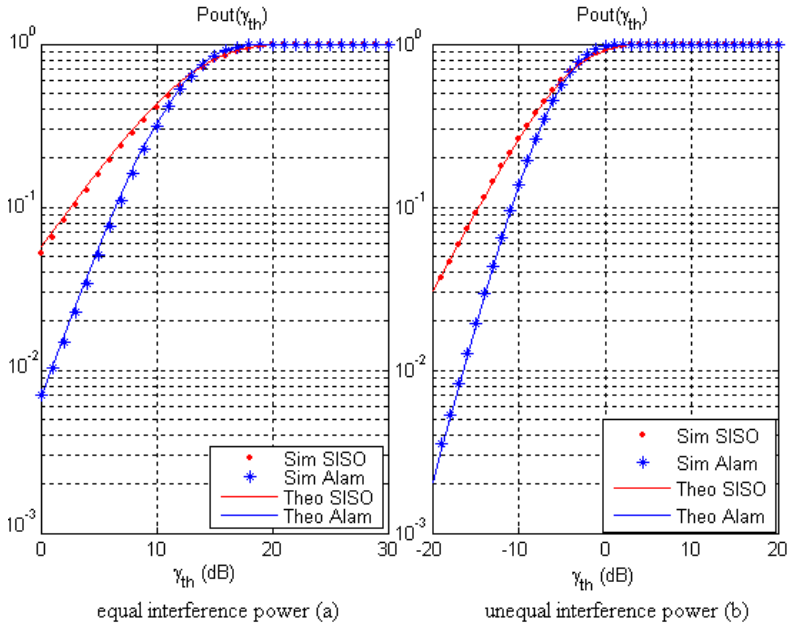

Figure 4: Probabilité de coupure P_{out} en fonction du SINR seuil pour les systèmes 2×1 MISO Alamouti et SISO dans le cas de puissances égales (a) et inégales (b) reçues des BSs interférentes (échelle logarithmique).

En figures 4 et 5, nous traçons les probabilités de coupure simulées et analytiques dans le cas EP (figure 4 (a), figure 5 (a)) et UEP (figure 4 (b), figure 5 (b)) pour le schéma Alamouti comparé à un système SISO respectivement dans une échelle linéaire et dans une échelle logarithmique. Pour le cas EP, nous considérons 6 BSs interférentes et un mobile à une distance $d = 0.2$ Km de sa BS serveuse (presque à égale distance des BSs interférentes). Pour le cas UEP, le mobile est à une distance $d = 0.5$ Km de sa BS et est interféré par 18 BSs. Dans les deux cas, l'effet de masque est considéré comme constant. Nous pouvons remarquer que dans la partie de faible SINR, le code d'Alamouti affiche une bien meilleure performance. En effet, d'après la figure 5, sa probabilité de coupure décroît beaucoup plus rapidement grâce à une plus grande pente, traduisant le gain de diversité égale à 2. Le code d'Alamouti permet donc d'avoir une meilleure couverture. Cependant dans la région de SINR élevé le système SISO est plus performant que le système Alamouti 2×1.

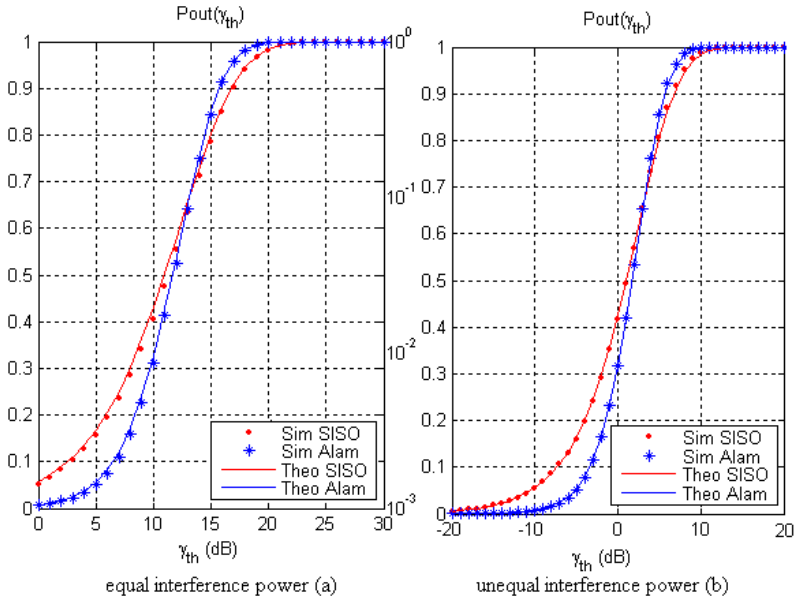

Figure 5: Probabilité de coupure P_{out} en fonction du SINR seuil pour les systèmes 2×1 MISO Alamouti et SISO dans le cas de puissances égales (a) et inégales (b) reçues de BSs interférentes (échelle linéaire).

Toujours dans le cas d'un effet de masque constant, nous traçons en figure 6 les probabilités de coupure simulées et analytiques du système Alamouti 2×1 que nous comparons à celles du système Alamouti 2×2 et 2×4 avec récepteur MRC. Les deux derniers systèmes présentent de meilleures performances avec des gains de diversité de réception respectifs de $G_R = 2$ et $G_R = 4$ en plus du gain du diversité de transmission $G_T = 2$.

La figure 7 présente l'influence de la variation aléatoire de l'effet de masque sur les performances des deux systèmes 2×1 Alamouti et 2×4 Alamouti avec récepteur MRC. Il est clair que l'effet de masque aléatoire dégrade considérablement les performances des deux systèmes. Nous pouvons constater que pour 1% de probabilité de coupure, la dégradation est de l'ordre de 10 dB pour le schéma 2×4 Alamouti avec récepteur MRC et de 7 dB pour le système 2×1 Alamouti. Les courbes montrent aussi une très bonne correspondance entre les résultats théoriques et les simulations.

En figure 8, nous comparons les résultats de simulations aux valeurs théoriques des probabilités de coupure des deux systèmes avec l'approximation du modèle fluide. Nous considérons un écart-type $\sigma = 4$ dB. Nous pouvons voir qu'il y a une bonne correspondance entre les deux résultats. Nous pouvons donc dire que le modèle fluide permet d'obtenir des formules de probabilité de coupure beaucoup plus simples sans une perte majeure en terme de précision.

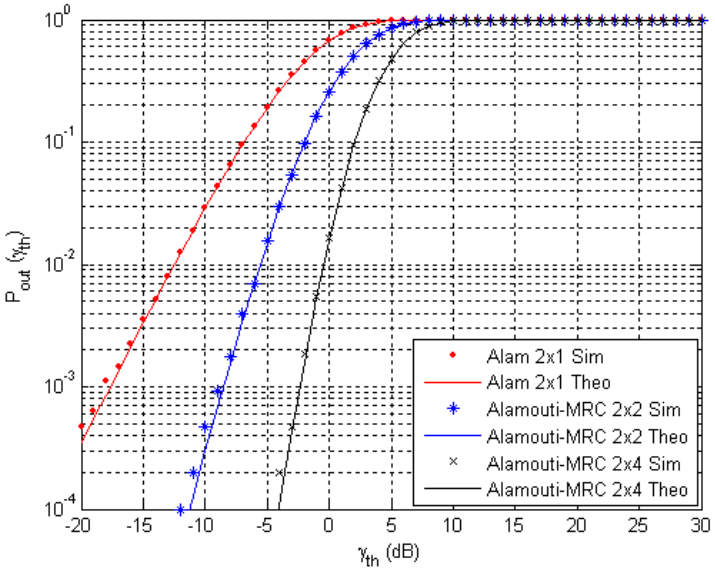

Figure 6: Probabilité de coupure P_{out} en fonction du SINR seuil pour les schémas 2×1 MISO Alamouti, 2×2 and 2×4 MIMO Alamouti avec récepteur MRC (18 BSs interférentes).

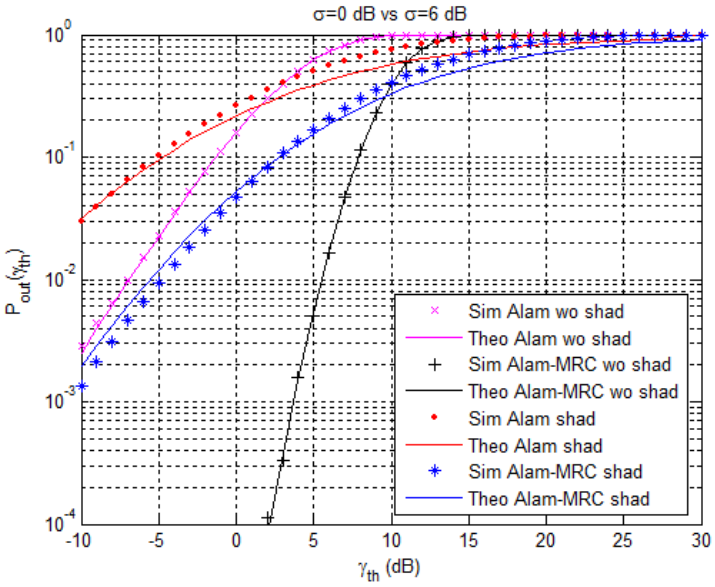

Figure 7: Probabilité de coupure P_{out} en fonction du SINR seuil pour le schéma 2×1 MISO Alamouti et le schéma 2×4 MIMO Alamouti avec récepteur MRC. Influence de l'effet de masque.

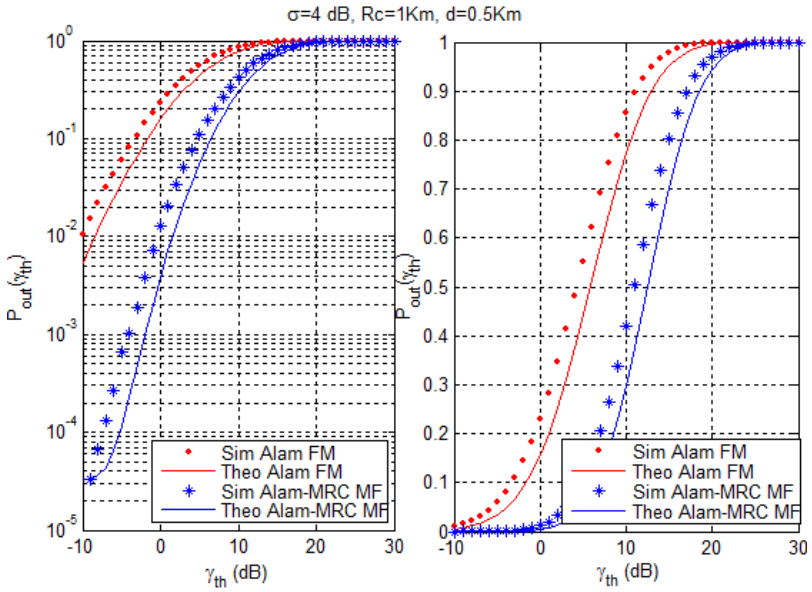

Figure 8: Probabilité de coupure P_{out} en fonction du SINR seuil pour le schéma 2×1 MISO Alamouti et le schéma 2×4 MIMO Alamouti avec récepteur MRC. Approximation modèle fluide.

Performance du précodage ZF dans un réseau cellulaire

Le précodage de forçage à zéro (ZF) est une technique de transmission qui permet d'éliminer les interférences multi-utilisateurs au niveau du transmetteur. Il consiste en la multiplication du vecteur d'information regroupant les données des utilisateurs par la matrice :

$$\mathbf{W} = \mathbf{H}^H(\mathbf{H}\mathbf{H}^H)^{-1}, \tag{3}$$

où $\mathbf{H}$ représente le canal entre la BS et les utilisateurs servis simultanément.

Dans ce chapitre, nous considérons un système multi-cellulaire où les BSs sont équipées de M antennes et servent simultanément $K < M - 1$. Nous avons tout d'abord pris l'hypothèse d'un effet de masque quasiment constant et nous avons obtenu une forme fermée de l'expression de la probabilité coupure. Par la suite, tenant compte de la variation aléatoire de l'effet de masque, nous avons pu proposer une forme intégrale de cette probabilité qui peut être calculée facilement et rapidement en utilisant des logiciels tels que Matlab et Mathematica.

En figure 9 nous présentons une comparaison entre les résultats simulés et les valeurs analytiques de la probabilité de coupure avec ZF sans prendre en compte l'effet de masque. Les BSs sont équipées de 6 antennes et servent 4 utilisateurs équipés d'une seule antenne chacun. Il y a une très bonne correspondance entre les deux types de résultats.

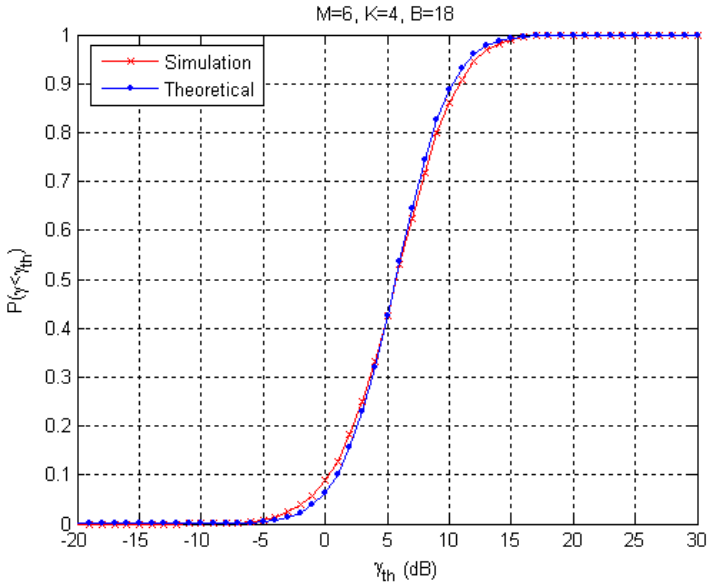

Figure 9: Probabilité de coupure P_{out} en fonction du SINR seuil pour un système multi-utilisateur multi-cellulaire utilisant le précodage ZF.

La figure 10 présente une comparaison des performances de la technique de transmission

ZF avec et sans variation aléatoire de l'effet de masque. Il est clair que la variation aléatoire de l'effet de masque dégrade considérablement les performances du système. En effet, pour 10% de probabilité de coupure la perte est de presque 4 dB au niveau du récepteur. Là, aussi nous pouvons voir qu'il y a un bon accord entre les résultats théoriques et les simulations.

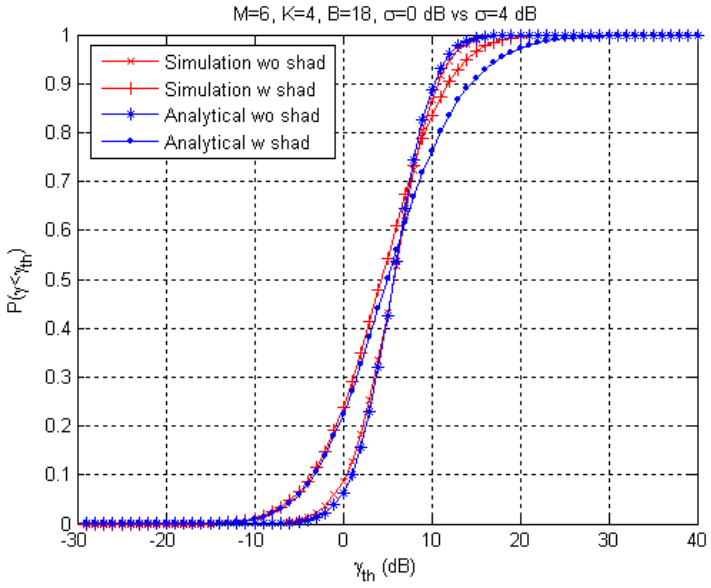

Figure 10: Influence de l'effet de masque sur la probabilité de coupure d'un système multi-utilisateur multi-cellulaire utilisant le précodage ZF.

Performance d'un système de coopération multi-point avec précodage MRT

La coordination multi-point (CoMP) est une nouvelle technique de transmission en cours de spécification dans le cadre du LTE-A. Elle consiste en une coopération entre BSs pour combattre l'interférence multi-cellulaire et atteindre de meilleures performances notamment en termes de débit des utilisateurs en bordure de cellule.

Ce schéma de transmission a été très peu étudié analytiquement dans la littérature [12, 13]. Dans ce chapitre, nous nous proposons d'étudier les performances analytiques du lien descendant d'un système de coopération multi-cellulaire avec transmission cohérente où les BSs sont équipées de plusieurs antennes et utilisent le précodage *Maximum Ratio Transmission* (MRT) comme technique de diversité de transmission. Cette technique est optimale en terme de maximisation du rapport signal à bruit (SNR) dans le cas d'une cellule isolée. Ce n'est plus le cas dans un réseau cellulaire à cause des interférences. Elle reste néanmoins une technique très facile à implémenter et admet des performances proches de l'optimal.

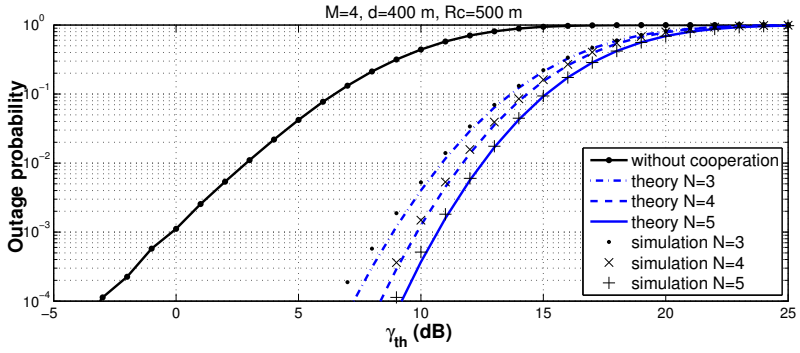

Figure 11: Comparaison entre les résultats de simulation et les valeurs analytiques de la probabilité de coupure avec et sans coopération pour différents nombres de BSs coopérantes.

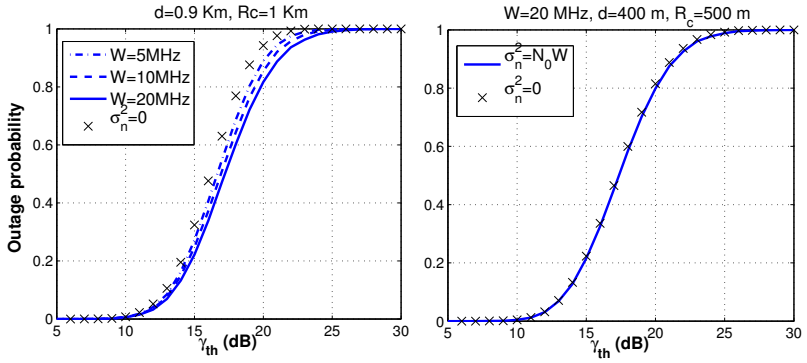

Figure 12: Impact de la puissance du bruit sur la probabilité de coupure.

Nous proposons donc une approximation de l'expression de la probabilité de coupure fondée sur la méthode CLCFM prenant en compte l'affaiblissement de parcours, les évanouissements rapides de Rayleigh et en supposant que l'effet de masque est très peu variable. Notre approche analytique vient donc consolider toutes les études numériques existantes.

La figure 11 présente une comparaison entre les valeurs simulées et théoriques de la probabilité de coupure. Nous considérons un réseau composé de 19 BSs équipées de 4 antennes chacune (cellule centrale et deux anneaux de BSs). Nous supposons trois cas de coopération fondés sur le nombre de BSs qui coopèrent: $N = 3,\ 4$ ou 5. L'utilisateur que nous considérons est servi par les N BSs offrant les affaiblissements de parcours les plus faibles. La figure montre que les valeurs théoriques sont en bon accord avec les résultats de simulations. Il apparaît aussi que notre approximation reste valable même pour un petit nombre de BSs dans le groupe de coopération ($N = 3$). Nous pouvons aussi voir la nette amélioration apportée par la coopération par rapport au cas classique de non coopération.

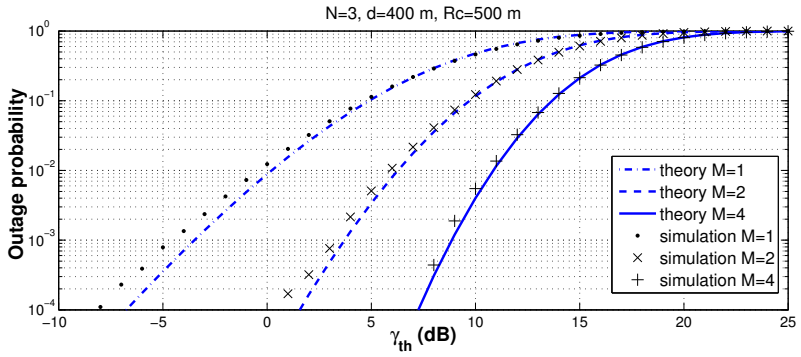

Figure 13: Probabilité de coupure en fonction du SINR seuil pour le lien descendant d'un système multi-cellulaire utilisant le CoMP avec $M = 1$, 2, 4 antennes par BS.

Dans notre étude, nous avons fait l'hypothèse d'un système limité par l'interférence où la puissance du bruit est négligeable par rapport à celle de l'interférence co-canal, ce qui est le cas dans un environnement urbain. En figure 12, à travers une comparaison entre les probabilités de coupure du SIR (sans bruit) et du SINR (avec bruit) pour des rayons de cellule $R_c = 500$ m et $R_c = 1$ Km, nous démontrons que notre hypothèse est bien fondée puisque les deux courbes sont superposées. Les deux courbes commencent à se distinguer pour le cas où $R_c = 1$ Km et pour des largeurs de bande $W \geq 10$ MHz. Cependant notre formule reste complètement valable pour la région de faible SINR pour des études de couverture par exemple.

En figure 13, nous fixons le nombre de BSs coopérantes à $N = 3$ et nous faisons varier le nombre d'antennes ($M = 1$, 2 et 4). Encore une fois, il y a un bon accord entre résultats analytiques et simulations. Notre formule d'approximation de la probabilité de coupure est valable pour différents nombres d'antennes. Un résultat attendu et qu'illustre cette figure est le fait qu'augmenter le nombre d'antennes améliore les performances des systèmes. C'est un résultat classique relative au gain de diversité du MRT.

Etude dynamique des performances des systèmes SISO, MISO et MIMO

Dans ce chapitre, nous proposons une étude fondée sur l'hypothèse d'une demande de trafic dynamique. Cette hypothèse courante a été considérée par Bonald et Poutrière dans [14] où ils ont proposé des expressions analytiques du débit moyen par utilisateur et de la capacité de la cellule en considérant différents critères de contrôle d'admission parmi lesquelles le nombre maximal d'utilisateurs actifs et le débit minimum par utilisateur. Dans leur étude, seul l'affaiblissement de parcours est pris en compte dans la modélisation du canal. Ce chapitre étend donc ces résultats en proposant une comparaison entre les performances analytiques des systèmes SISO, MISO Alamouti 2×1 et MIMO Alamouti $2 \times N$ avec un récepteur MRC dans un contexte multi-cellulaire. La cellule est divisée en anneaux

concentriques. Dans chaque anneau, nous calculons le débit physique moyen des utilisateurs en utilisant les distributions du SINR obtenues dans les chapitres précédents. À partir de ces résultats, nous pouvons calculer les débits moyens par utilisateur dans chaque anneau en présence d'arrivées et de départs d'utilisateurs.

La figure 14 présente une comparaison entre les débits moyens des systèmes SISO et MIMO Alamouti 2×1 en fonction de la charge de la cellule ρ lorsqu'il n'y a pas de contrôle d'admission. En termes de débits atteignables MISO Alamouti est légèrement plus performant que le SISO, en particulier dans les anneaux intérieurs. La tendance s'inverse en bordure de cellule.

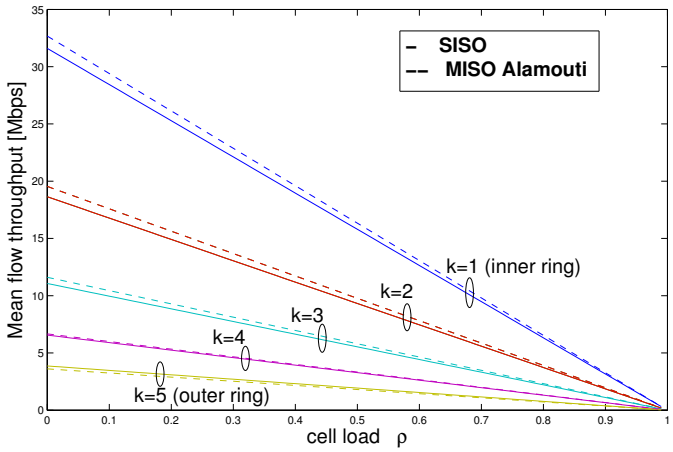

Figure 14: Débit des flux en fonction de la charge de la cellule pour les systèmes SISO et MIMO Alamouti 2×1.

La figure 15 présente une comparaison entre les débits moyens des systèmes MIMO Alamouti 2×2 avec récepteur MRC et MISO Alamouti 2×1, toujours sans contrôle d'admission. Nous pouvons voir que le système MIMO Alamouti avec MRC admet un gain de 4 Mbits/s dans l'anneau intérieur par rapport au système MISO Alamouti. Le gain reste considérable dans l'anneau extérieur.

Nous considérons ensuite un contrôle d'admission qui garantit un débit minimal $c_{min} = 0.5$ Mbits/s aux utilisateurs. En se fondant sur ce critère d'admission, nous comparons les performances de nos trois systèmes. Les nombres maximums d'utilisateurs actifs sont, respectivement, 12, 11 et 17 pour les systèmes SISO, MISO Alamouti et MIMO Alamouti avec MRC respectivement. La figure 16 illustre la comparaison entre le débit moyen des deux systèmes SISO et 2×1 Alamouti, en fonction de la charge de la cellule. Nous pouvons noter que quand la charge ρ tend vers 1, le débit des utilisateurs en bordure de cellule tends vers c_{min}. Les capacités cellulaires et les nombres maximums d'utilisateurs actifs étant similaires pour les deux systèmes, nous obtenons des résultats conformes à ce que

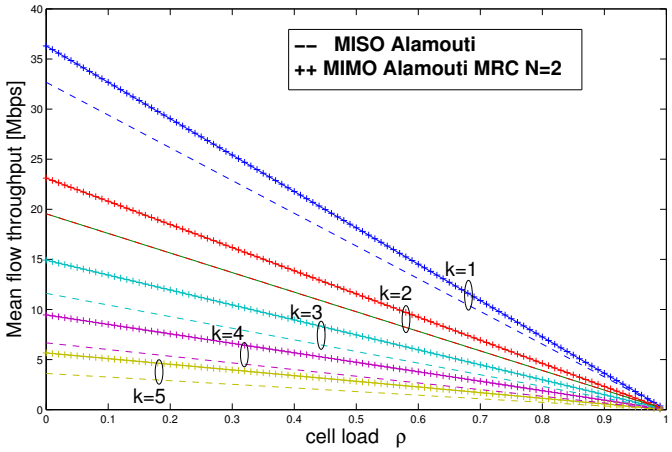

Figure 15: Débit des flux en fonction de la charge de la cellule pour les systèmes MISO Alamouti 2×1 et MIMO Alamouti 2×2 avec MRC.

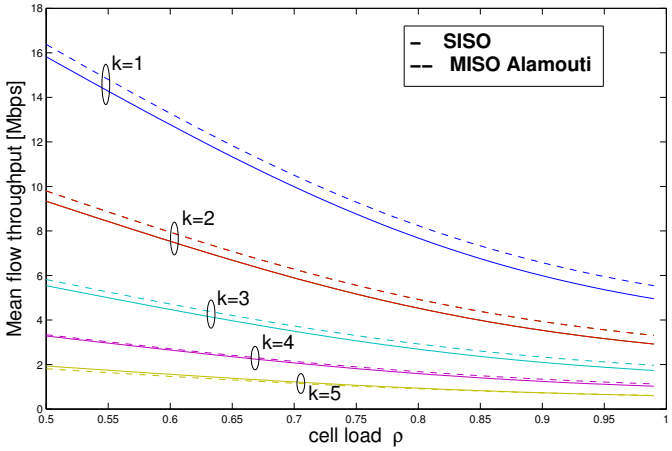

Figure 16: Débit des flux en fonction de la charge de la cellule pour les systèmes SISO et MISO Alamouti 2×1 avec contrôle d'admission ($c_{min} = 0.5$ Mbits/s).

nous avons pu observer dans le cas sans contrôle d'admission. La figure 17 illustre la comparaison entre les systèmes MISO et MIMO. Comme prévu, quand la charge est faible, MIMO est plus performant que MISO en termes de débit moyen du flux. Cependant, il est intéressant de voir que le débit dans les anneaux intérieurs est plus faible que celui obtenu avec un système MISO quand la charge est importante. Ce comportement peut être expliqué par le fait que le système MIMO accepte plus d'utilisateurs que le système MISO (17 au lieu de 11), la capacité, bien que plus grande, est donc divisée en plus de petits morceaux.

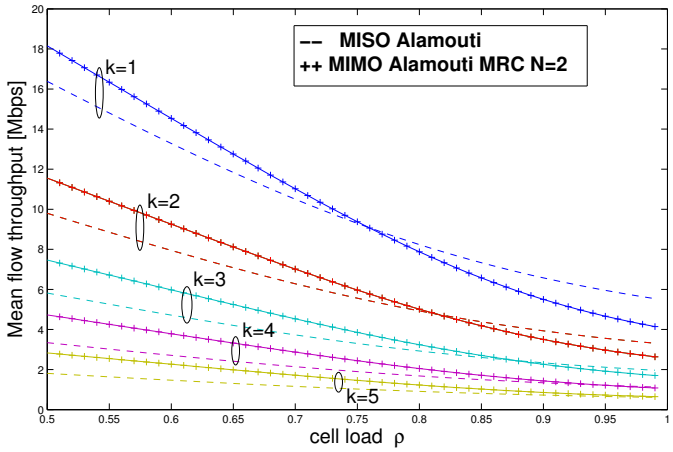

Figure 17: Débit des flux en fonction de la charge de la cellule pour les systèmes MISO Alamouti 2×1 et MIMO Alamouti 2×2 avec MRC avec contrôle d'admission ($c_{min} = 0.5$ Mbits/s).

Conclusion et perspectives

Les systèmes cellulaires présentent une vraie révolution dans les télécommunications d'aujourd'hui. Cependant, la conception d'un réseau cellulaire nécessite un dimensionnement préalable prenant en compte des exigences de qualité de service, tels que la couverture et le débit. Les estimations en termes d'infrastructure données par le processus de dimensionnement sont ensuite utilisées pour des études de planification détaillée. Une fois la planification du réseau finalisée, ces paramètres sont optimisés pour une efficacité maximale. Dans cette thèse, nous présentons des études de performances des systèmes cellulaires mettant en œuvre différentes techniques de transmission, à savoir le retournement temporel, le code Alamouti, le Zero Forcing ainsi que la coopération entre BSs (CoMP). Ces études ont été effectuées en analysant la probabilité de coupure. C'est en effet une métrique centrale pour l'évaluation aussi bien de la couverture que des débits atteignables. La plus grande partie de la thèse se fonde sur une hypothèse statique dans laquelle nous considérons un unique utilisateur pour lequel nous calculons la qualité du lien radio. Dans la toute dernière partie de la thèse, nous nous intéressons aux systèmes dynamiques avec un nombre variable d'utilisateurs et un trafic aléatoire. Nous étudions ces systèmes en termes de débit moyen par utilisateur en fonction de la charge et de capacité cellulaire. Ces paramètres sont des données primordiales dans le processus de dimensionnement.

À travers toutes nos études, nous considérons des systèmes avec une connaissance parfaite du canal au niveau de l'émetteur. C'est une hypothèse simplificatrice qui est communément utilisée, notamment pour les études analytiques de dimensionnement cellulaire.

Cependant elle n'est réellement valable que pour des systèmes avec des utilisateurs à faible mobilité. Il serait donc intéressant de considérer une connaissance imparfaite ou partielle du canal dans des études futures. Nous nous sommes par ailleurs focalisés sur la probabilité de coupure. En fait si le SINR descend en dessous d'un certain seuil pour une période très courte, la communication peut ne pas être coupée. Il serait donc judicieux d'étudier les *excursions* du SINR en dessous d'un certain seuil, c'est-à-dire la distribution des durées de coupures. Peu d'études sont pour le moment disponibles dans la littérature sur ce sujet. Notre étude sur le MIMO multi-utilisateur ZF peut être étendue en considérant cette même technique dans un contexte de coopération pour mettre en évidence l'apport de la transmission multi-cellulaire en terme de performances et pouvoir comparer ces performances à celles du MRT. Toujours dans le domaine du CoMP, l'étude de la qualité radio a montré que cette technique était très avantageuse pour l'utilisateur. Elle masque cependant le fait que les ressources de plusieurs BSs sont mobilisées pour un unique utilisateur. Il n'est donc pas évident que CoMP fournisse des performances acceptables s'il l'on considère une étude dynamique. Ce cas reste donc à étudier. Enfin, si le modèle de file d'attente M/G/1/PS fournit un cadre théorique appréciable pour l'étude de systèmes cellulaires dynamiques, il n'est pas adapté aux transmissions multi-utilisateurs MIMO. Un modèle de files d'attente simple pouvant couvrir ce cas serait donc très utile.

Chapter 1

Introduction

1.1 Cellular Networks Evolution

Although invented by Marconi in 1895, radio telecommunication took long to be part of the daily life of customers. The breakthrough of radio communication begins when the Federal Communications Commission (FCC) recognized the mobile radio as a new class of service in 1946. Then the deployment of the first cellular system by Nippon Telegraph and Telephone Corporation (NTT/Japan) marked the birth of the mobility concept. It was such an important progress that radio communication was baptized mobile communication.

In 1989, the Groupe Spécial Mobile (GSM) defined the European digital cellular standard, the first GSM call was made in 1991. After being deployed in the US in 1994, the GSM was relabeled Global System for Mobile Communication. The GSM marked the beginning of the 2^{nd} generation (2G) of communication systems age. Within the same family stands also the cdmaOne standard mainly deployed in the Americas and parts of Asia and the Personal Digital Cellular (PDC) used exclusively in Japan.

The GSM uses Gaussian Minimum Shift Keying (GMSK) modulation with time division multiple access (TDMA) over frequency division duplex (FDD) carriers and provides circuit-switched data services. These technologies make the GSM supports only voice services and slow data transmission. To enhance supported rates, the General Packet Radio Service (GPRS) was developed in the early 2000 adding packet-switched functionality to GSM. GPRS was hence the essential enabler for always-on applications such as web browsing. It was termed 2.5G. Investigation on novel modulation schemes were continued aiming to attain higher rates to meet the demands of wireless multimedia applications. These investigations resulted in six coding and modulation schemes adapted to different radio conditions promising up to 236.8 kbits/s. That was the birth of a new technology, Enhanced Data Rates for GSM Evolution (EDGE). The major change brought by this new technology is 8-Phase Shift Keying (8PSK) modulation that promises a considerable enhancement in data rates. It coexists with GMSK permitting hence at once to provide high data rates and to guarantee wide coverage.

The success of the GSM and its evolutions incited groups of telecommunications associations to collaborate and to form the 3rd Generation Group Project (3GPP) having as objective to make the 3rd generation specifications. In this context, the Universal Mobile Telecommunications Systems (UMTS) was developed promising up to 384 kbits/s of data rates. It is based on the Wideband Code Division Multiple Access (W-CDMA) technology and the Quadratic Phase shift Keying (QPSK) modulation. However, the UMTS was more oriented toward circuit-switched operation and thus was not well suitable for packet operation. Also, customers data speed demands surpassed the possibilities provided by the UMTS standard. The High Speed Packet Access (HSPA) was thus proposed as an evolution of the UMTS 3G and was labeled the 3.5G. It supports up to 14 Mbits/s in the downlink and 5.76 Mbits/s in the uplink with reduced latency. Instead of the QPSK, it implements the 16-Quadratic Amplitude Modulation (16QAM) offering hence higher data rates. Compared to the UMTS, HSPA provides better overall performance.

Always looking for higher achievable rates, an evolved version of the HSPA system termed HSPA+ or 3G+, has introduced multi-stream transmission through the use of Multiple Inputs Multiple Outputs (MIMO) technique. It enables the system not only to increase considerably achievable rates through spatial multiplexing but also to increase the robustness of the communication against bad channel conditions. In reality, this technique was already available within the UMTS standard (in the form of open loop and closed loop transmit diversity on the one hand, beamforming on the other hand) but operators chose to not exploit it mainly because of complexity and compatibility issues. HSPA+ is expected to be the first 3GPP standard to really exploit the MIMO technique. It is also referred to as dual stream transmit adaptive arrays. Adaptive because the dual-stream transmission is only performed in the case of favorable channel condition. Jointly with 64QAM, MIMO-HSPA+ in the downlink brings peak data rates to 42 Mbits/s.

In the quest of increased spectral efficiency, lower latency and optimized packed radio access technology, in 2004, the 3GPP began working on the Long Term Evolution (LTE) of the UMTS. Aware about the capability of MIMO systems to enhance data rates, the 3GPP has introduced this technique as an integral part of the LTE, indeed from the first version of LTE specification, the system has been designed to support up to four transmit and receive antenna in the downlink. The modulation modes adopted for the LTE are QPSK, 16QAM and 64QAM, promising hence up to 300 Mbits/s in the downlink and 75 Mbits/s in the uplink. Among the possible MIMO downlink transmission modes with LTE we can mention transmit diversity, open-loop and closed-loop spatial multiplexing, beamforming and multi-user MIMO (MU-MIMO). The LTE uses the Orthogonal Frequency Multiple Access (OFDMA) to multiplex users data in the downlink and the Single Carrier Frequency Division Multiple Access (SC-FDMA) for the uplink. Another standard promising near or even equivalent performance is the Worldwide Interoperability for Microwave Access (WiMax) that was developed by the Institute of Electrical and Electronics Engineers (IEEE). OFDMA has been adopted as the basic technique of the WiMax. The modulations used are BPSK, QPSK, 16QAM and 64QAM and two MIMO profiles are supported: the

first uses the Alamouti space time code transmit diversity (referred to as matrix A) with Maximum Ratio Combining (MRC) at the receiver. The second is 2×2 spatial multiplexing scheme (referred to as matrix B). The WiMax offers up to 75 Mbits/s transmission rate.

Aiming to reach even more significant enhancement in terms of performance and capability as higher peak data rate, higher spectral efficiency and lower latency, the 3GPP is now laying the foundations of the evolution of LTE referred to as the LTE-Advanced (LTE-A). Some potential techniques permitting to achieve these requirements are under study. Among them we can mention, enhanced multi-antenna transmission, coordinated multi-point (CoMP) transmission and the use of relays.

1.2 Cellular Network Dimensioning

Cellular networks was proposed as a revolutionary method ensuring mobility with low-power consumption. Indeed, the breakthrough idea was to subdivide a large geographical area into small coverage areas called cells. A base station (BS) serves users being inside the cell area. In mobile networks analytical studies, these cells are usually modeled by hexagons. However, this geographical communication reorganization has raised many concerns: how to subdivide the global coverage area into small areas to ensure an optimal use of the available resources while preserving a required Quality of Service (QoS) level. The engineering term for the way to deal with these concerns is the *dimensioning study*.

Cellular network dimensioning is the process consisting in finding the number of network elements and their configuration needed for achieving a certain QoS for a given environment. Network elements can be BSs, controllers, gateways of the core network, etc. The configuration of a BS includes for example the number of antennas, the transmit power, the antenna height, the number of base band boards, etc. The QoS requirements include coverage and capacity requirements. In terms of coverage, the operator may want to ensure that less than 2% of the cell users cannot decode the common control channel, its ultimate goal is to offer a service continuity. In terms of capacity, he may want to serve circuit switched services with a pre-defined blocking probability or packet switched services within a certain delay or with a certain data rate. The performance of the cellular network is highly dependent on the environment, according to the area type (urban, sub-urban or rural), propagation parameters are modified and have a significant impact on the coverage and the capacity. In this thesis, we focus on the dimensioning of the radio access link, which is the bottleneck of the network and which is also its most expensive part.

In a dimensioning study, we can distinguish three main phases using three complementary methods. In a first phase, engineers need to test and compare the performance of many network scenarios, assuming different BS densities, configurations in various environments or various frequency reuse schemes. Each evaluation should be performed relatively quickly because of the number of considered cases. In this phase, only analytical approaches as the ones presented in this thesis or based on link budgets can meet this requirement. Once few

configurations have been selected, detailed Monte Carlo simulations (using for example the software SOFFA in Orange Labs or the free software tool SEAMCAT [19]) can be launched in order to have more precise performance results. In a third phase, complex radio planning tool like Atoll [20] are used to refine the results based on digitalized maps and calibration measures from the field.

This last method is probably the most precise because it takes into account the details of the considered terrain, the exact antenna patterns, detailed propagation models, etc, and can even perform ray tracing. It cannot be however launched for many cases in a reasonable time and may require expensive measurements from the field. Monte Carlo simulation is a very generic method that provides accurate results. Any new technology, new technique, new protocol can be incorporated at very low cost (only good programmers are required) and evaluated. Accuracy however depends on the number of snapshots and here again the simulation time can be prohibitive in some circumstances.

This thesis focus on the first dimensioning method. It has, without doubts, some drawbacks. First of all, it is a very specific method, i.e., for each new technology, a new approach should be considered and new formulas should be derived. Then, it usually considers theoretical simple models. For example, cells are supposed to be hexagonal. Although there is now a large literature on stochastic geometry for cellular networks (see e.g. [21]), deployment models remain unrealistic. However, the analytical method has the advantage to give very quick results, especially with nowadays mathematical tools like Matlab or Mathematica. Provided they are compared with Monte Carlo simulations and provided that parameter ranges of validity are given, they provide reliable approximations of the performance. We will see in the next sections that for the analytical approach of cellular network dimensioning, outage probability is a crucial performance parameter.

1.2.1 Coverage Analysis

In cellular networks, the Signal to Interference-plus-Noise Ratio (SINR) is the essential input to lead a coverage study. Indeed, the outage probability defined as the probability of failure to reach a minimum SINR required to satisfy a given service or to decode common channels (it is defined in details in Section 5.44), is the principal indicator of the quality of coverage in a cell [4, 22, 23, 24]. To calculate the probability of outage at each point in the cell some inputs are required namely:

- *the radio propagation model*: path-loss, shadowing and fast fading models that depend on the radio communication environments.
- *the network parameters*: transmission power, cell range, antenna gains,...
- *the system specifications*: frequency reuse, modulation and coding schemes (MCS), number and nature of available resources, required QoS for nominal performance (for example, the required SINR in GSM is 9 dB [25], and the minimum required SINR for HSPA is 2.5 dB [26]).

Hence the choice of the appropriate channel model and specific network and system parameters permits to provide an efficient estimation of the probability of outage. Based on this metric, operators can undertake the necessary dimensioning procedure to meet coverage requirements.

1.2.2 Traffic Analysis

While coverage analysis studies the statistical channel quality of a single user in the cell, traffic analysis considers random arrivals and departures of users in the cell.

Traffic is usually modeled by considering a Poisson arrival process of users in the cell and random service times [27]. Mobility between cells can also be taken into account [28]. For a single circuit switched service (e.g. voice), the classical Erlang-B formula is used to derive the blocking probability and the average number of served calls [29]. In case of multiple such services, multi-Erlang-B is also commonly used in conjunction with the Kofman-Roberts algorithm [30].

Todays cellular networks are however fully packet oriented and there is no a priori reservation of resource for a given service. In this kind of network, users can achieve a data rate that is an increasing function of the SINR. They usually want to download a certain amount of data and a typical performance criterion for such users is the download duration. In this context, a traditional approach is to divide the cell area into equal data rate zones and to use the theory of Markov chains [31] and more specifically the M/G/1-PS queue [14].

In all these approaches, the SINR distribution appears as a crucial input. From this distribution, we are able to give the percentage of not covered users and to feed Markov chain approaches with the probabilities to obtain a certain throughput at a given location in the cell. This is the reason why we focus in this thesis on the SINR distribution or equivalently on the outage probability. We give however in Chapter 9, an example of application of our formulas to a dynamic study.

1.3 Contributions and Thesis Summary

The important enhancement in the achievable data rates have been made possible by the breakthroughs fulfilled in the physical layer. Typically, MIMO systems have been introduced as a very promising technique permitting to achieve considerable data rate gains. Since their implementation in the HSPA+ standard, MIMO systems have been prominently part of all 3GPP and even non 3GPP standards (WiMax). Operators and manufacturers have to take into account this technique in the dimensioning process. Multicell cooperation is another promising technique that was proven to bring a considerable improvement to the system capacity and especially to the cell-edge users throughputs. It is now under specification in the LTE-A standard. Dimensioning tools should evolve to take into consideration this newly coming transmission approach. Many other physical layer progress are nowadays under study such as the Time Reversal (TR) transmission that was proven to focalize the

energy in the targeted user reducing hence interference. It is a new factor to consider when conceiving dimensioning rules.

This thesis primary objective is to provide efficient analytical models to assess the performance of multicellular systems and to serve as inputs for operators dimensioning study. The dominant performance metric throughout this thesis is the outage probability. As already stated, this metric is primordial for coverage and capacity studies in wireless communication systems. In this present work, we provide easy-to-compute expressions of the outage probability for Single Input Single Output (SISO), Multiple Inputs Single Output (MISO) and MIMO systems in a multicellular context considering different transmission schemes and different channel models.

We first consider a SISO multicellular system and derive outage probability assuming different fading scales (path-loss, shadowing and fast fading). This first step introduces the main mathematical tools that will be used in the rest of the thesis and gives a benchmark for performance comparisons. We then consider the Time Reversal transmission technique and derive an outage probability formula in a cellular context.

Then we focus on multicellular MIMO systems, we provide analytical expressions of the probability of outage for single user MIMO (SU-MIMO) and multiuser MIMO (MU-MIMO) systems. For SU-MIMO systems, we study the performance of diversity transmission and reception techniques, Alamouti and MRC, used in many standards like UMTS (although it has not been implemented in practice), WiMAX, LTE. For MU-MIMO systems, we consider interference suppression beamforming technique namely the Zero Forcing Beamforming (ZFBF). MU-MIMO is standardized in LTE and enhancements are proposed for LTE-A. We shift towards CoMP transmission systems, in which case we study the performance of the joint transmission strategy with a multiple antenna diversity technique namely the Maximum Ratio Transmission (MRT).

While in the latter studies, assumed models are in nature static (a single user is considered at a given location), in a further study we show how SINR distribution can be efficiently used in a dynamic study considering a best effort traffic. In this context, we provide analytical expressions for the mean user throughput.

- **Chapter 2 - Radio Propagation Models and Performance Metrics**

  In the first part of this chapter we give a summary of the analytical models capturing the properties of radio propagation channels namely fast fading, path-loss and shadowing. We introduce three of the most commonly used flat fading channel models namely Rayleigh, Rice and Nakagami model. Furthermore, we describe the frequency selective channel model characterizing typically wideband communications. We briefly present some MIMO channel models as the Rayleigh flat fading MIMO channel and the frequency selective one and focus on the geometry-based 3GPP MIMO channel. We explain and justify the choices made in this thesis for the propagation models.

  In the second part, we first introduce the most pertinent performance metrics allowing to assess the behavior of different multicellular telecommunication schemes namely

the error probability, the outage probability and achievable rates. These QoS metrics are the key parameters for radio coverage and capacity study of telecommunication systems. Then, we present the dynamic performance study taking as inputs some of the previously presented metrics as well as a traffic model to provide outputs such as the mean user throughput and the cell capacity. Both coverage study and dynamic study provide the key metrics needed to deal with network dimensioning issues.

- **Chapter 3 - Overview of MIMO and CoMP Schemes**

  In this chapter, we first introduce the different MIMO communication contexts: point-to-point communication, multicellular MIMO communication and multiuser multicellular systems. For each system we present the principal gains offered by MIMO techniques namely the diversity gain, the multiplexing gain and the multiuser diversity gain. We present some existing transmission and/or reception schemes permitting to achieve one of these gains or a tradeoff between gains. Furthermore, we enumerate the telecommunication standards implementing MIMO techniques and we focus, in particular, on the LTE standard for which we detail the specified MIMO transmission modes. Then we give an overview of multicellular cooperation transmission, we present the cooperation strategies being specified in the LTE-A standard namely the coordinated beamforming/scheduling (CB/S-CoMP) and the joint processing (JP-CoMP). We also describe some existent selection algorithms for the BSs to cooperate. We highlight the two main overheads engendered by this promising technique: the feedback and the backhaul overheads and present some existent solutions to deal with these overheads. Finally, we go through some existent works on the joint precoding area considering different assumptions on the channel state information at the transmitter (CSIT).

- **Chapter 4 - Outage Probability of Multicellular SISO Systems**

  In this chapter, we propose an analytical study of a multicellular system performance through which we introduce the mathematical tools that will be used throughout this thesis. It is a kind of a benchmark chapter for the following chapters. We conduct an analysis of the joint impact of path-loss, shadowing and fast fading on cellular networks. Two analytical methods are developed to express the outage probability. The first one based on the Fenton-Wilkinson approach, approximates a sum of log-normal random variables by a log-normal random variable and approximates fast fading coefficients in interference terms by their average value. We denote it FWBM for Fenton-Wilkinson Based Method. The second one is based on the central limit theorem for causal functions. It allows to approximate a sum of positive random variables by a Gamma distribution. We denote it CLCFM for Central Limit Theorem for Causal Functions Method. Each method allows to establish a simple and easily computable outage probability formula, which jointly takes into account path-loss, shadowing and fast fading. We compute the outage probability, for mobile stations

located at any distance from their serving BS, by using a fluid model network that considers the cellular network as a continuum of BSs. We validate our approach by comparing all results to extensive Monte Carlo simulations performed in a traditional hexagonal network and we provide the limits of the two methods in terms of system parameters.

- **Chapter 5 - Outage Probability of Time Reversal in Multicellular Systems**

  In this chapter, we express the outage probability of the downlink of a multicellular system of a wideband communication in an indoor environment using Time Reversal transmission. It is a technique that uses the time reversed impulse response of the channel as a pre-filter at the transmitter allowing thus a time and space focusing of energy at the receiver. Time focusing is the concentration of the channel's energy into one predominant peak in time with low side lobes reducing thus inter symbol interference. Space focusing results in a power peak at the intended receiver position that vanishes rapidly when going farther from the focusing point so that inter user interference is reduced. This technique has been deeply investigated in the literature, thus we present some related works in SISO and in MISO/MIMO contexts as well as some original application of the TR.

  While previous works studied the performance of the Time Reversal technique from measurement and/or simulation perspectives, in this chapter, we derive an analytical study of the performance of TR pre-equalization in terms of outage probability for downlink multicellular Wideband (WB) indoor communication environments. We derive a closed form expression of the cumulative distribution function (CDF) of the output signal to interference ratio (SIR) or equivalently the outage probability for Rayleigh frequency selective fading channel. Even though we consider a frequency selective model we neglect the influence of inter-symbol interference (ISI) power in our study. This assumption is based upon the fact that the mean ISI power is negligible compared to mean inter-cell interference (ICI) power. This simplifying assumption is afterwards validated using Monte Carlo simulations by comparing the derived expression to the simulated outage probability when taking into consideration the ISI power.

- **Chapter 6 - Outage Probability of the Alamouti Scheme in a Multicellular Network**

  In this chapter, we study the performance in terms of outage probability of two downlink multicellular systems: a MISO system using the Alamouti code and a MIMO system using the Alamouti code at the transmitter side and a MRC as a receiver. The channel model includes path-loss, shadowing and fast fading and the system is considered interference limited. Two cases are distinguished: constant shadowing and log-normally distributed shadowing. In the first case, closed form expressions of the outage probability are proposed. For a log-normally distributed shadowing,

we derive easily computable expressions of the outage probability. The proposed expressions allow fast and simple performance evaluation for the two multicellular wireless systems: MISO Alamouti and MIMO Alamouti with MRC receiver. We use a fluid model approach to provide simpler outage probability expressions depending only on the distance between the considered user and its serving base station.

- **Chapter 7 - Outage probability of a Zero Forcing Precoded System**

  In this chapter, we propose an analytical expression of the outage probability of the zero forcing precoding technique in a multicellular multiuser context. The channel model includes path-loss shadowing and Rayleigh flat fading. Two cases are examined, the first one considers a slowly varying log-normal shadowing compared to the rapid fluctuation of the fast fading. In this case, a closed form expression of the outage probability is derived. In the second case, we consider a log-normal shadowing and we propose an easily computable integral form expression of the outage probability.

- **Chapter 8 - Outage Probability of an MRT CoMP Transmission**

  In this work, we study the performance of multiple antenna cooperative multicellular system in terms of outage probability. We consider the joint processing multiple antenna CoMP using the MRT technique. It is a diversity transmission scheme that each BS applies separately to the symbol to transmit intended to the user served in cooperation. A closed form expression of the outage probability is derived for Rayleigh flat fading channel model considering path-loss and constant shadowing. Analytical results are validated using Monte Carlo simulation results. In particular, we bring to the light the influence of the number of cooperating BSs and the number of antennas of each BS.

- **Chapter 9 - Dynamic System Performance of SISO, MISO and MIMO Systems**

  In this chapter, the performance of a SISO system, a 2×1 MISO Alamouti transmission system and a $2 \times N$ MIMO Alamouti transmission with MRC receiver system is studied in terms of mean flow throughput per user. A dynamic study (i.e. assuming a dynamic number of active users) is derived considering the downlink Rayleigh channel in a multicellular system. Two assumptions are considered: admission control based on a maximum number of users or no admission control. The studied cell is divided into concentric rings. Analytical expressions of the mean flow throughput of a user in each ring are proposed. A comparison between the performance of the different systems is presented and discussed.

List of Publications

- D. Ben Cheikh and A. Saadani, On the Outage Probability in Amplify-and-Forward Relay Channels, *In Proc. of IEEE conference on Wireless Communications and Networking Conference (WCNC), pages 1-5, May 2009.*
- D. Ben Cheikh, J.-M. Kélif, M. Coupechoux and P. Godlewski, Outage Probability in a Multi-Cellular Network Using Alamouti Scheme, *In Proc. of IEEE Sarnoff Symposium, pages 1-5, Apr. 2010.*
- D. Ben Cheikh, J.-M. Kélif, F. Abi-Abdallah and D.-T. Phan Huy, Time Reversal Outage Probability for Wideband Indoor Wireless Communications, *In Proc. of IEEE International Symposium on Personal Indoor and Mobile Radio Communications (PIMRC), pages 999-1003, Sept. 2010.*
- D. Ben Cheikh, J.-M. Kélif, M. Coupechoux and P. Godlewski, Multicellular Zero Forcing Precoding Performance in Rayleigh and Shadow Fading, *In IEEE Vehicular Technology Conference (VTC Spring), pages 1-5, May 2011.*
- D. Ben Cheikh, J.-M. Kélif, M. Coupechoux and P. Godlewski, Dynamic System Performance of SISO, MISO and MIMO Alamouti Schemes, *In Proc. of IEEE Sarnoff Symposium, pages 1-5, May 2011.*
- D. Ben Cheikh, J.-M. Kélif, M. Coupechoux and P. Godlewski, SIR Distribution Analysis in Cellular Networks Considering the Joint Impact of Path-Loss, Shadowing and Fast Fading, *EURASIP Journal on Wireless Communications and Networking, 2011:137, Oct. 2011.*
- D. Ben Cheikh, J.-M. Kélif, M. Coupechoux and P. Godlewski, Analytical Joint Processing Multi-Point Cooperation Performance in Rayleigh Fading, *IEEE Wireless Communications Letters, Vol. 1, Issue 4, pages 272-275, Aug. 2012.*
- D. Ben Cheikh, J.-M. Kélif, M. Coupechoux and P. Godlewski, Multicellular Alamouti Scheme Performance in Rayleigh and Shadow Fading, *to appear in Springer Annals of Telecommunications, 2012.*

Chapter 2

Radio Propagation Models and Performance Metrics

2.1 Introduction

The implementation of new communication techniques such as the MIMO and the CoMP transmission as a response to the growing demand for higher data rates has emerged the need for new dimensioning rules to take into consideration these evolutions. Indeed, the dimensioning process of wireless cellular networks is based around two main stages: a static study stage and a dynamic study one. The static study assumes fixed number of active users having full buffers and always ready to transmit. In this case, the study takes as inputs: the propagation model proper to the environment of study (path-loss, shadowing, fast fading), the network model (hexagonal, intercell distance, transmit powers,...) and strategies used such as multiple access scheme or the transmission and reception scheme (TR, MIMO, CoMP,...). As outputs, the study assesses metrics such as the instantaneous SINR, the outage probability, the error probability and the data rate. These metrics permits to have an idea about the radio coverage and the capacity of a telecommunication system. Dynamic study considers the case when users randomly enter the network, download a file during an active phase and go to sleep after download is over. The study takes as inputs the traffic demand model in the cell, the number of active users and scheduling method as well as some outputs provided by the static study such as the SINR distribution. The dynamic study assesses performance metrics such as the cell capacity, the blocking probability, the mean throughput per user and the average number of active users in the cell.

This chapter is composed of two parts. The first one presents some propagation models, the second one introduces the major metrics permitting to assess the radio performance of telecommunication systems. In the next section, we propose some models of fading, we distinguish the small scale propagation effect from the large scale one. In Section 2.3, we present some MIMO propagation models. In Sections 2.4 and 2.5, we present some perfor-

mance metrics. We distinguish the performance metrics when leading a static study from the metrics of a dynamic study. In Section 2.6, we explain the two stages of a dimensioning process and propose some references that have conducted either a static study or a dynamic one or with both studies. In Section 2.7, we conclude the chapter.

2.2 Fading Models

2.2.1 Small Scale Fading

Small scale fading is caused by the summation of different multipath replicas of the same signal arriving at slightly different times with different phase shifts. The addition of the different versions of the transmitted signal that can be constructive (when the waves are in-phase) or destructive (when the waves are in anti-phase) causes the fluctuation of the received signal over a short period of time.

The impulse response of a time-varying channel can be written as:

$$h(\tau, t) = \sum_i h_i(t)\delta(\tau - \tau_i(t)), \tag{2.1}$$

where $h_i(t)$ and $\tau_i(t)$ are respectively the attenuation and the time delay corresponding to the i^{th} path, $\delta(.)$ is the Dirac's delta function. The summation is over the set of resolvable multipath components, the difference between delays corresponding to any two multipath components being considerably higher than the symbol period.

From this expression of the channel filter, we can define the delay spread as the difference in propagation time between the first arriving version of the signal and the latest one, that can be written as:

$$\tau_d = \max_{i,j} |\tau_i(t) - \tau_j(t)| . \tag{2.2}$$

This time delay metric is very important since it allows to distinguish between two categories of channels. The flat fading channel and the frequency selective one. We talk about a flat fading when the delay spread of the channel is very small compared to the symbol period or equivalently if the transmitted signal bandwidth is very small compared to the coherence bandwidth of the channel (the coherence bandwidth characterizes the speed of the channel frequency variation). The channel is said frequency selective if the delay spread is considerably greater than the symbol period. In indoor environments, the delay spread is typically between 10 and 1000 nanoseconds, in urban environments, it ranges from 1 to 30 microseconds [32]. Hence, outdoor systems suffer more from inter-symbols interference (ISI) and thus tend to support lower data rates than indoor systems [33].

2.2.1.1 Flat Fading

The flat fading can be modeled by a one tap channel. In fact, if the delay spread is very small compared to the symbol duration, all the arriving multipath replicas are non

resolvable resulting in a single component. The channel can, thus, be written as:

$$h(t,\tau) = h(t)\delta(\tau). \tag{2.3}$$

- **Rayleigh Fading**
  In a rich scattering environment, the number of non resolvable components can be sufficiently high so that the central limit theorem can be used to statistically characterize $h(t)$ as a complex Gaussian random variable. If there is no line-of-sight (LOS) component, the magnitude of the channel tap $|h(t)|$ is hence Rayleigh distributed, the probability density function (PDF) is given by:

$$f(r) = \begin{cases} \frac{2r}{\Omega} e^{-\frac{r^2}{\Omega}} & r \geq 0 \\ 0 & r < 0 \end{cases}, \tag{2.4}$$

  where Ω is the mean power of the multipath fading. The squared magnitude $|h(t)|^2$ is exponentially distributed with density:

$$f(w) = \begin{cases} \frac{1}{\Omega} e^{-\frac{w}{\Omega}} & w \geq 0 \\ 0 & w < 0 \end{cases}. \tag{2.5}$$

- **Ricean Fading**
  If there is a line-of-sight component, the envelope of the received signal is described using a Rice distribution that is given by:

$$f(r) = \begin{cases} \frac{2r(\kappa+1)}{\Omega} e^{-\kappa-\frac{(1+\kappa)r^2}{\Omega}} I_0\left(2r\sqrt{\frac{\kappa(\kappa+1)}{\Omega}}\right) & r > 0 \\ 0 & r < 0 \end{cases}, \tag{2.6}$$

  where κ is the power of the line-of-sight component and $I_0(.)$ is the modified Bessel function of first kind of order zero. It can be clearly noticed that when κ tends to zero, the Rician distribution tends to a Rayleigh one.

  The squared form of a Ricean distributed envelope follows the non-central Chi-square distribution given by:

$$f(w) = \begin{cases} \frac{w(\kappa+1)}{\Omega} e^{-\kappa-\frac{(1+\kappa)w}{\Omega}} I_0\left(2\sqrt{\frac{\kappa(\kappa+1)w}{\Omega}}\right) & w \geq 0 \\ 0 & w < 0 \end{cases}. \tag{2.7}$$

- **Nakagami-m Fading**
  Another statistical model capturing with higher precision channels with large delay spread and different clusters of reflected waves is the Nakagami-m distribution. It is a variate of the Chi-square distribution and is given by:

$$f(r) = \begin{cases} \dfrac{2m^m r^{2m-1}}{\Gamma(m)\Omega^m} e^{-\frac{mr^2}{\Omega}} & r > 0 \\ 0 & r < 0 \end{cases}, \tag{2.8}$$

  where Γ is the Gamma function and m is a parameter of the distribution.

  The Nakagami-m distribution can be viewed as the generalization of a wide range of multipath distribution. Indeed, for $m = 1$ we find the Rayleigh distribution, with $m = \frac{(1+\kappa)^2}{1+2\kappa}$, we have the Ricean distribution [34] and when $m \to \infty$ it converges to the Additive White Gaussian Noise (AWGN) channel. It is the distribution modeling the best land-mobile and indoor-mobile multipath propagation [34].

  If $|h(t)|$ has a Nakagami-m distribution, then the distribution of the squared magnitude $|h(t)|^2$ is given by:

$$f(w) = \begin{cases} \left(\dfrac{m}{\Omega}\right)^m \dfrac{w^{m-1}}{\Gamma(m)} e^{-\frac{mw}{\Omega}} & w \geq 0 \\ 0 & w < 0 \end{cases}. \tag{2.9}$$

2.2.1.2 Frequency Selective Fading

In a very rich scattering environment, for instance an indoor or an urban environment, the transmission of a signal results in many resolvable multipath components arriving with different delays at the receiver end. Each resolvable component can be the result of a group of non resolvable components, the number of these components can be sufficiently large so that each resolvable component can be characterized by a complex Gaussian distribution referring to the central limit theorem.

The received signal is, thus, a sum of delayed copies of the original signal. This distortion causes inter-symbol interference if the symbol period is smaller than the delay spread of the channel meaning that:

$$T_s < \tau_d. \tag{2.10}$$

In the frequency domain, the channel exhibits different gains for different frequency components, this is typically why it is termed frequency-selective fading. The Orthogonal Frequency Division Multiplexing (OFDM) [35, 36] is a practical solution to eliminate ISI. Indeed it permits to subdivide a wide band into narrow sub-bands. The frequency selective channel is hence transformed into many flat fading sub-channels.

Note that the flat fading or the frequency-selective fading is not a property of the channel alone, but it characterizes the response of the signal through the channel transmission.

In this thesis, we have considered two different types of environments: the urban environment (Chapters 4, 6, 7, 8 and 9) and the indoor environment (Chapter 5). In the former case, the channel is usually modeled with normalized ($\Omega = 1$) Rayleigh flat fading because a line-of-sight propagation is very rare in such cases. The flat fading assumption is justified by the fact that for frequency selective channels the OFDM transmission can be applied to subdivide the bandwidth into small flat fading sub-channels. The OFDM technique is now the dominant transmission scheme on the downlink of cellular networks. In indoor environments, the time reversal transmission is studied considering a frequency selective channel for a large band communication, thus ISI has been taken into account. However, in Chapter 5, we will show that thanks to TR, this interference is negligible with respect to co-channel interference.

2.2.2 Large Scale Fading

Large scale fading is the attenuation of the average power of the signal due to the motion in a large area. We distinguish two kinds of large scale effects: path-loss and shadowing.

2.2.2.1 Path-loss

Path-loss traduces the degradation of the mean signal power as a function of the propagation distance and parameters related to the propagation environment (indoor, outdoor) and to other factors such as the antennas heights and the carrier frequency.

Many models of the path-loss effect have been proposed for different propagation environments among them we can mention the Egli model [37] used for a frequency range of 3 MHz-3 GHz, when there is a line-of-sight between a fixed transmit antenna and a mobile receive antenna, and the Okumara Hata model [38] proposed for mobile urban propagation environment for the frequency range 150 - 1500 MHz. Correction factors are available to make this model applicable for suburban environments or for different ranges of frequencies. However it is not applicable for indoor path-loss modeling.

Throughout this work we will consider a simplified commonly used model of the path-loss given by:

$$P_r = P_t A d^{-\eta}, \tag{2.11}$$

where P_r is the received power, P_t is the transmit power and A is a unit-less constant depending on the antennas characteristics, d is the relative distance of the receiver to the transmitter and η is the path-loss exponent characterizing the propagation environment and is in the range of $2.7 - 3.5$. Table 2.1 [33] illustrates the path-loss exponent for different environments.

In this thesis, we are not concerned about the details of the propagation characteristics, we let the reader free of choosing his favorite propagation model and adjust parameters A and η to fit the characteristics of the environment under study.

While for outdoor environments it is possible to have a generic model for the path-loss capturing a wide range of the propagation environments, for indoor communication, it is quite difficult to propose a precise model covering all types of indoor buildings (open factory, cubicle office,...). A simplified form of the COST 231 [39] indoor path-loss model for the frequency range $[0.8, 1.9]$ GHz was adopted by the International Telecommunication Union (ITU) for the evaluation of International Mobile Telecommunications (IMT) 2000 indoor systems and is given by [40]:

$$L(dB) = 37 + 30 \log_{10} d + 18.3^{(\frac{n+2}{n+1} - 0.45)}, \tag{2.12}$$

where d is the transmitter-receiver separation in meters and n the number of floors in the path. We will use this model for the study of the time reversal performance in Chapter 5.

Path-loss can be viewed as harmful effect for cell coverage however the rapid power decay with distance is also helpful since it permits to generate less interference to other cells operating on the same frequencies.

Table 2.1: Path-loss exponent in different communication environments.

environment	η range
urban macrocells	3.7-6.5
urban microcells	2.7-3.5
office building	1.6-3.5
home	3

2.2.2.2 Shadowing

A signal transmitted to a receiver is attenuated due to diffraction and reflection on the surrounding building surfaces, trees and many other obstacles encountered in the propagation environment, when moving over a distance of the order of these obstacles dimensions. To model the random attenuation effect on the transmitted signal the most commonly used statistic model is the log-normal shadowing [37]. The lognormal distribution is given by:

$$f_\Phi(\phi) = \frac{\omega}{\sqrt{2\pi}\sigma\phi} \exp\left[-\frac{(10 \log_{10} \phi - \mu)^2}{2\sigma^2}\right], \tag{2.13}$$

where $\omega = \frac{10}{\ln 10}$, μ (dB) and σ (dB) are respectively the mean and the variance of $10 \log_{10} \phi$. The standard deviation of the log-normal shadowing is between 0 and 8 dB [24] in outdoor and about 12 dB for indoor systems [40].

However, the lognormal model in composite fading/shadowing channels does not lead to closed-form expressions for the received signal power distribution which impedes further

analytical derivations. In the literature, we can find simpler statistical models for the shadowing as the Gamma distribution [41].

Compared to the multipath fading, the duration of shadow fading lasts much longer. Whereas the former typically lasts during tens of ms (depending of the velocity of the mobile and the carrier frequency), the latter lasts for tens of seconds or minutes. In traditional dimensioning studies of cellular networks (e.g. for GSM), fast fading is usually ignored since it is assumed to be efficiently processed by the physical layer. Once the useful signal has achieved a certain SINR threshold (for example 9 dB), it is assumed that voice has reached a sufficient quality even if fast fading induces a non zero residual frame error probability. In UMTS also, fast fading may be ignored in dimensioning studies because of the fast power control that partially compensates its negative effects. From HSDPA onwards however, fast fading should be considered as it has a crucial impact on fast scheduling algorithms and MIMO transmissions.

There are thus several approaches in the literature for dealing with fast and slow fading for dimensioning purposes. The first one is to simply ignore fast fading with the argument that it is efficiently taken into account by the physical layer (see e.g. [3] and [4]). The second one is to consider only fast fading and assuming a constant shadowing (see e.g. [42]). This can be explained by the considered time-scale: on a short duration, slow fading can be considered as constant. At last, many papers take the assumption of a joint effect of fast and slow fading in order to account with all variations of the channels (see e.g. [43]). In this thesis, we consider the only effect of fast fading assuming a constant shadowing in Chapters 5, 8 and 9 and the effect of both fast fading and shadowing in Chapters 4, 6 and 7. Our studies focus on the outage probability but cannot answer the question of how long outage takes place. For example, a very short outage should not interrupt a communication. The study of the *excursions* of the SINR below some given threshold is a possible future work.

2.3 MIMO Channel Models

Consider now a multiple inputs multiple outputs (MIMO) system with M transmit antennas and N receive antennas. The MIMO channel is modeled by a matrix whose elements represent the channel gains between the different transmit and receive antennas (figure 2.1).

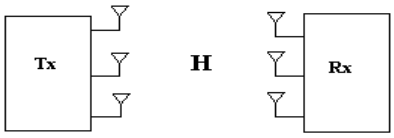

Figure 2.1: MIMO channel model.

2.3.1 Narrowband MIMO Channel

In a narrowband communication, the MIMO channel is modeled by a matrix which entries are flat fading channels. The channel matrix is hence given by:

$$\mathbf{H} = \begin{bmatrix} h_{1,1} & h_{1,2} & . & . & . & h_{1,N} \\ & & & . & & \\ & & & . & & \\ & & & & . & \\ h_{M,1} & h_{M,2} & . & . & . & h_{M,N} \end{bmatrix}, \tag{2.14}$$

where $h_{i,j}$ is the channel gain between antenna i of the receiver and antenna j of the transmitter.

If the MIMO channel matrix have independent circularly complex Gaussian distributed entries $h_{i,j}$ with zero mean unit variance, i.e., $h_{i,j} \sim CN(0,1)$ (most commonly used channel model) we speak about a flat fading Rayleigh MIMO channel model. If the matrix entries are non-zero mean independent complex Gaussian random variables, it is said a Rician MIMO channel and can be modeled as:

$$\mathbf{H} = \sqrt{\frac{\kappa}{\kappa+1}}\mathbf{H}_d + \sqrt{\frac{1}{\kappa+1}}\mathbf{H}_r, \tag{2.15}$$

where κ is Ricean factor defined as the ratio of the mean LOS signal power to the mean scattered signal power, $\sqrt{\frac{\kappa}{\kappa+1}}\mathbf{H}_d$ is the deterministic component of the channel (the mean of the channel) and $\sqrt{\frac{1}{\kappa+1}}\mathbf{H}_r$ is the random matrix component which entries are zero-mean complex Gaussian random variables.

Now if the entries of the channel matrix are dependent, the matrix $\mathbf{H}$ models a MIMO system where there are correlations between transmit and/or receive antennas. In this case $\mathbf{H}$ can be written as:

$$\mathbf{H} = \mathbf{R}_r^{1/2}\mathbf{H}_0\mathbf{R}_t^{1/2}, \tag{2.16}$$

where $\mathbf{H}_0$ is $N \times M$ matrix with complex Gaussian zero mean unit-variance independent and identically distributed (iid) elements, $\mathbf{R}_r$ and $\mathbf{R}_t$ are respectively the $N \times N$ receiver and the $M \times M$ transmitter correlation matrices.

2.3.2 Frequency Selective MIMO Channel

In a wideband communication, the channel response between a receive antenna i and a transmit antenna j is the sum of path gains with different delays. Hence each element $h_{i,j}$ can be expressed as:

$$h_{i,j}(\tau, t) = \sum_n \alpha_n(t)\delta(\tau - \tau_n), \tag{2.17}$$

where $\alpha_n(t)$ is the channel attenuation over path n at time t and τ_n is the delay corresponding to path n.

For quasi-static channels (constant during the transmission of a block or a packet), $h_{i,j}$ is only function of τ and (2.17) reduces to:

$$h_{i,j}(\tau) = \sum_n \alpha_n\delta(\tau - \tau_n). \tag{2.18}$$

As in the SISO case, MIMO frequency selective channels cause ISI. Equalization in this case becomes a very complex issue since it must be performed over time and over space. As for the SISO case, the OFDM technique may be the solution to mitigate ISI since it transforms the frequency selective MIMO channel into a set of narrowband MIMO channels.

2.3.3 3GPP MIMO Channel Model

The 3GPP proposed a spatial channel model for MIMO channels. It is a geometry-based stochastic model that enables the separation of propagation parameters and antennas.

As for the SISO case, a signal sent by a multiple antenna transmitter to a multiple antenna receiver follows different paths engendering different delayed versions of the original signal. In the 3GPP model each resolvable path is characterized by its own spatial MIMO channel parameters and all paths are assumed independent. These parameters are angle spread, angle of arrival and power azimuth spectrum. Figure 2.2 illustrates the angular parameters used in the model [1]. As can be seen from figure 2.2, each path consists of a number U of sub-paths. The n^{th} path channel coefficient between transmit antenna j and receive antenna i (between a BS and a MS) is given by [1]:

$$\begin{aligned} h_{i,j,n}(t) &= \sqrt{\frac{P_n\sigma_{SF}}{U}} \sum_{u=1}^{U} \sqrt{G_{BS}(\theta_{u,n,AoD})} \exp\left(j\left[kd_j \sin(\theta_{u,n,AoD}) + \phi_{u,n}\right]\right) \\ &\times \sqrt{G_{MS}(\theta_{u,n,AoA})} \exp\left(j\left[kd_i \sin(\theta_{u,n,AoA})\right]\right) \\ &\times \exp\left(jk \left\|v\right\| \cos(\theta_{u,n,AoA} - \theta_v)t\right), \end{aligned} \tag{2.19}$$

where AoA and AoD stand respectively for angle of arrival and angle of departure, table 2.2 defines the parameters used in (2.19). The path-loss and the lognormal shadowing are applied as bulk parameters to each of the sub-path components of the n^{th} path components

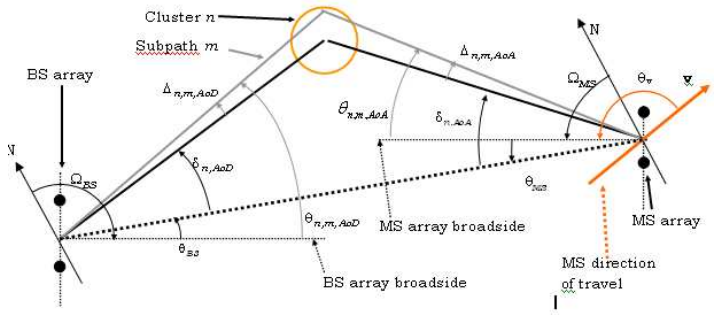

Figure 2.2: BS and Mobile Station (MS) angle parameters [1].

Table 2.2: 3GPP MIMO channel model parameters.

parameter	definition
P_n	power of the n^{th} path
σ_{SF}	lognormal shadow fading
U	number of sub-paths per-path
$\theta_{u,n,AoD}$	AoD for the u^{th} sub-path of the n^{th} path
$\theta_{u,n,AoA}$	AoA for the u^{th} sub-path of the n^{th} path
$G_{BS}(\theta_{u,n,AoD})$	BS antenna gain of each array element
$G_{MS}(\theta_{u,n,AoA})$	MS antenna gain of each array element
k	wave number $\frac{2\pi}{\lambda}$ where λ is the carrier wavelength in meters
d_j	distance in meters from BS antenna j to the reference ($j = 1$) antenna
d_i	distance in meters from MS antenna i to the reference ($i = 1$) antenna
$\phi_{u,n}$	phase of the u^{th} sub-path of the n^{th} path
$\|v\|$	magnitude of the MS velocity vector
θ_v	angle of the MS velocity vector

of the channel. For macrocell environments, the path-loss model is based on the modified COST 231 Hata [39] urban propagation model and on the COST 231 Walfish-Ikegami [39] for microcell environments.

In this thesis, we will use the Rayleigh flat fading MIMO channel. This choice can be justified by the fact that the principal aim of this work is to provide input elements to dimensioning studies. Rather than the complex 3GPP MIMO model that is not adapted for a rapid dimensioning application, the Rayleigh one is largely sufficient for this purpose. The 3GPP channel model is however perfectly adapted to the simulation phase of the dimensioning study. In this thesis, we have also ignored possible correlations between antennas, this is left for future studies.

2.4 Static Study Performance Metrics

2.4.1 Average SINR

Consider a downlink multicellular multiuser communication system. A user receives a useful signal from its serving BS, an interference signal consisting of signal intended to other users in the cell and a multicell interfering signal coming from the surrounding cells. The SINR expression is hence given by:

$$\gamma = \frac{P_u}{I_{int} + I_{ext} + \sigma_n^2}, \tag{2.20}$$

where P_u is the useful received power, I_{int} is the multi-user interference power and I_{ext} is the multicell interference power.

The instantaneous SINR is a very important performance indicator that we aim to maximize either using scheduling algorithms or by performing beamforming mechanisms or even by resorting to cooperation strategies that reduce or totally eliminate the interference power and maximize the useful power.

The statistical variation of the SINR over time is also of primordial importance. Indeed, the average SINR is probably the most useful performance metric for radio systems planning. Also, the distribution of the SINR permits to study the outage probability, the error probability, and the mean data rate which are three relevant performance metrics indicators.

2.4.1.1 Interference Limited Systems

In an interference limited system, the interference power is much larger than the noise power and hence the SINR reduces to an SIR that can be written as:

$$\gamma = \frac{P_u}{I_{int} + I_{ext}}, \tag{2.21}$$

CDMA systems are typically interference limited since many users transmits on the same frequency band. Interference can be reduced using sectorization and power control besides the interference reduction methods mentioned above.

Dense urban and urban environments characterized by small to moderate cell radii are also interference limited systems. They suffer from high level of ICI interference. The management of this kind of interference is hence of crucial importance in such systems, since it has a considerable impact on the performance. It can be reduced using multicell cooperation strategies.

2.4.1.2 Noise Limited Systems

In a noise limited system, the noise power is much higher than the interference power. It is the case in a isolated cell or in a multicell system whose out-of-cell interference is small compared with the thermal noise (e.g. in rural areas). We rather talk about SNR than SINR and hence the expression (2.20) reduces to:

$$\gamma = \frac{P_u}{\sigma_n^2}. \tag{2.22}$$

A noise limited system is more binding than an interference limited one since the thermal noise is produced through a physical process and cannot be avoided.

2.4.2 Outage Probability

The outage probability is defined as the probability that the SINR at the input of the receiver chain is falling below a given threshold value. Mathematically, the outage probability is the CDF of the SINR and is given by:

$$P_{out}(\gamma_{th}) = Pr[SINR < \gamma_{th}], \tag{2.23}$$

γ_{th} being the SINR threshold value.

The issue of expressing outage probability in cellular networks has been extensively addressed in the literature. In [3, 4, 5, 6, 7, 8], the authors derived outage probability expressions for multicellular SISO systems, considering different channel model assumptions: only path-loss and shadowing or only Rayleigh fading. In many cases, the authors resorted to simplifying statistical assumptions. The outage probability of multicellular MIMO systems was also investigated. In [9], the authors derived the outage probability expression for different receive diversity schemes such as the Maximum Ratio Combining (MRC), the Equal Gain combining (EGC) and the Selection Combining (SC) considering Rayleigh fading. In [10] the outage probability of the uplink of a multicellular MIMO system using the maximum ratio transmit diversity scheme considering path-loss, shadowing and Rayleigh was derived. In [11], the study provides analytical expressions of the outage probability

of MRT combined with one of two different receive antenna array schemes: MRC and interference cancellation (IC) considering Rayleigh channels.

Concerning multicell cooperation systems, very few works were devoted to the derivation of the outage probability. One of these works is [12], it provides an expression of the outage probability of a multicell processing system in the case of non-coherent transmission considering Rayleigh fading. Another analytical study of CoMP systems was proposed in [13] where the authors considered a cooperative MRT/MRC scheme. An analytical expression of the probability density function of the SIR was derived considering path-loss, shadowing and Rayleigh fading. However, the authors resorted to many assumptions: a cell-edge user served in cooperation is at equal distances from the cooperative BSs, a Gamma distributed shadowing and a Poisson spatial distribution of interfering transmitters. The obtained analytical results are not sufficiently accurate since they are significantly different from simulation results.

Our work in this thesis is a straight continuation of these studies since we propose outage probability expressions of multicellular systems with different transmission strategies considering different channel models.

For some wireless communication applications, the knowledge of the SINR CDF is not sufficient to characterize a system. The frequency and the mean duration of outage events may be of equivalent importance especially for adaptive communication. In this case, the outage probability is characterized not only by the CDF of the SINR but also the CDF of the outage duration. The outage probability is hence defined as [44]:

$$P_{out}(\gamma_{th}, \tau_m) = Pr[SINR < \gamma_{th}, \tau_{out} > \tau_m], \tag{2.24}$$

where τ_{out} is the outage duration and τ_m the minimum outage duration. In [44], the latter outage probability expression was approximated by:

$$P_{out} = f_{out}\, \bar{\tau}_{out}, \tag{2.25}$$

where f_{out} is the frequency of outage defined as the average rate of outage events and $\bar{\tau}_{out}$ is the average outage duration.

Based on this metric, the transmitter adapts the packet length or the slot duration reducing hence the data loss and retransmission requests.

2.4.3 Average Error Probability

The bit error probability has been deeply investigated in the literature. It permits to evaluate different transmission and detection schemes.

Usually the error probability is represented using the Q-function based on the Gaussian approximation of the perturbation due to the interference-plus-noise term. To compute the average error probability, one must hence evaluate the following integral [34]:

$$\bar{P}_e = \int_0^{\infty} Q(a\sqrt{\gamma}) f_\gamma d\gamma, \tag{2.26}$$

$f_\gamma(\gamma)$ being the PDF of the instantaneous SINR, $Q(.)$ the Q-function and a a constant depending on the specific modulation and detection combination.

Evaluating the expectation of the Q-function is a quite difficult issue, which aroused the interest in finding alternate representations, as well as approximations that are tight and analytically simple [34, 45, 46, 47].

As it can be noticed, to evaluate the error probability, the PDF of the SINR is needed. In this thesis, we provide the distribution of the SINR of various systems considering different communication scenarios.

The error probability can be reduced using space, frequency, time, polarization or angle diversity. To take most advantage of the different transmitted signal versions generated by these diversity techniques, some combining methods such as the MRC, EGC and the SC can be performed at the receiver. Many works compared the performance of these combining methods [48, 49, 50].

2.4.4 Data Rate

Enhancing the users achievable data rates is the principle motivation behind wireless communication standards evolution. It is hence important to propose transmission schemes to maximize this metric regarding the channel constraints.

In a single user M by N MIMO communication over a fading channel $\mathbf{H}$, if there is no Channel State Information (CSI) at the transmitter and full CSI at the receiver (CSIR) maximizing the data rate or equivalently achieving capacity is performed by an equal power allocation to the transmit antennas. The capacity is in this case given by [51]:

$$C = E_{\mathbf{H}}\left[\sum_{i=1}^{r} \log_2(1 + \frac{\lambda_i^2 P}{M\sigma_n^2})\right], \tag{2.27}$$

where λ_i is the i^{th} singular value of $\mathbf{H}$, r is the number of positive singular values (if $\mathbf{H}$ is a full-rank matrix, $r = \min\{M, N\}$) and P is the maximum power at the transmitter. Through this expression of capacity we can see that our system is equivalent to r parallel channels characterized by the r singular value of $\mathbf{H}$.

When CSI is available at the transmitter, a water-filling strategy can be performed to maximize data rate. It consists in investing power on the reliable channels among the r parallel channels. The capacity is in this case given by [33]:

$$C = E_{\mathbf{H}}\left[\max_{P_i:\sum_{i=1}^{r} P_i < P} \sum_{i=1}^{r} \log_2(1 + \frac{\lambda_i^2 P_i}{\sigma_n^2})\right]. \tag{2.28}$$

In a multiuser (K users) MIMO communication, the capacity is a region defined by the sets of K-users achievable rates. assuming full CSIT, it was proven that the Dirty Paper Coding

(DPC) scheme achieves the multi-user capacity region of the broadcast channel given by in MIMO broadcast channel. The broadcast capacity region is defined as [52]:

$$C_{BC}(P,\mathbf{H}) = C_o\left(\bigcup_{\pi,\mathbf{Q}} \mathbf{R}(\pi,\mathbf{Q})\right), \tag{2.29}$$

where $\pi(\cdot)$ denotes a permutation of the user indices and $\mathbf{Q} = (\mathbf{Q}_1, \mathbf{Q}_2, .., \mathbf{Q}_K)$ the set of covariance matrices of the signals transmitted to the K users and

$$\mathbf{R}(\pi,\mathbf{Q}) : R_{\pi(k)} = \log \frac{\left|\mathbf{I} + \mathbf{H}_{\pi(k)}(\sum_{j\geq k}\mathbf{Q}_j)\mathbf{H}^H_{\pi(k)}\right|}{\left|\mathbf{I} + \mathbf{H}_{\pi(k)}(\sum_{j>k}\mathbf{Q}_j)\mathbf{H}^H_{\pi(k)}\right|}, \quad k = 1...K. \tag{2.30}$$

This expression should be optimized over all possible user orderings. The capacity region (2.30) corresponds to a downlink multi-user system with perfect CSIT and CSIR. The capacity region of the same system without the assumption of perfect state information knowledge at both transmitter and receiver remains an open problem.

The complexity of the DPC makes it excluded from usage in practice. As an alternative, lower complexity sub-optimal schemes such as the Zero Forcing Beamforming (ZFBF) combined with multiuser diversity were proposed and were proven to achieve near-optimal capacity when the number of active users becomes large [53] (see Chapter 7).

The K-dimension capacity region is quite difficult to characterize when $K > 2$. Another metric much easier, defining the maximum throughput of a system is the sum-capacity region given by:

$$C_{BCSR} = \max_{R_1,...,R_K} \sum_{k=1}^{K} R_k. \tag{2.31}$$

The sum-rate capacity may not be fair in terms of rate allocation especially when there is large SNR imbalances between users however it remains an important metric permitting to evaluate MU-MIMO transmission and reception schemes.

When no CSIT is available, the BS cannot serve many users simultaneously since it is impossible to form spacial beams without any direction knowledge. In this case, a randomly chosen user is served by the BS and the maximum sum-rate in the high SNR regime reduces to:

$$E[R_{SR,no\ CSIT}] \underset{K\to\infty}{\longrightarrow} \min\{N, M\}\log(SNR). \tag{2.32}$$

However, in [54] Sharif and Hassibi showed that when the number of active users is large the sum-rate of the DPC scales like $M \log\log(KN)$.

As a design criterion for transmission or reception schemes, we can consider maximizing the minimum rate permitting hence to users with worst channel condition to benefit of a convenient rate level. The works [55, 56, 57] were proposed in this perspective.

2.5 Dynamic Study Performance Metrics

We speak about a dynamic study when we take into consideration the random nature of the traffic in the cell. This randomness is due to the dynamic variation of the active user set in the cell and of the traffic demand.

We consider a cellular network with a fair time shared downlink transmission and consider only data traffic. We assume a uniform traffic demand in the cell, file transfers or flows sizes are independent and identically distributed with a mean flow size equal to V and arrives in random times following a Poisson process with intensity λ. Users are assumed static during data transfers.

We also consider that a user at a distance r from its serving BS has a transmission rate given by the Shannon formula as:

$$\bar{R}(r) = \int_0^\infty W \log_2(1+\gamma(r)) f_\gamma(\gamma) d\gamma, \tag{2.33}$$

γ being the SINR at a distance r.

To calculate the transmission rate, we need the PDF of the SINR that we derived in this thesis for different communication systems.

The relevant performance metrics to assess in such a system are the cell capacity, the mean throughput per user and the mean number of active users. To introduce these metrics, we should first define the cell load. Referring to our traffic model presented above, in an infinitesimal area region dr, flows arrives with an intensity $\frac{\lambda dr}{A}$, A being the cell size. For each flow, an average transmission time is required and is given by [14]:

$$\bar{T} = \frac{V}{\bar{R}(r)}. \tag{2.34}$$

Denoting ρ the cell load, it can be written as:

$$\rho = \int_{cell} \frac{\lambda}{A} \frac{V}{\bar{R}(r)} dr. \tag{2.35}$$

The cell load must be kept under the threshold value 1 unless the number of active users grows indefinitely and the network is saturated.

- **Cell Capacity**

  In a dynamic system, the cell capacity can be defined as the maximum traffic intensity for which the cell is not saturated meaning that the cell load verifies $\rho < 1$. It is given by [14]:

  $$C = \left(\int_{cell} \frac{1}{A} \frac{dr}{R(r)} \right)^{-1}. \tag{2.36}$$

  From expression (2.36), the cell capacity can be viewed as a harmonic mean averaging the transmission rates.

- **Mean Throughput per User**

  Regarding the fair time slot allocation between active users, the variation of the number of active users in the cell is assimilated to the number of customers in a processor sharing queue with load ρ. Hence, the mean flow throughput of a user at a distance r from its serving BS that we denote φ is given by [58]:

  $$\varphi(r) = R(r)(1-\rho). \tag{2.37}$$

  From this expression we can see that the maximum mean flow throughput of a user is the theoretical transmission rate given by the Shannon formula $R(r)$ which is achieved when the cell load is tending to 0.

- **Average Number of Active Users**

  The key property of the processing sharing queue is the fact that the stationary distribution of the number of customers is insensitive to the distribution of service times and is given by [14]:

  $$\pi(k) = \rho^k(1-\rho). \tag{2.38}$$

  The mean number of active users denoted $\bar{K}$ is hence given by:

  $$\bar{K} = \frac{\rho}{1-\rho}. \tag{2.39}$$

  It can be noticed that even for high loaded cell the mean number of active users remains small, namely if the cell load is $\rho = 0.8$ the mean number of active users is only 4.

As it can be seen, by considering a time sharing scheduling, the cell capacity, the mean throughput number as well as the mean number of active users are independent on the flow size distribution.

2.6 Dimensioning of Multicellular Networks

The previously mentioned performance metrics are very important parameters when leading a dimensioning study. As already stated, the two major stages of a dimensioning study are the coverage study and the traffic analysis. These two research axes where deeply investigated in the literature, we will present some of the works done in these areas.

2.6.1 Coverage Study

The outage probability is a crucial metric for both coverage and capacity studies. In terms of coverage, mobile stations should be able to decode common control channels (like pilots or broadcast channels) and thus to attain a certain SINR threshold on these channels

with high probability. In this case, we are interested in the low SINR region of the SINR distribution to evaluate the cell coverage. In terms of capacity and for systems implementing link adaptation on shared downlink channels (such as HSPA or LTE), the whole SINR distribution is needed for performance evaluation. The ergodic capacity at a certain distance from the base station is indeed evaluated as an expectation of the Shannon classical formula over the channel variations. The cell capacity is obtained by integration over the cell area.

Many works were devoted to the coverage study of cellular systems. In [22, 23, 24], coverage studies were performed based on the outage probability. In [22], the authors considered a CDMA system with log-normal attenuation model, they proved that the soft handoff improves the cell coverage by a factor of 2 to 2.5. In [23], the authors considered shadowed-Rician/shadowed-Nakagami fading environments. In [24], only path-loss and shadowing were considered while studying the impact of the transmitting power reduction on coverage. It was proven that it is possible to drastically reduce the transmit power without any major loss in the QoS.

2.6.2 Traffic Study

The traffic analysis is the second stage of a dimensioning study after the coverage study. In the literature, the traffic analysis has been based either on simulations or on the Markov chain theory. Many studies have been led following the second approach. In [14], Bonald and Proutière conducted a dynamic traffic study, first for a single cell then for a multicell system considering only path-loss effect. The authors studied the performance of the two systems, assuming a uniform traffic demand in the cell and a Poisson distribution data flows arrival, considering different admission control criteria and different scheduling strategies. It was observed that multicell interference degrades considerably the capacity of the cell. It was also shown that considering a fair scheduling algorithm (Round Robin, proportional fair) or an opportunistic scheduling does not considerably improve the system performance compared to what can be observed in a static study. The authors considered two admission control schemes: the first one is based on the maximum number of active users and hence independent on users locations contrarily to the second scheme that is based on the minimum data rate. For a fixed blocking rate less than 10%, it was shown that both schemes are equivalent in terms of cell capacity. We based our dynamic study presented in Chapter 9 on this analysis.

In [15], Borst studied the performance of the proportional fair scheduling considering a dynamic system with random finite-size service demands. Assuming K classes of users where each class is characterized by an arrival rate λ_k, if the fluctuation in the feasible rates of the users are statistically identical, it was shown that the user-level performance may be evaluated by means of a multi-class Processor-Sharing (PS) model. This assumption is roughly valid when the users feasible rates are linear functions of the SNR. However in case of an asymmetric scenario where the users statistical rates fluctuations are different, the PS approach is no more valid. The system performance were evaluated in terms of mean

transfer delay and mean number of active users.

In [31], the authors considers the performance of a multicellular dynamic CDMA system handling two types of services: voice and data. The blocking probability, the dropping probability corresponding to each service and the mean throughput of the cell were calculated by subdividing the cell into concentric rings and characterizing each ring by its arrival rate. Different prioritization strategies between the two services are compared in terms of overall dropping probability and in terms of voice blocking probability. It is shown that prioritizing the service requiring the lower effective bandwidth (a notion introduced in [31] depending on the mobile position and on the SIR required for the service) permits to achieve a low dropping probability at an acceptable blocking rate for voice calls.

In [59], the authors proposes a two stages dimensioning methodology for an OFDMA network. In the coverage study, authors presented a semi-analytical approximation of the spatial SINR distribution based on a fitting of the simulated SINR distribution. This distribution is used to calculate the MCS probabilities. The second stage is traffic analysis taking as inputs the latter probabilities and through Markovian approach, provides dimensioning parameters as the average throughput per user, the average number of active users and the average duration of a transfer. This two stages study is performed considering different scheduling schemes and mixed traffic profiles.

2.7 Conclusion

In this chapter we have presented some models for large and small scale fading. For the small scale fading, different statistical channel models were proposed to capture the characteristics of a wide range of propagation environments. Many models may be suitable for the same environment, the choice of one rather than another can be motivated by the final purpose of the study. For example, for network dimensioning purpose, the use of Rayleigh channels to model the multipath fading can be sufficient. However, to accurately evaluate and compare the performance of different transmission technologies a sophisticated model such as the 3GPP MIMO channel is more suitable. Concerning large scale fading, we presented, amongst others, the models that will be used in this thesis: for the path-loss, a simplified commonly used model for outdoor environments and the COST 231 [39] for an indoor office environment, for the shadowing, the widely used log-normal model.

We also introduced the most relevant performance metrics in a static and in a dynamic system. The static system performance indicators are the pillars of the coverage study which purpose is to provide the best radio coverage while ensuring the required QoS. The dynamic system performance metrics are obtained using as inputs the coverage study outputs as well as a model for the traffic and are exploited as dimensioning parameters. Furthermore, we gave an overview on examples of studies proposed in the literature considering either a dynamic system or a static one.

In the present thesis, we first consider a static study of different systems. We provide outage probability or equivalently SINR CDF expressions considering different channel models and transmission schemes. We, then, propose an example of application of the derived SINR distributions to a dynamic study. We hence span the two stages of the dimensioning process namely the coverage study and the dynamic traffic analysis.

Chapter 3

Overview of MIMO and CoMP Schemes

3.1 Introduction

Due to the growing demand of higher data rates and the scarcity of the frequency spectrum, telecommunication actors have considered the MIMO technique as an ultimate solution. The capability of MIMO systems were first brought to light from a physical layer perspective, they were proven to achieve impressive gains in terms of capacity and reliability in particular in a point-to-point communication. In a multicellular context, the gains promised are hardly as considerable as that because of inter-cell interference. The cell-edge users are the most concerned by this performance loss.

Certainly, the peak data rate have a crucial importance from a marketing point of view, however, the end user average throughput is all the more important. This implies the need to find solutions to increase the cell-edge user throughput instead of addressing peak rates. In this context, a new transmission method termed CoMP by the 3GPP standardization body have been proposed as a key performance technique for the LTE-Advanced standard. In the literature many other terminologies were given to this technique like Multicell Processing (MCP), Multicell MIMO, Network MIMO or Distributed Antenna Systems (DAS). The idea behind the multicell cooperation is that instead of trying to mitigate multicell interference it is transformed to a useful signal or at least to non harmful signal. This technique was shown to improve the cell-edge user throughput.

In the first part of this chapter, we will present an overview of MIMO systems. We will introduce the different gains provided by this technique in a point-to-point communication and a multiuser context. We will propose some transmission schemes permitting to take advantage of MIMO systems gains. Then, we will explain the implementation of MIMO systems in the current standards. In the second part of this chapter, we introduce the CoMP transmission technique. We first present two main coordination strategies that

have been proposed for the LTE-A standard: the beamforming coordination (CB/S-CoMP) and the joint processing coordination (JP-CoMP). Then, we will introduce some selection algorithms for the BS (eNode-B in the LTE-A terminology) to cooperate, we will present the overheads that can be generated by this technique in terms of signaling and backhaul load, and speak about the solutions proposed in the literature to mitigate these overheads. Before concluding, we will focus on the joint precoding by going through some existing works in this area.

3.2 MIMO Systems

A pioneering work of Foschini [60] and Telatar [51] highlighted the performance gains promised by MIMO systems in reliability improvement as well as in capacity enhancement. In what follows we will distinguish two MIMO systems: point-to-point MIMO communication and multiuser MIMO communication and discuss the performance gains in each system. Before explaining the promised MIMO gains in these two systems we will first present a primordial notion conditioning the achievement of these gains which is the Channel State Information (CSI). Indeed, MIMO gains are obtained under the condition of the availability of CSI at the receiver (CSIR) and/or CSI at the transmitter (CSIT).

- **CSIR**
  Typically, obtaining the CSIR may be straightforward since it can be measured through the channel estimation via the transmission of pilots. The CSIR is an indispensable condition to achieve almost all MIMO gains.

- **CSIT**
  Unlike the CSIR, the CSIT is somewhat tricky to obtain especially in frequency division duplex (FDD) systems. In this case, the CSI is sent to the receiver via feedback signaling which can be constrained by a limited capacity and a high delay. However, in time division duplex (TDD) systems, CSIT is much easier to obtain since it relies on the uplink-downlink channel reciprocity assumption which is an idealist hypothesis. In reality, in cellular systems the reciprocity may be imperfect, which alters the quality of the CSIT.

3.2.1 Single User MIMO Communication Systems

3.2.1.1 Point-to-Point Communication

Consider an $M \times N$ point-to-point narrowband MIMO communication system. The signal at the receiver end $\mathbf{y}$ can be written as:

$$\underbrace{\begin{bmatrix} y_1 \\ . \\ . \\ . \\ y_N \end{bmatrix}}_{\mathbf{y}} = \sqrt{P} \underbrace{\begin{bmatrix} h_{1,1} & h_{1,2} & . & . & h_{1,N} \\ & & . & & \\ & & & . & \\ & & & & \\ h_{M,1} & h_{M,2} & . & . & h_{M,N} \end{bmatrix}}_{\mathbf{H}} \underbrace{\begin{bmatrix} x_1 \\ . \\ . \\ . \\ x_M \end{bmatrix}}_{\mathbf{x}} + \underbrace{\begin{bmatrix} n_1 \\ . \\ . \\ . \\ n_M \end{bmatrix}}_{\mathbf{n}}, \tag{3.1}$$

where $\mathbf{y} \in \mathbb{C}^{N\times 1}$ is the received signal, $\mathbf{x} \in \mathbb{C}^{M\times 1}$ is the transmitted symbol vector, $\mathbf{n} \in \mathbb{C}^{N\times 1}$ is the additive white Gaussian noise (AWGN) and P is received power including the path-loss and lognormal shadowing effect. When there is no CSIT, the total transmit power is equally shared between the transmit antennas, P is in this case given by:

$$P = \frac{P_t}{M} A d^{-\eta} 10^{\frac{\xi}{10}}, \tag{3.2}$$

where P_t is the total transmit power, A and η are respectively the path-loss constant and exponent and ξ is a zero mean normal random variable with variance σ.

MIMO systems have been proven to improve link performance through spatial diversity that permits a more reliable communication and spatial multiplexing which allows higher transmission rates.

3.2.1.2 Spatial Diversity Gain

Assuming sufficiently spaced transmit and receive antennas, a single symbol x_i experiences independent fadings. The different and independently faded replicas of the same signal allow for a more reliable detection reducing thus the error probability. A result from the information theory shows that the maximum diversity order of an N by M MIMO channel is $d = N \times M$ corresponding to the total number of independent fading gains [2]. Hence, increasing the number of transmit or receive antennas results in a considerable increase in the channel diversity order.

Extracting diversity gain without channel knowledge in the transmitter is possible using suitably designed coding schemes known as space time coding. The maximum achievable diversity gain d of a coding scheme is the diversity order of the channel, it is the negative slope of the bit error probability when plotted in a log-log scale versus SNR so that at high SNR, the bit error probability can be written as:

$$P_e \sim \frac{1}{SNR^d}. \tag{3.3}$$

3.2.1.3 Spatial Multiplexing Gain

Assuming the independence between transmit-receive antenna channel gains, a full rank of the MIMO channel matrix allows the creation of a maximum number of parallel spatial channels. The transmission of independent data streams through these parallel channels offers a linear increase in data rates. For an N by M MIMO channel, at high SNR, the ergodic capacity of the MIMO channel scales like [60]:

$$C(SNR) \sim \min(M, N) \log_2(SNR). \tag{3.4}$$

The spatial multiplexing gain is $\min\{M, N\}$ [60], it is also the number of degrees of freedom of the MIMO channel. The multiplexing gain hence represents the linear increasing slope of the MIMO channel capacity in the high SNR region. This gain is obtained without the need of additional power consumption. The achievement of this maximum multiplexing gain is conditioned by the channel information knowledge at the receiver side. A transmission scheme can achieve a multiplexing gain $r \leq \min\{M, N\}$.

3.2.1.4 Diversity Multiplexing Gain Tradeoff

There is a tradeoff between the maximum data rate transmission and the expected reliability. In fact, it was observed that, while achieving the full diversity gain, a MIMO scheme reduces the achievable multiplexing gain. A scheme achieves a diversity order $d^*(r)$ and a multiplexing gain r if [61]:

$$-\lim_{SNR\to\infty} \frac{\log(P_e(r\log_2(SNR)))}{\log(SNR)} = d^*(r). \tag{3.5}$$

In [2], D. Tse proposed a tradeoff formula describing the relation between both gains. For an N by M MIMO system the optimal tradeoff curve is obtained by a piece-wise linear function connecting the points $(r, d^*(r))$ for $r = 1...\min\{M, N\}$ (figure 3.1) where $d^*(r)$ is given by [2]:

$$d^*(r) = (M - r) \times (N - r). \tag{3.6}$$

3.2.1.5 Space-Time Block Coding (STBC)

The terminology space-time coding comes from the fact that, in MIMO systems, coding is performed over space (multiple antennas) and time (channel use period). Many space-time block codes were proposed in the literature to achieve full diversity as the Alamouti code [62] or the DAST [63], maximum multiplexing gain namely the V-BLAST code [64] or an optimal diversity multiplexing tradeoff as the Golden code [65]. Space-time codes are subject to some algebraic design criteria [61]. For instance, a Space-Time Block Code (STBC) achieves full diversity if the determinant of the difference between two distinct

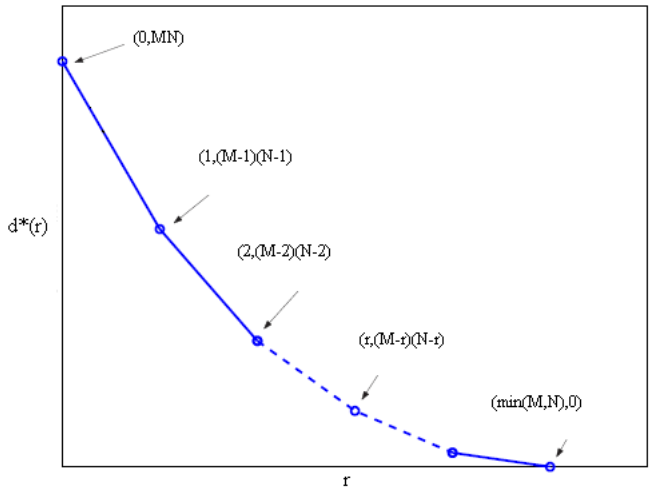

Figure 3.1: Piece-wise diversity-multiplexing tradeoff curve [2].

codewords matrices is nonzero. Typically, Orthogonal STBCs (OSTBC) constructed as that any pair of columns vectors taken from the coding matrix are orthogonal, achieve the maximal diversity gain.

When perfect CSI is available at the receiver side (coherent communication), the optimal decoder for space-time codes is the maximum likelihood algorithm. In particular, for OSTBC, the maximum likelihood detection reduces to a linear detection. However, for large number of antennas and high data rates, the maximum likelihood becomes too complex to use. The sphere decoder [66] was proposed as an alternative and was proven to engender much lower complexity and to have almost the same performance as the maximum likelihood algorithm.

3.2.2 Multiuser MIMO Communication Systems

Multiuser MIMO communication systems have arisen researchers interest. In fact, the spatial degrees of freedom of MIMO channels combined with multiuser multiplexing schemes can enhance considerably the system capacity.

3.2.2.1 Single Cell Multiuser MIMO System Model

Consider a single cell multiuser (K users) MIMO communication scenario. Each user k is equipped with N antennas. In a downlink communication (broadcast channel communica-

tion), the signal received at a user k can be written as:

$$\mathbf{y}_k = \sqrt{P_k}\mathbf{H}_k\mathbf{x}_k + \sum_{j=1, j\neq k}^{K} \sqrt{P_k}\mathbf{H}_k\mathbf{x}_j, \tag{3.7}$$

where $\sqrt{P}_k$ is the power received by the user k from the BS, $\mathbf{x}_k \in \mathbb{C}^{N\times 1}$ and $\mathbf{H}_k \in \mathbb{C}^{N\times M}$ is the channel between the user k and the BS. $\mathbf{y}_k$ can also be written as:

$$\mathbf{y}_k = \sqrt{P_k}\mathbf{H}_k\mathbf{x}, \tag{3.8}$$

where

$$\mathbf{x} = \sum_{j=1}^{K} \mathbf{x}_j. \tag{3.9}$$

$\mathbf{x}$ satisfies:

$$\mathrm{E}[\mathbf{x}\mathbf{x}^*] \leq P_t, \tag{3.10}$$

where P_t is the maximal transmit power of the BS.

Consider, now, the uplink communication (multiple access channel communication). The signal received at the BS from all users is given by:

$$\mathbf{y} = \sum_{k=1}^{K} \sqrt{P_k}\mathbf{H}_k^*\mathbf{x}_k. \tag{3.11}$$

The users are subject to a transmit power constraint given by:

$$\mathrm{E}[\mathbf{x}_k\mathbf{x}_k^*] \leq P_{kt}, \quad k = 1..K, \tag{3.12}$$

where P_{kt} is the maximum transmit power of the user equipment.

3.2.2.2 Multiuser Diversity

The multiuser diversity is the smart selection of users to serve at a given channel resource regarding their channel conditions. To obtain a multiuser diversity gain, instead of looking for fading mitigation, the system takes advantage of the channel variation in time to select users with good instantaneous channel conditions.

Assuming balanced users average SNR, it is known that the best user achieves an SNR $\log K$ higher than the average SNR received by all users [53]. This SNR gain is referred to as the multiuser diversity gain. It, asymptotically, enhances the sum-rate capacity of a multiuser system by a factor of $\log\log K$.

In a MU-MIMO system, the user scheduling can be combined with Space Division Multiple Access (SDMA) schemes to take advantage of both multiuser diversity gain and spatial multiplexing gain equal to $\min\{M, KN\}$. Typically the Time Division Multiple

Access (TDMA) scheme achieves a multiuser diversity gain $\log K$ but a multiplexing gain 1, while the Dirty Paper Coding (DPC) [67] achieves the same multiuser diversity gain and the full multiplexing gain M when $K > M$ regardless of N.

Many other transmission schemes (combination of beamforming and multiuser scheduling) were shown to achieve the optimal multiuser diversity and multiplexing gains [53, 68].

3.2.2.3 User Scheduling

Scheduling is the way of distributing the available resources between active users. The user or the set of users to be served with a given resource can be chosen randomly or can be subject to a specific criterion. For example, resources may be allocated periodically to each user. This is the Round-Robin scheduling [69], an obvious user selection approach when no CSIT is available. However, Round-Robin scheduling (RRS) does not provide any multiuser diversity gain since the multiuser system reduces, in this case, to a single user system. As already stated, to exploit multiuser diversity, the BS should distribute its resources based on the quality of the channel experienced by each user. In this case, the issue of fairness among users should be addressed. The RRS is the simplest form of a fair scheduling however it does not permit to benefit from multiuser diversity. On the other side, opportunistic scheduling [70] has no fairness but fully exploits multiuser diversity. The proportional fair [71] scheduling meets fairness while providing multiuser diversity gain. It consists in a simple algorithm assigning the channel resource to the user with the maximum throughput divided by its average past throughput.

3.2.2.4 Transmission Schemes

In a multiuser communication, interference is the key performance limiting factor since it ultimately limits the system capacity. To mitigate multiuser interference, scheduling is generally combined with additional pre-transmit signal processing techniques. In this context, many precoding techniques were proposed in the literature. Among them we can mention:

- **Dirty Paper Coding (DPC):** The DPC was proposed for the first time by [67] as a non linear multiuser precoding technique and was proven to achieve the entire capacity region of the MIMO broadcast channel [72] (see Section 2.4.4). Practically, DPC exploits the knowledge of multiuser interference in a broadcast channel to pre-substract this interference before broadcasting so that at the receiver end a user k only sees interference for users $\{k+1, ..., K\}$. Despite its optimal performance, the high implementation complexity of the DPC makes it almost impossible to use in practice. For this reason, suboptimal precoding techniques arouse more researchers interest.
- **Zero Forcing Beamforming (ZFBF):** It is a linear transmission strategy allowing a multiuser transmission without generating multiuser interference. Such beamforming

is possible when the number of BS transmit antennas M verifies $M \geq K$ (for single antenna users equipments). If the number of active users is higher than the number of transmit antennas, a user selection algorithm can be used to schedule $K^{'} \leq M$ users among the K active users so that the beamforming becomes possible. A simple precoding matrix for ZFBF can be given by the Moore-Penrose pseudo inverse of the channel matrix and is given as:

$$\mathbf{W} = \mathbf{H}^T(\mathbf{H}\mathbf{H}^T)^{-1}, \tag{3.13}$$

$\mathbf{H} \in \mathbb{C}^{K^{'} \times M}$ is the channel matrix between the $K^{'}$ users and the M antennas of the serving BS.

ZFBF is a suboptimal SDMA scheme that eliminates multiuser interference and presents the advantage of implementation simplicity. However, it was shown in [53], that the ZFBF combined with an appropriate scheduling approaches the sum-capacity achieved by the DPC when the number of users is very large. The ZFBF will be introduce with more details in Section 7.2.

- **Minimum Mean Square Error Beamforming (MMSE BF):** The MMSE BF is designed to minimize the error between the received and the transmitted signal caused by both interference and noise distortions. When the M antennas BS serves $K \leq M$ single antenna users, the MMSE precoding matrix is given by:

$$\mathbf{W} = \mathbf{H}^T(\mathbf{I} + \alpha\mathbf{H}\mathbf{H}^T)^{-1}, \tag{3.14}$$

where α is a regularization factor which is introduced to improve the performance of the ZFBF for rank-deficient or ill-conditioned matrix $\mathbf{H}$. However, it introduces a *crosstalk* multiuser interference. An optimal value of α can be determined by maximizing the SINR at each receiver as proposed in [73]. In this case $\alpha = \frac{M\sigma_n^2}{P}$.

The performance of MMSE BF is significantly better at low SNR and converges to that of ZF precoding at high SNR [74]. The ZFBF as well as MMSE BF necessitate both a perfect channel knowledge at the transmitter side and their performances are very sensitive to the quality of the CSIT. However, in large-user MIMO broadcast channels, it is quite hard to obtain perfect instantaneous CSI (especially for FDD systems). In this context random beamforming was proposed by [75].

- **Random Beamforming:** It consists in generating random beams so that the precoding matrix verifies:

$$\mathbf{W}\mathbf{W}^H = \mathbf{I}. \tag{3.15}$$

Each user calculates the SINR corresponding to each beam and feeds back the maximum SINR to the BS along with the corresponding beam index. Based on this information, the BS performs scheduling by mapping each user to the beam maximizing its SINR. This beamforming only requires low rate partial CSI at the transmitter

but has been proven to achieve poor sum-rate in the high SNR region due to multiuser interference [76].

- **Codebook Beamforming:** Always with the perspective of reducing the amount of feedback rates, the codebook beamforming was proposed as a limited feedback approach. It consists in using a beamformer from a set of N vectors called codebook where $N = 2^B$, B being the number of quantification bits. This codebook is available at both the receiver and the transmitter. The receiver provided with a perfect channel knowledge calculates the SINR using each beam. The index and the value of the highest SINR are then fed back to the BS that uses this information to generate the precoding matrix maximizing for example the sum-rate [77, 78].

3.2.3 Multi Cell MIMO Communication Systems

3.2.3.1 Multicellular Single User MIMO System Model

Consider a multicellular communication scenario (B BSs), where each BS i is equipped with M transmit antennas (figure 3.2), the users equipments with N antenna. The signal received at the user k served by a BS b can be written as:

$$\mathbf{y}_k = \sqrt{P_{b,k}}\mathbf{H}_{b,k}\mathbf{x}_k + \sum_{i=1,i\neq b}^{B} \sqrt{P_{i,k}}\mathbf{H}_{i,k}\mathbf{x}_i + \mathbf{n}_k, \tag{3.16}$$

where $\sqrt{P_{i,k}}$ is the power received by the user served by BS i, $\mathbf{H}_{i,k} \in \mathbb{C}^{N\times M}$ is the channel matrix between user k and BS i, $\mathbf{x}_i \in \mathbb{C}^{M\times 1}$ is the symbols vector transmitted to user i and $\mathbf{n}_k \in \mathbb{C}^{N\times 1}$ is the AWGN. The term $\sqrt{P_{b,k}}\mathbf{H}_{b,k}\mathbf{x}_k$ is the useful signal received by user k from its serving BS and the term $\sum_{i=1,i\neq b}^{B} \sqrt{P_{i,k}}\mathbf{H}_{i,k}\mathbf{x}_i$ is the multicell interference power received by user k from the surrounding BSs.

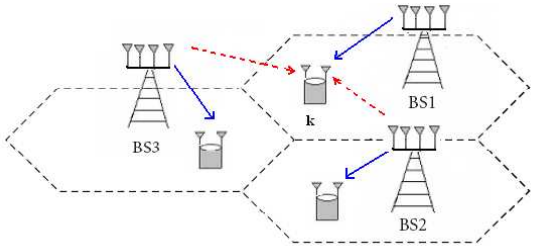

Figure 3.2: Multicellular single user MIMO communication system.

3.2.3.2 Multicell Multiuser MIMO System Model

Consider now a multicellular system (B BSs), where each BS serves K users simultaneously. Each user i is equipped with N antennas and each BS j with M antennas. In a downlink multiuser communication (broadcast communication), at a user k served by the BS b, the signal can be written as:

$$\mathbf{y}_k = \underbrace{\sqrt{P_{b,k}}\mathbf{H}_{b,k}\mathbf{x}_{b,k}}_{useful\ signal} + \underbrace{\sqrt{P_{b,k}}\mathbf{H}_{b,k}\sum_{j=1,j\neq k}^{K}\mathbf{x}_{b,j}}_{multiuser\ interference\ signal} + \underbrace{\sum_{i=1,i\neq b}^{B}\sqrt{P_{i,k}}\mathbf{H}_{i,k}\sum_{j=1}^{K}\mathbf{x}_{i,j}}_{multicell\ interference\ signal}, \tag{3.17}$$

where $\sqrt{P_{i,j}}$ is the power received by user k from BS i, $\mathbf{H}_{i,j} \in \mathbb{C}^{N\times M}$ is the channel between BS i and user j and $\mathbf{x}_{i,j} \in \mathbb{C}^{M\times 1}$ is the data information vector transmitted from BS i intended to user j. Assuming a same maximum transmit power for all BSs, the power constraint can be written as:

$$\mathrm{E}[\sum_{j=1}^{K}\mathbf{x}_j\mathbf{x}_j^*] \leq P_t, \quad k = 1..K. \tag{3.18}$$

As can be noticed, a multicell multiuser system suffers from the harmful effects of both multiuser interference and multicell interference. Some beamforming techniques such as the ZFBF can be used to mitigate multiuser interference. BS cooperation is a possible solution to combat multicell interference.

3.2.4 MIMO Systems in the Standards

The first commercial realization of MIMO was in wireless LAN in the IEEE 802.11n standard since it is easier to incorporate multiple antennas in laptops and PCs than in a mobile phone. The IEEE 802.11n support up to 4×4 MIMO systems promising hence a peak data rate of up to 600 Mbps in a bandwidth of 40 MHz.

The 3GPP introduced the multiple antennas transmission technique for the first time in the UMTS standard (Release 99). Two transmission diversity schemes are available in the downlink of a 2×1 MISO system: the open loop that does not require CSIT and the closed loop necessitating the feedback of CSI. For the open loop transmission, two diversity schemes are possible: the Space Time Transmit Diversity (STTD) implemented using the Alamouti code and the TSTD (Time Switched Transmit Diversity) where the transmission is alternated between the two antennas. As for the open loop transmission, two modes are possible for the closed loop one. The *mode 1* that is also called the Transmit Antenna Array (TxAA) permitting only a phase adjustment at the transmitter. The *mode 2* permits a phase and amplitude adaptation. Release 99 supports also three types of beamforming techniques. Although included in the UMTS standard, MIMO diversity and beamforming techniques are unexploited in practice.

MIMO gains have been verily exploited in the HSPA+ standard (Release 7) through the Double-TxAA (D-TxAA). It allows the transmission of two independent data streams permitting hence higher data rates (up to 42 Mbps when used jointly with 64-QAM). Four unitary precoding matrices are available at the transmitter. The choice of a precoding matrix is based on the information reported by the UE consisting in the Precoding Control Indication (PCI) and permitting to generate the matrix allowing an optimized decoding.

The LTE, introduced in 3GPP Release 8, uses the MIMO-OFDM technique and supports peak data rates of up to 300 Mbps in 4×4 MIMO systems and up to 150 Mbps in the downlink of a 2×2 MIMO systems and up to 75 Mbps in the uplink. The MIMO Transmission Modes (TM) available in the LTE are:

- **TM1**: In this case the transmitter uses only one antenna. If the receiver uses one antenna it reduces to a SISO system, the receiver can use multiple antennas for diversity.

- **TM2**: It is the transmission diversity mode, it uses two or four antennas. For the two antennas case, a frequency Alamouti code is performed, for the four antennas case, the same code is applied for each antenna pair.

- **TM3**: It is an open loop spatial multiplexing scheme, a maximum of two code words can be transmitted simultaneously. Having no information from the receiver, the transmitter uses either the identity matrix as a precoding matrix for the two transmit antennas case or 4 predefined precoding matrix in an alternative manner.

- **TM4**: It is a closed loop spatial multiplexing scheme. It consists in transmitting one or two code words using a precoding matrix chosen from a codebook of 3 matrices (two transmit antennas case) or 16 matrices (four transmit antennas case) based on the information fed back by the receiver. This transmission mode is suitable for users with low mobility.

- **TM5**: In this case, the code words are transmitted to two different users. It is called the MU-MIMO. It is performed for users sufficiently separated in space so that the transmitter can form beams to transmit data simultaneously to the two users without generating much interference.

- **TM6**: It is the rank one closed loop beamforming and is a special case of the TM5. In this case the transmitter sends only one code word using a rank one precoding matrix that is chosen based on the reported information from the UE.

- **TM7**: It is a beamforming mode, where the transmitter does not have any precoding related information. It can deduce this information using, for example, the Direction Of Arrival (DOA) estimations from the uplink. The eNode-B transmits a single code word to the intended user.

All the transmission modes previously presented are designed for the downlink. For the uplink, the MU-MIMO technique is standardized, the eNode-B can ask for a simultaneous transmission from multiple users. Each user transmits using a single antenna, the eNode-B receives the signal using its multiple antennas. If the UE has two antennas, the antenna selection transmission can be performed. In this case, the user transmits its data alternatively from each antenna. To select the suitable antenna it uses an information sent from the eNode-B based on the channel quality.

3.3 CoMP Transmission

3.3.1 CoMP Strategies

As already stated, the 3GPP is now laying the foundation of the LTE-A standard. The CoMP is a serious candidate technique to be part of this standard. Two CoMP strategies are under study: the Coordinated Beamforming/Scheduling (CB/S) scheme and the Joint Processing (JP) scheme.

3.3.1.1 Coordinated Beamforming/Scheduling

In the CB/S-CoMP strategy, the network is subdivided into clusters of cells. In each cluster there is a master cell, the other cells are considered as slave cells. A user in the master cell is served by only one base station while the others BSs schedule their users so as to generate the least interference possible. This can be either by completely silencing slave cells while the master cell BS transmits to its user (coordinated scheduling) or by performing beamforming in slave cells avoiding to generate interference to the master cell user (coordinated beamforming) [79]. The CB/S-CoMP does not necessitate to share users data but only scheduling signaling which is less constraining in terms of backhaul load.

3.3.1.2 Joint Processing

The JP strategy consists in sharing data, CSI and control information via the backhaul across coordinated BSs to serve users cooperatively. Instead of acting as interferers, several cells participate to provide a better signal to the user. The cooperating BSs act thus as a virtual MIMO system using distributed antennas. These BSs can perform jointly the transmission schemes initially intended to localized multiple antennas systems enhancing hence the SINR. The JP-CoMP permits thus to recover the MIMO gains loosed or reduced due to multicell interference. The JP coordination offers better performance compared to the CB/S strategy [79, 80, 81, 82] however it engenders a backhaul overhead due to the amount of data exchanged between cooperating BSs. Low latency backhaul links are required to ensure this data transit.

3.3.2 Selection Algorithms

When speaking about BSs cooperation, it is obvious that this cooperation concerns only a group of BSs (eNodes-B or access points) and not all the network. The BSs are hence grouped into *clusters*. In practice, these clusters should be composed of a limited number of BSs in order to generate affordable overheads. The selection of BSs to be part of a cluster is an issue that has recently aroused the interest of researchers. It is often called the clustering algorithm.

In the literature, we can find the disjoint clustering where each BS belongs to a unique cluster [83, 84], or the overlapping clustering where the clusters can have one or many BSs in common [85, 86]. Papers distinguish also the static clustering in which the BSs forming a cluster remain the same during time [85, 87] and the dynamic clustering where the organization into clusters of the BSs varies with time [84]. The cluster can be formed simply by the first r rings surrounding the BS with which they cooperate as described in [85], another intuitive way is to select the BSs with better channel conditions (path-loss and shadowing). The selection criterion can also be the maximization of the sum rate as in [84] where the authors proceeds to a greedy dynamic BS selection. In [86], a sphere-like-algorithm were proposed as an alternative to the greedy search in order to reduce the computation complexity. In [88] a joint precoding-BS selection algorithm was proposed with the objective of transmit power minimization for a target SINR.

3.3.3 CSI Feedback and Backhaul Load

Whether we are considering the CB/S-CoMP or the JP-CoMP, the cooperating BSs need CSI or scheduling information to jointly schedule or serve one or several users. This information is fed back by the UE (in a FDD context) to the BSs of its serving cluster. The feedback overhead is all the more important when the cluster is large. Therefore a natural way for mitigating these overheads is to limit the number of cooperating BSs per cluster. It is obvious that using limited static clustering reduces considerably the feedback overhead [85, 89, 87] while offering limited gains. Thus, there is a tradeoff between performance and overheads. In this context, a dynamic clustering algorithm was proposed in [84, 90] ensuring better performance than the static clustering with limited overhead increase.

Depending on the CoMP strategy considered, the backhaul load can be more or less important. In fact, as already stated, in CB/S-CoMP, the cooperating BSs need only to share users CSI information and synchronization signaling, generating hence a limited backhaul burden. On the contrary, in the JP-CoMP, the cooperating BSs not only share CSI and synchronization signaling but also data streams intended to the scheduled users, which engender a considerable backhaul burden. Ensuring a reliable exchange of this amount of information requires low latency backhaul links of higher capacity, which implies also higher deployment costs.

To make possible the practical deployment of the CoMP, it was compulsory to propose

methods permitting to reduce backhaul overhead. In [91], the authors propose to deal with this issue either by exchanging pre-processed and quantized signal values, or uncoded binary data of jointly pre-processed users. The two methods have limited backhaul requirement while ensuring good performance.

Inspired from the scheduling methods used for conventional cellular networks (without multicell cooperation) [92, 93], the authors in [94] propose a selection criterion for users to have access to feedback resources used jointly with BSs clustering algorithms. The proposed algorithm allows hence to relieve at the same time the feedback overhead and the backhaul load while offering good performance.

3.3.4 Joint Precoding Techniques

All the transmission schemes initially proposed for localized MIMO can be used for distributed antenna in a cooperation context. Generally, these schemes require full CSIT at the cooperating BSs which is not always possible in practice because of the backhaul imperfectness (limited capacity, high delay,...). In the literature, some works consider the idealistic assumption of perfect CSIT while others consider more realistic systems with partial or imperfect CSIT.

3.3.4.1 Full CSIT

Assuming an extreme case of cooperation where all BSs have perfect CSIT of all users, the multicell cooperation system reduces hence to a classical broadcast channel, where the DPC was proven to be the optimal strategy to maximize the multicell throughput [95, 96]. The complex implementation of the DPC motivates the exploration of more practical cooperative precoding schemes even if sub-optimal compared to the DPC. Among these schemes we can mention the joint processing zero forcing (JP-ZF). It totally eliminates interference between users and permits to asymptotically (for large number of users) approach the upper bound performance of the DPC when performed jointly with a suitable user scheduling algorithm [97]. The JP-MMSE and the JP null space decomposition (JP-decomp) described in [98] was proven to outperform the JP-ZF. The JP-MMSE offers sharply better performance in the low SNR region and converges to the JP-ZF one at high SNR [98]. The JP-decomp outperforms the JP-ZF and the JP-MMSE for all SNR values.

Now, since the assumption of a global network cooperation is practically impossible, in [99, 100, 101] the authors consider more practical cases where the cooperation BSs are grouped into clusters reducing hence the feedback overhead.

3.3.4.2 Partial CSIT

To relieve the backhaul burden caused by the cooperation process, some cooperation schemes have been proposed considering a partial CSIT knowledge. In this case, there is no need of CSIT exchange between BSs, only a local CSIT knowledge is assumed. In [102], the

authors proposed a multicell ZF beamforming using the data information of all users and a local CSIT. It was shown that, even with partial CSIT the cooperation scheme offers a sufficient reliability to the users. In [103], under the same assumption of partial CSIT, a distributed suboptimal precoder design is proposed ensuring efficient transmission with reasonable backhaul overhead.

3.3.4.3 Imperfect CSIT

The issue of CSIT imperfectness have been well addressed in the literature. Many studies investigate the influence of this imperfectness on the multicell schemes performance. Some cooperation methods are proposed to get around this impairment. In [104], it is assumed that the imperfectness of the CSIT can occur when each cooperating BS decodes independently the CSI or when only one BS decodes it and forwards subquantized versions of it to neighboring bases. In the first case, depending on the feedback channel quality, the decoded information may be different. A multicell team decision precoding scheme is proposed offering the possibility to tolerate the imperfect CSIT and hence to reduce communication requirements, at the expense of performance reduction. In [105], the model proposed assumes that each user feeds back quantized CSI of the desired and interfering channels to its BS that shares this information with the neighboring BSs. An upper bound for the mean loss in sum-rate due to CSI quantization is proposed and shown to be reasonably tight.

3.4 Conclusion

MIMO systems offered a new spatial dimension to wireless communication. This new dimension can be used either to improve communication reliability by providing diversity, or to enhance system capacity owning to the multiplexing gain or even to serve multiple users simultaneously. In this case, when a smart selection of the users to be served in a given time period is performed, MIMO systems offer the multiuser diversity gain enhancing thus the users achievable sum-rate.

In a multicellular context, in presence of intercell interference, the gains promised by the MIMO system over the SISO system shrinks considerably [106]. Traditional MIMO schemes are not sufficient in this case. The CoMP transmission strategies has been proposed as a solution improving capacities especially for cell-edge users. However, this promising technique is constrained by some implementation limitations since the requirements in terms of CSI cause additional overheads that may be unaffordable. The difficulties to provide perfect CSI is all the more important in a context of high mobility where the channel information arriving to the eNode-B may be outdated. Quantization or statistical CSI are hence preferable in practice. The challenging issue is to use the available partial information while achieving a major part of the promised gains.

Chapter 4

Outage Probability of Multicellular SISO Systems

4.1 Introduction

In this chapter, we are interested in characterizing the outage probability on the downlink of a SISO cellular network. Our goal is here to introduce the main mathematical tools used throughout the thesis and to provide a benchmark system for the following chapters.

Many works were devoted to the calculation of the outage probability in cellular networks, however few works considered the joint impact of path-loss, shadowing and fast fading due to the difficulty of the task. There are two classical assumptions: (1) considering only the shadowing effect, (2) considering both shadowing and fast fading effects. In the former case, authors mainly face the problem of expressing the distribution of the sum of log-normally random variables; several classical methods can be applied to solve this issue (see e.g. [3] [4]). In the latter case, formulas usually consist in many infinite integrals, which are uneasy to handle in a practical way (see e.g. [5]). In both cases, outage probability is always an explicit function of all distances from the user to interferers.

As the need for easy-to-use formulas for outage probability is clear, approximations need to be done. Working on the uplink, [107] derived the distribution function of a ratio of path-losses with shadowing, which is essential for the evaluation of external interference. For that, authors approximate the hexagonal cell with a disk of same area. Authors of [108] assume perfect power control on the uplink, while neglecting fast fading. On the downlink, Chan and Hanly [6] precisely approximate the distribution of the other-cell interference. They however provide formulas that are difficult to handle in practice and do not consider fast fading. Immovilli and Merani [43] take into account both channel effects and make several assumptions in order to obtain simplified formulas. In particular, they approximate interference by its mean value. Outage probability is however an explicit function of all distances from receiver to every interferer. In [109], Zorzi proposes a formula essentially

valid for packet radio networks rather than for cellular systems. Authors of [110] provide some interesting characterizations and upper bounds of the outage probability but neglects the slowly varying path-gains. In [111], authors consider both shadowing and fast fading but assume a single interferer.

In this chapter, we propose two methods to analyze the outage probability of mobile stations located at any distance r from their serving base station (BS). The first method, based on the Fenton-Wilkinson approach [16], approximates a sum of log-normal random variables as a log-normal random variable and approximates fast fading coefficients in interference terms by their average value. We denote it FWBM (for Fenton-Wilkinson Based Method). The second one is based on the central limit theorem for causal functions [17]. It allows to approximate a sum of positive random variables by a Gamma distribution. We denote it CLCFM (for Central Limit Theorem for Causal Functions Method). Each method allows to establish a simple and easily computable outage probability formula, which jointly takes into account path-loss, shadowing and fast fading. We compare our proposed formulas with results obtained with extensive Monte Carlo simulations in a classical hexagonal network. At last, we rely on fluid model proposed in [18] in order to express the outage probability as a simple analytical expression depending only on the distance to the serving BS. Such an expression allows further integrations much more easily than with existing formulas.

This chapter is organized as follows. FWBM is explained in Section 4.3. We derive the outage probability while considering first only path-loss and shadowing and then path-loss, shadowing and fast fading jointly. Section 4.4 develops the CLCF method. Outage probability is calculated while considering first only path-loss and fast fading and then path-loss, shadowing and fast fading jointly. The computation is based on the fluid model (Section 4.5). In Section 4.6, we validate our approach and compare analytical expressions with results obtained through Monte Carlo simulations.

All the results derived in this study were published in [112].

4.2 Interference Model

We first define the interference model assumed in this paper. We consider a hexagonal cellular network with frequency reuse one and we focus on the downlink. We are interested in evaluating the SIR at a mobile station u, served by base station BS_0 and interfered by N interfering base stations. We assume that mobile stations are attached to their closest BS.

4.2.0.4 Propagation Model

The power received by u depends on the radio channel state and varies with time due to fading effects (shadowing and fast fading). Let P_j be the transmission power of base station

j, the power $p_{j,u}$ received by u can be written as:

$$p_{j,u} = P_j C r_{j,u}^{-\eta} X_{j,u} Y_{j,u}. \tag{4.1}$$

The term $P_j C r_{j,u}^{-\eta}$, where C is a constant, represents the mean value of the received power at distance $r_{j,u}$ from the transmitter (BS_j). $X_{j,u}$ is a random variable (RV) representing the Rayleigh fading effects, whose pdf is $p_X(x) = e^{-x}$. The term $Y_{j,u} = 10^{\xi_{j,u}/10}$ is a log-normal RV characterizing shadowing. $\xi_{j,u}$ is a *Normal* distributed RV, with zero mean and standard deviation σ, which is typically between 0 and 8 dB. Parameter η, which is typically between 2.7 and 3.5, is the path-loss exponent.

4.2.0.5 SIR Calculation

The interference power received by a mobile u can be written as:

$$p_{ext,u} = \sum_{j=1}^{N} P_j C r_{j,u}^{-\eta} X_{j,u} Y_{j,u}. \tag{4.2}$$

We consider that the thermal noise is negligible (in a urban environment) and so we focus on the SIR rather than on the SINR. Considering moreover that all BSs transmit with the same power P_0, we can express the SIR expression (dropping index u and setting $r_{0,u} = r$):

$$\gamma = \frac{r^{-\eta} X_0 Y_0}{\sum_{j=1}^{N} r_j^{-\eta} X_j Y_j}. \tag{4.3}$$

4.2.0.6 Outage Probability

The outage probability is defined as the probability that the SIR at u falls below a given threshold δ. Note that while varying δ, we obtain the definition of the SIR CDF. We indifferently speak of outage probability or CDF.

$$\mathbb{P}\big(\gamma < \delta\big) = \mathbb{P}\left(\frac{r^{-\eta} X_0 Y_0}{\sum_{j=1}^{N} r_j^{-\eta} X_j Y_j} < \delta\right). \tag{4.4}$$

4.3 Fenton-Wilkinson Based Method

In this section, we propose a first method based on the Fenton-Wilkinson approximation. We first analyze the path-loss and shadowing impact. We then extend the result to the joint influence of path-loss, shadowing and fast fading based on the previous obtained result.

4.3.1 Path-Loss and Shadowing Impact

The power p_j received by u can be written in this case:

$$p_j = P_j C r_j^{-\eta} Y_j. \tag{4.5}$$

The probability density function (PDF) of this slowly varying received power is given by:

$$p_Y(s) = \frac{1}{a\sigma s\sqrt{\pi}} \exp\left[-\left(\frac{\ln(s) - am}{\sqrt{2}a\sigma}\right)^2\right], \tag{4.6}$$

where $a = \frac{\ln 10}{10}$, $m = \frac{1}{a}\ln(CP_j r_j^{-\eta})$ is the (logarithmic) received mean power expressed in decibels (dB), which is related to the path-loss and σ is the (logarithmic) standard deviation of the mean received signal due to the shadowing. The SIR at user u is now given by:

$$\gamma = \frac{r^{-\eta} Y_0}{\sum_{j=1}^{N} r_j^{-\eta} Y_j}. \tag{4.7}$$

We see that the SIR can be written $\gamma = 1/F$ with

$$F = \frac{\sum_{j=1}^{N} r_j^{-\eta} Y_j}{r^{-\eta} Y_0}. \tag{4.8}$$

The factor F is defined for any mobile u and it is thus location dependent. The numerator of this factor is a sum of log-normally distributed RVs, which can be approximated by a log-normally distributed RV [4]. The denominator of the factor is a log-normally distributed RV. F can thus be approximated by a log-normal RV. Using the Fenton-Wilkinson [16] method, we can calculate the logarithmic mean and standard deviation, m_f and s_f of F for any mobile at the distance r from its serving BS, BS_0 [113] (see Appendix A.1):

$$m_f = \frac{1}{a}\ln(f(r,\eta)H(r,\sigma)), \tag{4.9}$$

$$s_f^2 = 2(\sigma^2 - \frac{1}{a^2}\ln H(r,\sigma)), \tag{4.10}$$

where

$$H(r,\sigma) = e^{a^2\sigma^2/2}\left(G(r,\eta)(e^{a^2\sigma^2} - 1) + 1\right)^{-\frac{1}{2}}, \tag{4.11}$$

$$G(r,\eta) = \frac{\sum_j r_j^{-2\eta}}{\left(\sum_j r_j^{-\eta}\right)^2}, \tag{4.12}$$

$$f(r,\eta) = \frac{\sum_j r_j^{-\eta}}{r^{-\eta}}. \tag{4.13}$$

From equations (4.8) and (4.13), we notice that $f(r,\eta)$ represents the factor F *without shadowing*.

The outage probability is now defined as the probability for the SIR γ to be lower than a threshold value δ and can be expressed as:

$$\begin{aligned}\mathbb{P}\left(\gamma<\delta\right) &= 1-\mathbb{P}\left(\frac{1}{\delta}>F\right),\\ &= 1-\mathbb{P}\left(10\log_{10}(\frac{1}{\delta})>10\log_{10}(F)\right),\\ &= Q\left[\frac{10\log_{10}(\frac{1}{\delta})-m_f}{s_f}\right]. \end{aligned} \tag{4.14}$$

where Q is the complementary error function: $Q(u)=\frac{1}{2}erfc(\frac{u}{\sqrt{2}})$.

4.3.2 Path-Loss, Shadowing and Fast Fading Impact

In this case, the outage probability can be expressed as:

$$\mathbb{P}\big(\gamma<\delta\big)=1-\mathbb{P}\left(r^{-\eta}X_0Y_0>\delta\left(\sum_{j=1}^{N}r_j^{-\eta}X_jY_j\right)\right). \tag{4.15}$$

The interference power received by a mobile u due to fast fading effects varies with time. As a consequence, the fast fading can increase or decrease the power received by u. We consider that the increase of interfering power due to fast fading coming from some base stations are compensated by the decrease of interfering powers coming from other base stations. As a consequence, for the interfering power, only the slow fading effect has a significant impact on the SIR. We thus assume that $\forall j\neq 0,\ X_j\approx E[X_j]=1$ (this assumption will be validated by simulations in the next section), and we can write $\mathbb{P}\big(r^{-\eta}X_0Y_0>\delta(\sum_{j=1}^{N}r_j^{-\eta}X_jY_j)\big)\approx\mathbb{P}\big(r^{-\eta}X_0Y_0>\delta(\sum_{j=1}^{N}r_j^{-\eta}Y_j)\big)$.

So we have:

$$\begin{aligned}\mathbb{P}\big(\gamma<\delta\big) &= 1-\mathbb{P}\left(X_0Y_0>\delta\frac{1}{r^{-\eta}}\sum_{j=1}^{N}r_j^{-\eta}Y_j\right),\\ &= 1-\mathbb{P}\big(X_0>\delta F\big),\\ &= 1-\int_0^{\infty}\mathbb{P}\big(x>\delta F\big)p_X(x)dx,\\ &= 1-\int_0^{\infty}\mathbb{P}\big(10\log_{10}(\frac{x}{\delta})>10\log_{10}(F)\big)e^{-x}dx. \end{aligned} \tag{4.16}$$

As a consequence, the outage probability for a mobile **located at a distance r** from its serving BS, taking into account path-loss, shadowing and fast fading can be written as:

$$\mathbb{P}\big(\gamma < \delta\big) = \int_0^{\infty} Q\left[\frac{10\log_{10}(\frac{x}{\delta}) - m_f}{s_f}\right] e^{-x} dx. \tag{4.17}$$

4.4 Central Limit Theorem for Causal Functions Method

In this section, we adopt a different path for deriving the SIR CDF. We first express the outage probability by considering the path-loss and fast fading. Afterwards, we use this result in order to introduce the shadowing impact.

4.4.1 Path-Loss and Fast Fading Impact

Assuming only fast fading channel, the SIR is given by:

$$\gamma = \frac{r^{-\eta} X_0}{\sum_{j=1}^{N} r_j^{-\eta} X_j} = \frac{S}{I}, \tag{4.18}$$

where:

$$S = r^{-\eta} X_0, \qquad I = \sum_{j=1}^{N} r_j^{-\eta} X_j \tag{4.19}$$

are two independent RVs. To calculate the outage probability, we need to calculate first, the probability distribution function (PDF) $f_S(x)$ of S and the PDF $f_I(x)$ of I. The PDF of the useful power is given by [34]:

$$f_S(x) = \frac{1}{r^{-\eta}} e^{-\frac{x}{r^{-\eta}}}. \tag{4.20}$$

We now approximate the interference PDF using the central limit theorem for causal functions (see Appendix A.2) by a Gamma distribution given by:

$$f_I(y) = \frac{y^{\nu-1}}{\Gamma(\nu)\lambda^{\nu}} e^{-\frac{y}{\lambda}}, \tag{4.21}$$

where $\nu = \frac{\mathrm{E}[I]^2}{\mathrm{var}(I)}$ and $\lambda = \frac{\mathrm{var}(I)}{\mathrm{E}[I]}$. Since $\mathrm{E}[X_j] = 1$ and $\mathrm{var}(X_j) = 1$ for $j = 1, ..., N$, the mean of the interference power is given by:

$$\mathrm{E}[I] = \sum_{j=1}^{N} r_j^{-\eta} \mathrm{E}[X_j] = \sum_{j=1}^{N} r_j^{-\eta}. \tag{4.22}$$

The variance of I can be expressed as:

$$\text{var}(I) = \sum_{j=1}^{N} r_j^{-2\eta} \text{var}(X_j) = \sum_{j=1}^{N} r_j^{-2\eta}. \tag{4.23}$$

So we have:

$$\nu = \frac{(\sum_{j=1}^{N} r_j^{-\eta})^2}{\sum_{j=1}^{N} r_j^{-2\eta}}, \tag{4.24}$$

$$\lambda = \frac{\sum_{j=1}^{N} r_j^{-2\eta}}{\sum_{j=1}^{N} r_j^{-\eta}}. \tag{4.25}$$

The outage probability can now be derived as follows:

$$\begin{aligned} \mathbb{P}(\gamma < \delta) &= \int_0^{\infty} \mathbb{P}(S < I\gamma_{th} | I = y) f_I(y) dy, \\ &= \int_0^{\infty} F_S(\delta y) f_I(y) dy, \\ &= 1 - \frac{1}{(\frac{\lambda}{r^{-\eta}}\gamma_{th} + 1)^{\nu}}. \end{aligned} \tag{4.26}$$

Leading the same analysis as in Section 4.3.1, we can consider the case of equal interfering distances R_{eq} in which case λ and ν reduces to:

$$\lambda = R_{eq}^{-\eta}, \tag{4.27}$$

$$\nu = N. \tag{4.28}$$

Equivalent interfering distances means that I is the sum of N exponential random variables with equal mean R_{eq}. In this case the PDF of I is exactly the Gamma distribution (not an approximation) with shape N and scale R_{eq}.

4.4.2 Path-Loss, Shadowing and Fast Fading Impact

In this section, we will consider that the shadowing follows a log-normal distribution. We can again write $\gamma = S/I$ with now:

$$S = r^{-\eta} Y_0 X_0, \quad I = \sum_{j=1}^{N} r_j^{-\eta} Y_j X_j. \tag{4.29}$$

We again approximate the interference PDF using the Central Limit Theorem for Causal Functions. We thus need to compute the two quantities $\nu_s = \frac{\text{E}[I]^2}{\text{var}(I)}$ and $\lambda_s = \frac{\text{var}(I)}{\text{E}[I]}$. Since

involved RVs are independent, the average value of I is given by:

$$\begin{aligned} \mathrm{E}[I] &= \sum_{j=1}^{N} r_j^{-\eta} \mathrm{E}[Y_j]\mathrm{E}[X_j], \\ &= e^{\frac{a^2\sigma^2}{2}} \sum_{j=1}^{N} r_j^{-\eta}. \end{aligned} \tag{4.30}$$

In the same way, the variance of I is given by:

$$\begin{aligned} \mathrm{var}(I) &= \sum_{j=1}^{N} r_j^{-2\eta} \left(\mathrm{E}[Y_j^2]\mathrm{E}[X_j^2] - \mathrm{E}[Y_j]^2\mathrm{E}[X_j]^2 \right), \\ &= \left(2e^{2a^2\sigma^2} - e^{a^2\sigma^2} \right) \sum_{j=1}^{N} r_j^{-2\eta}. \end{aligned} \tag{4.31}$$

The two parameters ν_s and λ_s can now be obtained:

$$\nu_s = \frac{1}{2e^{a^2\sigma^2} - 1} \frac{\left(\sum_{j=1}^{N} r_j^{-\eta} \right)^2}{\sum_{j=1}^{N} r_j^{-2\eta}}, \tag{4.32}$$

$$\lambda_s = e^{\frac{a^2\sigma^2}{2}} \left(2e^{a^2\sigma^2} - 1 \right) \frac{\sum_{j=1}^{N} r_j^{-2\eta}}{\sum_{j=1}^{N} r_j^{-\eta}}. \tag{4.33}$$

Recall that Y_0 follows a log-normal distribution with logarithmic mean 0 and standard deviation σ. We can thus average the outage probability over the variations of Y_0:

$$\begin{aligned} \mathbb{P}(\gamma < \delta) &= \int \mathbb{P}(\gamma < \delta | Y_0) p_Y(y) dy, \\ &= \int \mathbb{P}\left(r^{-\eta} X_0 < \frac{\delta}{y} I \right) p_Y(y) dy, \\ &= 1 - \int_0^{\infty} \frac{1}{(\frac{\lambda_s}{r^{-\eta}} \frac{\delta}{y} + 1)^{\nu_s}} \times \frac{1}{ay\sigma\sqrt{2\pi}} \exp\!\left(-\frac{\ln(y)^2}{2a^2\sigma^2} \right) dy. \end{aligned} \tag{4.34}$$

Although this expression involves an infinite integral, it can be numerically calculated with e.g. Mathematica.

4.5 Analytical Fluid Model

With the two proposed methods, we obtain expressions of the SIR CDF at a given distance r from the serving base-station. We see however that expressions depend also from the

distances r_i between the considered mobile terminal and all interfering BSs. With FWBM, parameters m_f and s_f in (4.17) depend on the r_i (see equations (4.9) and (4.10)). With CLCFM, parameters ν_s and λ_s in (4.34) depend also on the r_i (see equations (4.32) and (4.33)). The presence of all distances r_i make proposed formulas sometimes uneasy to use for dimensioning purposes. In this section, we thus express the parameters m_f, s_f, ν_s and λ_s as functions dependent only on the distance r using the fluid model.

The fluid model approach has been developed e.g. in [114]. It consists in replacing on the downlink a given fixed finite number of transmitters (base stations) by an equivalent continuum of transmitters which are distributed according to some distribution function. For a homogeneous and regular cellular network, inteferers are now characterized by the interfering BS density ρ_{BS}. Let denote:

$$g(\eta) = \sum_{j=1}^{N} r_j^{-\eta}. \tag{4.35}$$

Introducing the dependence of g on r and assuming an infinite network, the fluid model allows us to approximate g by the following function [114] (see Appendix A.3 for more details):

$$g(r, \eta) = \frac{2\pi\rho_{BS}}{\eta - 2}(2R_c - r)^{2-\eta}, \tag{4.36}$$

where R_c is the half inter-BS distance.

In the FWBM method, parameters $f(r, \eta)$ and $G(r, \eta)$ given by equations (4.13) and (4.12) respectively, can be expressed as follows:

$$f(r, \eta) = \frac{g(r, \eta)}{r^{-\eta}}, \tag{4.37}$$

$$G(r, \eta) = \frac{g(r, 2\eta)}{g(r, \eta)^2}. \tag{4.38}$$

Parameters m_f and s_f can thus be written as functions only on the distance r to the serving BS. In the same way, for the CLCFM, we have:

$$\nu_s = \frac{1}{2e^{a^2\sigma^2} - 1} \frac{g(r, \eta)^2}{g(r, 2\eta)}, \tag{4.39}$$

$$\lambda_s = e^{\frac{a^2\sigma^2}{2}} \left(2e^{a^2\sigma^2} - 1\right) \frac{g(r, 2\eta)}{g(r, \eta)}. \tag{4.40}$$

4.6 Performance Evaluation

In this section, we compare the figures obtained with analytical expressions (4.17) and (4.34) to those obtained by Monte Carlo simulations. It is clear that several approximations have

been done in order to obtain easy-to-use closed-form formulas: (1) the Fenton-Wilkinson method is known to be accurate for low standard deviations; (2) the Central Limit Theorem for Causal Functions is an approximation for a finite number of BSs; (3) the fluid model also. It is thus important to know to what extent approximations are acceptable.

4.6.1 Monte Carlo Simulator

The simulator assumes a homogeneous hexagonal network made of fifteen rings around a central cell. The cell range is denoted R, the half-distance between BSs is set to $R_c = 1$ Km.

The simulation consists in computing at each snapshot the SIR for a uniformly random location in the central cell. This computation can be done independently of the BS output power because noise is supposed to be negligible both in simulations and analytical study. At each snapshot, shadowing (log-normal distribution with standard deviation σ) and fast fading (exponential distribution of mean 1) RVs are independently drawn between the MS and the serving BS and between MS and interfering BSs. We do not consider correlation between shadowing coefficients. SIR samples at a given distance from the central BS are recorded in order to compute the outage probability. Five thousand (5000) snapshots are considered.

4.6.2 Results

In this section, we compare obtained formulas with results obtained by Monte Carlo simulations in a hexagonal network. We study the robustness of our approaches while varying three important parameters: σ, the standard deviation of the shadowing, η, the path-loss exponent, and r, the distance to the serving BS.

Moreover, we compare the results for the following approaches:

- SIM: results obtained from Monte Carlo simulations;
- FWBM: the Fenton-Wilkinson Based Method in conjunction with the fluid model;
- CLCFM: the Central Limit Theorem for Causal Functions Method in conjunction with the fluid model;

In figure 4.1, we compare SIR CDF obtained with SIM, FWBM and CLCFM at $r = 0.2$ Km, for $\eta = 3.0$ and while varying σ from 3 to 8 dB. Parameter σ is definitely the coefficient that influences the most the difference between analysis and simulations. It is clear that the highest is σ, the highest is the error induced by approximations. For $\sigma = 8$ dB, the CLCFM is not valid anymore if we consider the whole CDF, but remains accurate for low SIR region. For $\sigma = 3$ dB, both methods provide very accurate results.

In figure 4.2, we study the influence of the distance to the serving BS for $\sigma = 4$ dB and $\eta = 3.0$. This distance has a small influence on the accuracy of the proposed methods, all analytical CDF fit well with the CDF obtained by simulations.

In figure 4.3, we study the path-loss exponent η with fixed $\sigma = 4$ dB and distance $r = 0.2$ Km. Here again, the parameter has a small influence on the globally good accuracy of the methods. Error seems however to increase with η.

For the sake of completeness, we present in tables 4.1 and 4.2 extensive results for the comparison of SIM, FWBM, and CLCFM. We set three probability thresholds (5, 50, and 90%) and we obtain the corresponding SIR thresholds in dB from the different CDF. Reported figures represent the difference in dB between the threshold obtained with SIM on the one side and the threshold obtained with FWBM or CLCFM on the other side. Excessive differences (more than 3 dB) are marked with a star. From these tables, we can draw some conclusions:

- CLCFM provides accurate results for $\sigma \leq 6$ dB and $\eta \leq 3.0$. For all $\sigma \leq 8$ dB, results are still accurate in the low SIR region; this is an interesting result for coverage issues where outage computations are involved.
- FWBM provides accurate results for $\sigma \leq 8$ dB and $\eta \leq 3.0$, η can be greater if σ is strictly less than 8 dB. At $\sigma = 8$ dB and for $\eta \leq 3.5$, results are still accurate in the low SIR region.

Theses results show that proposed methods, especially FWBM, can provide accurate results for typical values of parameters r, σ and η usually considered in cellular networks.

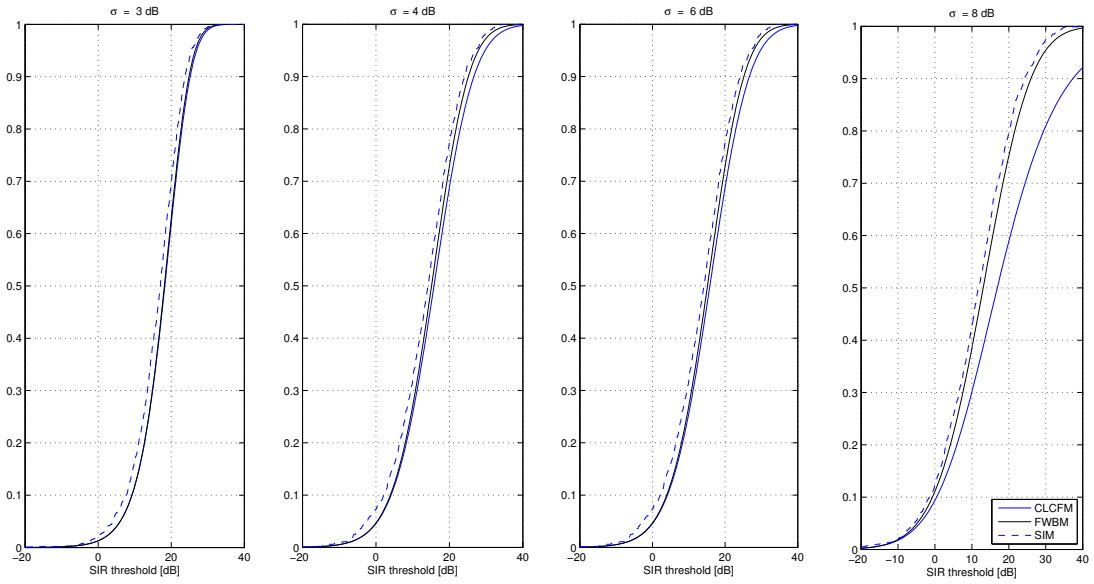

Figure 4.1: Influence of the shadowing standard deviation σ [dB] with $r = 0.2$ Km and $\eta = 3.0$.

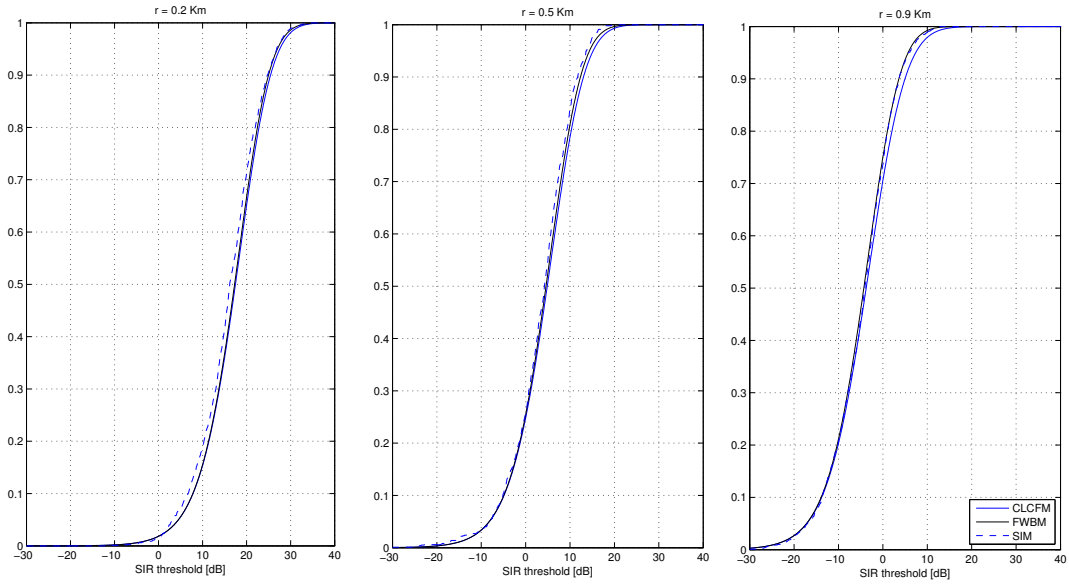

Figure 4.2: Influence of the distance to the serving BS r [Km] with $\sigma = 4$ dB and $\eta = 3.0$.

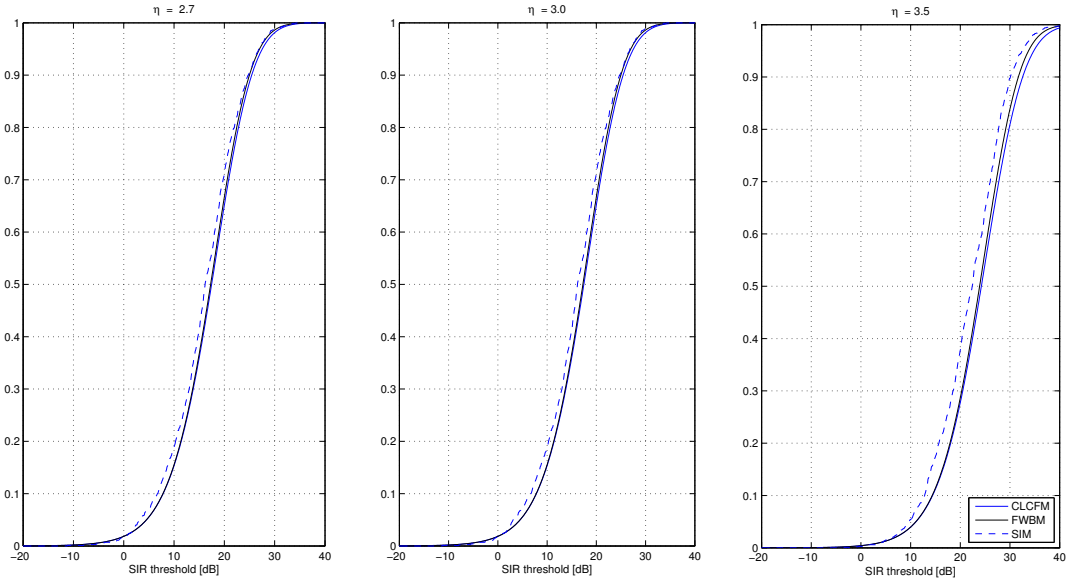

Figure 4.3: Influence of path-loss exponent η with $\sigma = 4$ dB and $r = 0.2$ Km.

Table 4.1: CDF difference in dB between Monte Carlo Simulations (SIM) on the one hand and CLCFM and FWBM on the other hand at 5%, 50% and 90% (σ =3, 4, 6 dB, * means greater than 3 dB).

σ[dB]	η	r[Km]	CLCF [dB]	FW [dB]
3.0	2.7	0.2	0.8, 0.6, 0.3	0.8, 0.5, 0.2
3.0	2.7	0.5	0.2, 0.1, 0.1	0.2, 0.0, 0.3
3.0	2.7	0.9	0.1, 0.1, 0.4	0.2, 0.2, 0.9
3.0	3.0	0.2	2.0, 1.2, 1.3	2.0, 1.1, 1.0
3.0	3.0	0.5	0.2, 0.6, 0.6	0.2, 0.5, 0.1
3.0	3.0	0.9	0.7, 0.6, 1.1	0.7, 0.2, 0.2
3.0	3.3	0.2	2.1, 1.9, 1.5	2.1, 1.7, 1.1
3.0	3.3	0.5	0.3, 0.8, 1.3	0.2, 0.6, 0.6
3.0	3.3	0.9	1.2, 0.8, 1.6	1.2, 0.3, 0.2
3.0	3.5	0.2	2.1, 1.6, 1.6	2.1, 1.3, 1.0
3.0	3.5	0.5	0.9, 1.4, 2.0	0.9, 1.1, 1.1
3.0	3.5	0.9	0.7, 0.6, 1.6	0.7, 0.0, 0.1
4.0	2.7	0.2	0.2, 0.5, 0.4	0.1, 0.4, 0.1
4.0	2.7	0.5	1.0, 0.3, 0.1	1.1, 0.5, 0.5
4.0	2.7	0.9	0.5, 0.1, 0.0	0.4, 0.2, 0.7
4.0	3.0	0.2	1.4, 1.3, 0.6	1.4, 1.1, 0.1
4.0	3.0	0.5	0.2, 0.6, 1.3	0.3, 0.3, 0.6
4.0	3.0	0.9	0.2, 0.3, 1.3	0.3, 0.2, 0.0
4.0	3.3	0.2	1.0, 1.6, 1.9	1.0, 1.3, 1.2
4.0	3.3	0.5	1.3, 1.6, 1.8	1.2, 1.2, 0.7
4.0	3.3	0.9	0.8, 1.0, 2.6	0.7, 0.2, 0.4
4.0	3.5	0.2	1.5, 1.8, 2.5	1.5, 1.4, 1.6
4.0	3.5	0.5	2.2, 1.7, 2.6	2.1, 1.2, 1.3
4.0	3.5	0.9	0.4, 1.8, 3.0	0.3, 0.8, 0.4
6.0	2.7	0.2	0.9, 0.8, 1.0	0.8, 0.4, 0.3
6.0	2.7	0.5	0.9, 0.7, 0.5	1.0, 0.1, 0.7
6.0	2.7	0.9	0.1, 0.6, 2.2	0.1, 0.4, 0.5
6.0	3.0	0.2	2.7, 1.6, 2.4	2.6, 0.9, 0.9
6.0	3.0	0.5	1.7, 1.5, 2.7	1.5, 0.5, 0.3
6.0	3.0	0.9	1.0, 1.9, *	0.7, 0.0, 0.0
6.0	3.3	0.2	1.3, 2.8, *	1.1, 1.8, 1.5
6.0	3.3	0.5	0.6, 2.3, *	0.3, 0.8, 1.3
6.0	3.3	0.9	0.5, *, *	0.1, 0.8, 0.7
6.0	3.5	0.2	1.8, *, *	1.6, 2.0, 1.9
6.0	3.5	0.5	2.6, *, *	2.3, 1.9, 1.7
6.0	3.5	0.9	1.7, *, *	1.1, 0.7, 0.7

Table 4.2: CDF difference in dB between Monte Carlo Simulations (SIM) on the one hand and CLCFM and FWBM on the other hand at 5%, 50% and 90% (σ =7 and 8 dB, * means greater than 3 dB).

d[Km]	η	σ[dB]	CLCF [dB]	FW [dB]
7.0	2.7	0.2	0.2, 0.9, 2.0	0.3, 0.1, 0.2
7.0	2.7	0.5	0.1, 1.1, 2.8	0.4, 0.1, 0.1
7.0	2.7	0.9	0.1, 2.4, *	0.6, 0.0, 0.1
7.0	3.0	0.2	1.5, 2.6, *	1.2, 1.1, 1.0
7.0	3.0	0.5	0.8, 3.0, *	1.2, 0.8, 1.2
7.0	3.0	0.9	2.4, *, *	1.7, 1.0, 1.4
7.0	3.3	0.2	0.2, *, *	0.6, 1.3, 2.8
7.0	3.3	0.5	2.3, *, *	1.7, 1.6, 2.4
7.0	3.3	0.9	2.6, *, *	1.6, 1.5, 2.0
7.0	3.5	0.2	2.9, *, *	2.4, 1.8, 2.2
7.0	3.5	0.5	1.3, *, *	0.6, 1.5, 2.4
7.0	3.5	0.9	1.7, *, *	0.5, 2.2, 2.7
8.0	2.7	0.2	0.4, 2.9, *	0.9, 0.8, 0.6
8.0	2.7	0.5	2.6, *, *	1.9, 0.4, 0.3
8.0	2.7	0.9	1.0, *, *	0.0, 0.4, 1.3
8.0	3.0	0.2	1.3, *, *	0.6, 1.1, 1.7
8.0	3.0	0.5	2.7, *, *	1.6, 1.1, 2.2
8.0	3.0	0.9	*, *, *	2.0, 1.7, 2.3
8.0	3.3	0.2	2.7, *, *	1.7, 2.6, 3.0
8.0	3.3	0.5	2.1, *, *	0.7, 1.9, *
8.0	3.3	0.9	2.9, *, *	0.5, 2.4, *
8.0	3.5	0.2	*, *, *	2.1, 3.0, *
8.0	3.5	0.5	2.7, *, *	1.0, 2.2, *
8.0	3.5	0.9	*, *, *	1.2, 2.2, *

4.7 Conclusion

In this chapter, we have established simple formulas of the outage probability in cellular networks, while considering path-loss, shadowing and fast fading. Using FWBM approach, we took into account path-loss and shadowing to first express the inverse of the SIR of a mobile located at a given distance of its serving BS as a lognormal random variable. We then, considered both path-loss, shadowing and fast fading and gave an analytical expression of the outage probability at a given distance of the serving BS. Using CLCFM approach, we took into account path-loss and fast fading to express the SIR of a mobile located at a given distance of its serving BS. We then, considered both path-loss, fast fading and shadowing and gave an analytical expression of the outage probability at a given distance of the serving BS. The fluid model allowed us to obtain formulas that only depend on the distance to the serving BS. The analytical model that was proposed was validated by comparisons with Monte Carlo simulations. The proposed framework is a powerful tool to study performances of cellular networks almost instantaneously and to design fine algorithms taking into account the distance to the serving BS, shadowing and fast fading. It can particularly easily be used for example to study frequency reuse schemes in OFDMA systems.

Chapter 5

Outage Probability of Time Reversal in Multicellular Systems

5.1 Introduction

Indoor communication were shown to achieve higher data rates than outdoor communication, however it suffers from the ISI caused by the time dispersion of the signal. Time Reversal (TR) mitigates this kind of interference. It is a technique that uses the time reversed impulse response of the channel as a pre-filter at the transmitter. This pre-filtering technique allows a time and space focusing of energy: time focusing consists in a concentration of the channels energy into one predominant peak in time with low side lobes. Space focusing results in a power peak at the intended receiver position that vanishes rapidly when going farther from the focusing point. Based on the above observations it can be shown the TR increases the percentage of captured energy at the target receiver leading to a more reliable and less complex equalization task.

This chapter studies the analytical performance of the time reversal transmission technique. A multicellular single user context is considered. Single user assumption is not a limitation to a scenario where only one user is active but refers to all systems where users are allocated orthogonal resources (time, frequency, code,...). TR precoding is performed at the BS side to encode data before transmission. In the first section of this chapter, we introduce the time reversal technique and give an overview of the existent studies in this area. In the next section, we present the system model we will consider in our analytical study. In the third section, we derive the outage probability expression. First, the PDF of the useful received power is calculated, then an approximation of the interference power PDF is provided. The mean ISI power is proved to be negligible compared to the mean multi-cell interference power which facilitates the outage probability derivation. Finally we present the simulations results that validate our outage probability expression. The main results of this chapter were published in [115].

5.2 Time Reversal Technique

5.2.1 Time Reversal Formulation

The time reversal consists in using the time reversed complex conjugate of the channel response as pre-equalizer to transmit the information signal.

Let $h(r_0, t)$ the channel impulse response between the intended receiver and the transmitter, the pre-equalizer used for this user is $h^*(r_0, -t)$. The effective channel at any location r is given by:

$$h_{eff}(r, t) = h^*(r_0, -t) \star h(r, t), \tag{5.1}$$

where $\star$ denotes the convolution operation with respect to the delay t. Hence, the effective channel is the autocorrelation of $h(r_0, t)$ defined as $h_{eff}(r_0, t) = R^{auto}(r_0, t)$ yielding a sharpened response at the target. At an off-target, the effective channel is the cross correlation $h_{eff}(r, t) = R^{cross}(r, t)$.

5.2.2 Time Reversal in the Literature

The advantages of this technique were experimentally demonstrated for rich scattering ultrasound and acoustic transmission mediums in [116, 117, 118]. These results have motivated many authors to investigate the utility of TR technique in wireless communications.

5.2.2.1 TR for SISO systems

In [119], the advantages of TR for wireless communication was, for the first time, experimentally predicted using static indoor channel (2-8 GHz band) measurements. The authors demonstrated the two principal properties of TR technique: space focusing and time focusing. Two cases where considered, the line of sight (LOS) scenario and the non line of sight (NLOS) scenario. It was shown that the time focusing is all the more significant for the NLOS case, while the two scenarios present almost the same spatial focusing property.

In [120] a measurement based analysis of the performance of TR for Ultra-Wideband (UWB) communication in an indoor propagation environment showed that the power delay profile is remarkably compressed when using TR. It was also shown that increasing the bandwidth reduces the temporal side lobes of the received time reversed signal. In [121], through a deep simulation and measurement study, the advantages and drawbacks of TR technique in broadband communication systems were presented. The principal disadvantage of TR technique consists in that it imposes a power allocation strategy that is not optimal in terms of capacity. However it is close to optimal in the low SNR region. The measurement analysis emphasized the time and spatial TR focusing gain for LOS and NLOS scenarios. For the LOS case, the time focusing is shown to be less important because of the correlation caused by the deterministic component that results in strong side lobes. It was also shown that the space focusing gain increases with the bandwidth while the time focusing gain presents an opposite behavior. In [122], based on a numerical study, it was noticed that

TR, when applied to an indoor UWB signal transmission, reduces significantly multiuser interference for sufficiently separated users owning to the spatial focusing.

All the previously mentioned studies were interested in TR applied to UWB communication exploiting the large delay spread and the richness introduced by this kind of channels. It is hence interesting to comfort all these measurement and simulation results by a theoretical study of the statistical performance of TR technique for a wideband indoor multicellular communication through the evaluation of the outage probability.

5.2.2.2 Time Reversal for MIMO Systems

Regarding the space-time focusing properties of TR technique, the use of this scheme was extended to multiple antenna systems. Consider an M antennas BS transmitting to K single antenna users. The received signal at the j^{th} user can be written as [123]:

$$y_j(t) = s_j(t) \star \sum_{i=1}^{M} h_{i,j}^*(-t) \star h_{i,j}(t) + \sum_{i=1}^{M} \sum_{k=1;k\neq j}^{K} s_k(t) \star h_{i,j}^*(-t) \star h_{i,k}(t) + n_j, \qquad (5.2)$$

where s_j is the signal intended to the j^{th} user/receiving antenna. The expression (5.2) corresponds also to an $M \times K$ single user system.

In [123], the authors showed that the TR permits to serve up to five users simultaneously while guaranteeing a BER of 10^{-3} with an SNR of 15 dB. In many works, TR was investigated in a single user MISO context. In [124], through a measurement study, it was shown that MISO TR scheme permits to reduce the delay spread by a factor of 3 reducing hence considerably the ISI effect. Always with an experimental approach, it was shown in [125] that the peak of the time reversed impulse response of a 4×1 MISO system is twice as that of a SISO one assuming sufficiently separated transmit antennas. In [126], using simulation based on the measured impulse channel response, it was observed that while for a SISO system the bit error rate (BER) reaches a floor from a given SNR value, this is not the case for the MISO system where the BER continue to decrease when the SNR gets higher.

Owning to its spatial focusing property, TR was presented as an interesting technique to be investigated in a multiuser context. In [126], using the measures of the impulse channel response, it was shown that in a system with 2 sufficiently separated concurrent users and 8 transmit antennas, the TR permits to achieve a high mean SIR value (around 17 dB). It was also proven that TR permits a better spatial focusing than the Singular Value Decomposition (SVD) technique while ensuring lower complexity.

Many works proposed modified approaches of the TR technique performed in a multiuser context achieving each time higher gains and better performance than the classical version of TR [126, 125, 127].

5.2.2.3 Combination of Time Reversal with Other Techniques

As already mentioned TR is a technique permitting to reduce ISI. However, an UWB communication suffers from very high ISI and the use of TR does not prevent the prohibitive character of this interference component. Hence comes the idea of combining TR with other transmission techniques. For example in [128], TR was combined with the ZF transmission technique in order to minimize the BER at the intended receiver. The authors considered a MISO communication system. They proposed a beamformer that achieves perfect channel equalization in the ZF sense while taking advantage from the focusing property of the TR. Using a measurement and a simulation approach, it was shown that the joint TR-ZF transmission not only permits to reduce considerably the BER at the target user especially for high SNRs but also to have a BER approaching 0.5 at an off-target proving a significant spatial focusing. In [129], TR was combined with the MMSE equalizer. It was shown that, for a given BER target, TR significantly reduces the number of taps that the receiver needs to estimate. For example for 10^{-3} of BER target, with TR technique the receiver needs to estimate only the 10 strongest taps instead of 90 taps with a regular transmission.

All previously presented works studied the TR using a measurement or a simulation-measurement approach. To the best of our knowledge no analytical approach was performed to study the performance of the TR. In what follows, we will try to investigate the performance of the TR technique from an analytical point of view considering a SISO system in a multicellular context.

5.3 System Model

In this section, we will present the system model we will use to study the analytical performance of the TR. The time reversed signal can be written as:

$$\tilde{x}(t) = x(t) \star h^*(-t), \tag{5.3}$$

where $\star$ denotes the time convolution, $h^*(-t)$ the time reversed complex conjugated channel gain and $x(t)$ is the information signal. We assume perfect knowledge of the channel at the transmitter side.

Consider a downlink, multicell single user communication. A user in a cell receives a useful signal from its serving BS and an interfering signal from the L neighboring BSs. The transmission scheme is given by the figure 5.1. Considering a Double Sideband (DSB) pulse amplitude modulation (PAM) [35], the signal $x_i(t)$ transmitted from BS i is given by:

$$x_i(t) = \sum_{n=0}^{\infty} s_n^i g(t - nT), \tag{5.4}$$

where $\{s_n^i\}$ represents the discrete sequence of i.i.d symbols, T is the symbol period and

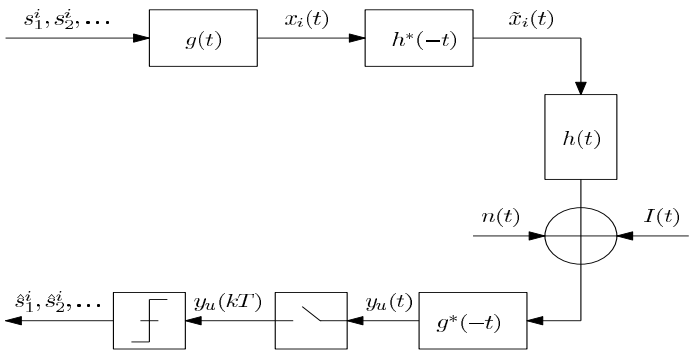

Figure 5.1: Transmission scheme.

$g(t)$ is a pulse occupying the allowed bandwidth and verifying:

$$\frac{1}{T}\int_{-\infty}^{\infty}|g(t)|^2dt = 1. \tag{5.5}$$

The received signal at a user u served by a BS b is given by:

$$\begin{aligned} y_u(t) &= \sqrt{P_b}x_b(t) \star h^*(-t) \star h(t) \star g^*(-t) \\ &+ \sum_{l=1}^{L}\sqrt{P_l}x_l(t) \star c_l^*(-t) \star d_l(t) \star g^*(-t) \\ &+ \underbrace{n(t) \star g^*(-t)}_{z(t)}, \end{aligned} \tag{5.6}$$

where $x_b(t)$ is the signal transmitted by BS b to the user u, $h^*(-t)$ is the complex conjugate time reversed channel response between user u and its serving BS, $g^*(-t)$ is the filter matched to the transmitted pulse shape, $c_l^*(-t)$ is the complex conjugate time reversed channel response between BS l and its user and $d_l(t)$ is the channel response between user u and the BS l. $n(t)$ represents the zero mean additive white Gaussian noise with power spectral density N_0. P_b is the power received by user u from BS b and can be written as:

$$P_b = P_T\frac{10^{X_b/10}}{L(d_{b,u})}, \tag{5.7}$$

where $L(d_{b,u})$ is the path-loss term and $d_{b,u}$ is the distance between the user u and its serving BS b. The term $10^{X_b/10}$ is the log-normal shadowing effect where X_b is a normally distributed random variable with a standard deviation σ (as stated in Section 2.2.2.2, a typical value of σ in an indoor office environment is 12 dB [40]).

The ITU profiles present the channel time dispersion model as a discrete tapped-delay-line with N taps:

$$h(t) = \sum_{i=1}^{N} h_i \delta(t - \tau_i). \tag{5.8}$$

The tapped-delay-line model represents a wide sense stationary uncorrelated scattering (WSSUS) where $h_{i\{i=1..N\}}$ are zero mean complex uncorrelated Gaussian random processes (Rayleigh fading). τ_i for $i = 1...N$ represents the propagation delays.

Substituting the indoor channel model given by (5.8) and the transmitted signal expressed in (5.4) in the equation (5.6) and after sampling the filtered signal at a period T, the output signal can be written as the sum of a useful power, an ISI term and an ICI term as follows:

$$\begin{aligned} y_u(kT) &= \underbrace{\sqrt{P_b} s_k^b \sum_{i=1}^{N}\sum_{j=1}^{N} h_i h_j^* \rho_g(\tau_{ij})}_{Useful\ power} \\ &+ \underbrace{\sqrt{P_b} \sum_{p\neq k}^{\infty} s_p^b \sum_{i=1}^{N}\sum_{j=1}^{N} h_i h_j^* \rho_g((p-k)T + \tau_{ij})}_{ISI} \\ &+ \underbrace{\sum_{l=1}^{L} \sqrt{P_l} \sum_{m=1}^{N}\sum_{q=1}^{N} c_{lm}^* d_{lq} \sum_{n=1}^{\infty} s_n^l \rho_g((n-k)T + \tau_{lmq})}_{ICI} \\ &+ z(kT), \end{aligned} \tag{5.9}$$

where $\rho_g(t) = g(t) \star g^*(-t)$, $\tau_{ij} = \tau_i - \tau_j$ and $\tau_{lmq} = \tau_{lm} - \tau_{lq}$. Let now write:

$$a_{ij} = \mathrm{E}[|s_k^b|^2]\rho_g(\tau_{ij}), \tag{5.10}$$

$$b_{ij} = \sum_{p\neq k}^{\infty} \mathrm{E}[|s_p^b|^2]\rho_g((p-k)T + \tau_{ij}) \tag{5.11}$$

and

$$f_{lmq} = \sum_{n=1}^{\infty} \mathrm{E}[|s_n^l|^2]\rho_g((n-k)T + \tau_{lmq}). \tag{5.12}$$

The output SINR at the u^{th} user can be expressed as:

$$SINR_u = \frac{X}{Y + Z + \sigma_z^2}, \tag{5.13}$$

where

$$X = \left| \sum_{i=1}^{N} \sum_{j=1}^{N} h_i h_j^* a_{ij} \right|^2 P_b, \tag{5.14}$$

$$Y = \sum_{l=1}^{L} \left| \sum_{m=1}^{N} \sum_{q=1}^{N} c_{lm}^* d_{lq} f_{lmq} \right|^2 P_l, \tag{5.15}$$

$$Z = \left| \sum_{i=1}^{N} \sum_{j=1}^{N} h_i h_j^* b_{ij} \right|^2 P_b. \tag{5.16}$$

In this work, we assume that the noise power and the ISI power are negligible with respect to the ICI power. This assumption will be verified in the discussion section. Hence, we will study the outage probability of the SIR_u given by:

$$SIR_u = \frac{X}{Y}. \tag{5.17}$$

For simplification reasons and without loss of generality, we also assume that the shadowing and the path-loss are constant, we also consider that:

$$P_l = P, \quad \forall\, l = 1...L. \tag{5.18}$$

5.4 Outage Probability

The outage probability is a relevant metric for the evaluation of the quality of service. It measures the probability of failing to achieve an output SIR threshold value required for a desired service. It is given by the CDF of the output SIR, i.e., for a user u [34]:

$$P_{out} = P[SIR_u < \gamma_{th}], \tag{5.19}$$

where γ_{th} is the threshold SIR value. To calculate the outage probability for the SIR_u expressed in (5.17), we need to calculate first, the PDF of the useful power and the PDF of the ICI power.

5.4.1 Useful Power PDF

The useful power expression is given by:

$$X = \left| \sum_{i=1}^{N} \sum_{j=1}^{N} h_i h_j^* a_{ij} \right|^2 P_b, \tag{5.20}$$

where $\{h_j\}_{j=1}^{N}$ are complex Gaussian fading channel gains with variances σ_j^2. It can be easily observed that (5.20) can be written as:

$$X = |\mathbf{h}^\dagger \mathbf{A} \mathbf{h}|^2 P_b, \tag{5.21}$$

where $\mathbf{h}^\dagger = [h_1^*, .., h_N^*]$ and $\mathbf{A}$ is a symmetric $N \times N$ matrix with elements a_{ij}. X can be written as:

$$X = U^2, \tag{5.22}$$

where $U = \mathbf{h}^\dagger \mathbf{A} \mathbf{h} \sqrt{P_b}$, $\mathbf{A}$ being a positive symmetric matrix so that $\sqrt{\mathbf{A}}$ exists. U can be written as:

$$U = \mathbf{v}\mathbf{v}^\dagger \sqrt{P_b}, \tag{5.23}$$

where $\mathbf{v} = \sqrt{A}\mathbf{h}$. $\mathbf{v}$ can be written as [130]:

$$\mathbf{v} = \sum_{i=1}^{N} z_i \mathbf{u}_i, \tag{5.24}$$

where $\{z_i\}_{(i=1,..,N)}$ are zero mean complex Gaussian random variables with variances the eigenvalues of the matrix $\mathbf{A}\,\mathrm{E}[\mathbf{h}\mathbf{h}^\dagger]$ and $\mathbf{u}_i$ are complex mutually orthonormal vectors. U can hence be expressed as:

$$U = \sum_{i=1}^{N} |z_i|^2 \sqrt{P_b}. \tag{5.25}$$

From the expression (5.25), U is the sum of independent chi-square random variables with unequal means λ_i, which are the eigenvalues of $P_b \mathbf{A}\,\mathrm{E}[\mathbf{h}\mathbf{h}^\dagger]$. In case of unequal variances (i.e $\sigma_{h_j}^2 \neq \sigma_{h_i}^2$ for $i \neq j$) the distribution of U is hence given by [130]:

$$f_U(u) = \sum_{j=1}^{N} \frac{\pi_j}{\lambda_j} \exp\{-\frac{u}{\lambda_j}\}. \tag{5.26}$$

Some $\sigma_{h_j}^2$ may be equal, in this case, it was shown in [131] that by separating the equal values by a very small amount the distribution (5.26) still holds and yields results closed to the exact approach. The PDF of X can be directly derived from the PDF of U (5.26) and is given:

$$f_X(x) = \frac{1}{2\sqrt{x}} \sum_{j=1}^{N} \frac{\pi_j}{\lambda_j} \exp\{-\frac{\sqrt{x}}{\lambda_j}\}, \tag{5.27}$$

where $\pi_j = \prod_{p=1, p\neq j}^{N} \frac{\lambda_j}{\lambda_j - \lambda_p}$.

5.4.2 Interference Power PDF

The interference power coming from all the BSs (except from the serving BS) received by user u is given by:

$$Y = \sum_{l=1}^{L} \left| \sum_{m=1}^{N} \sum_{q=1}^{N} c_{lm}^{*} d_{lq} f_{lmq} \right|^2 P, \tag{5.28}$$

$$= \sum_{l=1}^{L} \left| \sum_{m=1}^{N} c_{lm}^{*} \underbrace{\sum_{q=1}^{N} d_{lq} f_{lmq} \sqrt{P}}_{v_{lm}} \right|^2, \tag{5.29}$$

$$= \sum_{l=1}^{L} \left| \sum_{m=1}^{N} c_{lm}^{*} v_{lm} \right|^2, \tag{5.30}$$

where v_{lm} is a Gaussian complex random variable because it is the sum of N independent Gaussian complex random variables, with variance:

$$\sigma_{v_{lm}}^2 = \sum_{q=1}^{N} \sigma_{d_{lq}}^2 f_{lmq}^2 P. \tag{5.31}$$

To the best of our knowledge, no closed form expression is available for the interference power distribution. However, an approximation of this distribution can be deduced by applying the Central Limit Theorem for Causal Functions [17]. The theorem is presented in details in Appendix A.2. The PDF of the interference power can be approximated by a Gamma distribution given by:

$$f_Y(y) \approx \frac{y^{\alpha-1} \exp(-\frac{y}{\beta})}{\beta^{\alpha} \Gamma(\alpha)} \qquad y > 0 \quad \alpha, \beta > 0, \tag{5.32}$$

where $\beta = \frac{\mathrm{var}(y)}{\mathrm{E}(y)}$ and $\alpha = \frac{\mathrm{E}(y)^2}{\mathrm{var}(y)}$. To calculate $\mathrm{E}[y]$ and $\mathrm{var}(y)$ we need first to find out the mean and the variance of the term $\nu_l = \left| \sum_{m=1}^{N} c_{lm}^{*} v_{lm} \right|^2$. We will proceed as follows:

$$\mathrm{E}[\nu_l] = \mathrm{E}[(\sum_{m=1}^{N} c_{lm}^{*} v_{lm})(\sum_{j=1}^{N} c_{lj} v_{lj}^{*})], \tag{5.33}$$

$$= \sum_{m=1}^{N} \sum_{j=1}^{N} \mathrm{E}[c_{lm}^{*} v_{lm} c_{lj} v_{lj}^{*}]. \tag{5.34}$$

Assuming zero mean independent vectors $\mathbf{c}_l = [c_{l1}, .., c_{lN}]$ and $\mathbf{v}_l = [v_{l1}, .., v_{lN}]$, we can easily derive:

$$\mathrm{E}[\nu_l] = \sum_{j=1}^{N} \sigma^2_{c_{lj}} \sigma^2_{v_{lj}}. \tag{5.35}$$

In the same way, we can show that:

$$\mathrm{E}[|\nu_l|^2] = 4 \sum_{j=1}^{N} \sigma^4_{c_{lj}} \sigma^4_{v_{lj}} + 2 \sum_{m=1}^{N} \sum_{p \neq m}^{N} \sigma^2_{c_{lm}} \sigma^2_{c_{lp}} \sigma^2_{v_{lm}} \sigma^2_{v_{lp}}. \tag{5.36}$$

Hence, the variance of ν_l is given by:

$$\begin{aligned} \mathrm{var}(\nu_l) &= 4 \sum_{j=1}^{N} \sigma^4_{c_{lj}} \sigma^4_{v_{lj}} + 2 \sum_{m=1}^{N} \sum_{p \neq m}^{N} \sigma^2_{c_{lm}} \sigma^2_{c_{lp}} \sigma^2_{v_{lm}} \sigma^2_{v_{lp}} - (\sum_{j=1}^{N} \sigma^2_{c_{lj}} \sigma^2_{v_{lj}})^2, \\ &= 3 \sum_{j=1}^{N} \sigma^4_{c_{lj}} \sigma^4_{v_{lj}} + \sum_{m=1}^{N} \sum_{p \neq m}^{N} \sigma^2_{c_{lm}} \sigma^2_{c_{lp}} \sigma^2_{v_{lm}} \sigma^2_{v_{lp}}. \end{aligned} \tag{5.37}$$

The variance and the mean of y are, hence, given by:

$$\mathrm{E}[y] = L \, \mathrm{E}[\nu_l] \tag{5.38}$$

and

$$\mathrm{var}(y) = L \, \mathrm{var}(\nu_l), \tag{5.39}$$

which allows us to calculate the parameters α and β.

5.4.3 Outage Probability Calculation

Using the useful power PDF and the interference power PDF approximation, we calculate the outage probability as follows:

$$\begin{aligned} P_{out} &= P[SIR < \gamma_{th}], \\ &= P[\frac{X}{Y} < \gamma_{th}], \\ &= \int_0^{\infty} P(X < \gamma_{th} y | Y = y) f_Y(y) dy, \\ &= \int_0^{\infty} F_X(\gamma_{th} y) f_Y(y) dy, \end{aligned} \tag{5.40}$$

where $F_X(\gamma_{th} y)$ is the CDF of the useful power and is given by:

$$F_X(\gamma_{th} y) = \sum_{i=1}^{N} \pi_i \left(1 - \exp\left(- \frac{\sqrt{\gamma_{th} y}}{\lambda_i} \right) \right). \tag{5.41}$$

Replacing $F_X(\gamma_{th}y)$ and $f_Y(y)$ by their expressions in (5.40), the probability of outage can be derived as:

$$P_{out} = \sum_{j=1}^{N}(1 - \frac{1}{\beta^{\alpha}\Gamma(\alpha)} \underbrace{\int_0^{\infty} y^{\alpha-1} \exp\left(-\frac{\sqrt{\gamma_{th}y}}{\lambda_j}\right) \exp\left(-\frac{y}{\beta}\right)}_{I}). \tag{5.42}$$

The integral I can be calculated using [132] and is given by:

$$I = 2^{-2\alpha+1}\beta^{\alpha}\Gamma(2\alpha)U(\alpha, \frac{1}{2}, \frac{\gamma_{th}\beta}{4\lambda_j^2}). \tag{5.43}$$

Replacing I by its expression in (5.42), we show that the outage probability can be obtained as [132]:

$$P_{out} = \sum_{i=1}^{N} \pi_i \left(1 \; - \; 2^{-2\alpha+1}\frac{\Gamma(2\alpha)}{\Gamma(\alpha)}U(\alpha, \frac{1}{2}, \frac{\gamma_{th}\beta}{4\lambda_i^2})\right), \tag{5.44}$$

where $\pi_i = \prod_{p=1, p\neq i}^{N} \frac{\lambda_i}{\lambda_i - \lambda_p}$, $\Gamma(.)$ is the gamma function, $U(.,.,.)$ is the confluent hypergeometric function of second kind and is defined as:

$$U(a, b, z) = \frac{1}{\Gamma(a)} \int_0^{\infty} e^{-zt} t^{a-1}(1+t)^{b-a-1} dt. \tag{5.45}$$

5.5 Simulation Results and Discussions

5.5.1 Mean ISI Power and Mean ICI Power

In this section, we will show that our assumption stipulating that the ISI power is negligible regarding the ICI power is valid. We will calculate the mean ISI power and the mean ICI power and compare them for different numbers of interfering BSs.

The ISI power PDF can be derived in the same way as for the useful power PDF and is given by:

$$f_Z(z) = \sum_{i=1}^{N} \frac{\Delta_i}{\delta_i} \frac{1}{2\sqrt{z}} \exp\{\frac{\sqrt{z}}{\delta_i}\}, \tag{5.46}$$

denoting the matrix $B = [b_{ij}]$, δ_i for $i = 1...N$ the eigenvalues of the matrix $\sqrt{P_b}B\mathrm{E}[\mathbf{h}\mathbf{h}^{\dagger}]$ and $\Delta_i = \prod_{i\neq n}^{N} \frac{\delta_i}{\delta_i - \delta_n}$. The mean ISI power can, hence, be calculated as:

$$\begin{aligned} \mathrm{E}[z] &= \sum_{i=1}^{N} \frac{\Delta_i}{\delta_i} \int_0^{\infty} \frac{z}{2\sqrt{z}} \exp\{\frac{\sqrt{z}}{\delta_i}\} dz, & (5.47) \\ &= \Gamma(3) \sum_{i=1}^{N} \delta_i^2 \Delta_i. & (5.48) \end{aligned}$$

The mean ICI power can be derived as:

$$\begin{aligned} \mathrm{E}[y] &= \int_0^\infty y \frac{y^{\alpha-1}\exp(-\frac{y}{\beta})}{\beta^\alpha \Gamma(\alpha)} dy, \\ &= \beta \frac{\Gamma(\alpha+1)}{\Gamma(\alpha)}. \end{aligned} \tag{5.49}$$

In figure 5.2, we plot the calculated mean ISI power and mean ICI power as a function of the number of interfering BSs. We considered path-loss and constant shadowing. We can see that the mean ICI power increases with the number of interfering BSs, however the mean ICI power is a near to zero constant. Our assumption is, hence, valid.

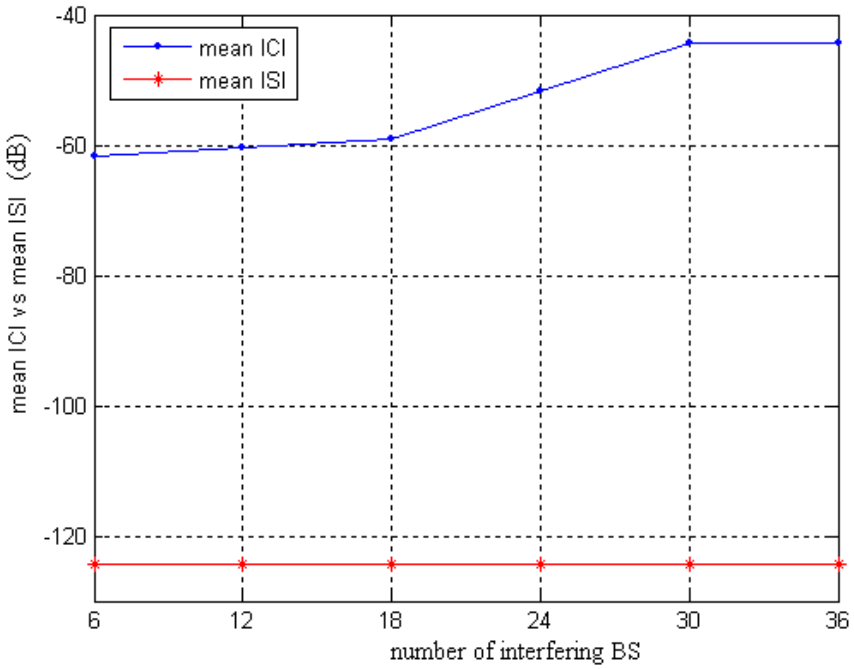

Figure 5.2: Mean ISI power and mean ICI power as function of the number on interfering BSs considering ITU IMT-2000 indoor office channel model.

5.5.2 Simulation Results

In our simulations we consider the ITU IMT-2000 model [40] which is characterized by a 6 taps indoor office channel, for a bandwidth of 2 Ghz. The 6 taps Rayleigh channels are

generated using the Jakes model [133] with respective variances in dB {0;-3.6;-7.2;-10.8;-18;-25.2} dB, and with relative delays {0;100;200;300;500;700} ns. The considered carrier frequency is $f_c = 2$ GHz and we suppose that the users move at a velocity of 3 km/h inside a building. We use identical square root raised cosine filters at the transmitter and the receiver with a roll-off coefficient equal to 0.22. We consider a cell radius of 50 m, and a user at a distance $d = 15$ m from its serving BS.

Figure 5.3 presents a comparison between the approximated PDF of the interference power and simulations. For the analytical results, we compare the PDF curves for simulated and analytical parameters α and β. We note a better accuracy in the approximation for 18 interfering BSs since it is based on a central limit theorem.

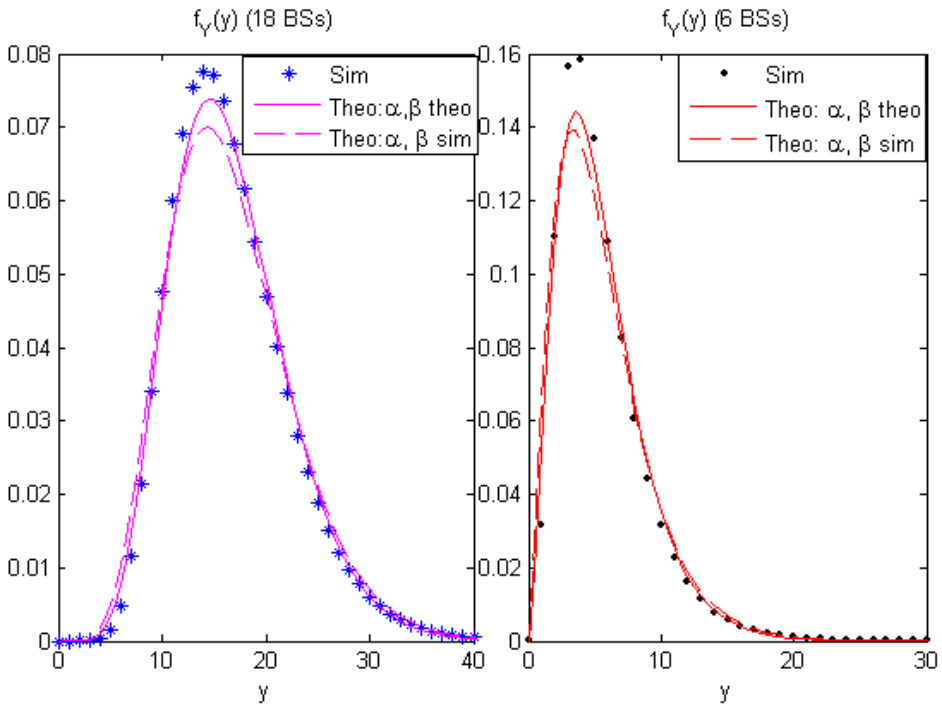

Figure 5.3: Comparison between simulations and analytical result (simulated and theoretical parameters α and β) for the interference power PDF (18 interfering BSs vs 6 interfering BSs)

In figure 5.4, we present a comparison between simulated and analytical outage probability without ISI power using time reversal pre-filtering in the case of 18 interfering BSs corresponding to the two first rings of BSs in a hexagonal network. Table 5.1 summaries the simulation parameters used to draw the curves. Theoretical results are given by the expression (5.44). It can be seen from this figure that there is a good match between simulations

Table 5.1: Indoor propagation parameters for simulations.

Shadowing standard deviation σ	12 dB
Number of floors n	3 for the useful signal 3 for the first ring of interferers 6 for the second ring of interferers

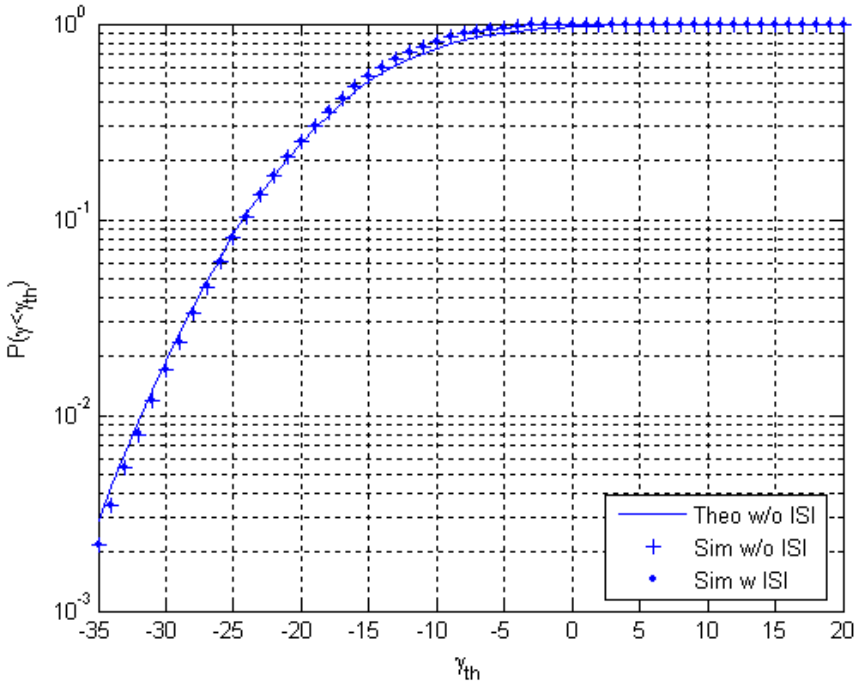

Figure 5.4: Comparison between simulations and analytical results for the outage probability with and without ISI power using time reversal for 18 interfering BSs.

and analytical results. It can also be noticed that the assumption of neglecting the ISI power compared to ICI power is valid since the simulated curves of the outage probability with and without ISI are superposed.

In figure 5.5, we highlight the influence of the number of channel taps when using time reversal transmission technique. In this perspective we compare the performance of TR when considering 6 taps ITU channel and when considering a 12 taps channel. We consider the same system parameters as for figure 5.4 except for the number of interfering BSs that we fix to 6. It can be noticed that increasing the number of taps leads to better performance. This result confirms the conclusions reached by Emami in [134] stating that the beneficial effect of the TR is all the more important when the number of significant resolvable taps is

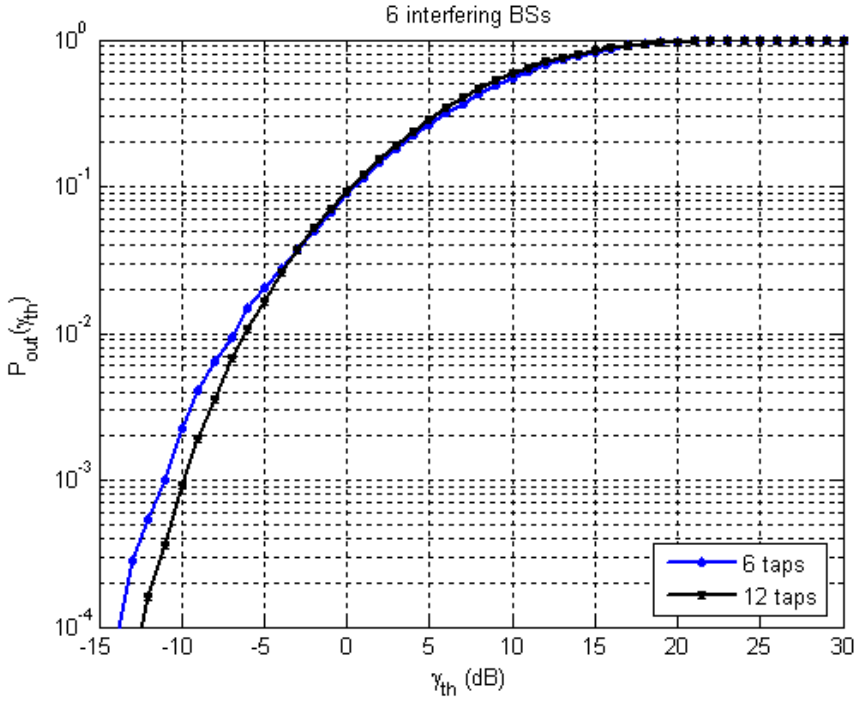

Figure 5.5: Outage probability using time reversal when considering 6 taps channels and 12 taps.

larger. Indeed, it can be seen from figure 5.5 that for an outage probability of 10^{-3} the 12 taps channel system attain a minimum SINR threshold of -10 dB, this minimum falls to -11 dB when using a 6 taps channel. Thus, doubling the number of channel taps engenders a gain of about 1 dB in the SINR, for an outage probability lower than 10^{-2}.

In figure 5.6, we compare the outage probability of system using TR transmission in presence of 6 dominant interfering BSs and in presence of 18 dominant interfering BSs. We use the initially presented 6 taps ITU channel model. We consider 2 scenarios: scenario 1 (sc=1) considers a number of crossed roofs $n = 2$ for the first ring of interfering BSs signals and $n = 3$ for the second ring of BSs interfering signals. Scenario 2 (sc=2) considers $n = 3$ and $n = 6$ respectively. In the first scenario, we can notice the degradation of performance due to the increasing number of interfering BSs. In the second scenario, the curves of outage probability for 6 and 18 interfering BSs are superposed. Indeed, the high attenuation of the interfering signal coming from the second ring of BSs due to the crossed roofs makes the influence of these BSs negligible.

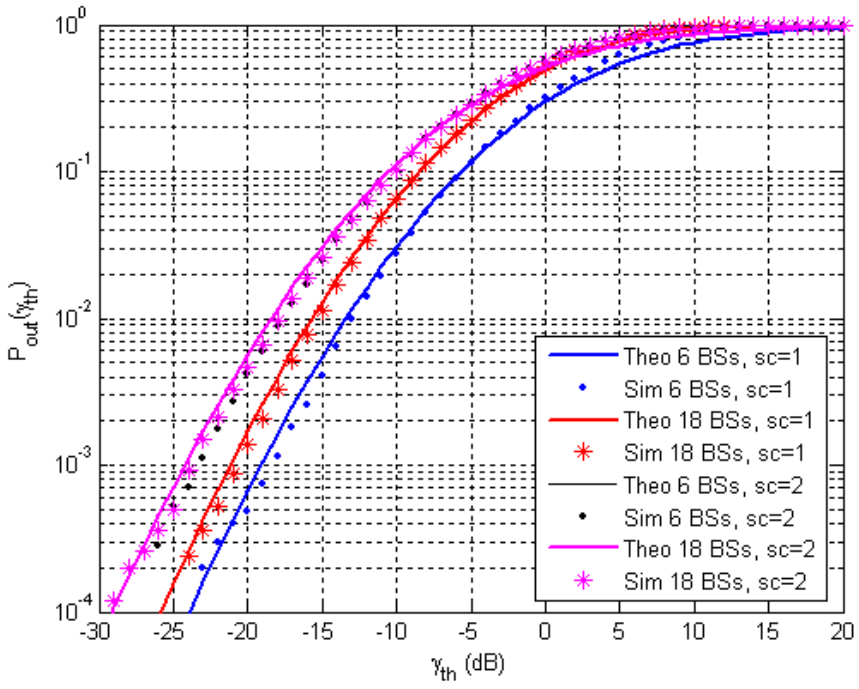

Figure 5.6: Comparison between simulations and analytical result of the outage probability using time reversal when considering 6 interfering BSs and 18 interfering BSs.

5.6 Conclusion

In this chapter, we derived a simple closed-form expression of outage probability of a multicellular system using time reversal pre-equalization. Analytical and simulation results comparison showed the validity of our expression. Our analytical study is an additional contribution to the diverse measurements and simulations existent studies.

Although time reversal is an interesting technique and is very simple to implement, it requires perfect CSIT, which cannot always be available in practice. An interesting future work can be an analytical study of the effect of the CSIT imperfectness on TR performance. In this chapter, we also assumed a constant shadowing. It could be interesting to study the influence of random variation of the shadowing. Another possible extension of this work, is to apply the TR technique to a MIMO system.

We have up to now studied SISO systems (with or without time reversal), we will concentrate in the following chapters on MISO and MIMO systems in cellular networks, starting in the next chapter with the Alamouti scheme. We will then evaluate the performance of a multi-user ZF precoded system and of a MRT CoMP transmission. There is

an interesting connection between TR and MRT. Of course, time reversal is typically an interesting technique for wideband communication in rich scattering environments modeled using a frequency selective channel with large number of resolvable paths. However, applying time reversal to a flat fading (one tap) channels reduced obviously to performing the MRT technique (see Chapter 8).

Chapter 6

Outage Probability of the Alamouti Scheme in a Multicellular Network

6.1 Introduction

The exploitation of the spatial dimension yielded through the use of multiple antennas at the transmitter and/or the receiver permits to increase capacity [60, 51] and to improve reliability [2]. In this context OSTBC [135] have been proposed to provide a tradeoff between a capacity enhancement through the multiplexing gain and a reliability improvement through the diversity gain. Among the proposed codes, the Alamouti [62] scheme has attracted much attention thanks to its simple implementation and decoding. It is also an interesting scheme since it achieves the full transmission diversity for two transmit antennas. Unlike the receive diversity schemes such as the EGC [136], the Optimum Combining (OC) [137] and the MRC [49], the Alamouti scheme removes the burden to the transmitter side.

In a point-to-point communication with Rayleigh channel, the Alamouti code was studied in terms of outage capacity probability in [138] and in terms of bit error rate (BER) with transmit antenna selection in [139]. In [140], different transmission strategies were compared. The Alamouti scheme was analyzed in single cell multiuser MISO (2×1) and MIMO (2×2) system scenarios for LOS and NLOS channels in terms of network outage probability. In [141], the Alamouti code performance was examined in the case of single cell multiuser uplink communication. The outage probability was derived for a MIMO system in Rayleigh fading channels. In [142], the authors showed that, in a single cell multiuser system, the Alamouti STBC transmission approach combined with the MRC receiver provides high system throughputs when there is a big unbalance in users channels gains. In [143], an analytical study of Almouti-MRC systems was derived in a single cell context. A closed form expression of the BER was proposed.

Some papers have conducted MIMO Alamouti systems performance evaluations consid-

ering multicell interference. In [144], authors rely on Monte Carlo simulations, whereas we propose an analytical study. In [145] and [146], authors mainly focus their investigation on a scenario, where interferers are received with equal average powers. An approximation of the SINR distribution is given for only two interferers received with unequal average powers. In this chapter, we derive the outage probability for a 2×1 multicellular Alamouti system and a $2 \times N$ multicellular Alamouti system with an MRC receiver when taking into account Rayleigh fading, shadowing and path loss. The results derived in this chapter have been published in [147], more results and discussions are available in [148].

6.2 Alamouti Code

Alamouti code is a STBC that was proposed for the first time by Alamouti in 1998 [62]. The Alamouti code is an interesting scheme since it achieves the full transmission diversity for two transmit antennas without requiring channel knowledge and is very simple to implement. It was adopted for the downlink transmission of WiMax (IEEE 802.16m), UMTS and CDMA2000 standards. In the LTE, a "frequential" version of the Alamouti code as a transmit diversity scheme for the 2 transmit antenna case [149]. The Alamouti code matrix is given by [62]:

$$\mathbf{X} = \begin{bmatrix} s_1 & -s_2^* \\ s_2 & s_1^* \end{bmatrix}, \tag{6.1}$$

where $\{s_i\}_{i=1,2}$ are the transmitted complex symbols. It consists in transmitting the symbols s_1 and s_2 from the two antennas in the first channel use period and $-s_2^*$, s_1^* in the second channel use period. It is hence a rate 1 code since two symbols are transmitted during two channel use periods. In [135], it has been proved that, for more than two transmit antennas, the orthogonal design for complex signals with linear decoding complexity achieving full-diversity rate-one transmission is not available.

6.3 MISO (2×1) Alamouti Scheme

Consider a downlink, multicell single user communication. Each BS is equipped with two antennas and each user equipment (UE) with a single antenna. At the receiver side, the signal can be represented in the following form:

$$\mathbf{y} = \sqrt{\frac{P_0}{2}} \underbrace{\begin{bmatrix} h_{1,0} & h_{2,0} \\ h_{2,0}^* & -h_{1,0}^* \end{bmatrix}}_{\mathbf{H}_0} \underbrace{\begin{bmatrix} s_{1,0} \\ s_{2,0} \end{bmatrix}}_{\mathbf{x}_0} + \sum_{j=1}^{B} \sqrt{\frac{P_j}{2}} \begin{bmatrix} h_{1,j} & h_{2,j} \\ h_{2,j}^* & -h_{1,j}^* \end{bmatrix} \underbrace{\begin{bmatrix} s_{1,j} \\ s_{2,j} \end{bmatrix}}_{\mathbf{x}_j} + \mathbf{n}, \tag{6.2}$$

where $\mathbf{y} = [y_1 \; y_2^*]^T$, y_k is the received signal at time instant k, $s_{i,j}$ is the symbol transmitted from the antenna i of the BS j, $h_{i,j}$ is the flat fading Rayleigh channel gain between the antenna i of the BS j and the considered user and B is the number of interfering BSs. The

flat fading is assumed quasi-static over the two channel use periods and $\mathbf{n}$ is the additive white Gaussian noise vector with covariance matrix $\sigma_n^2\mathbf{I}$. P_j is the received power from the j^{th} BS (P_0 is the power received from the serving BS) including path-loss and shadowing terms and is given by:

$$P_j = P_T K d_j^{-\eta} 10^{\frac{\xi_j}{10}}, \tag{6.3}$$

where P_T is the transmit power, K is a constant, d_j is the distance between the considered user and BS j, η is the path-loss exponent and is characteristic of the propagation environment and ξ_j is a Normal random variable with zero mean and standard deviation σ. By pre-multiplying the received signal by the channel transpose conjugate (operator ^{H}) of the channel $\mathbf{H}_0$, the signal at the receiver becomes:

$$\begin{aligned}
\mathbf{H}_0^H\mathbf{y} &= \sqrt{\frac{P_0}{2}}\begin{bmatrix} |h_{1,0}|^2+|h_{2,0}|^2 & 0 \\ 0 & |h_{1,0}|^2+|h_{2,0}|^2 \end{bmatrix}\mathbf{x}_0 \\
&+ \sum_{j=1}^{B}\sqrt{\frac{P_j}{2}}\begin{bmatrix} h_{1,0} & h_{2,0} \\ h_{2,0}^* & -h_{1,0}^* \end{bmatrix}^H\begin{bmatrix} h_{1,j} & h_{2,j} \\ h_{2,j}^* & -h_{1,j}^* \end{bmatrix}\mathbf{x}_j \\
&+ \begin{bmatrix} h_{1,0} & h_{2,0} \\ h_{2,0}^* & -h_{1,0}^* \end{bmatrix}^H\mathbf{n}.
\end{aligned} \tag{6.4}$$

The SINR per symbol is, thus, given by:

$$\gamma = \frac{\frac{P_0}{2}(|h_{1,0}|^2+|h_{2,0}|^2)}{\sum_{j=1}^{B}\frac{P_j}{2}\left(\frac{|h_{1,0}^*h_{1,j}+h_{2,0}h_{2,j}^*|^2+|h_{1,0}^*h_{2,j}-h_{2,0}h_{1,j}^*|^2}{|h_{1,0}|^2+|h_{2,0}|^2}\right)+\sigma_n^2}. \tag{6.5}$$

6.4 Outage Probability of (2×1) MISO Alamouti Scheme

The SINR expressed in (6.5) can be written as: $\gamma = \frac{X}{Y+\sigma_n^2}$, where

$$X = \frac{P_0}{2}(|h_{1,0}|^2+|h_{2,0}|^2), \tag{6.6}$$

and

$$Y = \sum_{j=1}^{B}\frac{P_j}{2}\frac{|h_{1,0}^*h_{1,j}+h_{2,0}h_{2,j}^*|^2+|h_{1,0}^*h_{2,j}-h_{2,0}h_{1,j}^*|^2}{|h_{1,0}|^2+|h_{2,0}|^2}. \tag{6.7}$$

We consider an interference limited cellular system where the background noise is assumed to be negligible, the SINR can, thus, be approximated by: $SINR \approx \frac{X}{Y}$. To calculate the outage probability we need to calculate first, the Probability Density Function (PDF) of X and the PDF of Y.

6.4.1 Constant Shadowing

In this section, we consider the case of very slowly varying shadowing compared to the small scale fading so that we model the shadowing by a multiplicative constant. Since $|h_{i,j}|$ are zero mean unit variance Rayleigh distributed channel gains, it can be easily shown that X is Gamma distributed and that the PDF of X is given by:

$$f_X(x) = \frac{4x}{P_0^2} e^{-\frac{2x}{P_0}}. \tag{6.8}$$

The received powers from the different interfering BSs can be written as:

$$Y = \sum_{j=1}^{B} \frac{P_j}{2} Z_j, \tag{6.9}$$

where Z_j is given by:

$$Z_j = |c_j|^2 + |d_j|^2, \tag{6.10}$$

and $c_j = \frac{\mathbf{h}_0 \mathbf{h}_j^t}{||\mathbf{h}_0||}$, $d_j = \frac{\mathbf{h}_0 \mathbf{g}_j^t}{||\mathbf{h}_0||}$, where

$$\mathbf{h}_0 = [h_{1,0}^* \; h_{2,0}], \tag{6.11}$$

$$\mathbf{h}_j = [h_{1,j} \; h_{2,j}^*] \tag{6.12}$$

and

$$\mathbf{g}_j = [h_{1,j} \; -h_{2,j}^*] \tag{6.13}$$

Since the channels are assumed Rayleigh distributed, the elements of $\mathbf{h}_0$, $\mathbf{h}_j^t$ and $\mathbf{g}_j^t$ are zero mean complex Gaussian. In this case, it was demonstrated in [49] (the demonstration is detailed in the Appendix A.4) that c_j and d_j are also complex Gaussian independent of $\mathbf{h}_0$. Z_j is, hence, the sum of two correlated exponentially distributed variables. In [150], Alouini and Holm propose a distribution for the sum of two correlated exponential variates with parameters κ_1 and κ_2 and a correlation coefficient ρ, given by:

$$\begin{aligned} f_U(u) &= \left[\exp\left(-\frac{\kappa_1 + \kappa_2 - \sqrt{(\kappa_1+\kappa_2)^2 - 4\kappa_1\kappa_2(1-\rho)}}{2\kappa_1\kappa_2(1-\rho)} u \right) \right. \\ &- \left. \exp\left(-\frac{\kappa_1 + \kappa_2 + \sqrt{(\kappa_1+\kappa_2)^2 - 4\kappa_1\kappa_2(1-\rho)}}{2\kappa_1\kappa_2(1-\rho)} u \right) \right] \\ &\times \left(\sqrt{(\kappa_1+\kappa_2)^2 - 4\kappa_1\kappa_2(1-\rho)} \right)^{-1}. \end{aligned} \tag{6.14}$$

In our case $\kappa_1 = \kappa_2 = 1$, thus, the PDF of Z_j is given by [150]:

$$f_{Z_j}(z) = \frac{1}{\sqrt{\rho_z}} \exp\left(-\frac{z}{1-\rho_z} \right) \sinh\left(\frac{\sqrt{\rho_z}}{1-\rho_z} z \right), \quad \text{for} \;\; z > 0. \tag{6.15}$$

where ρ_z is the correlation coefficient between the two correlated random variables $|c_j|^2$ and $|d_j|^2$. It is a constant obtained by simulation $\rho_z = 0.0167$.

6.4.1.1 Equal Interference Power Assumption

In this section, we will assume that $P_j = P, \forall j = 1, ..., B$. This assumption allows us to derive a simple closed form expression of the outage probability. However this scenario is not completely unrealistic. It can correspond to the case where the considered user is close to its serving BS mainly interfered by the first surrounding ring of cells. The interference power Y can be written as:

$$Y = \sum_{j=1}^{B} \frac{P}{2}(|c_j|^2 + |d_j|^2), \tag{6.16}$$

where

$$c_j = \frac{\mathbf{h}_0 \mathbf{h}_j^t}{||\mathbf{h}_0||}, \tag{6.17}$$

$$d_j = \frac{\mathbf{h}_0 \mathbf{g}_j^t}{||\mathbf{h}_0||}, \tag{6.18}$$

and $\mathbf{h}_0 = [h_{1,0}^* \ h_{2,0}]$, $\mathbf{h}_j = [h_{1,j} \ h_{2,j}^*]$ and $\mathbf{g}_j = [h_{1,j} \ -h_{2,j}^*]$. As proven in [49], c_j and d_j are complex Gaussian random variables independent of $\mathbf{h}_0$. Hence, Y is the sum of two correlated Gamma distributed random variables. In [150], Holm and Alouini proved that the distribution of the sum of two dependent Gamma variates with the same shape parameter ω, different scale parameters κ_1 and κ_2 and a correlation coefficient ρ, is the type I McKay distribution given by:

$$f_U(u) = \frac{\sqrt{\pi}(c^2-1)^{a+\frac{1}{2}} u^a}{2^a b^{a+1} \Gamma(a+\frac{1}{2})} e^{-u\frac{c}{b}} I_a(\frac{u}{b}), \tag{6.19}$$

where

$$a = \omega, \tag{6.20}$$

$$b = \frac{2\kappa_1\kappa_2(1-\rho)}{\sqrt{(\kappa_1+\kappa_2)^2 - 4\kappa_1\kappa_2(1-\rho)}}, \tag{6.21}$$

$$c = \frac{\kappa_1+\kappa_2}{\sqrt{(\kappa_1+\kappa_2)^2 - 4\kappa_1\kappa_2(1-\rho)}}. \tag{6.22}$$

In our case $\omega = B$, $\kappa_1 = \kappa_2 = \frac{P}{2}$, by replacing these values in (6.20), (6.21) and (6.22) we can obtain the probability distribution of Y that is given by:

$$f_Y(y) = \frac{2\sqrt{\pi}}{P(1-\rho)^B \Gamma(B)} \left(\frac{2y}{P^2\delta}\right)^{B-\frac{1}{2}} \exp(-\frac{2y}{P(1-\rho)}) I_{B-\frac{1}{2}}(\delta y), \tag{6.23}$$

where ρ is the correlation coefficient between the two correlated variables $Y_c = \sum_{j=1}^{B} |c_j|^2$ and $Y_d = \sum_{j=1}^{B} |d_j|^2$ and can be expressed as $\rho = \frac{Cov(Y_c, Y_d)}{\sqrt{\text{var}(Y_c)\text{var}(Y_d)}}$, $\delta = \frac{2\sqrt{\rho}}{P(1-\rho)}$ and $I_n(.)$ is

the n^{th} order modified Bessel function of first kind. Using the PDF expressions (6.8) and (6.23), the outage probability can be derived as follows:

$$\begin{aligned} P(\frac{X}{Y} < \gamma_{th}) &= \int_0^{\infty} F_X(\gamma_{th} y) f_Y(y) dy \\ &= \int_0^{\infty} (1 - e^{-\frac{2\gamma_{th}}{P_0} y}(1 + \frac{2\gamma_{th}}{P_0} y)) f_Y(y) dy. \end{aligned} \tag{6.24}$$

Substituting $f_Y(y)$ by its expression and using the following formula [150]:

$$\int_0^{\infty} x^{\mu-1} e^{-\eta x} I_\nu(\beta x) dx = \frac{\beta^\nu}{2^\nu \eta^{\mu+\nu}} \frac{\Gamma(\mu+\nu)}{\Gamma(\nu+1)} {}_2F_1\left(\frac{\mu+\nu}{2}, \frac{\mu+\nu+1}{2}; \nu+1; \frac{\beta^2}{\eta^2}\right), \tag{6.25}$$

the outage probability is given by:

$$\begin{aligned} P_{out}(\gamma_{th}) = 1 &- \frac{C}{P^{2B-1}\varsigma^{2B}} \frac{\Gamma(2B)}{\Gamma(B+\frac{1}{2})} \Big({}_2F_1(B, B+\frac{1}{2}; B+\frac{1}{2}; \frac{\delta^2}{\varsigma^2}) \\ &+ \frac{4B}{\varsigma} \frac{\gamma_{th}}{P_0} {}_2F_1(B+\frac{1}{2}, B+1; B+\frac{1}{2}; \frac{\delta^2}{\varsigma^2}) \Big), \end{aligned} \tag{6.26}$$

where $C = \frac{2\sqrt{\pi}}{P(1-\rho)^B \Gamma(B)}$, $\varsigma = \frac{2\gamma_{th}}{P_0} + \frac{2}{P(1-\rho)}$ and ${}_2F_1(.,.;.;.)$ is the Gauss hypergeometric function [132] given by:

$${}_2F_1(e, f; g; x) = \sum_{n=0}^{\infty} \frac{e(e+1)..(e+n-1) f(f+1)..(f+n-1)}{n! g(g+1)..(g+n-1)} x^n. \tag{6.27}$$

From [151], for $e = g$ or $f = g$ using the binomial theorem the Gauss' hypergeometric function reduces to:

$${}_2F_1(e, f; e; x) = {}_2F_1(f, e; e; x) = (1-x)^{-f}, \tag{6.28}$$

where $|x| < 1$. Using this property in (6.27), the probability of outage can be written as:

$$\begin{aligned} P_{out}(\gamma_{th}) = 1 &- \frac{C}{P^{2B-1}\varsigma^{2B}} \frac{\Gamma(2B)}{\Gamma(B+\frac{1}{2})} \left(1 - \frac{\delta^2}{\varsigma^2}\right)^{-(B+\frac{1}{2})} \\ &\times \left(1 + \frac{4B}{\varsigma} \frac{\gamma_{th}}{P_0} \left(1 - \frac{\delta^2}{\varsigma^2}\right)^{-\frac{1}{2}}\right). \end{aligned} \tag{6.29}$$

6.4.1.2 Unequal Interference Power Assumption

Since the equal power assumption does not cover many possible scenarios, we will try to derive an expression for the outage probability in the case of unequal received power. When the received powers from the different interfering BSs are unbalanced, it is more difficult to find a closed form expression for the interference power PDF. From the expression (6.9) of the interference power, we can approximate the PDF $f_Y(y)$ using the central limit theorem for causal functions [17] (see Appendix A.2) by a Gamma distribution given by:

$$f_Y(y) = \frac{y^{\alpha-1}\exp(-\frac{y}{\beta})}{\Gamma(\alpha)\beta^{\alpha}}, \tag{6.30}$$

where $\alpha = \frac{\mathrm{E}[Y]^2}{\mathrm{var}(Y)}$ and $\beta = \frac{\mathrm{var}(Y)}{\mathrm{E}[Y]}$. Note that the application of the central limit theorem for causal functions requires that interference powers are independent but not necessarily identically distributed [17]. Let us derive the expressions of α and β. As Z_j for $j = 1, ..., B$ are independent random variables, the mean of the interference power is given by:

$$\mathrm{E}[Y] = \sum_{j=1}^{B} \frac{P_j}{2}\mathrm{E}[Z_j] = \sum_{j=1}^{B} P_j. \tag{6.31}$$

The variance of Y can be expressed as:

$$\mathrm{var}(Y) = \sum_{j=1}^{B} \frac{P_j^2}{4}\mathrm{var}(Z_j). \tag{6.32}$$

$\mathrm{E}[Z_j]$ can be derived as:

$$\mathrm{E}[Z_j] = \mathrm{E}[|c_j|^2] + \mathrm{E}[|d_j|^2] = 2, \tag{6.33}$$

and $\mathrm{E}[Z_j^2]$ can be calculated using the PDF of Z_j as follows:

$$\begin{aligned}
\mathrm{E}[Z_j^2] &= \int_0^{\infty} \frac{z^2}{\sqrt{\rho_z}} \exp\left(\frac{-z}{1-\rho_z}\right) \sinh\left(\frac{\sqrt{\rho_z}}{1-\rho_z} z\right) dz, \\
&= \frac{1}{\sqrt{\rho_z}} \frac{\Gamma(3)}{2} \left[\left(\frac{1-\sqrt{\rho_z}}{1-\rho_z}\right)^{-3} - \left(\frac{1+\sqrt{\rho_z}}{1-\rho_z}\right)^{-3} \right], \\
&= 2(3+\rho_z).
\end{aligned} \tag{6.34}$$

The parameters α and β in (6.30) are, thus given by:

$$\alpha = \frac{2}{1+\rho_z} \frac{(\sum_{j=1}^{B} P_j)^2}{\sum_{j=1}^{B} P_j^2}, \quad \beta = \frac{1+\rho_z}{2} \frac{\sum_{j=1}^{B} P_j^2}{\sum_{j=1}^{B} P_j}. \tag{6.35}$$

As already stated, the random variables c_j and d_j are independent of $\mathbf{h}_0$ (see Appendix A.4), and since Y is given by:

$$Y = \sum_{j=1}^{B} \frac{P_j}{2}|c_j|^2 + |d_j|^2. \tag{6.36}$$

Y is also independent of $\mathbf{h}_0$, and since X can be written as:

$$X = \frac{P_0}{2}\left\|\mathbf{h}_0\right\|^2, \tag{6.37}$$

it can be asserted that Y is independent of X. The outage probability can thus be derived as follows:

$$\begin{aligned} P(\frac{X}{Y} < \gamma_{th}) &= \int_0^\infty F_X(\gamma_{th}y) f_Y(y) dy, \\ &= \int_0^\infty (1 - e^{-\frac{2\gamma_{th}}{P_0}y}(1 + \frac{2\gamma_{th}}{P_0}y)) f_Y(y) dy. \end{aligned} \tag{6.38}$$

Substituting $f_Y(y)$ by its expression, the outage probability can be written as:

$$P_{out}(\gamma_{th}) = 1 - \left(\frac{P_0}{2\gamma_{th}\beta + P_0}\right)^{\alpha} \left(1 + \frac{2\gamma_{th}\beta}{2\gamma_{th}\beta + P_0}\frac{\Gamma(\alpha+1)}{\Gamma(\alpha)}\right). \tag{6.39}$$

6.4.2 Log-Normal Shadowing

In this section, we will consider that the shadowing follows a log-normal distribution. The PDF of the received power can be expressed as:

$$f_{P_j}(x) = \frac{1}{ax\sigma\sqrt{2\pi}} \exp\left(-\frac{(\ln(x) - a\mu_j)^2}{2a^2\sigma^2}\right), \tag{6.40}$$

where $a = \frac{\ln 10}{10}$ and $\mu_j = \frac{1}{a}\ln\left(KP_T d_j^{-\eta}\right)$.

Following the same reasoning as for the equation (6.39), we will derive an expression for the outage probability for the 2×1 MISO Alamouti system. Considering the PDF of the received power given by (6.40), the outage probability conditioned on the useful received power can be written as:

$$P_{out}(\gamma_{th}|P_0 = x) = 1 - \left(\frac{x}{2\gamma_{th}\beta_s + x}\right)^{\alpha_s} \left(1 + \frac{2\gamma_{th}\beta_s}{2\gamma_{th}\beta_s + x}\frac{\Gamma(\alpha_s + 1)}{\Gamma(\alpha_s)}\right), \tag{6.41}$$

where $\alpha_s = \frac{\mathrm{E}[Y]^2}{\mathrm{var}(Y)}$ and $\beta_s = \frac{\mathrm{var}(Y)}{\mathrm{E}[Y]}$, the subscript $_s$ refers to the shadowing. To calculate α_s and β_s we will consider the log-normal distribution of the received powers P_j. The mean of Y is, hence, given by:

$$\mathrm{E}[Y] = \sum_{j=1}^{B} \mathrm{E}[\frac{P_j}{2}]\mathrm{E}[Z_j]. \tag{6.42}$$

Using (6.40), the mean of P_j is given by:

$$\mathrm{E}[P_j] = e^{a\mu_j + \frac{a^2\sigma^2}{2}}. \tag{6.43}$$

Since $\mu_j = \frac{1}{a}\ln\left(KP_T d_j^{-\eta}\right)$, $E[P_j]$ can be written as:

$$\mathrm{E}[P_j] = e^{\frac{a^2\sigma^2}{2}} KP_T d_j^{-\eta}. \tag{6.44}$$

The mean of Y can, thus, be written as:

$$\mathrm{E}[Y] = e^{\frac{a^2\sigma^2}{2}} \sum_{j=1}^{B} KP_T d_j^{-\eta}. \tag{6.45}$$

The variance of the interference power can be derived as:

$$\mathrm{var}(Y) = \sum_{j=1}^{B} \mathrm{E}[\frac{P_j^2}{4}]\mathrm{E}[Z_j^2] - \frac{1}{4}\mathrm{E}[P_j]^2\mathrm{E}[Z_j]^2, \tag{6.46}$$

where $\mathrm{E}[P_j^2]$ is given by:

$$\mathrm{E}[P_j^2] = e^{2a^2\sigma^2}\left(KP_T d_j^{-\eta}\right)^2. \tag{6.47}$$

Hence, the variance of Y can be expressed as:

$$\begin{aligned} \mathrm{var}(Y) &= \sum_{j=1}^{B} e^{2a(\mu_j + a\sigma^2)}\frac{1}{2}(3+\rho_z) - e^{2a(\mu_j + \frac{a\sigma^2}{2})}, \\ &= (\frac{1}{2}(3+\rho_z)e^{2a^2\sigma^2} - e^{a^2\sigma^2})\sum_{j=1}^{B}\left(KP_T d_j^{-\eta}\right)^2. \end{aligned} \tag{6.48}$$

The parameters α_s and β_s are, thus given by:

$$\alpha_s = \frac{1}{\frac{1}{2}(3+\rho_z)e^{a^2\sigma^2} - 1}\frac{(\sum_{j=1}^{B} d_j^{-\eta})^2}{\sum_{j=1}^{B} d_j^{-2\eta}}, \tag{6.49}$$

$$\beta_s = \left(\frac{1}{2}(3+\rho_z)e^{a^2\sigma^2} - 1\right)e^{\frac{a^2\sigma^2}{2}} KP_T \frac{\sum_{j=1}^{B} d_j^{-2\eta}}{\sum_{j=1}^{B} d_j^{-\eta}}. \tag{6.50}$$

The outage probability can be derived by integrating the conditional outage probability over the PDF of the received power given by (6.40) as follows:

$$\begin{aligned} P_{out}(\gamma_{th}) &= 1 - \int_0^{\infty}\left(\frac{x}{2\gamma_{th}\beta_s + x}\right)^{\alpha_s}\left(1 + \frac{2\gamma_{th}\beta_s}{2\gamma_{th}\beta_s + x}\frac{\Gamma(\alpha_s+1)}{\Gamma(\alpha_s)}\right) \\ &\times \frac{1}{ax\sigma\sqrt{2\pi}}\exp\left(-\frac{(\ln(x) - a\mu_0)^2}{2a^2\sigma^2}\right)dx, \end{aligned} \tag{6.51}$$

where $\mu_0 = \frac{1}{a}\ln\left(KP_T d_0^{-\eta}\right)$, d_0 is the distance between the considered user and its serving BS.

6.5 MIMO $(2 \times N)$ Alamouti Scheme with MRC Receiver

In this case, we consider the same system as in the previous section, the receiver is however equipped, here, with N receive antennas. At the receiver side, the signal can be written as:

$$\mathbf{y} = \sqrt{\frac{P_0}{2}} \underbrace{\begin{bmatrix} h_{1,1,0} & h_{1,2,0} \\ h^*_{1,2,0} & -h^*_{1,1,0} \\ . & . \\ . & . \\ h_{N,1,0} & h_{N,2,0} \\ h^*_{N,2,0} & -h^*_{N,1,0} \end{bmatrix}}_{\mathbf{H}_0} \underbrace{\begin{bmatrix} s_{1,0} \\ s_{2,0} \end{bmatrix}}_{\mathbf{x}_0} + \sum_{j=1}^{B} \sqrt{\frac{P_j}{2}} \begin{bmatrix} h_{1,1,j} & h_{1,2,j} \\ h^*_{1,2,j} & -h^*_{1,1,j} \\ . & . \\ . & . \\ h_{N,1,j} & h_{N,2,j} \\ h^*_{N,2,j} & -h^*_{N,1,j} \end{bmatrix} \underbrace{\begin{bmatrix} s_{1,j} \\ s_{2,j} \end{bmatrix}}_{\mathbf{x}_j} + \mathbf{n}, \tag{6.52}$$

where $h_{i,j,k}$ is the Rayleigh flat fading channel between i^{th} antenna of the receiver and the antenna j of the BS k. The MRC receiver combines the received signals from the N antennas. The received signal is multiplied by the complex conjugate of the channel $\mathbf{H}_0$. The SINR per symbol is, hence, given by:

$$\gamma = \frac{\frac{P_0}{2}\sum_{n=1}^{N}(|h_{n,1,0}|^2 + |h_{n,2,0}|^2)}{\sum_{j=1}^{B}\frac{P_j}{2}\left(\frac{|\sum_{n=1}^{N} h^*_{n,1,0}h_{n,1,j} + h_{n,2,0}h^*_{n,2,j}|^2 + |\sum_{n=1}^{N} h^*_{n,1,0}h_{n,2,j} - h_{n,2,0}h^*_{n,1,j}|^2}{\sum_{n=1}^{N}(|h_{n,1,0}|^2 + |h_{n,2,0}|^2)}\right) + \sigma_n^2}. \tag{6.53}$$

6.6 Outage Probability for the $2 \times N$ MIMO Alamouti System with MRC Receiver

As in the previous section, in an interference limited system, the SINR per stream of a MIMO Alamouti scheme with MRC receiver given by (6.53) can be approximated as: $SINR \approx \frac{X_{MRC}}{Y_{MRC}}$, where X_{MRC} and Y_{MRC} are given by the expressions:

$$X_{MRC} = \frac{P_0}{2}\sum_{n=1}^{N}(|h_{n,1,0}|^2 + |h_{n,2,0}|^2), \tag{6.54}$$

and

$$Y_{MRC} = \sum_{j=1}^{B}\frac{P_j}{2}\left(\frac{|\sum_{n=1}^{N} h^*_{n,1,0}h_{n,1,j} + h_{n,2,0}h^*_{n,2,j}|^2 + |\sum_{n=1}^{N} h^*_{n,1,0}h_{n,2,j} - h_{n,2,0}h^*_{n,1,j}|^2}{\sum_{n=1}^{N}(|h_{n,1,0}|^2 + |h_{n,2,0}|^2)}\right). \tag{6.55}$$

6.6.1 Constant Shadowing

From the expression of X_{MRC} and since $|h_{i,j,b}|$ are zero mean unit variance Rayleigh distributed channel gains, it can be easily shown [34] that X_{MRC} is the sum of two Gamma distributed random variables $G(N, P_0/2)$ and that $X_{MRC} \sim G(2N, P_0/2)$, the PDF of X_{MRC} is hence given by:

$$f_{X_{MRC}}(x) = \frac{x^{2N-1}}{(\frac{P_0}{2})^{2N}(2N-1)!} e^{-\frac{2x}{P_0}}. \tag{6.56}$$

6.6.1.1 Equal Interference Power Assumption

As in Section 6.4.1.1, we will assume that $P_j = P, \forall j = 1, ..., B$. The interference power Y_{MRC} can then be written as:

$$Y_{MRC} = \sum_{j=1}^{B} \frac{P}{2}(|C_j|^2 + |D_j|^2), \tag{6.57}$$

where $C_j = \frac{\tilde{\mathbf{h}}_0 \tilde{\mathbf{h}}_j}{||\tilde{\mathbf{h}}_0||}$ and $D_j = \frac{\tilde{\mathbf{h}}_0 \tilde{\mathbf{g}}_j}{||\tilde{\mathbf{h}}_0||}$, $\tilde{\mathbf{h}}_0$, $\tilde{\mathbf{h}}_j$ and $\tilde{\mathbf{g}}_j$ being:

$$\begin{aligned}
\tilde{\mathbf{h}}_0 &= [h^*_{1,1,0} \,..\, h^*_{N,1,0}\; h_{1,2,0} \,..\, h_{N,2,0}], &(6.58)\\
\tilde{\mathbf{h}}_j &= [h_{1,1,j} \,..\, h_{N,1,j}\; h^*_{1,2,j} \,..\, h^*_{N,2,j}]^T, &(6.59)\\
\tilde{\mathbf{g}}_j &= [h_{1,2,j} \,..\, h_{N,2,j}\; -h^*_{1,1,j} \,..\, -h^*_{N,1,j}]^T, &(6.60)
\end{aligned}$$

where ^{T} is the transpose operator. As proven in Section 6.4.1.1, Y_{MRC} is the sum of two correlated Gamma distributed random variables with shape parameter B and scale parameter $\frac{P}{2}$, hence the PDF of Y_{MRC} is given by [150]:

$$f_{Y_{MRC}}(y) = \frac{2\sqrt{\pi}}{P(1-\rho_{mrc})^B \Gamma(B)} \left(\frac{2y}{P^2 \delta_{mrc}}\right)^{B-\frac{1}{2}} \exp(-\frac{2y}{P(1-\rho_{mrc})}) I_{B-\frac{1}{2}}(\delta_{mrc} y), \tag{6.61}$$

where ρ_{mrc} is the correlation coefficient between the two correlated variables $Y_C = \sum_{j=1}^{B} |C_j|^2$ et $Y_D = \sum_{j=1}^{B} |D_j|^2$ and can be expressed as $\rho_{mrc} = \frac{\mathrm{Cov}(Y_C, Y_D)}{\sqrt{\mathrm{var}(Y_C)\mathrm{var}(Y_D)}}$, $\delta_{mrc} = \frac{2\sqrt{\rho_{mrc}}}{P(1-\rho_{mrc})}$ and $I_n(.)$ is the n^{th} order modified Bessel function of first kind. Using the PDF expressions (6.56) and (6.61), the outage probability can be derived as in (6.24):

$$P_{out}^{MRC}(\gamma_{th}) = \int_0^{\infty} F_{X_{MRC}}(\gamma_{th} y) f_{Y_{MRC}}(y) dy, \tag{6.62}$$

where

$$\begin{aligned} F_{X_{MRC}}(\gamma_{th}y) &= 1 - e^{-\frac{2\gamma_{th}y}{P_0}} \sum_{k=0}^{2N-1} \frac{(\gamma_{th}y)^k}{k!(\frac{P_0}{2})^k}, \\ &= \frac{1}{\Gamma(2N)}\gamma(2N, \frac{2\gamma_{th}y}{P_0}), \end{aligned} \tag{6.63}$$

where $\gamma(.,.)$ is the lower incomplete Gamma function defined as [152]:

$$\gamma(a,x) = \int_0^x t^{a-1}e^{-t}dt. \tag{6.64}$$

Using the integration formula (6.25), the outage probability is given by:

$$\begin{aligned} P_{out}^{MRC}(\gamma_{th}) = 1 \quad - \quad & \frac{C_{mrc}\delta_{mrc}^{B-\frac{1}{2}}}{2\varsigma_{mrc}^{2B}\Gamma(B+\frac{1}{2})} \sum_{k=0}^{2N-1} \frac{(2\gamma_{th})^k\Gamma(2B+k)}{(\varsigma_{mrc}P_0)^k k!} \\ & {}_2F_1(B+\frac{k}{2}, B+\frac{k+1}{2}; B+\frac{1}{2}; \frac{\delta_{mrc}^2}{\varsigma_{mrc}^2}), \end{aligned} \tag{6.65}$$

where $C_{mrc} = \frac{2\sqrt{\pi}}{P(1-\rho_{mrc})\Gamma(B)}\left(\frac{2}{P^2\delta_{mrc}}\right)^{B+\frac{1}{2}}$, $\varsigma_{mrc} = \frac{2}{P(1-\rho_{mrc})} + \frac{2\gamma_{th}}{P_0}$ and ${}_2F_1(.,.;.;.)$ is the Gauss hypergeometric function [132].

6.6.1.2 Unequal Interference Power Assumption

For the unequal power case, P_j for $j = 1, ..., B$ can be different. To derive the interference power PDF, we use the same Gamma approximation as in Section 6.4:

$$f_{Y_{MRC}}(y) = \frac{y^{\nu-1}\exp(-\frac{y}{\lambda})}{\Gamma(\nu)\lambda^\nu}, \tag{6.66}$$

where $\nu = \frac{\mathrm{E}[Y_{MRC}]^2}{\mathrm{var}(Y_{MRC})}$ and $\lambda = \frac{\mathrm{var}(Y_{MRC})}{\mathrm{E}[Y_{MRC}]}$.

In order to compute $\mathrm{E}[Y_{MRC}]$ and $\mathrm{var}(Y_{MRC})$, we will note $Y_{MRC} = \sum_{j=1}^{B}\frac{P_j}{2}V_j$. V_j is given by:

$$V_j = |C_j|^2 + |D_j|^2, \tag{6.67}$$

where $C_j = \frac{\tilde{\mathbf{h}}_0\tilde{\mathbf{h}}_j}{||\tilde{\mathbf{h}}_0||}$ and $D_j = \frac{\tilde{\mathbf{h}}_0\tilde{\mathbf{g}}_j}{||\tilde{\mathbf{h}}_0||}$, $\tilde{\mathbf{h}}_0$, $\tilde{\mathbf{h}}_j$ and $\tilde{\mathbf{g}}_j$ being:

$$\tilde{\mathbf{h}}_0 = [h_{1,1,0}^* \,..\, h_{N,1,0}^* \; h_{1,2,0} \,..\, h_{N,2,0}], \tag{6.68}$$

$$\tilde{\mathbf{h}}_j = [h_{1,1,j} \,..\, h_{N,1,j} \; h_{1,2,j}^* \,..\, h_{N,2,j}^*]^T, \tag{6.69}$$

$$\tilde{\mathbf{g}}_j = [h_{1,2,j} \,..\, h_{N,2,j} \; -h_{1,1,j}^* \,..\, -h_{N,1,j}^*]^T, \tag{6.70}$$

where ^{T} is the transpose operator. As proven in Section 6.4, C_j and D_j are complex Gaussian random variables independent of $\tilde{\mathbf{h}}_0$ meaning that V_j is the sum of two correlated exponentially distributed variables. As explained in Section 6.4.1, the PDF of V_j is given by:

$$f_V(v) = \frac{1}{\sqrt{\rho_v}} \exp\left(-\frac{v}{(1-\rho_v)}\right) \sinh\left(\frac{\sqrt{\rho_v}}{(1-\rho_v)} v\right), \quad \text{for } v > 0, \tag{6.71}$$

where $\rho_v = 3.9267.10^{-4}$ (obtained by simulations) is the correlation coefficient between the two correlated random variables $|C_j|^2$ and $|D_j|^2$. $\mathrm{E}[V_j]$ and $\mathrm{E}[V_j^2]$ can be derived as in Section 6.4 and are given by: $\mathrm{E}[V_j] = 2$ and $\mathrm{E}[V_j^2] = 2(3+\rho_v)$. Since V_j for $j = 1, ..., B$ are independent random variables, the mean of the interference power is given by:

$$\mathrm{E}[Y_{MRC}] = \sum_{j=1}^{B} \frac{P_j}{2} \mathrm{E}[V_j] = \sum_{j=1}^{B} P_j. \tag{6.72}$$

The variance of Y_{MRC} can be expressed as:

$$\mathrm{var}(Y_{MRC}) = \sum_{j=1}^{B} \frac{P_j^2}{4} \mathrm{var}(V_j) = \sum_{j=1}^{B} \frac{P_j^2}{2}(1+\rho_v). \tag{6.73}$$

The parameters ν and λ in (6.66) are, thus given by:

$$\nu = \frac{2}{1+\rho_v} \frac{(\sum_{j=1}^{B} P_j)^2}{\sum_{j=1}^{B} P_j^2}, \quad \lambda = \frac{(1+\rho_v)}{2} \frac{\sum_{j=1}^{B} P_j^2}{\sum_{j=1}^{B} P_j}. \tag{6.74}$$

Since Y_{MRC} is independent of $\tilde{\mathbf{h}}_0$, it is consequently independent of $X_{MRC} = \tilde{\mathbf{h}}_0 \tilde{\mathbf{h}}_0^H$, the outage probability can be derived using the formula (6.38) and is given by:

$$P_{out}^{MRC}(\gamma_{th}) = 1 - \sum_{k=0}^{2N-1} \frac{(2\gamma_{th}\lambda)^k P_0^\nu}{k!(2\gamma_{th}\lambda + P_0)^{k+\nu}} \frac{\Gamma(k+\nu)}{\Gamma(\nu)}. \tag{6.75}$$

6.6.2 Log-Normal Shadowing

As in the previous section, we will try to find out the outage probability when we consider the log-normal distribution of the received power. The Gamma approximation of the interference power PDF is always valid, however, we have to calculate the new parameters ν_s and λ_s of the Gamma distribution.

Following the same approach of Section 6.4.2, and considering the log-normal random variation of the received power, the mean and the variance of Y_{MRC} are given by:

$$\mathrm{E}[Y_{MRC}] = e^{\frac{a^2\sigma^2}{2}} \sum_{j=1}^{B} K P_T d_j^{-\eta}, \tag{6.76}$$

and

$$\mathrm{var}(Y_{MRC}) = e^{a^2\sigma^2}\left(\frac{3+\rho_v}{2}e^{a^2\sigma^2}-1\right). \tag{6.77}$$

Hence, ν_s and λ_s can be expressed as:

$$\nu_s = \frac{1}{\left(\frac{3+\rho_v}{2}e^{a^2\sigma^2}-1\right)}\frac{(\sum_{j=1}^{B} d_j^{-\eta})^2}{\sum_{j=1}^{B} d_j^{-2\eta}}, \tag{6.78}$$

$$\lambda_s = e^{\frac{a^2\sigma^2}{2}}\left(\frac{3+\rho_v}{2}e^{a^2\sigma^2}-1\right)KP_T\frac{\sum_{j=1}^{B} d_j^{-2\eta}}{\sum_{j=1}^{B} d_j^{-\eta}}. \tag{6.79}$$

Conditioned on the useful received power, the outage probability of a MIMO Alamouti system with an MRC receiver is given by:

$$P_{out}^{MRC}(\gamma_{th}|P_0=x) = 1-\sum_{k=0}^{2N-1}\frac{(2\gamma_{th}\lambda_s)^k P_0^{\nu_s}}{k!(2\gamma_{th}\lambda_s+P_0)^{k+\nu_s}}\frac{\Gamma(k+\nu_s)}{\Gamma(\nu_s)}. \tag{6.80}$$

Averaging over the distribution of P_0, the outage probability when considering the log-normal shadowing is given by:

$$\begin{aligned} P_{out}^{MRC}(\gamma_{th}) = 1 &- \sum_{k=0}^{2N-1}\frac{(2\gamma_{th}\lambda_s)^k}{k!a\sigma\sqrt{2\pi}}\frac{\Gamma(k+\nu_s)}{\Gamma(\nu_s)} \\ &\times \int_0^{\infty}\frac{x^{\nu_s-1}}{(2\gamma_{th}\lambda_s+x)^{k+\nu_s}}\exp\left(-\frac{(\ln(x)-a\mu_0)^2}{2a^2\sigma^2}\right)dx. \end{aligned} \tag{6.81}$$

6.7 Fluid Model Approach

We have seen in the previous section that several parameters depend on the distances d_j between the user and each of the interfering base-stations. For dimensioning purposes (e.g. for the computation of the coverage probability at cell edge or of the achievable throughput at a given distance), it is very interesting to obtain formulas that depend only on the distance to the serving station. In this section, we thus use the fluid model that was presented for the first time in [153] to derive an outage probability expression depending only on the distance between the considered user and the serving BS. The fluid model concept consists in replacing a fixed number of BSs by an equivalent continuum characterized by a given density. Denoting:

$$g(\eta) = \sum_{j=1}^{B} d_j^{-\eta}, \tag{6.82}$$

for a homogeneous network and a BS density ρ_{BS} and admitting an infinite network radius, the fluid model permits to write $g(\eta)$ as (the approach is explained in details in Appendix A.3):

$$g(\eta) = \frac{2\pi\rho_{BS}}{\eta - 2}(2R_c - d_0)^{2-\eta}, \tag{6.83}$$

where R_c is the considered cell radius. In terms of $g(\eta)$, the parameters of the outage probability of the 2×1 Alamouti system α_s (6.49) and β_s (6.50) can be written as:

$$\alpha_s = \frac{1}{(\frac{3+\rho}{2}e^{a^2\sigma^2} - 1)} \frac{g(\eta)^2}{g(2\eta)}, \tag{6.84}$$

$$\beta_s = e^{\frac{a^2\sigma^2}{2}} \left(\frac{3+\rho}{2} e^{a^2\sigma^2} - 1 \right) KP_T \frac{g(2\eta)}{g(\eta)}. \tag{6.85}$$

Similarly, the parameters of the MIMO $(2 \times N)$ system with MRC receiver ν_s (6.79) and λ_s (6.79) are given by:

$$\nu_s = \frac{1}{\left(\frac{3+\rho_v}{2}e^{a^2\sigma^2} - 1\right)} \frac{g(\eta)^2}{g(2\eta)}, \tag{6.86}$$

$$\lambda_s = e^{\frac{a^2\sigma^2}{2}} \left(\frac{3+\rho_v}{2} e^{a^2\sigma^2} - 1 \right) KP_T \frac{g(2\eta)}{g(\eta)}. \tag{6.87}$$

6.8 Simulation Results

In this section, we compare obtained formulas with results obtained by Monte Carlo simulations in a hexagonal network. The common simulations parameters used in this section are:

- the cell radius is $R_c = 1$ Km;
- the standard deviation of the log-normal shadowing is taken $\sigma = 6$ dB;
- the path-loss exponent is taken $\eta = 3.41$.

The Jakes model [133] is used to generate zero mean unit variance Rayleigh independent fading channels. We compare the results for the following systems:

- SISO: for equal and unequal interference power constant shadowing over the period of study;
- MISO Alamouti: for equal and unequal interference power considering constant and log-normal shadowing;

- MIMO Alamouti with MRC receiver: for unequal interference power considering constant and log-normal shadowing;

In figures 6.1 and 6.2, we plot simulated and analytical outage probability in the case of equal received interference power (figure 6.1 (a), figure 6.2 (a)) and in the case of unequal received interference power (figure 6.1 (b), figure 6.2 (b)) for the Alamouti scheme compared to a SISO system respectively in a linear and logarithmically y-axis scale. For the equal interference power simulation, we consider 6 interfering BSs, the mobile station is at a distance $d = 0.2$ Km from the BS and the interfering BSs are at distance $d_{int} = 2R_c$. For the unequal power results, we consider a user at a distance $d = 0.5$ Km from its serving BS and 18 dominant interfering BSs (two rings of BS in a hexagonal network). In the two cases the shadowing is considered constant over the period of study.

It can be seen that, in the low SINR regime, the Alamouti scheme achieves better performance. In fact, as can be seen in figure 6.2 that the outage probability of the Alamouti scheme decreases faster owning to a higher slope corresponding to the diversity gain of the scheme $G_D = 2$. Thus, the Alamouti scheme allows a better coverage. However, at high SINR, we can see, from figure 6.1 that the SISO system outperforms the 2×1 MISO Alamouti precoded system. This unexpected behavior can be explained by the fact that, as the power is equally shared equally between two antennas for the MISO case, to get back the maximum of this power at the receiver two very good channels are needed. However, when all power is transmitted over one single antenna one good channel is needed. Since the probability to have one good channel is higher than the probability of two good channels event, the outage probability of the Alamouti scheme at high SINR is higher than the outage probability of the SISO system. In other words, at high SINR, the diversity has an inverse effect.

In figure 6.3, we plot simulated and analytical outage probability for the MISO Alamouti scheme compared to a 2×2 an 2×4 MIMO Alamouti schemes with MRC receiver. We consider a user at a distance $d = 0.5$ Km from its serving BS and 18 dominant interfering BSs (two rings of BSs in a hexagonal network). The shadowing is considered constant over the period of study.

It can be seen that the MIMO Alamouti coded system with MRC receiver achieves better performance. In fact, as can be seen in figure 6.3, the outage probability of this scheme decreases faster owning to a higher slope corresponding to the additional (the transmit diversity gain achieved by the Alamouti code $G_T = 2$) receiver diversity gain ($G_R = 2$ for 2×2 MIMO system and $G_R = 4$ for the 2×4 MIMO system) achieved by the MRC receiver. Thus, the Alamouti scheme associated with the MRC receiver allows a better coverage. The simulated curves fit well the analytical ones.

Figure 6.4 shows that the central limit approximation used to derive the outage probability is valid even when considering 6 interfering BSs.

Figure 6.6 presents a comparison between the simulated performance of the Alamouti scheme in a single cell communication and in a multicellular system with the simulated

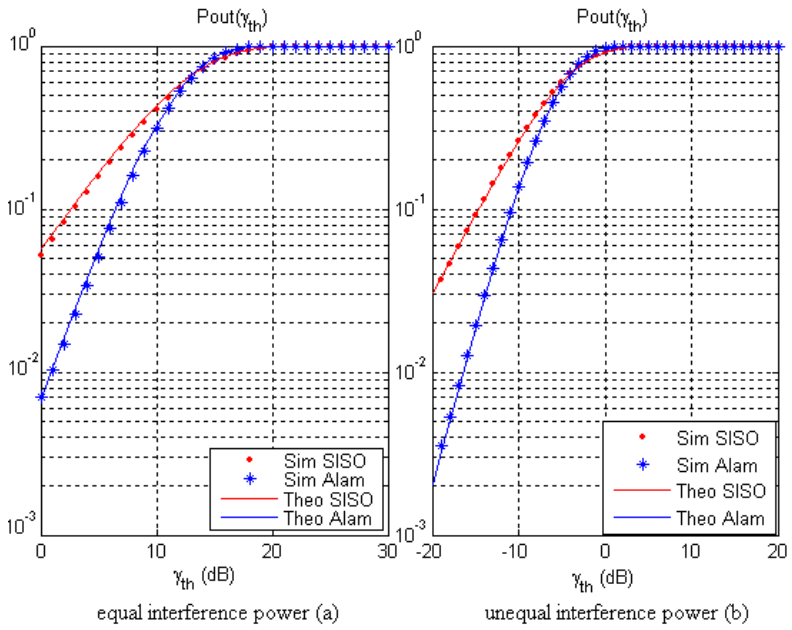

Figure 6.1: P_{out} versus SINR threshold for 2×1 MISO Alamouti and SISO systems in case of equal (a) and unequal (b) received interference power (logarithmic y-axis scale).

performance of a SISO system for the same scenarios. The performance gain of the Alamouti scheme over the SISO system degrades considerably in a multicellular context compared to the single cell case. This degradation can be explained by the fact that, as for the useful signal, the Alamouti scheme induces a diversity gain on the interference channel.

Figure 6.6 presents also a comparison between the simulated performance of the 2×1 MISO Alamouti scheme in a single cell and in a multicellular system with the simulated performance of the 2×2 MIMO Alamouti coded system with MRC receiver for the same scenarios. The performance of the two systems degrades considerably in the multicellular scenario compared to the single cell case. We can also see that the performance gain of the 2×2 MIMO Alamouti scheme jointly with the MRC receiver over the 2×1 MISO Alamouti scheme remains the same when moving from a single cell to a multicellular context.

Figure 6.7 presents the influence of the shadowing on the performance of the two systems 2×1 Alamouti and 2×4 Alamouti with MRC receiver. Simulated and analytical curves are displayed for a user at a distance $d = 0.5$ Km from its serving BS and 18 dominant interfering BSs. It can be noticed that the log-normal random variation of the shadowing degrades the performance of the two systems. It can be remarked that for an outage probability of 1%, the loss in terms of SINR is about 10 dB for the Alamouti with MRC receiver scheme and 7 dB for the Alamouti scheme. From the same figure, we can also see

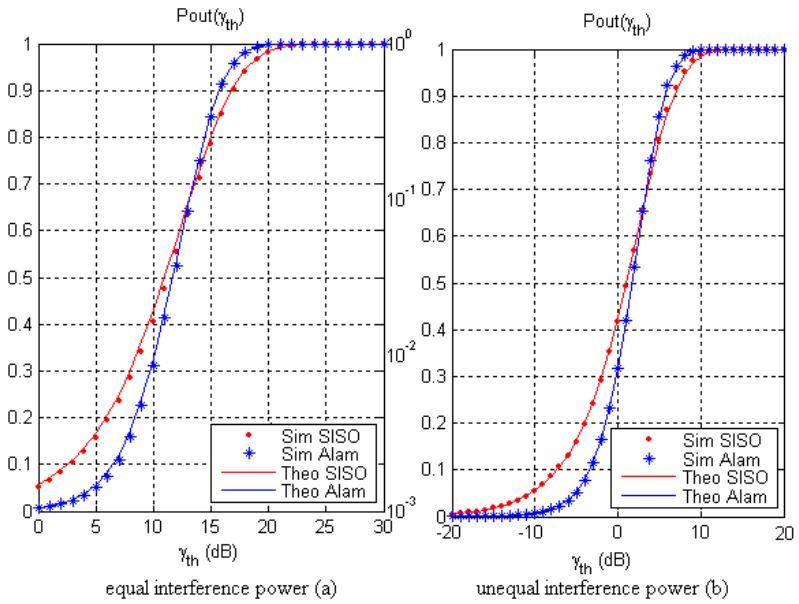

Figure 6.2: P_{out} versus SINR threshold for 2×1 MISO Alamouti and SISO systems in case of equal (a) and unequal (b) received interference power (linear y-axis scale).

that there is a good match between theoretical results and simulations.

In figure 6.8, we present a comparison between simulated and theoretical outage probability results for the two systems when using the fluid model approach. We consider the same system parameters as for figure 6.7 except for the shadowing standard deviation set to 4 dB. It can be seen that there is a good agreement between analytical results and simulations. The fluid model approximation allows us to derive simpler expressions of the outage probability parameters without major loss in the results accuracy.

It is at last interesting to see on figure 6.9 that the well known 3 dB difference between Alamouti 2×1 and MRC 1×2 [62] can also be observed in a multicellular environment. Curves have been here obtained using the fluid model, $R_c = 1$ Km and $d = 0.5$ Km.

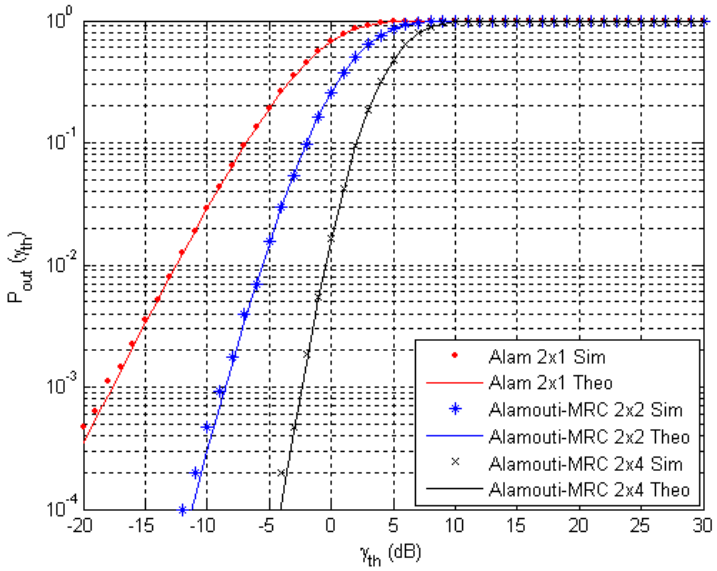

Figure 6.3: P_{out} versus SINR threshold for 2×1 MISO Alamouti, 2×2 and 2×4 MIMO Alamouti with MRC receiver systems (18 interfering BSs).

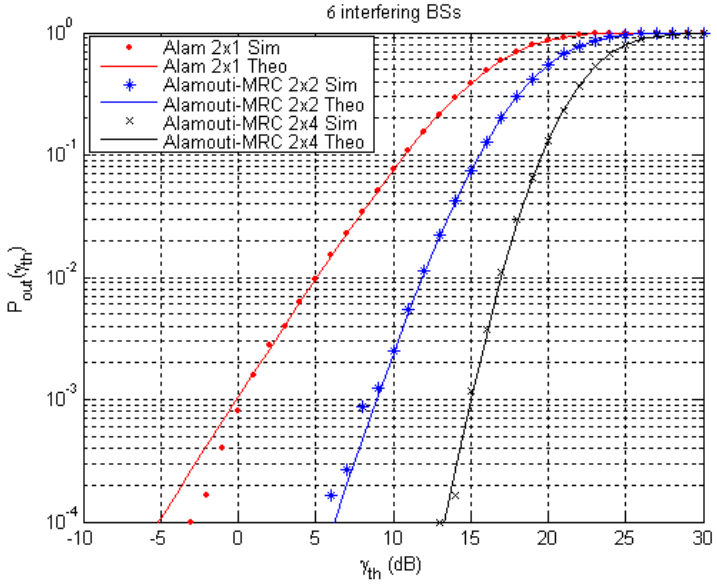

Figure 6.4: P_{out} versus SINR threshold for 2×1 MISO Alamouti, 2×2 and 2×4 MIMO Alamouti with MRC receiver systems (6 interfering BSs).

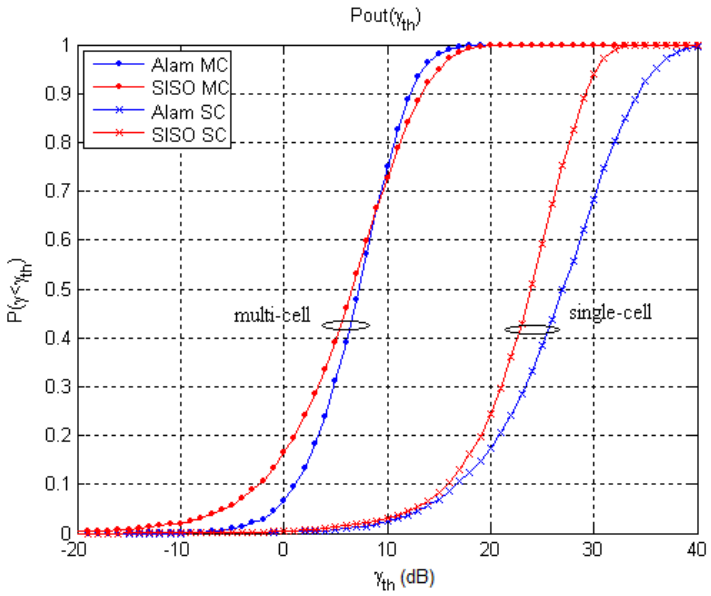

Figure 6.5: P_{out} versus SINR threshold for 2×1 MISO Alamouti and SISO systems in a single-cell (SC) and in a multicellular (MC) communications.

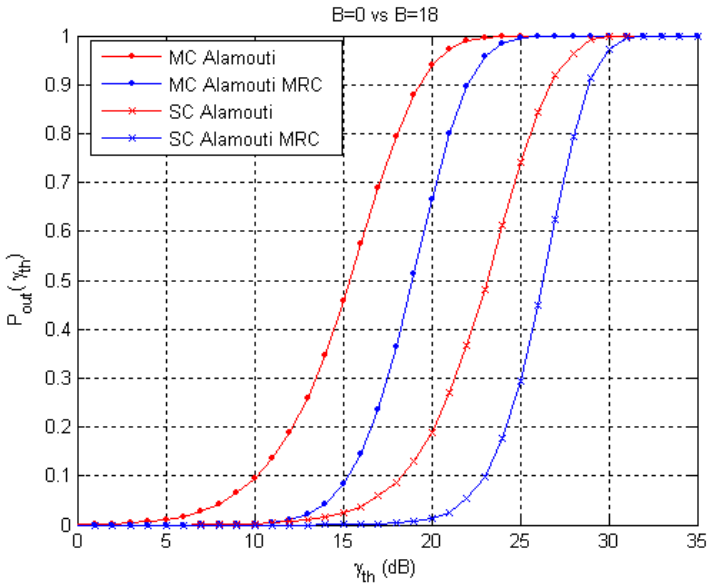

Figure 6.6: P_{out} versus SINR threshold for 2×1 MISO Alamouti and 2×2 Alamouti with MRC receiver schemes in a single-cell (SC) and in a multicellular (MC) communications.

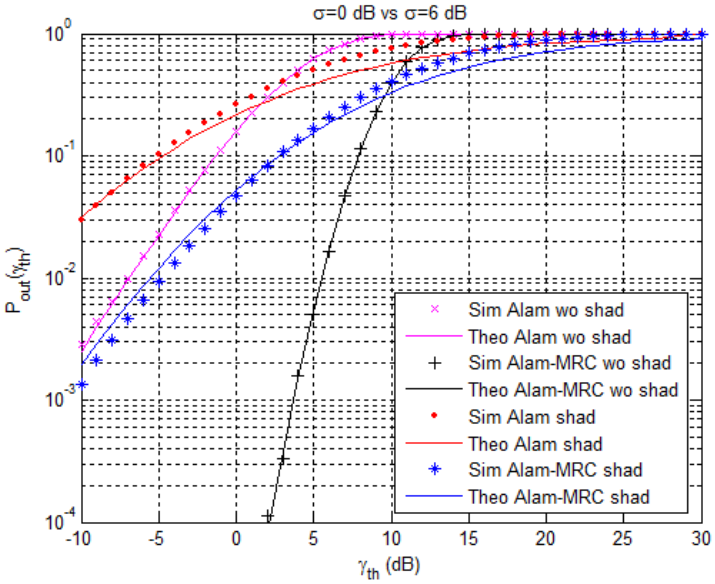

Figure 6.7: Influence of the shadowing: P_{out} versus SINR threshold for 2×1 MISO Alamouti and the 2×4 MIMO Alamouti with MRC receiver systems.

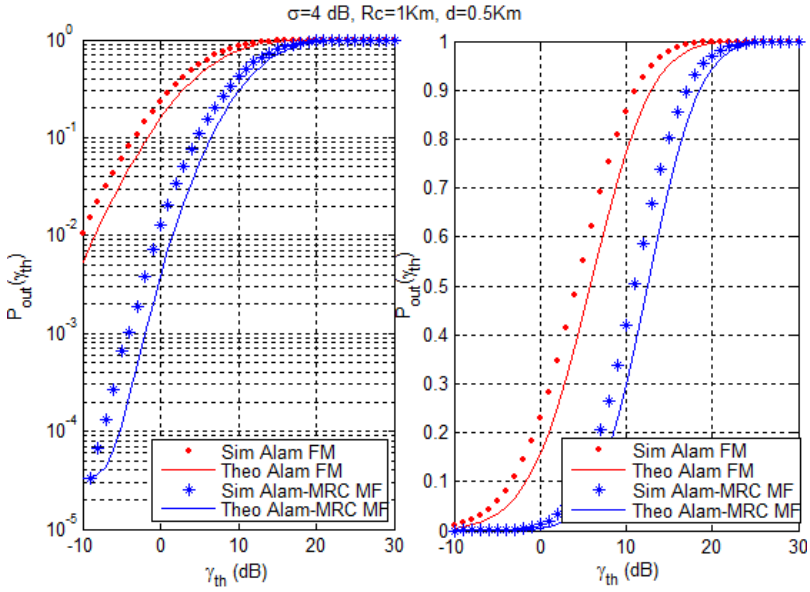

Figure 6.8: Fluid model (FM) approximation: P_{out} versus SINR threshold for 2×1 MISO Alamouti and 2×4 MIMO Alamouti with MRC receiver systems.

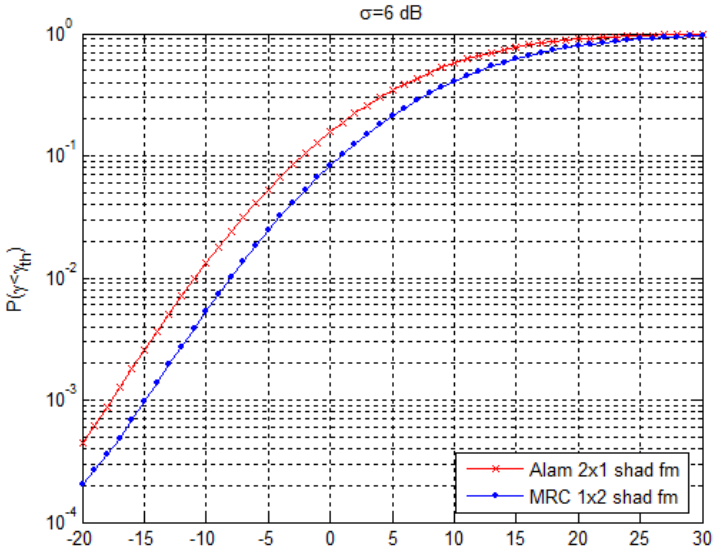

Figure 6.9: P_{out} versus SINR threshold for Alamouti 2×1 and with MRC 1×2 systems assuming fluid model (FM).

6.9 Conclusion

In this chapter, the performance of the Alamouti scheme was studied in two multicellular network interference limited systems: a 2×1 MISO and a $2\times N$ MIMO using a MRC receiver. Outage probability expressions for the case of constant shadowing and the case of log-normal shadowing were derived. In the two cases, a comparison between the performance of the two multicellular systems were illustrated. The fluid model approach permits to derive expressions of outage probability depending only on the distance between the considered user and its serving BS without a major loss in terms of precision.

Chapter 7

Outage probability of a Zero Forcing Precoded System

7.1 Introduction

In the previous chapter, we have studied the performance of a SU-MIMO diversity scheme in a multicellular context. In this chapter, we will focus on a MU-MIMO spatial multiplexing scheme which is the ZF precoding. We will study the performance of this scheme in a multicellular context in terms of outage probability.

The ZF precoding performance was studied in [154] in terms of symbol error rate. Analytical distributions of the SIR of a ZF precoded system was proposed for a broadcast channel in a single cell system for a Rayleigh channel without considering shadowing. In [155], the performance of the ZF precoding was investigated in the case of imperfect channel estimation in terms of bit error rate for a broadcast single cell MIMO system. In [156], an asymptotic analysis of linear precoding techniques (ZF and MMSE) was conducted for small cells multiuser multicellular systems where the inter-cell interference affects enormously the system performance. The authors showed a dramatic decrease in the achievable sum-rate due to multicell interference. In [157] and [53], it was shown that for a MIMO broadcast channel and using an adequate user selection algorithm, the ZF precoding approaches the performance of the DPC for a large number of users in the cell.

In the literature, the ZF performance has been studied in a single cell context without considering multicell interference and for a Rayleigh channel except in [156] where the multicellular case has been studied in terms of sum-rate capacity for small-cell systems. In this work, we propose an analytical study of the performance of the ZF precoding in a multiuser multicellular system. Two assumptions will be considered: constant shadowing during the period of study and lognormal random shadowing.

This chapter is organized as follows: the next section is dedicated to the system model description. In Section 7.3, two outage probability expressions are derived, the first one

concerns the case of Rayleigh fading channels, the second expression is obtained when considering path-loss, shadowing and fast fading. In Section 7.4, simulation results are presented and discussed. Some conclusions are proposed in Section 7.5.

The results derived in this chapter were published in [158].

7.2 Zero Forcing MISO System Model

Consider a downlink, multicellular multiuser system. Each base station (BS) is equipped with M antennas and there are K users per cell with a single antenna each, as presented in figure 7.1. Let us recall the principle of the ZF transmission scheme that has been briefly

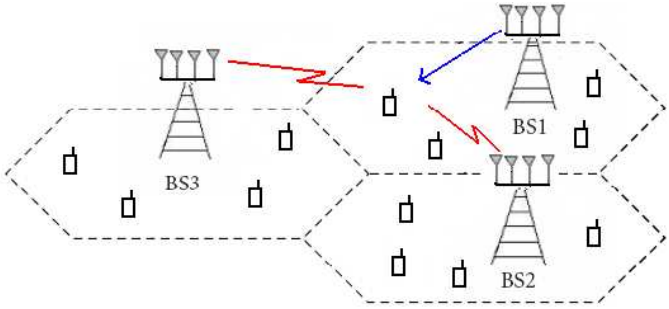

Figure 7.1: System model

introduced in Section 3.2.2.4. The ZFBF is a linear precoding technique that eliminates the multiuser interference at the transmitter level. It consists of multiplying the information vector by the ZF precoding matrix given by:

$$\mathbf{W} = \mathbf{H}^H(\mathbf{H}\mathbf{H}^H)^{-1}, \tag{7.1}$$

where $\mathbf{H}$ is the channel between the BS and the users served simultaneously. $\mathbf{H}$ is a $K \times M$ matrix with complex Gaussian distributed entries, i.e, $h_{i,j}$ the channel between the user i and the antenna j of the BS is $CN(0,1)$. Hence the transmitted signal is given by:

$$\mathbf{x} = \sqrt{P_T}\frac{\mathbf{W}\mathbf{s}}{\sqrt{\delta}}, \tag{7.2}$$

where P_T is the transmit power, $\mathbf{s} = [s_1, s_2, ...s_K]$ the symbol information vector intended to the K users and δ is a normalization factor introduced to satisfy the transmission power constraint and to ensure: $\|\mathbf{x}\|^2 = P_T$. δ is given by:

$$\delta = \|\mathbf{W}\mathbf{s}\|^2. \tag{7.3}$$

The maximum number of users that can be served by a BS is $K = M$. When $K > M$, M among the K users can be scheduled to be served by the BS simultaneously. The scheduling algorithms are beyond the scope of this study.

In a multicellular system (B BSs), the signal received by a user k served by the BS 0 is given by:

$$y_k = \sqrt{P_k}\mathbf{h}_{0,k}\frac{\mathbf{W}_0\mathbf{s}_0}{\sqrt{\delta_0}} + \sum_{j=1}^{B}\sqrt{P_j}\mathbf{h}_{j,k}\frac{\mathbf{W}_j\mathbf{s}_j}{\sqrt{\delta_j}} + n_k, \tag{7.4}$$

where $\mathbf{h}_{j,k} \in \mathbb{C}^{1\times M}$ is the channel between the BS j and user k, $\mathbf{W}_j \in \mathbb{C}^{M\times K}$ is the precoding matrix used by the BS j, $\mathbf{s}_j$ is the information symbol vector intended to the users of BS j, δ_j is the normalization factor used by the BS j and n_k is the AWGN. P_j is the power received from the BS j including path-loss and shadowing terms and is given by:

$$P_j = P_T K d_j^{-\eta} 10^{\frac{\xi_j}{10}}, \tag{7.5}$$

where K is a constant, d_j is the distance between the considered user and BS j, η is the path-loss exponent and is characteristic of the propagation environment and ξ_j is a Normal random variable with zero mean and standard deviation σ.

From (7.4) we can write:

$$y_k = \frac{P_0}{\sqrt{\delta_0}}s_{0,k} + \sum_{j=1}^{B}P_j\mathbf{h}_{j,k}\frac{\mathbf{W}_j\mathbf{s}_j}{\sqrt{\delta_j}} + n_k. \tag{7.6}$$

The SINR at the user k can, hence be written as:

$$\gamma = \frac{P_0}{\delta_0\left(\sum_{j=1}^{B}P_j\frac{\left\|\mathbf{h}_{j,k}\mathbf{W}_j\right\|^2}{\delta_j} + \sigma_n^2\right)}, \tag{7.7}$$

where σ_n is the noise variance.

Considering an interference limited system where the noise power can be neglected compared to the interference power, the SINR can be approximated as:

$$\gamma \approx \frac{P_0}{\delta_0\left(\sum_{j=1}^{B}P_j\frac{\left\|\mathbf{h}_{j,k}\mathbf{W}_j\right\|^2}{\delta_j}\right)}. \tag{7.8}$$

7.3 Outage Probability

In this section, we will calculate the probability of outage of the ZFBF scheme in a multicellular context. The probability of outage is defined as

$$P_{out} = P[\gamma < \gamma_{th}], \tag{7.9}$$

where γ_{th} is the SINR threshold value. Writing the SINR given by (7.8) as:

$$SINR \approx \frac{X}{Y}, \tag{7.10}$$

where

$$X = \frac{P_0}{\delta_0}, \tag{7.11}$$

and

$$Y = \sum_{j=1}^{B} P_j \frac{\|\mathbf{h}_{j,k}\mathbf{W}_j\|^2}{\delta_j}, \tag{7.12}$$

we need to calculate the probability density function (PDF) of X and Y to derive the outage probability expression.

7.3.1 Constant Shadowing

In this section, we will assume that the shadowing remains constant during the period of study. This assumption allows us to derive a simple closed form expression of the outage probability.

If we assume standard Gaussian information symbols, i.e., the entries of $\mathbf{s}_0$, $s_{0,i}$ are $CN(0,1)$, the PDF of $X = \frac{P_0}{\delta_0}$ is a scaled F-distribution [154] that is given by:

$$f_X(x) = \frac{P_0(M-K+1)}{K} F(x, 2(M-K+1), 2K), \tag{7.13}$$

$$= \frac{M!}{(K-1)!(M-K)!} \frac{P_0^K x^{M-K}}{(P_0+x)^{M+1}}. \tag{7.14}$$

In order to gain insight in this expression, we consider a commonly used approximation of the F-distribution based on the Chi-square distribution [154]. It approximates the F-distribution $F(x, n_1, n_2)$ by a Chi-square distribution with degrees of freedom n_1. In our case $n_1 = 2(M-K+1)$. The PDF of X can hence be expressed as:

$$f_X(x) \approx \frac{K^{M-K+1}}{P_0^{M-K+1}(M-K)!} e^{-\frac{K\,x}{P_0}}\, x^{M-K}. \tag{7.15}$$

The approximation of the useful power X by a Chi-square distribution reveals, in a way, the diversity order of the ZF precoding that cannot be seen from the F-distribution which is $G_{ZF} = M - K + 1$. This conclusion about the diversity order of the ZFBF is somehow expected since the antennas that are not used for the multiplexing gain will necessarily participate to bring diversity to the transmitted signal.

To derive the density power function of the inter-cell interference power Y given by (7.12), we can notice that Y is the sum of positive random variables. Hence, using the central limit theorem for causal functions [17] (see Appendix A.2), the distribution of Y can be approximated by a Gamma distribution that can be written as:

$$f_Y(y) = \frac{y^{\nu-1}\exp(-\frac{y}{\mu})}{\Gamma(\nu)\mu^\nu}, \tag{7.16}$$

where $\nu = \frac{\mathrm{E}[Y]^2}{\mathrm{var}(Y)}$ and $\mu = \frac{\mathrm{var}(Y)}{\mathrm{E}[Y]}$.

To derive the analytical expressions of the parameters ν and μ, let us write Y as:

$$Y = \sum_{j=1}^{B} P_j z_j, \tag{7.17}$$

where

$$z_j = \frac{\|\mathbf{h}_{j,k}\mathbf{W}_j\|^2}{\delta_j}. \tag{7.18}$$

Assuming independent received signals from the interfering BSs, the mean and the variance of Y can be written as:

$$\mathrm{E}[Y] = \sum_{j=1}^{B} P_j \mathrm{E}[z_j], \tag{7.19}$$

$$\mathrm{var}(Y) = \sum_{j=1}^{B} P_j^2 \mathrm{var}(z_j). \tag{7.20}$$

To calculate the mean and the variance of z_j, we can write z_j as:

$$z_j = \frac{U}{V}, \tag{7.21}$$

where $U = \frac{1}{\delta_j}$ and $V = \frac{1}{\|\mathbf{h}_{j,k}\mathbf{W}_j\|^2}$. It can be seen that U and V have the same PDF as X, hence, using the same Chi-square approximation as for the useful power PDF (7.15) (with $P_0 = 1$ in this case), z_j can be seen as the ratio of two correlated Gamma distributed random variables (U and V). From [159], and denoting $\alpha = M - K + 1$, the mean and the second moment of z_j are given by:

$$\mathrm{E}[z_j] = \frac{(1-\rho^2)+\alpha-1}{\alpha-1}, \tag{7.22}$$

$$\mathrm{E}[z_j^2] = \frac{6(1-\rho^2)^2 + 4(\alpha-2)(1-\rho^2)}{(\alpha-1)(\alpha-2)} + 1, \tag{7.23}$$

for $\alpha > 2$, i.e., $M > K+1$, (note that for $\alpha < 2$ the second moment does not exist). $\rho = \frac{\mathrm{Cov}(U,V)}{\sqrt{\mathrm{var}(U)\mathrm{var}(V)}}$ is the correlation coefficient between the two correlated random variables U and V.

Using (7.22) and (7.23), we can derive the variance of z_j that is given by:

$$\mathrm{var}(z_j) = \frac{(5\alpha-4)(1-\rho^2)^2 + 2(\alpha-1)(\alpha-2)(1-\rho^2)}{(\alpha-1)^2(\alpha-2)}. \tag{7.24}$$

Defining $\theta = (1-\rho^2)$, the expressions (7.22) and (7.24) allows us to derive the parameters ν and μ that are given by:

$$\nu = (1-\frac{2(2\alpha-1)\theta^2-(\alpha-1)^2(\alpha-2)}{(5\alpha-4)\theta^2+2(\alpha-1)(\alpha-2)\theta})\frac{\left(\sum_{j=1}^{B} P_j\right)^2}{\sum_{j=1}^{B} P_j^2}, \tag{7.25}$$

$$\mu = \frac{(5\alpha-4)\theta^2+2(\alpha-1)(\alpha-2)\theta}{(\alpha-1)(\alpha-2)\theta+(\alpha-1)^2(\alpha-2)}\frac{\sum_{j=1}^{B} P_j^2}{\sum_{j=1}^{B} P_j}. \tag{7.26}$$

The outage probability can then be calculated as follows:

$$\begin{aligned} P(\gamma < \gamma_{th}) &= \int_0^{\infty}\int_0^{\gamma_{th}y} f_X(x)dx f_Y(y)dy, \\ &= \int_0^{\infty} \frac{1}{(\alpha-1)!}\gamma(\alpha, \frac{K\gamma_{th}y}{P_0})\frac{y^{\nu-1}\exp(-\frac{y}{\mu})}{\Gamma(\nu)\mu^{\nu}}dy. \end{aligned} \tag{7.27}$$

where $\gamma(.,.)$ is the lower incomplete Gamma function as defined in (6.64).

The outage probability expression is given by (equation (6.455-2), page 663 of [132]):

$$P_{out}(\gamma_{th}) = \frac{\Gamma(\nu+\alpha)}{\Gamma(\nu)\mu^{\nu}\alpha!}\frac{P_0^{\nu}(K\gamma_{th})^{\alpha}}{(\gamma_{th}K+\frac{P_0}{\mu})^{\nu+\alpha}}\,{}_2F_1(1,\nu+\alpha;\alpha+1;\frac{\gamma_{th}K}{\gamma_{th}K+\frac{P_0}{\mu}}) \tag{7.28}$$

where ${}_2F_1(.,.;.;.)$ is the Gauss hypergeometric function defined as (6.27).

Using the relation [160]:

$${}_2F_1(a,b;c;x) = (1-x)^{c-a-b}\,{}_2F_1(c-a,b-c;c;x), \tag{7.29}$$

we can write the outage probability (7.28) as:

$$P_{out}(\gamma_{th}) = \frac{1}{B(\alpha,\nu)}\left(\frac{K\gamma_{th}}{K\gamma_{th}+\frac{P_0}{\mu}}\right)^{\alpha}\,{}_2F_1(\alpha,1-\nu,\alpha+1,\frac{K\gamma_{th}}{K\gamma_{th}+\frac{P_0}{\mu}}), \tag{7.30}$$

where $B(.,.)$ is the Beta function defined as $B(p,q) = \frac{\Gamma(p)\Gamma(q)}{\Gamma(p+q)}$. (7.30) is an easily computable closed-form outage probability expression, as it expressed using well known tabulated functions available in most software computation packages such as Matlab.

Let us see how the outage probability behaves near 0. From [160], ${}_2F_1(a,b;c;0) = 1$, then for small $\epsilon > 0$ we can write:

$$P_{out}(\epsilon) \propto \left(\frac{K\mu}{P_0}\epsilon\right)^{\alpha}. \tag{7.31}$$

The asymptotic expression of the outage probability confirms the diversity order of the ZF precoding equal to $\alpha = M-K+1$.

7.3.2 Log-Normal Shadowing

In this section, we will consider the case of a randomly varying shadowing following a log-normal distribution. We will derive an easily computable expression for the outage probability.

In this case, the received power P_j is a log-normal random variable with PDF given by:

$$f_{P_j}(x) = \frac{1}{ax\sigma\sqrt{2\pi}} \exp\left(-\frac{(\ln(x) - a\, m_j)^2}{2a^2\sigma^2}\right), \tag{7.32}$$

where $a = \frac{\ln 10}{10}$ and $m_j = \frac{1}{a} \ln\left(AP_T d_j^{-\eta}\right)$.

For the interference power distribution, the Gamma approximation is still valid, however new expressions of the parameters μ and ν will be given taking into consideration the log-normal variation of the received powers. Referring to the shadowing, we will call these parameters: μ_s and ν_s.

Let us start by recalculating the mean and the variance of the interference power considering this new assumption.

The mean and variance of Y are given by:

$$\mathrm{E}[Y] = \sum_{j=1}^{B} \mathrm{E}[P_j]\mathrm{E}[z_j], \tag{7.33}$$

and

$$\mathrm{var}(Y) = \sum_{j=1}^{B} \mathrm{E}[P_j^2]\mathrm{E}(z_j^2) - \mathrm{E}[P_j]^2\mathrm{E}[z_j]^2. \tag{7.34}$$

From (7.32), we can derive $\mathrm{E}[P_j]$ and $\mathrm{E}[P_j^2]$ that are given by:

$$\mathrm{E}[P_j] = e^{\frac{a^2\sigma^2}{2}} AP_T d_j^{-\eta}, \tag{7.35}$$

$$\mathrm{E}[P_j^2] = e^{2a^2\sigma^2} \left(AP_T d_j^{-\eta}\right)^2. \tag{7.36}$$

Using the expressions (7.22) and (7.35), the mean of Y can be derived and is given by:

$$\mathrm{E}[Y] = e^{\frac{a^2\sigma^2}{2}} AP_T \frac{\theta + \alpha - 1}{(\alpha - 1)} \sum_{j=1}^{B} d_j^{-\eta}. \tag{7.37}$$

From (7.22), (7.24) and (7.36), the variance Y can be calculated and is given by:

$$\mathrm{var}(Y) = (AP_T)^2 G(K, \sigma^2, \theta) \sum_{j=1}^{B} d_j^{-2\eta}, \tag{7.38}$$

where

$$\begin{aligned} G(K,\sigma^2,\theta) &= e^{2a^2\sigma^2}\left(\frac{6\theta^2}{(\alpha-1)(\alpha-2)}+\frac{4\theta}{\alpha-1}+1\right) \\ &- e^{a^2\sigma^2}\left(\frac{\theta^2}{(\alpha-1)^2}+\frac{2\theta}{(\alpha-1)}+1\right). \end{aligned} \tag{7.39}$$

Using the expressions of the mean (7.37) and the variance (7.38), we can easily derive the expressions of the parameters ν_s and μ_s that are given by:

$$\nu_s = \frac{e^{a^2\sigma^2}(\theta+\alpha-1)^2}{(\alpha-1)^2 G(K,\sigma^2,\theta)}\frac{(\sum_{j=1}^{B} d_j^{-\eta})^2}{\sum_{j=1}^{B} d_j^{-2\eta}}, \tag{7.40}$$

$$\mu_s = \frac{(AP_T)^2 G(K,\sigma^2,\theta)(\alpha-1)}{e^{\frac{a^2\sigma^2}{2}}(\theta+\alpha-1)}\frac{\sum_{j=1}^{B} d_j^{-2\eta}}{\sum_{j=1}^{B} d_j^{-\eta}}. \tag{7.41}$$

From (7.28), the outage probability when considering the log-normal shadowing conditioned on the useful received power is given by:

$$P_{out}(\gamma_{th}|P_0) = \frac{1}{B(\alpha,\nu_s)}\left(\frac{K\gamma_{th}}{K\gamma_{th}+\frac{P_0}{\mu_s}}\right)^{\alpha} {}_2F_1(\alpha, 1-\nu_s, \alpha+1, \frac{K\gamma_{th}}{K\gamma_{th}+\frac{P_0}{\mu_s}}). \tag{7.42}$$

Averaging over the distribution of P_0, the outage probability can be written in an integral form as:

$$\begin{aligned} P_{out}(\gamma_{th}) &= \frac{(K\gamma_{th})^{\alpha}}{B(\alpha,\nu_s)}\int_0^{\infty}\frac{1}{(1+\frac{x}{K\gamma_{th}\mu_s})^{\alpha}} \\ &\times {}_2F_1(\alpha, 1-\nu_s; \alpha+1; \frac{1}{1+\frac{x}{K\gamma_{th}\mu_s}}) \\ &\times \frac{1}{a\,x\sigma\sqrt{2\pi}}\exp\left(-\frac{(\ln(x)-a\,m_0)^2}{2a^2\sigma^2}\right)dx. \end{aligned} \tag{7.43}$$

The outage probability (7.43) involves a quickly computable expression using software such as Matlab or Mathematica.

7.4 Simulation Results

In this section, we will begin by verifying the sensitivity of the Gamma approximation given by (7.16) of the interference power PDF to the number of interfering BSs. Figure 7.2 shows a comparison between the Gamma distribution and the simulated PDF when considering 6 and 18 interfering BSs. We can see that the approximation is all the more precise when the

number of surrounding BSs is larger which is predictable since the Gamma approximation is based on the central limit theorem.

To emphasize the degradation of performance induced by the multicell interference, we simulated the outage probability of a single cell system compared to the multicell case (figure 7.3). For the multicell performance, the considered user receives a useful signal from its BS and an interfering signal from the two surrounding rings of BSs (18 interferers). All BSs transmit $P_T = 20$ W, the cell radius is $R_c = 1$ Km and the considered mobile station is at a distance $d = 0.5$ Km from its serving BS. The standard deviation of the log-normal shadowing is taken $\sigma = 6$ dB and the path-loss exponent is $\eta = 3.41$. Each BS serves 4 single antenna users simultaneously. The total bandwidth allocated to the 4 users is $W = 10$ MHz. It can be seen that for an outage probability of 10% we have a loss of more than 10 dB in the SINR.

Figure 7.4 presents a comparison between simulated and analytical performance of the ZF precoding without shadowing. As for the previous figure, we considered cellular system where the BSs are equipped with 6 antennas and we assumed 4 active single antenna terminals per cell. These values corresponds to a typical urban environment. It can be seen that there is a good match between simulated and analytical results.

Figure 7.5 presents a comparison between the performance of the ZF transmission technique when considering log-normal shadowing and without shadowing. We considered the same simulation parameters as for figure 7.4 except the standard deviation of the log-normal shadowing which is set to $\sigma = 4$ dB. From the figure, we can see the degradation of performance induced by the shadowing effect. In fact, for 10% of outage probability, we have a loss of 4 dB in the SINR at the receiver level. We can also see that there is a good agreement between simulation and analytical results.

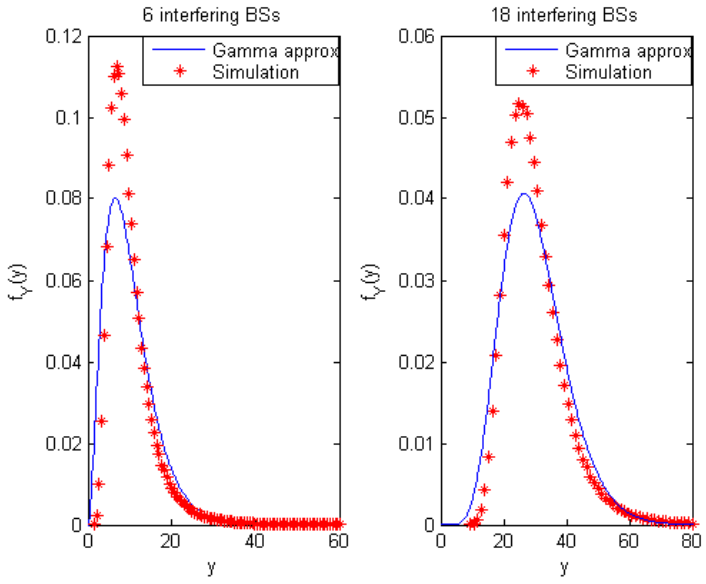

Figure 7.2: Comparison between the simulated PDF and the Gamma approximation.

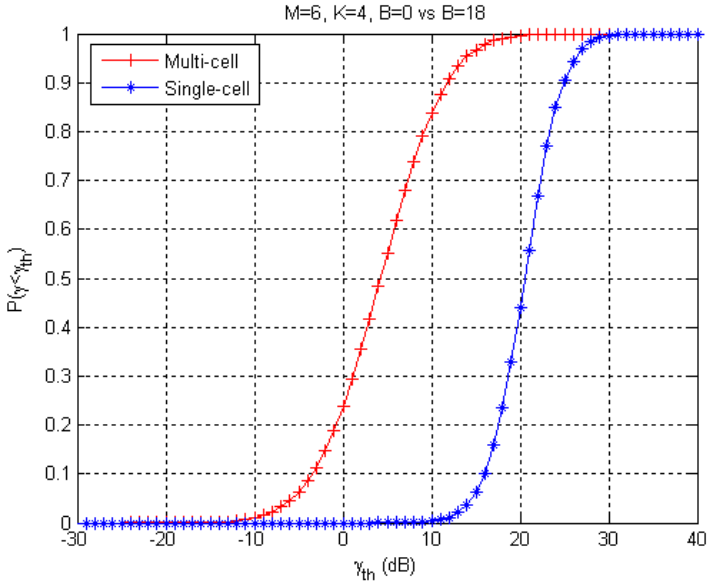

Figure 7.3: Comparison between the ZF precoding performance in a single cell system versus multicell system.

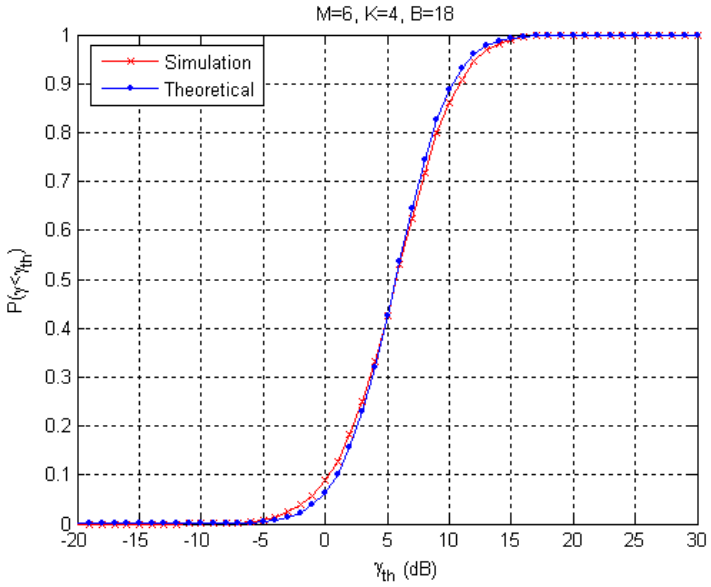

Figure 7.4: P_{out} versus SINR threshold for a multiuser multicellular ZF precoded system (constant shadowing).

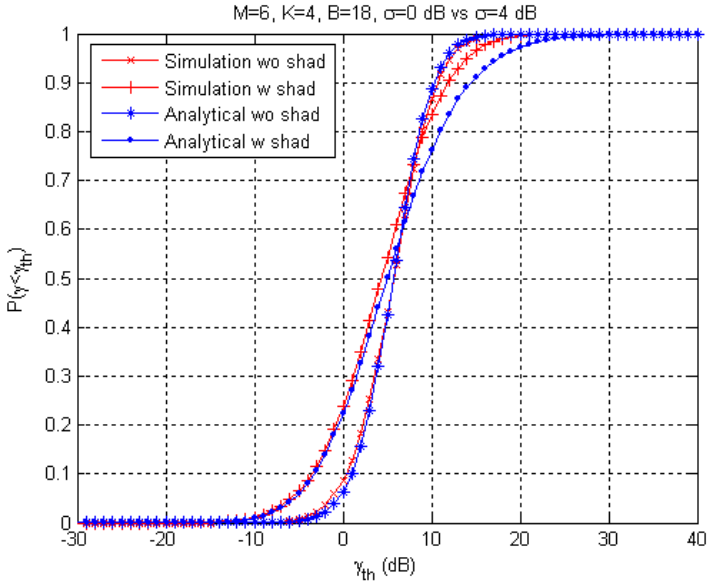

Figure 7.5: Influence of the shadowing on the outage probability of the ZF precoded multiuser multicellular system.

7.5 Conclusion

In this chapter, the performance of the zero forcing linear precoding technique was studied in terms of outage probability. Two expressions have been proposed. The first one corresponds to the case of a slowly varying shadowing compared to the variation of the fast fading in which case we derived a closed form expression involving commonly known tabulated functions. The second expression takes into consideration the log-normal random variation of the shadowing along the time and is in the form of a quickly computable integral.

As a future work, the newly derived expressions can be used for a dynamic study of a system that considers and models arrivals and departures of users in the cell. Another possible extension of this work is to envisage a joint ZF transmission scheme in a multicell cooperation context. In the next chapter, we will consider a cooperative system a diversity transmission scheme namely the MRT.

Chapter 8

Outage Probability of an MRT CoMP Transmission

8.1 Introduction

Coordinated multi-point (CoMP) transmission is a new technique targeted to the LTE-A standard and promising better cellular performance. It consists in a multicell cooperation scheme that takes advantage of the distributed antenna formed by the neighboring cells to mitigate multicell interference and to improve cell-edge and system throughput [161]. In the 3GPP LTE-A, two main schemes were highlighted [162]: the CB/S-CoMP and the JP-CoMP. These two techniques were presented in Section 3.3.1. In this chapter, we will focus on the JP-CoMP scheme. It consists in sharing information across coordinated BSs to serve users cooperatively. The surrounding BSs contribute to transmit the useful signal to the user instead of acting as inteferers. The JP-CoMP was deeply studied in the literature. In [163], a measurement study showed that multicell cooperation attain larger mean capacity than an isolated cell when considering a sufficiently high capacity and a low latency backbone. In [164], a field trial was performed to confirm the throughput enhancement introduced by JP-CoMP strategy. In [165, 98], a numerical study of different joint processing schemes showed the potential of this technique to enhance the overall system performance. In [166], the performance of the femtocell coordination strategy was studied for the ZF and the MRT schemes. Two power allocation algorithms were proposed and compared.

In [163, 164, 98, 166], authors performed simulation, measurement or field study but no theoretical studies were conducted. In [12], an analytical expression of the capacity outage probability was derived for an open-loop Alamouti-like CoMP downlink transmission in Rayleigh fading. The proposed SINR expression can only be achieved when using a distributed Alamouti for two cooperating BSs. In [13], an analytical study of a multicell multi-antenna cooperative MRT/MRC scheme was conducted. An analytical expression of the PDF of the SIR was derived considering path-loss, shadowing and Rayleigh fading.

However, the authors resorted to many assumptions: a cell-edge user served in cooperation is at equal distances from the cooperative BSs, a Gamma distributed shadowing and a Poisson spatial distribution of interfering transmitters. Furthermore, there is a significant difference between simulation and theoretical results.

In this chapter, our main contribution is to perform an analytical study of a downlink coherent multicell cooperation system using the MRT precoding technique. The MRT [167] is a transmission technique achieving maximum transmit diversity and maximizing the SNR. We propose an approximate outage probability expression of the downlink multiple antenna JP-CoMP using the MRT precoding considering path-loss, constant shadowing and Rayleigh fading. Our analytical approach consolidates the numerical performance studies provided in the literature.

The main results presented in this chapter have been published in [168].

8.2 MRT Scheme

The maximum ratio transmission scheme was proposed for the first time in [167]. It is a transmission diversity technique that, unlike the MRC, moves the burden from the receiver to the transmitter side. Unlike the Alamouti scheme which is also a well-known transmission diversity scheme, the MRT has as objective to maximize the SNR at the receiver.

Assume a single cell single user $M \times N$ MIMO system, the received signal can be written as:

$$\mathbf{y} = \mathbf{H}\mathbf{W}s + \mathbf{n}, \tag{8.1}$$

where $\mathbf{H} \in \mathbb{C}^{N \times M}$ is the channel matrix, $\mathbf{W} \in \mathbb{C}^{M \times 1}$ satisfying $\|\mathbf{W}\|^2 \leq 1$ is the precoding vector, s is the information symbol and $\mathbf{n} \in \mathbb{C}^{N \times 1}$ is the AWGN. The SNR is hence given by:

$$\gamma = \frac{\|\mathbf{H}\mathbf{W}\|^2}{\sigma_n^2} \mathrm{E}[|s|^2], \tag{8.2}$$

where σ_n^2 is the AWGN variance. The scheme that maximizes $\|\mathbf{H}\mathbf{W}\|^2$ under the constraint $\|\mathbf{W}\|^2 \leq 1$ is the MRT. In general $\|\mathbf{H}\mathbf{W}\|^2$ verifies:

$$\frac{\|\mathbf{H}\mathbf{W}\|^2}{\|\mathbf{W}\|^2} \leq \lambda_{max}(\mathbf{H}^H\mathbf{H}), \tag{8.3}$$

where $\lambda_{max}(\mathbf{H}^H\mathbf{H})$ is the largest eigenvalue of $\mathbf{H}^H\mathbf{H}$. The MRT precoder is in this case the normalized eigenvector associated to $\lambda_{max}(\mathbf{H}^H\mathbf{H})$.

If we now consider a single antenna receiver, i.e., $N = 1$, we have:

$$\left|\mathbf{h}^T\mathbf{W}\right|^2 \leq \|\mathbf{h}\|^2 \|\mathbf{W}\|^2 = \|\mathbf{h}\|^2, \tag{8.4}$$

where $\mathbf{h} \in \mathbb{C}^{1\times M}$. In (8.4), the equality is verified if $\mathbf{W}$ is proportional to $\mathbf{h}^T$, the MRT precoder is hence, in the MISO case, given by:

$$\mathbf{W} = \frac{\mathbf{h}^T}{\|\mathbf{h}\|}. \tag{8.5}$$

In multicellular systems, the MRT is no more optimal because of the presence of ICI interference, however it remains an interesting technique due to its implementation simplicity and near optimal performance.

8.3 JP-CoMP MRT System Model

Consider a downlink multicellular (B base stations) multiuser system (K active users) and consider multiple antenna BSs (M antennas) and single antenna user equipments. Let a *cluster* be a subset of BSs cooperating to serve a user. The clusters are disjoint. Some selection algorithms of the BSs in a cluster have been introduced in Section 3.3.2. In this chapter, we consider the simple criterion based on the minimization of the distance depending path-loss. A cluster of BSs transmits to a single user per Transmit Time Interval (TTI). BSs use the MRT to transmit their data. We assume coherent multicell transmission which needs a tight synchronization across transmitting BSs (like in [169]) that can be ensured using low-latency and high-capacity backhaul communication. The information data intended to a user are shared by all BSs in its cooperation cluster. CSI between the considered user and the cooperating BSs are estimated using feedback for the frequency division duplex (FDD) mode or uplink-downlink channel reciprocity for the time division duplex (TDD) mode. The cluster of BSs serving a user k is denoted B_k. The signal received by a user k is given by [170]:

$$y_k = \sum_{b\in B_k} \sqrt{p_{b,k}}\mathbf{h}_{b,k}\mathbf{x}_{b,k} + \sum_{i=1,i\neq k}^{K} \sum_{j\in B_i} \sqrt{p_{j,k}}\mathbf{h}_{j,k}\mathbf{x}_{j,i} + n, \tag{8.6}$$

where $p_{b,k}$ is the power received by user k from BS b, $\mathbf{h}_{b,k} \in \mathbb{C}^{1\times M}$ is the complex Gaussian channel between user k and BS b, n is the AWGN and $\mathbf{x}_{b,k} \in \mathbb{C}^{M\times 1}$ is the MRT data vector transmitted from BS b to the user k and is given by:

$$\mathbf{x}_{b,k} = \frac{\mathbf{h}_{b,k}^T}{\|\mathbf{h}_{b,k}\|} s_k, \tag{8.7}$$

where $s_k \in \mathbb{C}$ is the normalized information symbol intended to user k from BS b. Denoting P_T the total transmit power of BS b, it can be clearly seen that this power is the same regardless of the number of transmit antennas M and hence the transmitted signal meets the total transmit power constraint. The received power $p_{b,k}$ includes path-loss and shadowing:

$$p_{b,k} = P_T C d_{b,k}^{-\eta} 10^{\frac{\xi_{b,k}}{10}}, \tag{8.8}$$

where C is a constant, $d_{b,k}$ is the distance between the considered user and BS b, η is the path-loss exponent and $\xi_{b,k}$ is a Normal random variable with zero mean and standard deviation σ.

The output SINR perceived by a user k is given by:

$$\gamma_k = \frac{\left(\sum_{b\in B_k}\sqrt{p_{b,k}}\mathbf{h}_{b,k}\frac{\mathbf{h}_{b,k}^T}{\|\mathbf{h}_{b,k}\|}\right)^2}{\sum_{i=1,i\neq k}^{K}\left|\sum_{j\in B_i}\sqrt{p_{j,k}}\mathbf{h}_{j,k}\frac{\mathbf{h}_{j,i}^T}{\|\mathbf{h}_{j,i}\|}\right|^2+\sigma_n^2}, \tag{8.9}$$

$$= \frac{\left(\sum_{b\in B_k}\sqrt{p_{b,k}}\,\|\mathbf{h}_{b,k}\|\right)^2}{\sum_{i=1,i\neq k}^{K}\left|\sum_{j\in B_i}\sqrt{p_{j,k}}\mathbf{h}_{j,k}\frac{\mathbf{h}_{j,i}^T}{\|\mathbf{h}_{j,i}\|}\right|^2+\sigma_n^2}. \tag{8.10}$$

In a dense urban interference limited system, the noise power can be neglected compared to the interference power, thus the SINR can be approximated as:

$$\gamma_k \approx \frac{X}{Y}, \tag{8.11}$$

where

$$X = \left(\sum_{b\in B_k}\sqrt{p_{b,k}}\,\|\mathbf{h}_{b,k}\|\right)^2, \tag{8.12}$$

$$Y = \sum_{i=1,i\neq k}^{K}\left|\sum_{j\in B_i}\sqrt{p_{j,k}}\mathbf{h}_{j,k}\frac{\mathbf{h}_{j,i}^T}{\|\mathbf{h}_{j,i}\|}\right|^2. \tag{8.13}$$

8.4 Outage Probability

The outage probability is defined as:

$$P_{out} = P[\gamma_k < \gamma_{th}] \approx P[\frac{X}{Y} < \gamma_{th}], \tag{8.14}$$

where γ_{th} is the SINR threshold value characterizing the considered service. To determine the outage probability expression we need the probability density function (PDF) of X (8.12) and Y (8.13).

8.4.1 Useful Power PDF

Let us derive the PDF of X. X can be written as:

$$X = U^2, \quad U = \sum_{b\in B_k}\sqrt{p_{b,k}}\,\|\mathbf{h}_{b,k}\|\,. \tag{8.15}$$

U can also be written as:

$$U = \sum_{b \in B_k} \sqrt{p_{b,k}} \sqrt{\sum_{i=1}^{M} |h_{b,k,i}|^2}. \tag{8.16}$$

To the best of our knowledge, there is no possible closed form expression for the PDF of U. We will hence use the central limit approximation for causal functions [17] (Appendix A.2). It permits to approximate the sum of positive independent and not necessarily identically distributed random variables by a Gamma distribution given by:

$$f_U(u) = \frac{u^{\nu-1} e^{-\frac{u}{\theta}}}{\Gamma(\nu)\theta^{\nu}}. \tag{8.17}$$

where $\nu = \frac{\mathrm{E}[U]^2}{\mathrm{var}(U)}$ and $\theta = \frac{\mathrm{var}(U)}{\mathrm{E}[U]}$.

To derive ν and θ, let us calculate the mean and the variance of U, $\mathrm{E}[U]$ can be derived as follows:

$$\mathrm{E}[U] = \sum_{b \in B_k} \sqrt{p_{b,k}} \mathrm{E}\left[\sqrt{\sum_{i=1}^{M} |h_{b,k,i}|^2} \right]. \tag{8.18}$$

Denoting $V = \sqrt{\sum_{i=1}^{M} |h_{b,k,i}|^2}$, it can be noticed, that V is a square root of a Gamma distributed random variable and thus we can write the PDF of V as:

$$f_V(v) = \frac{2}{(M-1)!} v^{2M-1} e^{-v^2}. \tag{8.19}$$

$\mathrm{E}[V]$ can be derived using (8.19) and is given by:

$$\begin{aligned} \mathrm{E}[V] &= \int_0^{\infty} \frac{2}{(M-1)!} v^{2M} e^{-v^2} dv, \\ &= \frac{(2M-1)!!}{2^M (M-1)!} \sqrt{\pi}, \end{aligned} \tag{8.20}$$

where $(2N+1)!! = 1 \times 3 \times 5 ... \times (2N+1)$ and $(2N)!! = 2 \times 4 \times ...(2N)$. From (8.18), $\mathrm{E}[U]$ is given by:

$$\mathrm{E}[U] = \frac{(2M-1)!!}{2^M (M-1)!} \sqrt{\pi} \sum_{b \in B_k} \sqrt{p_{b,k}}. \tag{8.21}$$

The variance of U can be derived as follows:

$$\begin{aligned}
\mathrm{var}(U) &= \mathrm{E}[\sum_{b\in B_k}\sqrt{p_{b,k}}\,\|\mathbf{h}_{b,k}\|\sum_{n\in B_k}\sqrt{p_{n,k}}\,\|\mathbf{h}_{n,k}\|] \\
&- (\mathrm{E}[\sum_{b\in B_k}\sqrt{p_{b,k}}\,\|\mathbf{h}_{b,k}\|])^2, \\
&= \sum_{b\in B_k} p_{b,k}\mathrm{E}[\|\mathbf{h}_{b,k}\|^2] + \sum_{b\in B_k}\sum_{j\in B_k, j\neq b}\sqrt{p_{b,k}}\sqrt{p_{j,k}}\mathrm{E}[\|\mathbf{h}_{b,k}\|]\mathrm{E}[\|\mathbf{h}_{j,k}\|] \\
&- \sum_{b\in B_k}\sum_{j\in B_k, j\neq b}\sqrt{p_{b,k}}\sqrt{p_{j,k}}\mathrm{E}[\|\mathbf{h}_{b,k}\|]\mathrm{E}[\|\mathbf{h}_{j,k}\|] - \sum_{b\in B_k} p_{b,k}(\mathrm{E}[\|\mathbf{h}_{b,k}\|])^2, \\
&= \sum_{b\in B_k} p_{b,k}\mathrm{E}[\|\mathbf{h}_{b,k}\|^2] - \sum_{b\in B_k} p_{b,k}(\mathrm{E}[\|\mathbf{h}_{b,k}\|])^2. \qquad (8.22)
\end{aligned}$$

Having $\mathrm{E}[\|\mathbf{h}_{b,k}\|^2] = M$ and $\mathrm{E}[\|\mathbf{h}_{b,k}\|] = \frac{(2M-1)!!}{2^M(M-1)!}\sqrt{\pi}$, var(U) can be written as:

$$\mathrm{var}(U) = (M - \pi(\frac{(2M-1)!!}{2^M(M-1)!})^2)\sum_{b\in B_k} p_{b,k}. \qquad (8.23)$$

The parameters ν and θ are thus given by:

$$\nu = \frac{(2M-1)!!^2}{M2^{2M}(M-1)!^2 - \pi(2M-1)!!^2}\frac{(\sum_{b\in B_k}\sqrt{p_{b,k}})^2}{\sum_{b\in B_k} p_{b,k}}, \qquad (8.24)$$

$$\theta = \frac{M2^{2M}(M-1)!^2 - \pi(2M-1)!!^2}{2^M(M-1)!(2M-1)!!\sqrt{\pi}}\frac{\sum_{b\in B_k} p_{b,k}}{\sum_{b\in B_k}\sqrt{p_{b,k}}}. \qquad (8.25)$$

Using the Gamma approximation of the PDF of U, we can derive the CDF of X as follows:

$$\begin{aligned}
F_X(v) &= \int_0^{\sqrt{v}} \frac{u^{\nu-1}e^{-\frac{u}{\theta}}}{\Gamma(\nu)\theta^\nu}du, \\
&= \frac{\gamma(\nu, \frac{\sqrt{v}}{\theta})}{\Gamma(\nu)}, \qquad (8.26)
\end{aligned}$$

where $\gamma(.,.)$ is the lower incomplete Gamma function defined as (6.64) and $\Gamma(.)$ is the Gamma function.

It is clear from (8.21) and (8.23) that adding new cooperating BSs improves the mean useful signal power but increases also its variability. We can also show that the mean and the variance are increasing with M (figures 8.1 and 8.2).

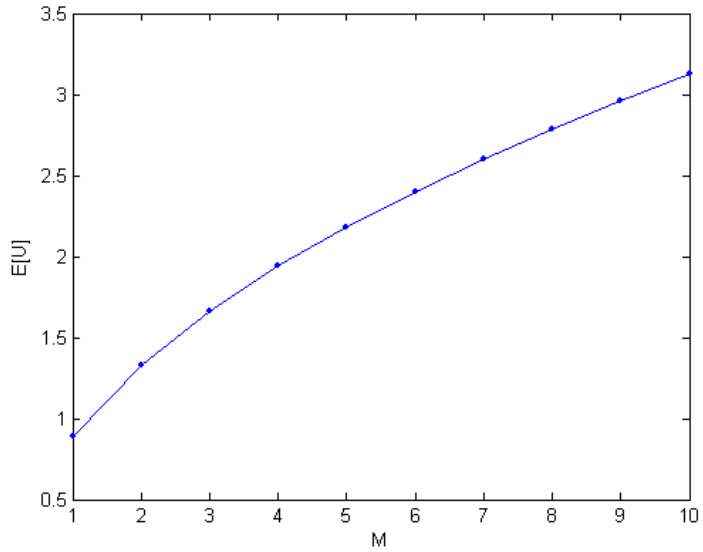

Figure 8.1: Mean of U versus the number of antennas M.

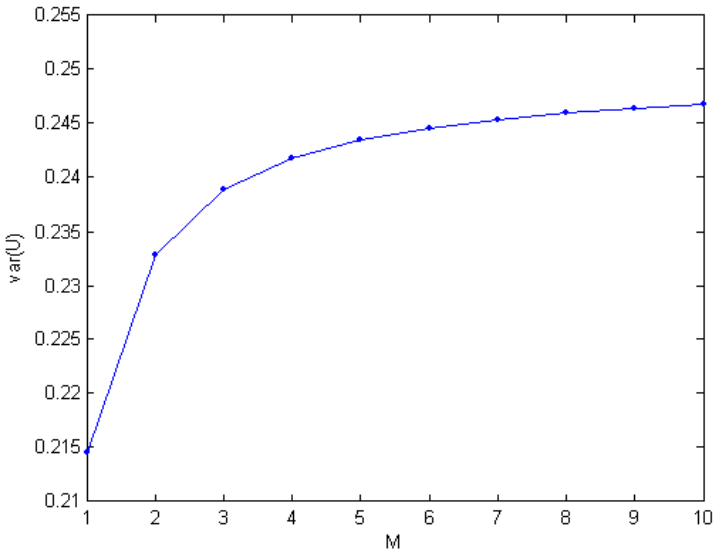

Figure 8.2: Variance of U versus the number of antennas M

8.4.2 Interference Power PDF

Having the useful power PDF, we need to derive the interference power PDF to calculate the outage probability expression. We can write the expression (8.13) as:

$$Y = \sum_{i=1, i\neq k}^{K} \left| \sum_{j \in B_i} \sqrt{p_{j,k}} g_{j,k,i} \right|^2, \tag{8.27}$$

where $g_{j,k,i} = \mathbf{h}_{j,k} \frac{\mathbf{h}_{j,i}^T}{\|\mathbf{h}_{j,i}\|}$. It was proven in [49] (see Appendix A.4), that, since the elements of $\mathbf{h}_{j,k}$ and $\mathbf{h}_{j,i}$ are zero-mean complex Gaussian random variables, $g_{j,k,i}$ is also complex Gaussian independent of $\mathbf{h}_{j,i}$. Let $c_{k,i} = \sum_{j \in B_i} \sqrt{p_{j,k}} g_{j,k,i}$, it is the sum of independent complex Gaussian random variables. Y can be written as:

$$Y = \sum_{i=1, i\neq k}^{K} |c_{k,i}|^2, \tag{8.28}$$

$\{c_{k,i}\}_{i=1...K, i\neq k}$ being independent zero-mean complex Gaussian elements with variances:

$$\lambda_{i,k} = \mathrm{var}(c_{k,i}) = \sum_{j \in B_i} p_{j,k}. \tag{8.29}$$

The PDF of Y can hence be derived in the same way as in Section 5.4.1, and is given by given by [130]:

$$f_Y(y) = \sum_{i=1, i\neq k}^{K} \frac{\Pi_i}{\lambda_{i,k}} \exp(-\frac{y}{\lambda_{i,k}}), \tag{8.30}$$

where $\Pi_i = \prod_{p=1..K, p\neq k, p\neq i} \frac{\lambda_{p,k}}{\lambda_{p,k} - \lambda_{i,k}}$.

Some $\{\lambda_{p,k}\}_{p=1..K, p\neq k}$ may be equal. In this case, a very small number can be added to differentiate equal terms [130] and hence the distribution (8.30) is still valid and yields good results.

8.4.3 Outage Probability

Having the PDFs of X and Y, and since they are independent random variables, we derive the outage probability as follows:

$$\begin{aligned} P(\gamma_k < \gamma_{th}) &= \int_0^\infty F_X(\gamma_{th} y) f_Y(y) dy, \\ &= \sum_{i=1, i\neq k}^{K} \frac{\Pi_i}{\lambda_{i,k} \Gamma(\nu)} \int_0^\infty \exp(-\frac{y}{\lambda_i}) \gamma(\nu, \frac{\sqrt{\gamma_{th} y}}{\theta}) dy. \end{aligned} \tag{8.31}$$

The outage probability is given by [132]:

$$P(\gamma_k < \gamma_{th}) = \sum_{i=1, i\neq k}^{K} \Pi_i \left(\frac{\sqrt{\gamma_{th}\lambda_{i,k}}}{2\theta} \right)^{\nu} U\left(\frac{\nu}{2}, \frac{1}{2}, \frac{\gamma_{th}\lambda_{i,k}}{4\theta^2} \right), \tag{8.32}$$

where $U(.,.,.)$ is the confluent hypergeometric function of second kind defined as [171]:

$$U(a,b;z) = \frac{1}{\Gamma} \int_0^{\infty} e^{-zt} t^{a-1} (1+t)^{b-a-1} dt. \tag{8.33}$$

Expression (8.32) is a closed form approximation of the outage probability. It is a finite sum over the number of the active users in the network of easily computable elements allowing for rapid evaluation of the cooperative MISO system performance.

Asymptotically, the confluent hypergeometric function is approximated as [171]:

$$U(a,b;z) \underset{z\to 0}{\longrightarrow} \left(\frac{1}{z} \right)^{a}. \tag{8.34}$$

We can hence conclude that, when $\gamma_{th} \to 0$, the outage probability varies as:

$$P_{out}(\gamma_{th}) \propto \left(\frac{\gamma_{th}}{4\theta^2} \right)^{\nu}. \tag{8.35}$$

The diversity order of the MRT scheme is hence given by: $G = \nu$, ν being the shape parameter of the Gamma distribution approximating the useful power given by:

$$\nu = \frac{(2M-1)!!^2}{M2^{2M}(M-1)!^2 - \pi(2M-1)!!^2} \frac{(\sum_{b\in B_k} \sqrt{p_{b,k}})^2}{\sum_{b\in B_k} p_{b,k}}. \tag{8.36}$$

Let us see how ν varies with the number of cooperating BSs and the number of antennas per BS. If we assume equal received powers $p_{b,k} = p$ for $b \in B_k$, ν can be written as:

$$\nu = \frac{(2M-1)!!^2}{M2^{2M}(M-1)!^2 - \pi(2M-1)!!^2} Np. \tag{8.37}$$

Drawing ν as a function of M, we can see from figure 8.3, that ν is a linear function of M. Hence, $\nu \sim N \times M$. The intuitive diversity order product of the number of transmit antennas and of the number of cooperating BSs emerges.

8.5 Simulation results

Figure 8.4 presents a comparison between simulated and theoretical outage probability. We consider a network of 19 BSs equipped with 4 antennas (the central cell and two surrounding rings of BSs). We consider $N = 3,\ 4$ or 5 cooperating BSs and 5 interfering clusters of BSs

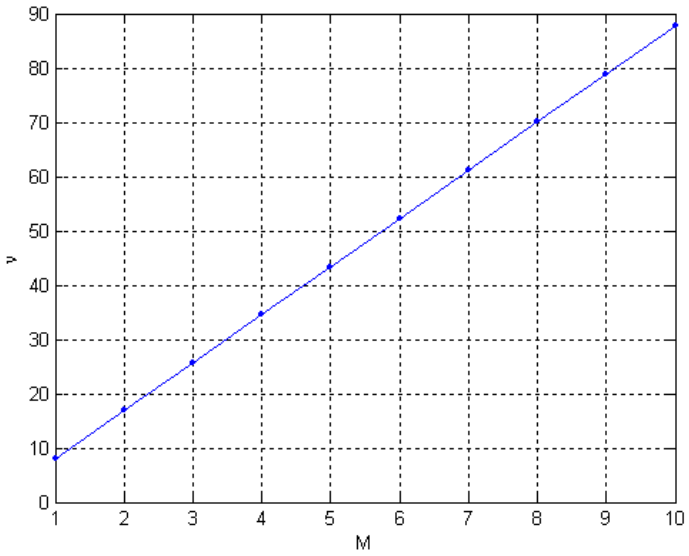

Figure 8.3: ν versus the number of transmit antennas M.

so that $K = 6$. A user is served by the N BSs with smallest path-loss degradation. We first generate 19 realizations of the shadowing using a log-normal random variable with $\sigma = 6$ dB standard deviation. In each iteration of our Monte Carlo simulation, the SINR is calculated using these same realizations. All BSs emit a power of 20 W. The cell radius is $R_c = 500$ m and the considered mobile station is at a distance $d = 400$ m from the central BS (cell-edge user). We assume that we are in an urban environment with path-loss exponent $\eta = 3.41$, carrier frequency $f_0 = 2$ GHz, and path-loss constant $C = 4.95 \times 10^{-4}$ [24]. The figure shows that there is a good match between simulations and analytical results. We can see that the approximation is all the more precise when the number of BSs is larger; however, it still holds even for a small number of cooperating BSs (3 or 4 BSs). We can also notice the considerable gain of performance of the CoMP strategy over the non cooperative case.

In figure 8.5, we plot the outage probability of the SIR and of the SINR for $R_c = 500$ m and $R_c = 1$ Km. Thermal noise power is computed as $\sigma_n^2 = N_0 W$ where $N_0 = -174$ dBm/Hz is the noise power density and W is the system bandwidth. Considering the same system parameters as for figure 8.4, it can be seen that for a dense urban environment where $R_c \leq 500$ m and for a bandwidth of $W = 20$ MHz, the two curves are superposed, thus the influence of the noise power is negligible compared to the interference power. In this case, the system is said *interference limited*. The difference between SIR and SINR outage probability becomes significant only for large cell ranges ($R_c \geq 1$ Km), large system bandwidths ($W \geq 10$ MHz) and high SINR. On figure 8.5, we can note however that even for $R_c = 1$ Km, $W = 20$ MHz, our formula can be efficiently used in the low SINR region

(for coverage studies for example).

In figure 8.6, we fix $N = 3$ and varies $M = 1$, 2 or 4. Again, we notice that our formula provides a good approximation of the outage probability. As an expected result, we can observe that increasing the number of antennas per BS enhances the system performance and that the improvement is decreasing with M. This is a classical result related to the diversity gain brought by multiple antenna at the BSs.

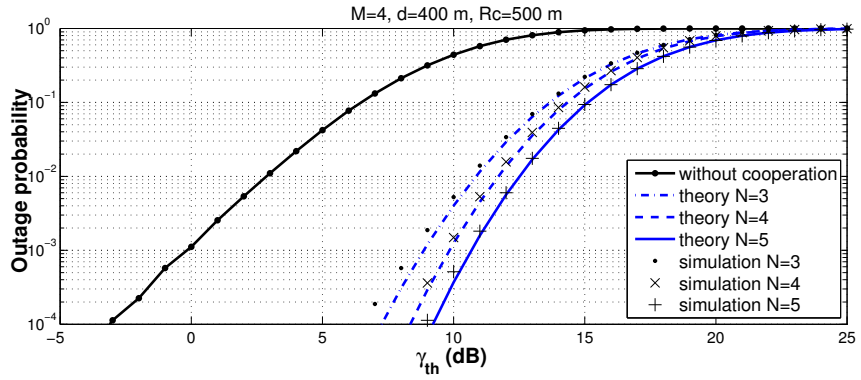

Figure 8.4: Comparison between simulated and analytical results of the outage probability without CoMP and with CoMP MRT strategy for 3, 4 or 5 cooperating BSs.

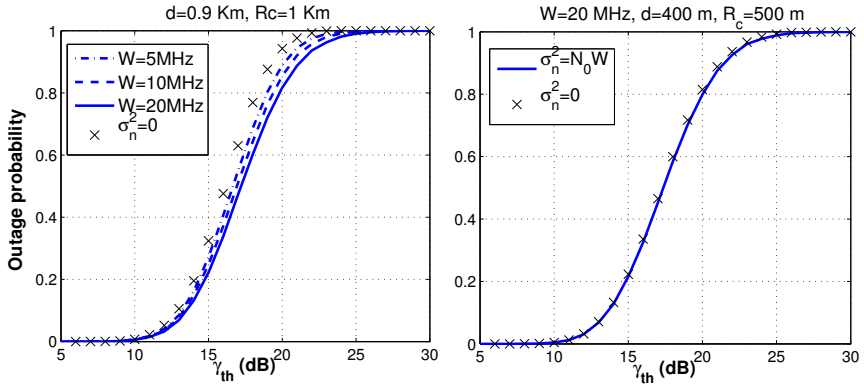

Figure 8.5: Impact of the noise power on the outage probability.

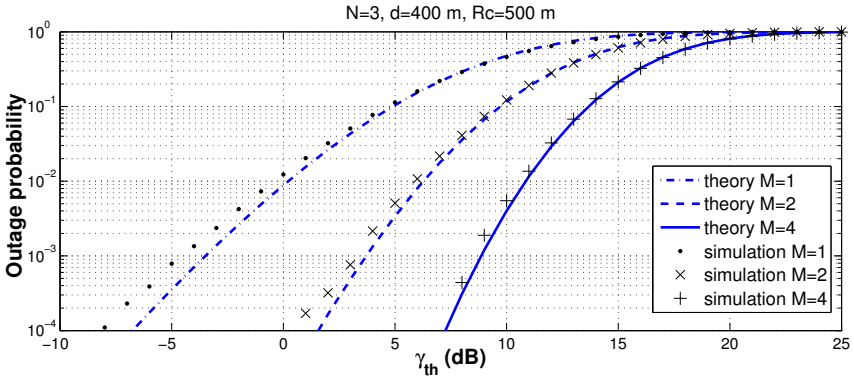

Figure 8.6: Outage probability versus SINR threshold for a downlink multicellular system using CoMP and $M = 1$, 2, 4 antennas per BS.

8.6 Conclusion

In this chapter, the performance of the joint processing maximum ratio transmission technique was studied in terms of outage probability. A closed-form expression has been derived using a Gamma approximation of useful power PDF and an exact interference power PDF. Simulation validates the derived outage probability expression. Our model is definitely optimistic since we assume perfect CSI at the transmitter. A more realistic approach should take into consideration the imperfectness of the CSI or consider open loop diversity achieving techniques, e.g., space time coding.

Chapter 9

Dynamic System Performance of SISO, MISO and MIMO Systems

9.1 Introduction

In this chapter, we propose an example of application of some of the previously obtained SIR distributions to a dynamic study. We will consider a dynamic traffic demand. This assumption has been considered in [14], where authors derived an analytical performance study for downlink data channels with dynamic traffic demand in a single cell system considering path-loss effect. In [58], the same authors, derived upper and lower bounds of the flow throughput in a multicell SISO system taking into consideration again the path-loss effect. In [15], the author studied the influence of the proportional fair channel-aware scheduling on the mean user throughput when considering a dynamic set of users. We extend these results by an analytical performance comparison between SISO, 2×1 MISO Alamouti and $2 \times N$ Alamouti with MRC receiver systems in a dynamic traffic demand context for downlink multicellular systems. We consider a time-shared system where each user transmits in a different time slot. The cell being divided into concentric rings, we compare the flow throughput of each system in each ring with or without admission control.

This chapter is organized as follows. In Section 9.2, we recall the three system models and, based on the obtained SIR CDFs, we propose the SINR PDFs as well as their fluid model formulation. Section 9.3 presents the dynamic traffic model used in our analysis and the analytical expressions of the mean flow throughput. In Section 9.4, systems performance is presented and discussed. Finally, in Section 9.5 some concluding remarks are proposed.

The results of the study conducted in this chapter were presented in [172].

9.2 System Models

In this section, results obtained in Chapters 4 and 6 are recalled for completeness. This part can be skipped by the reader having read these chapters.

9.2.1 SISO System

Consider a SISO multi-cellular system and consider a single user per cell. The base-station (BS) common transmit power is denoted P_T. The signal received by a user served by the BS 0 and interfered by B BSs is given by:

$$y = \sqrt{P_0} h_0 x_0 + \sum_{j=1}^{B} \sqrt{P_j} h_j x_j + n, \tag{9.1}$$

where h_j is the flat fading Rayleigh channel gain between the BS j and the considered user, x_j is the signal transmitted by BS j and n is the additive white Gaussian noise. $P_j = K P_T d_j^{-\eta}$ is the power received by the user from BS j including the path-loss term, where K is a constant, d_j is the distance between BS j and the considered user and $\eta > 2$ is the path-loss exponent.

The output SINR at the considered user can be written as:

$$\gamma_{SISO} = \frac{P_0 |h_0|^2}{\sum_{j=1}^{B} P_j |h_j|^2 + \sigma_n^2}. \tag{9.2}$$

In an interference limited system the SINR can be approximated by:

$$\gamma_{SISO} \approx \frac{X_{SISO}}{Y_{SISO}}, \tag{9.3}$$

where

$$X_{SISO} = P_0 |h_0|^2, \quad \text{and} \quad Y_{SISO} = \sum_{j=1}^{B} P_j |h_j|^2. \tag{9.4}$$

Since we considered Rayleigh flat fading, it can be easily noticed that X_{SISO} is exponentially distributed with probability density function (PDF):

$$f_{X_{SISO}}(x) = \frac{1}{P_0} e^{-\frac{x}{P_0}}. \tag{9.5}$$

Using the central limit theorem for causal function [17], the PDF of Y_{SISO} can be approximated by a Gamma distribution and is given by:

$$f_{Y_{SISO}}(y) = \frac{y^{\nu-1}}{\Gamma(\nu)\delta^{\nu}} e^{-\frac{y}{\delta}}. \tag{9.6}$$

where $\nu = \frac{\mathrm{E}(y)^2}{\mathrm{var}(y)}$ and $\delta = \frac{\mathrm{var}(y)}{\mathrm{E}(y)}$ are given by [112]:

$$\nu = \frac{(\sum_{j=1}^{B} P_j)^2}{\sum_{j=1}^{B} P_j^2},\ \delta = \frac{\sum_{j=1}^{B} P_j^2}{\sum_{j=1}^{B} P_j}. \tag{9.7}$$

Using the PDFs (9.5) and (9.6) we can derive the PDF of the SINR for a SISO system as:

$$\begin{aligned} f_{\gamma_{SISO}}(\gamma) &= \int_0^{\infty} f_{X_{SISO}}(\gamma y) f_{Y_{SISO}}(y) y dy, \\ &= \frac{P_0^{\nu} \delta \nu}{(\delta\gamma + P_0)^{\nu+1}}. \end{aligned} \tag{9.8}$$

9.2.2 MISO Alamouti System

Consider, now, a MISO Alamouti multi-cellular system where each BS is equipped with two antennas and the users equipment with a single antenna. All BSs use the Alamouti code to transmit their data. At the receiver the signal is multiplied by the Alamouti receiver (see e.g. [173]).

By pre-multiplying the received signal by the channel transpose conjugate of the channel $\mathbf{H}_0$, the signal at the receiver becomes:

$$\begin{aligned} \mathbf{H}_0^H \mathbf{y} &= \sqrt{\frac{P_0}{2}} \begin{bmatrix} |h_{1,0}|^2 + |h_{2,0}|^2 & 0 \\ 0 & |h_{1,0}|^2 + |h_{2,0}|^2 \end{bmatrix} \mathbf{x}_0 \\ &+ \sum_{j=1}^{B} \sqrt{\frac{P_j}{2}} \begin{bmatrix} h_{1,0} & h_{2,0} \\ h_{2,0}^* & -h_{1,0}^* \end{bmatrix}^H \begin{bmatrix} h_{1,j} & h_{2,j} \\ h_{2,j}^* & -h_{1,j}^* \end{bmatrix} \mathbf{x}_j \\ &+ \begin{bmatrix} h_{1,0} & h_{2,0} \\ h_{2,0}^* & -h_{1,0}^* \end{bmatrix}^H \mathbf{n}. \end{aligned} \tag{9.9}$$

where $\mathbf{x_j}$ is the symbols vector transmitted by BS j, $h_{i,j}$ is the flat fading Rayleigh channel gain between the antenna i of BS j and its user (the flat fading is assumed to be quasi-static over the two channel use periods), and $\mathbf{n}$ is the additive white Gaussian noise vector with covariance matrix $\sigma_n^2\mathbf{I}$. P_j is the received power from the j^{th} BS (P_0 is the power received from the serving BS) including path-loss.

The output SINR per stream is, hence, given by:

$$\gamma_{Alam} = \frac{\frac{P_0}{2}(|h_{1,0}|^2 + |h_{2,0}|^2)}{\sum_{j=1}^{B} \frac{P_j}{2} \frac{|h_{1,0}^* h_{1,j} + h_{2,0} h_{2,j}^*|^2 + |h_{1,0}^* h_{2,j} - h_{2,0} h_{1,j}^*|^2}{|h_{1,0}|^2 + |h_{2,0}|^2} + \sigma_n^2}. \tag{9.10}$$

In an interference limited system, the SINR of the MISO Alamouti system can be again

approximated as: $\gamma_{Alam} \approx X_{Alam}/Y_{Alam}$, where

$$X_{Alam} = \frac{P_0}{2}(|h_{1,0}|^2 + |h_{2,0}|^2), \tag{9.11}$$

$$Y_{Alam} = \sum_{j=1}^{B} \frac{P_j}{2} \frac{|h_{1,0}^* h_{1,j} + h_{2,0} h_{2,j}^*|^2 + |h_{1,0}^* h_{2,j} - h_{2,0} h_{1,j}^*|^2}{|h_{1,0}|^2 + |h_{2,0}|^2}. \tag{9.12}$$

From [147], the PDF of X_{Alam} is given by:

$$f_{X_{Alam}}(x) = \frac{4x}{P_0^2} e^{-\frac{2x}{P_0}}. \tag{9.13}$$

and the PDF of Y_{Alam} is approximated by:

$$f_{Y_{Alam}}(y) = \frac{y^{\alpha-1} \exp(-\frac{y}{\beta})}{\Gamma(\alpha)\beta^\alpha}, \tag{9.14}$$

where $\alpha = \frac{\mathrm{E}[Y]^2}{\mathrm{var}(Y)}$ and $\beta = \frac{\mathrm{var}(Y)}{\mathrm{E}[Y]}$. α and β are given by [147]:

$$\alpha = \frac{2}{1+\epsilon} \frac{(\sum_{j=1}^{B} P_j)^2}{\sum_{j=1}^{B} P_j^2}, \; \beta = \frac{1+\epsilon}{2} \frac{\sum_{j=1}^{B} P_j^2}{\sum_{j=1}^{B} P_j}, \tag{9.15}$$

and $\epsilon = -0.0187$. Following the same method as for (9.8), the distribution of γ_{Alam} is given by:

$$f_{\gamma_{Alam}}(z) = 4\beta^2 P_0^\alpha \alpha(\alpha+1) \frac{z}{(2\beta z + P_0)^{\alpha+2}}. \tag{9.16}$$

9.2.3 MIMO Alamouti System with MRC Receiver

We now assume that BSs are equipped with 2 antennas and user equipments with N antennas. An MRC receiver combines the received signals from the N antennas. In a interference limited environment, the SINR can still be written as: $\gamma_{MRC} \approx X_{MRC}/Y_{MRC}$, where

$$X_{MRC} = \frac{P_0}{2} \sum_{n=1}^{N} (|h_{n,1,0}|^2 + |h_{n,2,0}|^2), \tag{9.17}$$

$$\begin{aligned} Y_{MRC} &= \sum_{j=1}^{B} \frac{P_j}{2} \Bigg(\frac{|\sum_{n=1}^{N} h_{n,1,0}^* h_{n,1,j} + h_{n,2,0} h_{n,2,j}^*|^2}{\sum_{n=1}^{N} (|h_{n,1,0}|^2 + |h_{n,2,0}|^2)} \\ &+ \frac{|\sum_{n=1}^{N} h_{n,1,0}^* h_{n,2,j} - h_{n,2,0} h_{n,1,j}^*|^2}{\sum_{n=1}^{N} (|h_{n,1,0}|^2 + |h_{n,2,0}|^2)} \Bigg), \end{aligned} \tag{9.18}$$

and $h_{n,i,j}$ is the flat fading Rayleigh channel gain between the i^{th} antenna of BS j and the n^{th} antenna of the served user. In Section 6.5, the distributions of X_{MRC} and Y_{MRC} were derived and are given by:

$$f_{X_{MRC}}(x) = \frac{x^{2N-1}}{(\frac{P_0}{2})^{2N}(2N-1)!}e^{-\frac{2x}{P_0}}, \tag{9.19}$$

$$f_{Y_{MRC}}(y) = \frac{y^{\upsilon-1}\exp(-\frac{y}{\tau})}{\Gamma(\upsilon)\tau^{\upsilon}}, \tag{9.20}$$

where υ and τ are given by:

$$\upsilon = \frac{2}{1+\zeta}\frac{(\sum_{j=1}^{B}P_j)^2}{\sum_{j=1}^{B}P_j^2}, \quad \tau = \frac{(1+\zeta)}{2}\frac{\sum_{j=1}^{B}P_j^2}{\sum_{j=1}^{B}P_j}. \tag{9.21}$$

and $\zeta = 0.0043$.

The distribution of γ_{MRC} can be calculated as for (9.8), and is given by:

$$f_{\gamma_{MRC}}(u) = \frac{\Gamma(2N+\upsilon)\left(\frac{P_0}{2}\right)^{\upsilon}}{(2N-1)!\Gamma(\upsilon)\tau^{\upsilon}}\frac{u^{2N-1}}{(u+\frac{P_0}{2\tau})^{2N+\upsilon}}. \tag{9.22}$$

Note that setting $N = 1$ in (9.22) yields (9.16).

9.2.4 Fluid Model Approximation

To derive an outage probability expression depending only on the distance between the considered user and the serving BS we use the fluid model (Appendix A.3) approximation described in [153]. The fluid model concept consists in replacing a fixed number of BSs by an equivalent continuum characterized by a given density. Let us define:

$$g(\eta) = \sum_{j=1}^{B} d_j^{-\eta}. \tag{9.23}$$

For an infinite homogeneous network and a BS density ρ_{BS}, the fluid model permits to write $g(\eta)$ as:

$$g(\eta) = \frac{2\pi\rho_{BS}}{\eta-2}(2R_c - r)^{2-\eta}, \tag{9.24}$$

where R_c is the considered cell radius and r is the distance between the considered user and its serving BS.

In terms of $g(\eta)$, the parameters of the outage probability of the multi-cellular SISO system given by ν and δ (9.7) can be written as:

$$\nu = \frac{g(\eta)^2}{g(2\eta)}, \quad \delta = KP_T\frac{g(2\eta)}{g(\eta)}. \tag{9.25}$$

Similarly, the parameters of the MISO Alamouti system α and β (9.15) are given by:

$$\alpha = \frac{2}{1+\epsilon}\frac{g(\eta)^2}{g(2\eta)}, \quad \beta = \frac{1+\epsilon}{2}KP_T\frac{g(2\eta)}{g(\eta)}, \tag{9.26}$$

and the parameters of the MIMO Alamouti with MRC receiver system υ and τ (9.21) are given by:

$$\upsilon = \frac{2}{1+\zeta}\frac{g(\eta)^2}{g(2\eta)}, \quad \tau = \frac{1+\zeta}{2}KP_T\frac{g(2\eta)}{g(\eta)}, \tag{9.27}$$

9.3 Dynamic Traffic Study

We now assume a dynamic system where users randomly enter the network, download a file and go out of the system. We are interested in the user throughput.

9.3.1 Traffic Model

We consider a cellular network with a time-shared downlink. The scheduler is fair in slots: when there are n active users, each one receives $1/n$ proportion of time for data transmission. We assume a uniform traffic demand in the cell, flow sizes are independent and identically distributed with a mean flow size equal to V. The data flow arrival process is Poisson with an intensity per surface area λ.

Let us divide the cell in K' concentric rings around BS 0 defined by ranges R_k, $k \in \{1, ..., K'\}$, $R_{K'} = R_c$ and $R_0 = 0$. The arrival rate in ring k is $\lambda_k = p_k\lambda\pi R_c^2$, with $p_k = (R_k^2 - R_{k-1}^2)/R_c^2$. The service time in ring k is V/c_k, where c_k is the average throughput in ring k. So the load generated by ring k is $\rho_k = \lambda\pi R_c^2 V p_k/c_k$ and the cell load is:

$$\begin{aligned}\rho &= \sum_{k=1}^{K'}\rho_k, \\ &= \lambda\pi R_c^2 V\sum_{k=1}^{K'}\frac{p_k}{c_k}, \\ &= \frac{\lambda\pi R_c^2 V}{C},\end{aligned} \tag{9.28}$$

where

$$C = \left(\sum_k^{K'}\frac{p_k}{c_k}\right)^{-1} \tag{9.29}$$

is the cell capacity.

With the model proposed in the previous section, we are able to compute c_k:

$$c_k = \int_{R_{k-1}}^{R_k} \frac{2rD(r)dr}{R_k^2 - R_{k-1}^2}, \tag{9.30}$$

where $D(r)$ is the mean achievable rate at distance r and is given by:

$$D(r) = W \int_0^\infty \log_2(1+\gamma(r)) f_\gamma(\gamma(r)) d\gamma. \tag{9.31}$$

In case of no admission control, the flow throughput of a user in the ring k is then given by [14]:

$$\varphi_k = c_k(1-\rho). \tag{9.32}$$

We now consider an admission control based on a maximum number m of active users. This number of users can be chosen in order to ensure a minimum rate c_{min}, hence,

$$m = \left\lfloor \frac{C}{c_{min}} \right\rfloor. \tag{9.33}$$

In this case, the flow throughput in ring k is given by [14]:

$$\varphi_k = c_k \frac{(1-\rho)(1-\rho^m)}{1-(m+1)\rho^m + m\rho^{m+1}}. \tag{9.34}$$

We now derive the mean achievable rate $D(r)$ for each considered system.

9.3.2 SISO System Mean Rate

The mean achievable rate at a distance r for a SISO system, is given by:

$$\begin{aligned} D(r) &= \frac{W}{\log(2)} \int_0^\infty \log(1+\gamma(r)) f_{\gamma_{SISO}}(\gamma(r)) d\gamma, \\ &= \frac{W}{\log(2)} (\frac{P_0}{\delta})^\nu \int_0^\infty (1+\gamma)^{-1} (\gamma + \frac{P_0}{\delta})^{-\nu} d\gamma, \\ &= \frac{W}{\log(2)} \frac{P_0}{\delta\nu} {}_2F_1(1,1;\nu+1;1-\frac{P_0}{\delta}). \end{aligned} \tag{9.35}$$

where ${}_2F_1$ is the hypergeometric function, and $\nu(r)$ and $\delta(r)$ are given in Section 9.2.4.

9.3.3 MISO Alamouti Mean Rate

The mean achievable rate at a distance r for the MISO Alamouti system, is given by:

$$\begin{aligned} D_{MISO}(r) &= \frac{W}{\log(2)} \int_0^\infty \log(1+\gamma) f_{\gamma_{Alam}}(\gamma) d\gamma, \\ &= \frac{W}{\log(2)} \frac{P_0}{2\beta} \int_0^\infty \gamma \log(1+\gamma) (\gamma + \frac{P_0}{2\beta})^{-(\alpha+2)} d\gamma. \end{aligned} \tag{9.36}$$

After integration by parts, $D(r)$ can be written as:

$$\begin{aligned} D_{MISO}(r) &= \frac{W}{\log(2)}\frac{P_0}{2\beta}\Big(\frac{1}{\alpha}\,{}_2F_1(1,1;\alpha+1;1-\frac{P_0}{2\beta}) \\ &+ \frac{1}{\alpha+1}\,{}_2F_1(1,2;\alpha+2;1-\frac{P_0}{2\beta})\Big). \end{aligned} \tag{9.37}$$

9.3.4 MIMO Alamouti with MRC Receiver Mean Rate

At a distance r, the mean achievable rate for a MIMO Alamouti coded system with an MRC receiver can be written as:

$$\begin{aligned} D_{MIMO}(r) &= \frac{W}{\log(2)}\int_0^\infty \log(1+\gamma) f_{\gamma_{MRC}}(\gamma)d\gamma, \\ &= \frac{W}{\log(2)}\frac{\Gamma(2N+\upsilon)\left(\frac{P_0}{2}\right)^\upsilon}{(2N-1)!\Gamma(\upsilon)\tau^\upsilon}\int_0^\infty \log(1+\gamma)\frac{\gamma^{2N-1}}{(\gamma+\frac{P_0}{2\tau})^{2N+\upsilon}}d\gamma. \end{aligned} \tag{9.38}$$

9.4 Systems performance

In this section, we will study the performance of the three previously introduced systems with and without admission control.

9.4.1 Assumptions

In all case, we consider a mean flow size of $V = 2$ Mbits, a channel bandwidth of 5 MHz and a cell radius $R_c = 1$ Km. The cell is divided into five concentric rings characterized by radii 0.2, 0.4, 0.6, 0.8 and 1 Km.

Average throughputs c_k are obtained using Mathematica from (9.30). As suggested in [174] for LTE, the Shannon formula has been multiplied by a loss factor of 0.6 in order to take into account imperfect rate adaptation. Moreover, in all calculations, we consider that users are located at distances higher than 0.05 Km from the BS.

9.4.2 No Admission Control

Based on the equation (9.32), we calculate the mean flow throughput in each ring for the SISO, the MISO Alamouti and the MIMO Alamouti with MRC systems. Figure 9.1 presents a comparison between the mean flow throughput of the SISO system and the 2×1 Alamouti system as a function of the cell load ρ. In terms of achievable throughputs, MISO Alamouti slightly outperforms SISO, especially in the inner rings. Performances are lower at cell edge. Note that our analysis does not focus on the outage probability, which Alamouti is clearly advantageous for.

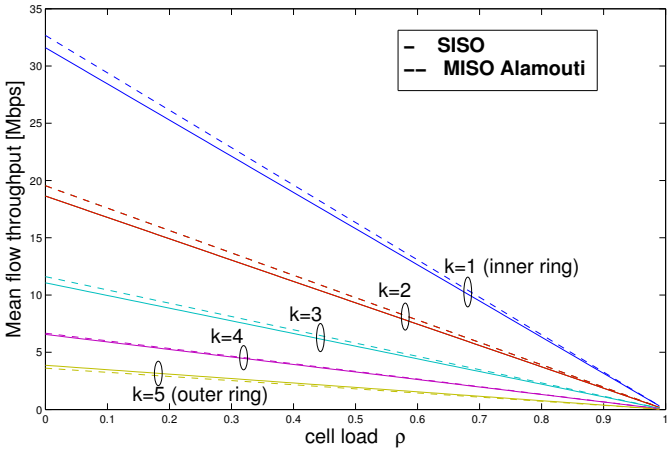

Figure 9.1: Flow throughput vs cell load for SISO and 2×1 MISO Alamouti.

Figure 9.2 shows a comparison between the 2×2 MIMO Alamouti with MRC system and the 2×1 MISO Alamouti system for the same values of the arrival rate. It can be seen that the MIMO Alamouti with MRC receiver system achieves a gain of about 4 Mbits/s in the inner ring compared to the MISO Alamouti system. The gain remains important in the outer ring.

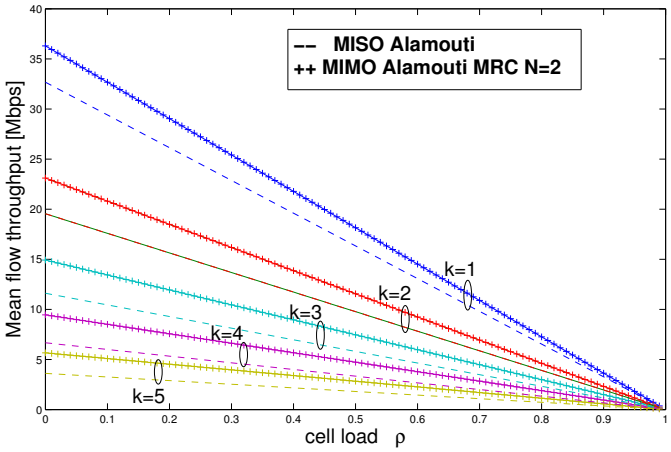

Figure 9.2: Flow throughput vs cell load for 2×1 MISO Alamouti and 2×2 MIMO Alamouti MRC.

For SISO, MISO Alamouti and MIMO Alamouti with MRC, the cell capacities are re-

spectively 6.17, 5.99 and 8.83 Mbps (see (9.29)). This confirms the phenomenon observed in [147]: although Alamouti scheme greatly improves the outage probability at cell edge compared to SISO, it also provides relatively lower SINR at cell center. The two effects almost compensate and the cell capacities are similar. In contrast, the use of MRC significantly improves cell capacity.

9.4.3 With Admission Control

We now consider a minimum guaranteed rate $c_{min} = 0.5$ Mbits/s. The maximum number of active users in the cell can be obtained using (9.33) and is 12, 11 and 17 for SISO, MISO Alamouti and MIMO Alamouti with MRC respectively. Based on this admission criterion, we compare the performance of our three systems.

Figure 9.3 illustrates a comparison between the flow throughput of the SISO system and the 2×1 Alamouti system as a function of the cell load. We notice that when $\rho \to 1$, the throughput of cell edge users tends to c_{min}. Then, cell capacities and maximum number of users being similar for the two systems, we obtain results in conformity with what has been observed without admission control.

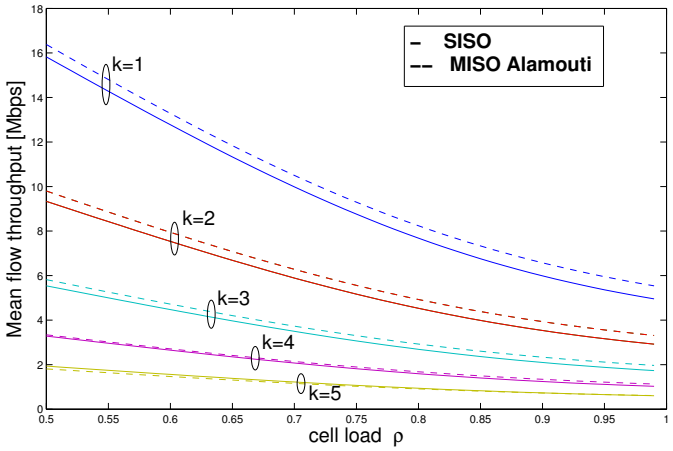

Figure 9.3: Flow throughput vs cell load for SISO and 2×1 MISO Alamouti with admission control ($c_{min} = 0.5$ Mbits/s).

Figure 9.4 illustrates the comparison between MISO and MIMO. As expected, when the load is low, MIMO outperforms MISO in terms of flow throughput. It is however interesting to see that the flow throughput of MIMO users in inner rings fall below the throughput achieved by MISO users when the load is high.

From a mathematical point of view, it is not difficult to see that (9.34) decreases more rapidly when m increases. More intuitively, the MIMO system accepts more users (17

instead of 11), so that the cell capacity (although higher) is divided in smaller pieces than with MISO. The loss is particularly visible for inner rings, i.e., for users in the center of the cell.

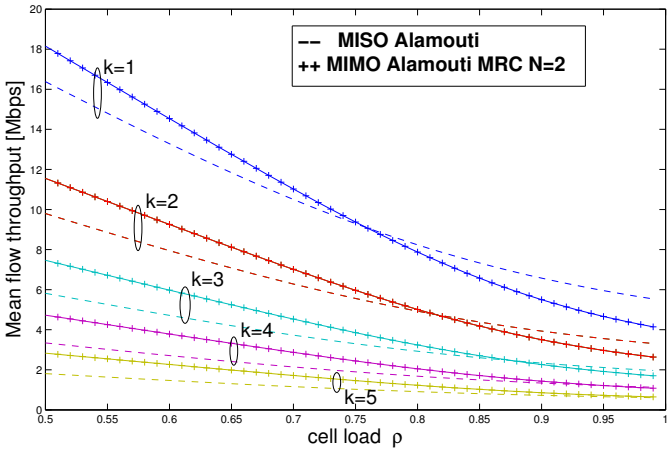

Figure 9.4: Flow throughput vs cell load for 2×1 MISO Alamouti and 2×2 MIMO Alamouti MRC with admission control ($c_{min} = 0.5$ Mbits/s).

9.5 Conclusion

In this chapter, analytical expressions of the mean flow throughput have been derived for three systems: a SISO system, a MISO Alamouti scheme with and without MRC receiver. The performance study has been derived assuming or not admission control. Performance results show that the MISO scheme does not bring enhancement over SISO in terms of flow throughput, although gains are obtained in terms of outage probability. Only the addition of MRC at the receiver, on top of the Alamouti scheme at the transmitter, brings significant improvements.

Conclusion

In this concluding chapter, we will first summarize the main results obtained in this thesis then we will give some possible further works that may extend these results.

Summary of Contributions

In this thesis, we have evaluated the performance of different multicellular communication systems through static and dynamic studies.

In the first part of the thesis we have considered static multicellular SISO, MISO and MIMO systems either in a single user or in a multiuser communication context. In Chapter 4, we began our analyses with a narrowband multicellular single user SISO system. In this context, we proposed two approximation methods we denoted CLCFM and FWBM, to derive the expression of the outage probability when considering the joint impact of path-loss, shadowing and Rayleigh fading. Two easy-to-compute outage probability expressions were obtained. A fluid model approximation allowed us to derive expressions depending only on the distance between the user and its serving BS. In conjunction with the fluid model, both methods provide accurate results for low values of shadowing standard variation, however the CLCFM is no more valid for high standard deviation values.

In Chapter 5, we have assumed a multicellular single user wideband communication system implementing the Time Reversal transmission. It is a technique that mitigates inter-cell and inter-symbol interference (ISI). By neglecting the ISI power effect, we have derived an outage probability expression for a Rayleigh fading channel. Simulations showed that our approximation is valid since there is a good match between the numerical outage probabilities with and without considering ISI power and our analytical expression.

In Chapter 6, we have studied the performance of MISO and MIMO systems in a multicellular context. We considered the Alamouti scheme transmission for the two systems and the MRC receiver for the MIMO case. We provided outage probability expressions when considering path-loss and Rayleigh fading and two assumptions about the shadowing variation: very slow varying shadowing (actually assumed constant in the calculations) and randomly varying shadowing. For the first case, we have obtained closed form expressions. For the second case, easy-to-compute integral form expressions were derived. The comparison between the two systems showed that both take advantage of the transmit diversity

gain of the Alamouti scheme equal to 2. The MRC MIMO system benefits in addition from a receive diversity gain equal to the number of receive antennas.

Considering a multiuser communication context, in Chapter 7, we have studied the performance of the ZFBF as a SDMA technique to serve a set of users simultaneously. The ZFBF permits to eliminate multiuser interference. We have derived an outage probability expression taking into account path-loss, shadowing and Rayleigh fast fading.

Having studied so far, the effect of inter-cell interference on MIMO systems performance, we devoted Chapter 8 to the study of a cooperation scenario permitting to mitigate this kind of interference. Indeed, we have considered multiple antenna BSs organized into clusters, each cluster serving cooperatively a single user. The BSs are assumed to use the MRT scheme to transmit their data. Considering path-loss, constant shadowing and Rayleigh fast fading, we have derived a closed-form outage probability expression.

So far, our analysis assumed a static system communication with a single user or a multiuser transmission. We devoted the last part of this thesis to the dynamic study where users randomly enter the network, download a file and go out of the system. We take as inputs the already derived CDFs of the SIR for the narrowband SISO, the MISO and MIMO Alamouti schemes and a traffic model assuming a fair time-shared transmission. We derived analytical expressions of the mean user throughput and the cell capacity.

Through the static and the dynamic studies we have gone through two major steps of network dimensioning process namely the coverage estimation and the traffic analysis. We have hence provided analytical models allowing for rapid and accurate cellular networks design.

Further Works

Throughout this thesis we have considered either no CSIT or perfect channel knowledge at the transmitter. The latter assumption is commonly used but may be realistic exclusively for low mobility users, whose CSI does not change rapidly. It permits to simplify considerably the studied issues especially in an analytical study. However, in practice this may not be the case. It would be hence interesting to study the impact of CSIT imperfectness on the performance of TR technique, ZFBF and cooperative MRT transmission. In this perspective, the latter case is of particular importance since it involves CSIT transfer between BSs.

We have also studied the distribution of the SIR without taking into account the outage duration. This is however an interesting metric to look at, since it conditions the continuity of the service. Indeed, if the SIR drops below a threshold value for a short period, the communication can be maintained. It would, hence, be judicious to study the excursions of the SIR below the threshold value. In the literature, few works were devoted to this kind of study.

Another interesting extension of the present work is to study the performance of the

ZFBF in a cooperation context, where a cluster of BSs serve the same set of users cooperatively. Compared to the performance of the system we studied in Chapter 7, the analysis may bring to light the advantages of multicell cooperation with ZFBF.

The study of the radio performance of CoMP showed that it is a very advantageous technique for the end user, as it is shown in Chapter 8 in a static study. However, this approach masks the fact that resources of many BSs are mobilized to serve a single user. The performance of the CoMP technique may be unsatisfactory when considering now a dynamic study. This case may be interesting to investigate.

Finally, the M/G/1/PS queue model, while offering a suitable theoretical framework for single user systems (see Chapter 9 for SISO, MISO or MIMO), is not adapted to a multiuser MIMO communication. In this case, indeed, several transmissions for different users can occur simultaneously and the choice of the served users according to their channel conditions plays a crucial role in the system performance. A simple queue model suitable for this kind of systems would be very useful for network dimensioning.

Appendix A

Some Intermediate Results

A.1 Sum of Lognormal Random Variables

In this section, we derive the logarithmic mean and standard deviation of F (see equation (4.8)) using the Fenton-Wilkinson method. Several classical techniques exist in the literature in order to approximate a sum of log-normal RVs, e.g. Schwartz-Yeh [175] and Farley [176]. The former needs complex recursive calculations, the latter assumes identical means and standard deviations for the considered RVs. On the contrary, the Fenton-Wilkinson method provides a closed-form formula for non identical distributed log-normal RVs.

Each term of the sum in the numerator of F is a RV following a log-normal distribution. We can write $\ln(r_j^{-\eta} Y_j) \propto \mathcal{N}(am_j, a^2\sigma^2)$, where $a = \ln(10)/10$ and $m_j = \frac{1}{a}\ln(r_j^{-\eta})$. The sum $S = \sum_{j=1}^{N} r_j^{-\eta} Y_j$ can itself be approximated by a log-normal RV: $\ln(S) \propto \mathcal{N}(am, a^2\sigma_s^2)$ with:

$$am = \ln\left(\sum_{j=1}^{N} e^{am_j}\right) + \frac{a^2\sigma^2}{2} - \frac{a^2\sigma_s^2}{2}, \tag{A.1}$$

$$a^2\sigma_s^2 = \ln\left[\left(e^{a^2\sigma^2} - 1\right)\frac{\sum_{j=1}^{N} e^{2am_j}}{\left(\sum_{j=1}^{N} e^{am_j}\right)^2} + 1\right]. \tag{A.2}$$

These two expressions simplify to:

$$am = \ln\left(\sum_{j=1}^{N} r_j^{-\eta}\right) + \frac{a^2\sigma^2}{2} - \frac{a^2\sigma_s^2}{2}, \tag{A.3}$$

$$a^2\sigma_s^2 = \ln\left[\left(e^{a^2\sigma^2} - 1\right)\frac{\sum_{j=1}^{N} r_j^{-2\eta}}{\left(\sum_{j=1}^{N} r_j^{-\eta}\right)^2} + 1\right]. \tag{A.4}$$

Taking now into account the denominator in the expression of F, the logarithmic mean value of F is simply $am_f = am - (-\eta \ln(r))$ and the logarithmic standard deviation of F is $a^2 s_f^2 = a^2\sigma_s^2 + a^2\sigma^2$. The ratio of two log-normal RVs is indeed a log-normal RV with mean, the difference of the means, and variance, the sum of the variances. With the definitions of f, G and H, we obtain equations (4.9) and (4.10). Note that m_f and s_f are expressed in dB.

A.2 Causal Form of the Central Limit Theorem

The following sections are taken from [17] (Chapter 11, Section 3, pages 227-236).

A.2.1 Central limit Theorem

"The central limit theorem states that if the densities $f_1(t), ..., f_n(t)$ are not lattices, then, under certain general conditions, the product $F(w)$ of their Fourier transforms

$$F_1(w), ..., F_n(w), \tag{A.5}$$

tends to a Gaussian function as $n \to \infty$

$$F(w) \sim e^{-\sigma^2 w^2/2 - j\eta w} \quad \text{for } n \to \infty, \tag{A.6}$$

where σ and η are given by:

$$\eta = \eta_1 + \eta_2 + ... + \eta_n, \tag{A.7}$$
$$\sigma^2 = \sigma_1^2 + \sigma_2^2 + ... + \sigma_n^2, \tag{A.8}$$

η_i and σ_i^2 being:

$$\eta_i = \int_{-\infty}^{+\infty} t f(t) dt, \tag{A.9}$$
$$\sigma_i^2 = \int_{-\infty}^{+\infty} (t - \eta_i)^2 f(t) dt. \tag{A.10}$$

From (A.6) and a limit argument, known as Helly's theorem, it can be concluded that the inverse transform of $F(w)$, tends also to a Gaussian function:

$$f(t) \sim \frac{1}{\sigma\sqrt{2\pi}} e^{\frac{-(t-\eta)^2}{2\sigma^2}}, \quad \text{for } n \to \infty \tag{A.11}$$

i.e., to the inverse of the limit of $F(w)$.
Two conditions ensure the validity of this approximation; though they are not the most general, they cover a wide range of applications:

- The third moment of the functions $f_i(t)$ is finite, and for every i it is smaller than an arbitrary constant C.
- The sum of the variances of $f_i(t)$ tends to infinity with n:

$$\sigma^2 = \sigma_1^2 + \sigma_2^2 + ... + \sigma_n^2 \underset{n\to\infty}{\longrightarrow} \infty. \tag{A.12}$$

"

A.2.2 Causal form of the central limit theorem

"Often the functions $f_i(t)$ are causal, and, obviously, the same is true for their convolution, however, the Gaussian estimate (A.11) of $f(t)$ is not zero for $t < 0$, no matter how large η is. In this case, a modification would be brought to the central-limit theorem so that $f(t)$ tends to a causal function as $n \to \infty$. This can be treated as follows.
Consider the function:

$$s(t) = \frac{t^\alpha e^{-\frac{t}{\beta}}}{\beta^{\alpha+1}\Gamma(\alpha+1)} U(t), \tag{A.13}$$

where $U(t)$ is the step function. Its Fourier transform is given by:

$$S(w) = \frac{1}{(1+j\beta w)^{\alpha+1}}. \tag{A.14}$$

Clearly, $S(w)$ can be written as the product of n characteristic functions where n is the nearest integer to α. Therefore, according to (A.6) and (A.11), $s(t)$ is a causal approximation to a Gaussian function provided α is large. We thus have the following version of the central limit for causal functions:

$$f(t) \approx \frac{t^\alpha e^{-\frac{t}{\beta}}}{\beta^{\alpha+1}\Gamma(\alpha+1)} \quad for\ n \to \infty, \tag{A.15}$$

where the constants α and β are such that the mean and the variance of the two sides of (A.15) are equal, hence:

$$\begin{aligned} \eta &= \frac{1}{\beta^{\alpha+1}\Gamma(\alpha+1)} \int_0^\infty t \times t^\alpha e^{-\frac{t}{\beta}} dt, \\ &= (\alpha+1)\beta. \end{aligned} \tag{A.16}$$

and

$$\begin{aligned} \sigma^2 + \eta^2 &= \frac{1}{\beta^{\alpha+1}\Gamma(\alpha+1)} \int_0^\infty t^2 \times t^\alpha e^{-\frac{t}{\beta}} dt, \\ &= (\alpha+1)(\alpha+2)\beta^2. \end{aligned} \tag{A.17}$$

Therefore α and β are given by:

$$\alpha + 1 = \frac{\eta^2}{\sigma^2} \quad \beta = \frac{\sigma^2}{\eta}, \tag{A.18}$$

and (A.15) gives a causal estimate to $f(t)$."

A.3 Fluid Model

In this appendix, we shortly recall the fluid model approach, that will allow us to simplify equation (4.35). The fluid model approach consists of replacing a given fixed finite number of interfering BS by an equivalent continuum of transmitters which are uniformly distributed with density ρ_{BS}. Fluid model has been first proposed in [153]. Detailed simulations presented in [177] show its validity in many scenarios.

We consider a central cell and a round shaped network around this cell with radius R_{nw} (see figure A.1). The inter-site distance is $2R_c$. Let us consider a mobile u at a distance r_u from its serving BS and the function g defined as:

$$g(\eta) = \sum_{j=1}^{N} r_j^{-\eta}, \tag{A.19}$$

where the sum is over the set of interfering BSs and r_j is the distance from the user to BS j.

In the fluid model, each elementary surface $zdzd\theta$ at a distance z from u contains $\rho_{BS}zdzd\theta$ BS which contribute to function g. Their contribution to the sum over j is $\rho_{BS}zdzd\theta z^{-\eta}$ ($\eta > 2$). We approximate the integration surface by a ring with centre u, inner radius $2R_c - r_u$, and outer radius $R_{nw} - r_u$ (see figure A.2). Re-writing g as a function of r_u and η, we obtain:

$$\begin{aligned} g(r_u, \eta) &= \int_0^{2\pi} \int_{2R_c - r_u}^{R_{nw} - r_u} \rho_{BS} z^{-\eta} z dz d\theta, \\ &= \frac{2\pi\rho_{BS}}{\eta - 2} \left[(2R_c - r_u)^{2-\eta} - (R_{nw} - r_u)^{2-\eta} \right]. \end{aligned} \tag{A.20}$$

If the network is large, i.e., R_{nw} is large in front of R_c, g can be further approximated by (dropping subscript u):

$$g(r, \eta) = \frac{2\pi\rho_{BS}}{\eta - 2} (2R_c - r)^{2-\eta}. \tag{A.21}$$

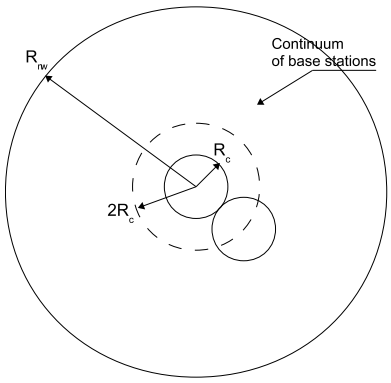

Figure A.1: Network and cell of interest in the fluid model; the minimum distance between the BS of interest and interferers is $2R_c$ and the interfering network is made of a continuum of base stations.

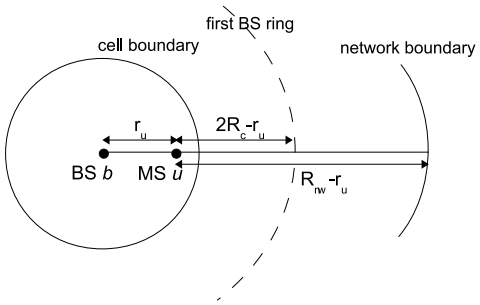

Figure A.2: Integration limits for external interference computation.

A.4 Independance of Random Variables

Consider zero mean complex Gaussian vectors $\mathbf{h}_0 = [h_{1,0}, h_{2,0}, ..., h_{N,0}]^H$ and $\mathbf{h}_j = [h_{1,j}, h_{2,j}, ..., h_{N,j}]^H$ and let g_j be a random variable given by:

$$g_j = \frac{\mathbf{h}_0^H \mathbf{h}_j}{\|\mathbf{h}_0\|}. \tag{A.22}$$

Since the elements of $\mathbf{h}_j$ are i.i.d zero mean complex Gaussian, g_j conditioned on $\mathbf{h}_0$ is also zero-mean complex Gaussian. The mean and the variance of g_j can be calculated as follows:

$$\mathrm{E}[g_j|\mathbf{h}_0] = \frac{\mathbf{h}_0^H}{\|\mathbf{h}_0\|}\mathrm{E}[\mathbf{h}_j] = 0, \tag{A.23}$$

$$\begin{aligned} \mathrm{E}[|g_j|^2|\mathbf{h}_0] &= \frac{\mathbf{h}_0^H \mathrm{E}[\mathbf{h}_j \mathbf{h}_j^H]\mathbf{h}_0}{\|\mathbf{h}_0\|^2}, \\ &= \frac{\mathbf{h}_0^H \mathbf{I}_N \mathbf{h}_0}{\|\mathbf{h}_0\|^2}, \\ &= 1, \end{aligned} \tag{A.24}$$

$\mathbf{I}_N$ being the identity matrix of dimension N.
The PDF of g_j conditioned on $\mathbf{h}_0$ can, thus be written as:

$$f_{g_j}(g_j/\mathbf{h}_0) = \frac{1}{\pi}\exp(-|g_j|^2). \tag{A.25}$$

From the expression of the pdf, it can be clearly stated that g_j is independent of $\mathbf{h}_0$.

Bibliography

[1] 3GPP TR 25.996. Spatial Channel Model for Multiple Input Multiple Output (MIMO) Simulations. *Release V10.0.0*, Mar. 2011.

[2] L. Zheng and D.N.C Tse. Diversity and Multiplexing: a Fundamental Tradeoff in Multiple-Antenna Channels. *IEEE Transactions on Information Theory*, 49(5):1073–1096, May 2003.

[3] M. Pratesi, F. Santucci, F. Graziosi, and M. Ruggieri. Outage Analysis in Mobile Radio Systems with Generically Correlated Log-normal Interferers. *IEEE Transactions on Communications*, 48(3):381–385, Mar. 2000.

[4] G. L. Stuber. *Principles of Mobile Communications - 2nd Edition*. Kluwer Academic Publishers, Massachusetts, USA, 1958.

[5] J.-P.M.G. Linnartz. Exact Analysis of the Outage Probability in Multiple-User Mobile Radio. *IEEE Transactions on Communications*, 40(1):20–23, Jan. 1992.

[6] C.C. Chung and S.V. Hanly. Calculating the Outage Probability in a CDMA Network with Spatial Poisson Traffic. *IEEE Transactions on Vehicular Technology*, 50(1):183–204, Jan. 2001.

[7] S.J. Grant and J.K. Cavers. Analytical Calculation of Outage Probability for a General Cellular Mobile Radio System. In *Proc. of Vehicular Technology Conference (VTC Fall)*, pages 1372–1376, Sep. 1999.

[8] Y. Weichen and A.M. Haimovich. Outage Probability of Cellular CDMA Systems with Space Diversity, Rayleigh Fading, and Power Control Error. *IEEE Communications Letters*, 2(8):220–222, Aug. 1998.

[9] Y. Song, S.D. Blostein, and J. Cheng. Outage Probability Comparisons for Diversity Systems with Cochannel Interference in Rayleigh Fading. *IEEE Transactions on Wireless Communications*, 4(4):1279 – 1284, Jul. 2005.

[10] Y. Tokgoz and B. D. Rao. Performance Analysis of Maximum Ratio Transmission Based Multi-Cellular MIMO Systems. *IEEE Transactions on Wireless Communications*, 5(1):1536–1276, Jan. 2006.

[11] J. P. Pená Martin, J. M. Romero-Jerez, G. Aguilera, and A. J. Goldsmith. Performance Comparison of MRC and IC Under Transmit Diversity. *IEEE Transactions on Wireless Communications*, 8(5):2484–2493, May 2009.

[12] V. Garcia, N. Lebedev, and J.-M. Gorce. Capacity Outage Probability for Multi-Cell Processing under Rayleigh Fading. *IEEE Communication Letters*, 15(8):801–803, Aug. 2011.

[13] X. Ge, K. Huang, C-X. Wang, X. Hong, and X. Yang. Capacity Analysis of a Multi-Cell Multi-Antenna Cooperative Cellular Network with Co-Channel Interference. *IEEE Transactions on Wireless Communications*, 10(10):3298–3309, Oct. 2011.

[14] T. Bonald and A. Proutière. Wireless Downlink Data Channels: User Performance and Cell Dimensioning. In *Proc. of The Annual International Conference on Mobile Computing and Networking (MobiCom)*, pages 339–352, Sep. 2003.

[15] S. Borst. User-Level Performance of Channel-Aware Scheduling Algorithms in Wireless Data Networks. *IEEE/ACM Transactions on Networking*, 13(3):636–647, Jun. 2005.

[16] L. Fenton. The Sum of Log-Normal Probability Distributions in Scatter Transmission Systems. *IRE Transactions on Communications Systems*, 8(1):57–67, Mar. 1960.

[17] A. Papoulis. *The Fourier Integral and Its Applications*. McGraw-Hill, New York, NY, 1962.

[18] J.-M. Kelif. Admission Control on Fluid CDMA Networks. In *Proc. of International Symposium on Modeling and Optimization in Mobile, Ad Hoc and Wireless Networks (WiOPt)*, pages 1–7, Apr. 2006.

[19] `www.seamcat.org`.

[20] `http://www.forsk.com`.

[21] B. Blaszczyszyn and R. Schott. Approximate Decomposition of Some Modulated Poisson-Voronoi Tessellations. *Advances in Applied Probability*, 35:847–862, Dec. 2003.

[22] A.J. Viterbi, A.M. Viterbi, K.S. Gilhousen, and E. Zehavi. Soft Handoff Extends CDMA Cell Coverage and Increases Reverse Link Capacity. *IEEE Journal on Selected Areas in Communications*, 12(8):1281–1288, Oct. 1994.

[23] J.-C. Lin, W.-C. Kao, Y.T. Su, and T.-H. Lee. Outage and Coverage Considerations for Microcellular Mobile Radio Systems in a Shadowed-Rician/Shadowed-Nakagami Environment. *IEEE Transactions on Vehicular Technology*, 48(1):66 –75, Jan. 1999.

[24] J.-M. Kelif, M. Coupechoux, and F. Marache. Limiting Power Transmission of Green Cellular Networks: Impact on Coverage and Capacity. In *Proc. of IEEE International Conference on Communications (ICC)*, pages 1–6, May 2010.

[25] J. Hämäläinen. Cellular Network Planning and Optimization Part V: GSM. Technical report, `http://www.comlab.hut.fi/studies/3275/Cellular_network_planning_and_optimization_part5.pdf`, 2008.

[26] T. Heikkilä. HSDPA Radio Network Planning. Technical report, `http://digitus.itk.ppke.hu/~takacsgy/26_hsdpa_rnp.pdf`, Feb. 2006.

[27] A.W. Massey and W. Whitt. A Stochastic Model to Capture Space and Time Dynamics in Wireless Communication Systems. *Probability in the Engineering and Informational Sciences*, 8:541–569, 1994.

[28] X. Lagrange and P. Godlewski. Performance of a Hierarchical Cellular Network with Mobility-Dependent Hand-Over Strategies. In *Proc. of IEEE Vehicular Technology Conference (VTC)*, pages 1868–1872, Apr. 1999.

[29] G. Haring, R. Marie, R. Puigjaner, and K. Trivedi. Loss Formulas and their Application to Optimization for Cellular Networks. *IEEE Transactions on Vehicular Technology*, 50(3):644–673, May 2001.

[30] M-K. Karray. Analytical Evaluation of QoS in the Downlink of OFDMA Wireless Cellular Networks Serving Streaming and Elastic Traffic. *IEEE Transactions on Wireless Communications*, 9:1799–1807, May 2010.

[31] S.-E. Elayoubi and T. Chahed. Admission Control in the Downlink of WCDMA/UMTS. In Gabriele Kotsis and Otto Spaniol, editors, *Wireless Systems and Mobility in Next Generation Internet*, volume 3427 of *Lecture Notes in Computer Science*, pages 136–151. Springer Berlin / Heidelberg, 2005.

[32] T.S. Rappaport. *Wireless Communications: Principles and Practice*. Prentice Hall, Upper Saddle River, NJ, 1996.

[33] A. Goldsmith. *Wireless Communications*. Cambridge University Press, New York, NY, 2005.

[34] M.K. Simon and M.-S. Alouini. *Digital Communication over Fading Channels*. John Wiley & Sons, New York, NY, second edition, 2005.

[35] John G. Proakis. *Digital Communictions*. McGraw-Hill Series in Electrical Engineering, Singapore, 1983.

[36] A. R. S. Bahai, B. R. Saltzberg, and M. Ergen. *Multi-Carrier Digital Communications: Theory and Applications of OFDM*. Springer, second edition, 2004.

[37] J.J. Egli. Radio Propagation above 40 Mc over Irregular Terrain. *Proceedings of the Instiute of Radio Engineers*, 45(10):1383–1391, Oct. 1957.

[38] M. Hata. Empirical Formula for Propagation Loss in Land Mobile Radio Services. *IEEE Transactions on Vehicular Technology*, 29(3):317–325, Aug. 1980.

[39] COST Action 231. Digital Mobile Radio towards Future Generation Systems Final Report. *European Cooperation in the Field of Scientific and Technical Research*, 1999.

[40] Recommendation ITU-R M.1225. Guidelines For Evaluation of Radio Transmission Technologies for IMT-2000. 1997.

[41] A. Abdi, W.-C Lau, M.-S. Alouini, and M. Kaveh. A New Simple Model for Land Mobile Satellite Channels: First- and Second-Order Statistics. *IEEE Transactions on Wireless Communications*, 2(2):519–528, May 2003.

[42] S. Kandukuri and S. Boyd. Optimal Power Control in Interference-Limited Fading Wireless Channels With Outage-Probability Specifications. *IEEE Transactions on Wireless Communications*, 1(1):46–55, Jan. 2002.

[43] G. Immovilli and M.L. Merani. Simplified Evaluation of Outage Probability for Cellular Mobile Radio Systems. *IEEE Electronics Letters*, 27(15):1365–1367, Jul. 1991.

[44] N.B. Mandayam, P.C. Chen, and J.M. Holtzman. Minimum Duration Outage for Cellular Systems: A Level Crossing Analysis. In *Proc. of IEEE Vehicular Technology Conference (VTC Spring)*, pages 879–883, Apr. 1996.

[45] Y. Isukapalli and B. Rao. An Analytically Tractable Approximation for the Gaussian Q-Function. *IEEE Communications Letters*, 12(9):669–671, Sep. 2008.

[46] C. Tellambura and A. Annamalai. Efficient Computation of erfc(x) for Large Arguments. *IEEE Transactions on Communications*, 48:529–532, Apr. 2000.

[47] M. Chiani, D. Dardari, and M.K. Simon. New Exponential Bounds and Approximations for the Computation of Error Probability in Fading Channels. *IEEE Transactions on Wireless Communications*, 2(4):840–845, Jul. 2003.

[48] J. M. Romero and A. J. Goldsmith. Receive Antenna Array Strategies in Fading and Interference: An Outage Probability Comparison. *IEEE Transactions on Wireless Communications*, 7(3):1536–1276, Mar. 2008.

[49] A. Shah and A. Haimovich. Performance Analysis of Maximum Ratio Combining and Comparison with Optimum Combining for Mobile Radio Communications with Cochannel Interference. *IEEE Transactions on Vehicular Techology*, 49(4):1454–1463, Jul. 2000.

[50] M.-S. Alouini and M.K. Simon. An MGF-based Performance Analysis of Generalized Selection Combining over Rayleigh Fading Channels. *IEEE Transactions on Communications*, 48(3):401–415, Mar. 2000.

[51] E. Telatar. Capacity of Multi-Antenna Gaussian Channels. *European Transactions on Telecommunications*, 10(6):585–595, Oct. 1995.

[52] H. Weingarten, Y. Steinberg, and S. Shmai (Shitz). The Capacity Region of the Gaussian Multiple-Input Multiple-Output Broadcast Channel. *IEEE Transactions on Information Theory*, 52(9):3936–3964, Sep. 2006.

[53] T. Yoo and A. Goldsmith. On the Optimality of Multiantenna Broadcast Scheduling Using Zero-Forcing Beamforming. *IEEE Journal on Selected Areas in Communications*, 24(3):528–541, Mar. 2006.

[54] M. Sharif and B. Hassibi. A Comparison of Time-Sharing, DPC, and Beamforming for MIMO Broadcast Channels With Many Users. *IEEE Transactions on Communications*, 55(1):11–15, Jan. 2007.

[55] M. Stojnic, H. Vikalo, and B. Hassibi. Rate Maximization in Multi-Antenna Broadcast Channels with Linear Preprocessing. In *Proc. of IEEE Global Telecommunications Conference (GLOBECOM)*, pages 3957–3961, Nov. 2004.

[56] M. K. Karakayali, G. J. Foschini, R. A. Valenzuela, and R. D Yates. On the Maximum Common Rate Achievable in a Coordinated Network. In *Proc. of IEEE International Communications Conference (ICC)*, pages 4333–4338, Jun. 2006.

[57] A. Tajer, N. Prasad, and W. Xiaodong. Robust Beamforming for Multi-Cell Downlink Transmission. In *Proc. of IEEE International Symposium on Information Theory (ISIT)*, pages 2063–2067, Jun. 2010.

[58] T. Bonald, S. Borst, N. Hegde, and A. Proutière. Wireless Data Performance in Multi-Cell Scenarios. In *Proc. of International Conference on Measurement and Modeling of Computer Systems (SIGMETRICS)*, pages 378–387, Jun. 2004.

[59] M. Masood, M. Coupechoux, P. Godlewski, S. Doirieux, B. Baynat, and V. Capdevielle. Dimensioning Methodology for OFDMA Networks. In *Proc. of Wireless World Research Forum (WWRF)*, May 2009.

[60] G. J. Foschini and M. J. Gans. On Limits of Wireless Communications in a Fading Environment When Using Multiple Antennas. *Springer Wireless Personal Communications*, 6:311–335, Mar. 1998.

[61] F. Oggier, J.-C. Belfiore, and E. Viterbo. Cyclic Division Algebras: A Tool for Space-Time Coding. *Foundations and Trends in Communications and Information Theory*, 4(1):1–95, 2007.

[62] S. M. Alamouti. A Simple Transmit Diversity Technique for Wireless Communications. *IEEE Journal on Selected Areas in Communications*, 16(8):1451–1458, Oct. 1998.

[63] M. O. Damen, K. Abed-Meraim, and J.-C. Belfiore. Diagonal Algebraic Space-Time Block Codes. *IEEE Transations on Information Theory*, 48:628–636, Mar. 2002.

[64] G. J. Foschini. Layered Space-Time Architecture for Wireless Communication in a Fading Environment When Using Multi-Elements Antennas. *Bell Labs Technical Journal*, pages 41–59, Aug. 1996.

[65] J-C. Belfiore, G. Rekaya, and E. Viterbo. The Golden Code: A 2×2 Full-Rate Code with Non-Vanishing Determinants. *IEEE Transactions on Information Theory*, 51(4):1432–1436, Jul. 2005.

[66] B. Hassibi and H. Vikalo. On Sphere Decoding Algorithm. I. Expected Complexity. *IEEE Transactions on Signal Processing*, 53:2806–2818, Aug. 2005.

[67] M. Costa. Writing on Dirty Paper (corresp.). *IEEE Transactions on Information Theory*, 29(3):439–441, May 1983.

[68] M.-A. Maddah-Ali, M. Ansari, and A.K. Khandani. An Efficient Signaling Scheme for MIMO Broadcast Systems: Design and Performance Evaluation. Technical report, University of Waterloo, Jul. 2005.

[69] O.-S. Shin and K. Bok. Antenna-Assisted Round Robin Scheduling for MIMO Cellular Systems. *IEEE Communcation Letters*, 7(3):109–111, Mar. 2003.

[70] P. Viswanath, D.N.C. Tse, and R. Laroia. Opportunistic Beamforming Using Dumb Antennas. *IEEE Transactions on Information Theory*, 48(6):1277–1294, Jun. 2002.

[71] T. Park, O.-S. Shin, and K.B. Lee. Proportional Fair Scheduling for Wireless Communication with Multiple Transmit and Receive Antennas. In *Proc. of IEEE Vehicular Technology Conference (VTC Fall)*, pages 1573–1577, Oct. 2003.

[72] N. Jindal, S. Vishwanath, S. Jafar, and A. Goldsmith. Duality, Dirty Paper Coding and Capacity for Multiuser Wireless Channels. In *Proc. of DIMACS Workshop on Signal Processing for Wireless Transmisson*, pages 1–16, Oct. 2002.

[73] C.B. Peel, B.M. Hochwald, and A.L. Swindlehurst. A Vector Perturbation Technique for Near-Capacity Multiantenna Multiuser Comunication - Part I. *IEEE Transactions on Communications*, 53(1):195–202, Jan. 1983.

[74] F. Kaltenberger, M. Kountouris, L. Cardoso, R. Knopp, and D. Gesbert. Capacity of Linear Multi-User MIMO Precoding Schemes with Measured Channel Data. In *Proc. of IEEE Workshop on Signal Processing Advances in Wireless Communications (SPAWC)*, pages 580–584, Jul. 2008.

[75] M. Sharif and B. Hassibi. On the Capacity of MIMO Broadcast Channels with Partial Side Information. *IEEE Transactions on Information Theory*, 51(2):506–522, Feb. 2005.

[76] T. Yoo. *Sum-Capacity, Scheduling, and Multi-User Diversity in MIMO Broadcast Systems*. PhD thesis, Stanford University, 2007.

[77] F. Shu, W. Gang, X. Yue, and L. Shao-Qian. Multi-User MIMO Linear Precoding with Grassmannian Codebook. In *Proc. of International Conference on Communications and Mobile Computing (CMC)*, pages 250–255, Jan. 2009.

[78] T.H. Kim, R.W Heath, and S. Choi. Multiuser MIMO Downlink with Limited Feedback Using Transmit-Beam Matching. In *Proc. of IEEE International Conference on Communications (ICC)*, pages 3506–3510, May 2008.

[79] J. Zhu and H.-C. Yang. Low-Complexity Coordinated Beamforming Transmission for Multiuser MISO Systems and its Performance Analysis. In *Proc. of IEEE Global Telecommunications Conference (GLOBECOM)*, pages 1–5, Dec. 2010.

[80] M. Boldi, C. Botella, F. Boccardi, V. DŠAmico, E. Hardouin, M. Olsson, H. Pennanen, P. Rost, V. Savin, T. Svensson, and A. Tölli. D1.8 Intermediate Report on CoMP (Coordinated Multi-Point) and Relaying in the Framework of CoMP. *CELTIC CP5-026 WINNER+*, Nov 2009.

[81] J. Li, E. Lu, and I.-T. Lu. Performance Benchmark for Network MIMO Systems: A Unified Approach for MMSE Transceiver Design and Performance Analysis. In *Proc. of IEEE Global Telecommunications Conference (GLOBECOM)*, pages 1–6, Dec. 2010.

[82] Y. Rui, M. Li, P. Chengo, Y. Luo, and A. Guo. Achievable Rates of Coordinated Multi-Point Transmission Schemes under Imperfect CSI. In *Proc. of IEEE International Communications Conference (ICC)*, pages 1–5, Jun. 2011.

[83] N. Lee and K. Lee. Base Station Selection Technique for MMSE Joint Transmission in Downlink Cooperative MIMO System. In *Proc. of IEEE Wireless Communication and Networking Conference (WCNC)*, pages 1–5, Apr. 2009.

[84] A. Papadogiannis, D. Gesbert, and E. Hardoin. Dynamic Clustering Approach in Wireless Networks with Multi-Cell Cooperative Processing. In *Proc. of IEEE International Communication Conference (ICC)*, May 2008.

[85] S. Venkatesan, A. Lozano, and R. Valenzuela. Network MIMO: Overcoming Intercell Interference in Indoor Wireless Systems. In *Proc. of Asilomar Conference on Signals, Systems and Computers (ACSSC)*, pages 83–87, Nov. 2007.

[86] M. Kamoun and L. Mazet. Base-Station Selection in Cooperative Single Frequency Cellular Network. In *Proc. of Workshop on Signal Processing Advances in Wireless Communications (SPAWC)*, pages 1–5, Jun. 2007.

[87] P. Marsch and G. Fettweis. Static Clustering for Cooperative Multi-Point (CoMP) in Mobile Communications. In *Proc. of IEEE International Conference on Communications (ICC)*, pages 1–6, Jun. 2011.

[88] Z. Yong, E. Gunawan, L.G. Yong, and L. Jin. Joint Base Station Selection and Linear Precoding for Cellular Networks with Multi-Cell Processing. In *Proc. of IEEE Region 10 Conference TENCON*, pages 1976–1981, Nov. 2010.

[89] F. Boccardi and H. Huang. Limited Downlink Network Coordination in Cellular Networks. In *Proc. of IEEE Personal Indoor and Mobile Radio Communications (PIMRC)*, pages 1–5, Sep. 2007.

[90] F. Boccardi, H. Huang, and A. Alexiou. Network MIMO with Reduced Backhaul Requirements by MAC Coordination. In *Proc. of Asilomar Conference on Signals, Systems and Computers (ACSSC)*, pages 1125–1129, Oct. 2008.

[91] P. Marsch and G. Fettweis. A Framework for Optimizing the Downlink of Distributed Antenna Systems Under a Constrained Backhaul. In *Proc. of European Wireless Conference (EWC)*, Apr. 2007.

[92] D. Gesbert and M.-S. Alouini. How Much Feedback Multi-User Diversity Really Worth? In *Proc. of IEEE International Conference on Communications (ICC)*, pages 234–238, Jun. 2004.

[93] V. Hassel, D. Gesbert, M.-S. Alouini, and G.E Oien. A Threshold-Based Channel State Feedback Algorithm for Modern Cellular Systems. *IEEE Transactions on Wireless Communications*, 6(7):2422–2426, Jul. 2007.

[94] A. Papadogiannis, H.J. Bang, D. Gesbert, and E. Hardouin. Efficient Selective Feedback Design for Multicell Cooperative Networks. *IEEE Transactions on Vehicular Technology*, 60(1):196–205, Jan. 2011.

[95] S. Shamai and B.M. Zaidel. Enhancing the Cellular Downlink Capacity via Co-Processing at the Transmitting End. In *Proc. of IEEE Vehicular Technology Conference (VTC Spring)*, pages 1745–1749, May 2001.

[96] O. Somekh, B.M Zaidel, and S. Shamai. Sum Rate Characterization of Joint Multiple Cell-Site Processing. *IEEE Transactions on Information Theory*, 53(12):4473–4497, Dec. 2007.

[97] O. Somekh, O. Simeone, Y. Bar-Ness, and A.M Haimovich. Distributed Multi-Cell Zero-Forcing Beamforming in Cellular Downlink Channels. In *Proc .of IEEE Global Telecommunications Conference (GLOBECOM)*, pages 1–6, Dec. 2006.

[98] H. Zhang and H. Dai. Cochannel Interference Mitigation and Cooperative Processing in Downlink Multicell Multiuser MIMO Networks. *EURASIP Journal on Wireless Communications and Networking*, 2004(2):222–235, 2004.

[99] J. Zhang, R. Chen, J.G. Andrews, A. Ghosh, and R.W. Heath. Networked MIMO with Clustered Linear Precoding. *IEEE Transactions on Wireless Communications*, 8(4):1910–1921, Apr. 2009.

[100] S. Kaviani and W.A. Krzymien. Optimal Multiuser Zero Forcing with Per-Antenna Power Constraints for Network MIMO Coordination. *EURASIP Journal on Wireless Communications and Networking*, 2011:190461, Mar. 2011.

[101] A. Silva, R. Holakouei, and A. Gameiro. Power Allocation Strategies for Distributed Precoded Multicell Based Systems. *EURASIP Journal on Wireless Communications and Networking*, 2011:1, May 2011.

[102] M. Kobayashi, M. Debbah, and J.-C. Belfiore. Outage Efficient Strategies for Network MIMO with Partial CSIT. In *Proc. IEEE International Symposium on Information Theory (ISIT)*, pages 249–253, Jun. 2009.

[103] R. Zakhour and D. Gesbert. Distributed Multicell-MISO Precoding Using the Layered Virtual SINR Framework. *IEEE Transactions on Wireless Communications*, 9(8):2444–2448, Aug. 2010.

[104] R. Zakhour and D. Gesbert. Team Decision for the Cooperative MIMO Channel with Imperfect CSIT Sharing. In *Proc. of Information Theory and Applications Workshop (ITA)*, pages 1–6, Feb. 2010.

[105] R. Bhagavatula and R.W Heath. Sum-Rate Maximizing Beamforming in Multicell Systems with Limited Feedback. In *Proc. of Asilomar Conference on Signals, Systems and Computers (ACSSC)*, pages 1838–1842, Nov. 2009.

[106] S. Catreux, P.F. Driessen, and L.J. Greenstein. Simulation Results for an Interference-Limited Multiple-Input Multiple-Output Cellular System. *IEEE Communications Letters,*, 4(11):334–336, Nov. 2000.

[107] J.S. Evans and D. Everitt. Effective Bandwidth-Based Admission Control for Multiservice CDMA Cellular Networks. *IEEE Transactions on Vehicular Technology*, 48(1):36–46, Jan. 1999.

[108] V.V. Veeravalli and A. Sendonaris. The Coverage-Capacity Tradeoff in Cellular CDMA Systems. *IEEE Transactions on Vehicular Technology*, 48(5):1443–1450, Sep. 1999.

[109] M. Zorzi and S. Pupolin. Outage Probability in Multiple Access Packet Radio Networks in the Presence of Fading. *IEEE Transactions on Vehicular Technology*, 43(3):604–610, Aug. 1994.

[110] J. Papandriopoulos, J. Evans, and S. Dey. Outage-Based Optimal Power Control for Generalized Multiuser Fading Channels. *IEEE Transactions on Communications*, 54(4):693–703, Apr. 2006.

[111] A.G. Williamson and J.D. Parsons. Outage Probability in a Mobile Radio System Subject to Fading and Shadowing. *IEEE Electronics Letters*, 21(14):622–623, Apr. 1985.

[112] D. Ben Cheikh, J.-M. Kelif, M. Coupechoux, and P. Godlewski. SIR Distribution Analysis in Cellular Networks Considering the Joint Impact of Path-Loss, Shadowing and Fast Fading. *EURASIP Journal on Wireless Communications and Networking*, 2011:137, Oct. 2011.

[113] J.-M. Kelif and M. Coupechoux. Joint Impact of Pathloss Shadowing and Fast Fading - An Outage Formula for Wireless Networks. *ArXiv*, arxiv:1001.1110, Jan. 2010.

[114] J.-M. Kelif, M. Coupechoux, and P. Godlewski. Spatial Outage Probability for Cellular Networks. In *Proc. of IEEE Global Telecommunications Conference (GLOBECOM)*, pages 4445 –4450, Nov. 2007.

[115] D. Ben Cheikh, J.-M. Kelif, F. Abi-Abdallah, and D.-T. Phan-Huy. Time Reversal Outage Probability for Wideband Indoor Wireless Communications. In *Proc. of IEEE International Symposium on Personal Indoor and Mobile Radio Communications (PIMRC)*, pages 999–1003, Sep. 2010.

[116] A. Derode, P. Roux, and M. Fink. Robust Acoustic Time Reversal With High Order Multiple Scattering. *Physical Review Letters*, 75:4206–4209, Dec. 1995.

[117] M. G. Heinmann, A. Larazza, and K. B. Smith. Acoustic Communications in an Enclosure Using Single-Channel Time-Reversal Acoustics. *Applied Physics Letters*, 80:694–696, Nov. 2002.

[118] G. F. Edelmann, T. Akal, W. S. Hodgkiss, S. Kim, W. A. Kuperman, and H. C. Song. An Initial Demonstration of Underwater Acoustic Communications Using Time Reversal. *IEEE Journal of Oceanic Engineering*, 27(3):602–609, Jul. 2002.

[119] S. M. Emami, J. Hansen, A.D. Kim, G. Papanicolaou, A. J. Paulraj, D. Cheung, and C. Prettie. Predicted Time Reversal Performance in Wireless Communications Using Channel Measurements. Technical report, `http://math.stanford.edu/~papanico/pubftp/ComLet.pdf`, 2002.

[120] A. Khalegi. Measurement and Analysis of Ultra-Wideband Time Reversal for Indoor Propagation Channels. *Springer Wireless Personal Communications*, 54(2):307–320, May 2009.

[121] C. Oestges, J. Hansen, S. M. Emami, A.D. Kim, G. Papinicolaou, and A.J. Paulraj. Time Reversal Techniques for Broadband Wireless Communication Systems. In *Proc. of European Microwave Conference (Workshop)*, pages 49–66, Oct. 2004.

[122] S. Q. Xio, J. Chen, B.-Z. Wiang, and X. F. Liu. A Numerical Study on Time Reversal Electromagnetic Wave For Indoor Ultra-Wideband Signal Transmission. *Progress in Electomagnetics Research, PIER 77*, pages 329–342, 2007.

[123] H. T. Nguyen, I. Z. Kovacs, and P. C. F. Eggers. A Time Reversal Transmission Approach for Multiuser UWB Communications. *IEEE Transactions on Antenna and Propagation*, 54(11):3216–3224, Nov. 2006.

[124] P. Kyritsi, G. Papanicolaou, P. Eggers, and A. Oprea. MISO Time Reversal and Delay-Spread Compression for FWA Channels at 5 Ghz. *IEEE Antennas and Wireless Propagation Letters*, 3:96–99, Dec. 2004.

[125] R. Qiu, C. Zhou, N. Guo, and J. Zhang. Time Reversal with MISO for Ultrawideband Communications: Experimental Results. *IEEE Antennas and Wireless Propagation Letters*, 5:269–273, Dec. 2006.

[126] H. T. Nguyen, J.B. Andersen, G. F. Pedersen, P. Kyritsi, and P. C. F. Eggers. Time Reversal in Wireless Communications: A Measurment-Based Investigation. *IEEE Transactions on Wireless Communications*, 5(8), Aug. 2006.

[127] I. H. Naqvi, A. Khaleghi, and G. El Zein. Multiuser Time Reversal UWB Communication System: A Modified Transmission Approach. In *Proc. of IEEE International Symposium on Personal, Indoor and Mobile Radio Communications (PIMRC)*, pages 1–5, Sep. 2009.

[128] P. Kyritsi, P. Stoica, G. Papanicolaou, P. Eggers, and A. Oprea. Time Reversal and Zero-Forcing Equalization for Fixed Wireless Access Channels. In *Proc. of Asilomar Conference on Signals, Systems and Computers (ACSSC)*, pages 1297–1301, Nov. 2005.

[129] T. Strohmer, M. Emami, J. Hansen, G. Papanicolaou, and A.J. Paulraj. Application of Time-Reversal with MMSE Equalizer to UWB Communications. In *Proc. of IEEE Global Telecommunications Conference (GLOBECOM)*, pages 3123–3127, Dec. 2004.

[130] R. Visoz and E. Bejjani. Matched Filter Bound for Multichannel Diversity Over Frequency-Selective Rayleigh-Fading Mobile Channels. *IEEE Transactions on Vehicular Technology*, 49(5):1832–1844, Sep. 2000.

[131] C. Schlegel. Error Probability for Multibeam Rayleigh Channels. *IEEE Transactions on Communications*, 44(3):290–293, Mar. 1996.

[132] I.S. Gradshteyn and I.W.Ryzhik. *Table of integrals series and products.* Academic Press, Moscow, 1963.

[133] W. C. Jakes. *Microwave Mobile Communications.* IEEE Press, Piscataway, NJ, second edition, 1994.

[134] M. Emami, F. Lee, and A. Paulraj. Communications through High Delay Spread x Bandwidth (HDB) Channels: Opportunities and Challenges. In *Proc. of AIM Workshop on Time-Reversal Communications in Richly Scattering Environments*, Oct. 2004.

[135] V. Tarokh, H. Jafarkhani, and A. R. Calderbank. Space-Time Block Codes from Orthogonal Designs. *IEEE Transactions on Information Theory*, 45(5):1456–1467, Jul. 1999.

[136] M.-S. Alouini and M. K. Simon. Performance Analysis of Coherent Equal Gain Combining Over Nakagami-m Fading Channels. *IEEE Transactions on Vehicular Technology*, 50(6):1449–1463, Nov. 2001.

[137] M. Kang, L. Yang, and M.-S. Alouini. Outage Probability of MIMO Optimum Combining in Presence of Unbalanced Co-channel Interferers and Noise. *IEEE Transactions on Wireless Communications*, 5(7):1536–1276, Jul. 2006.

[138] L. Yang. Outage Performance of OSTBC in Double Scattering MIMO Channels. *Springer Wireless Personal Communications*, 45:225–230, Oct. 2007.

[139] Z. Chen, J. Yuan, B. Vucetic, and Z. Zhou. Performance of Alamouti Scheme with Transmit Antenna Selection. In *Proc. of IEEE International Symposium on Personal, Indoor and Mobile Radio Communications (PIMRC)*, pages 1135 – 1141, Sep. 2004.

[140] C. Schnurr, S. Stanczak, and A. Sezgin. The Impact of Different MIMO Strategies on the Network Outage Performance. In *Proc. of International ITG/IEEE Workshop on Smart Antennas (WSA)*, Feb. 2007.

[141] B. K. Chalise and A. Czylwik. Exact Outage Probability Analysis for a Multiuser MIMO Wireless Communication System with Space-Time Block Coding. *IEEE Transactions on Vehicular Technology*, 57(3):1502–1512, May 2008.

[142] N. Reider and G. Fodor. On Opportunistic Power Control for Alamouti and Spatial Multiplexing MIMO Systems. *Springer Wireless Personal Communications*, pages 1–24, Aug. 2011.

[143] F. Javier Lopez-Martýnez, E. Martos-Naya, K.-K. Wong, and J. Tomas Entrambasaguas. Closed-Form BER Analysis of Alamouti-MRC Systems with ICSI in Ricean Fading Channels. *IEEE Communications Letters*, 15(1):46–48, Jan. 2011.

[144] M. Rahman, E. de Carvalho, and R. Prasad. Impact of MIMO Co-Channel Interference. In *Proc. of IEEE Personal, Indoor, Mobile Radio Communications Conference (PIMRC)*, Athens, Greece, Sept. 2007.

[145] W. Choi, N. Himayat, S. Talwar, and M. Ho. The Effects of Co-Channel Interference on Spatial Diversity Techniques. In *Proc. of IEEE Wireless Communications and Networking Conference (WCNC)*, Hong Kong, China, Mar. 2007.

[146] Y. Li, L. Cimini, and N. Himayat. Performance Analysis of Space Time Block Coding with Co-Channel MIMO Interferers. In *Proc. of IEEE Global Communications Conference (GLOBECOM)*, New Orleans, LA, Nov. 2008.

[147] D. Ben Cheikh, J.-M. Kelif, M. Coupechoux, and P. Godlewski. Outage Probability in a Multi-Cellular Network Using Alamouti Scheme. In *Proc. of IEEE Sarnoff Symposium*, pages 1–5, Apr. 2010.

[148] D. Ben Cheikh, J.-M. Kelif, M. Coupechoux, and P. Godlewski. Multicellular Alamouti Scheme Performance in Rayleigh and Shadow Fading. *to appear in Springer Annals of Telecommunications*, 2012.

[149] J. Lee, J.-K. Han, and J. Zhang. MIMO Technologies in 3GPP LTE and LTE-Advanced. *EURASIP Journal on Wireless Communications and Networking*, 2009:302092, Jul. 2009.

[150] H. Holm and M-S. Alouini. Sum and Difference of Two Squared Correlated Nakagami Variates in Connection with the McKay Distribution. *IEEE Transactions on Communications*, 52(8):1367–1376, Aug. 2004.

[151] A. Bagdasaryan. A Note on the 2F1 Hypergeometric Function. *ArXiv*, arxiv:0912.0917v1, Dec. 2009.

[152] `http://mathworld.wolfram.com/IncompleteGammaFunction.html`.

[153] J-M. Kelif and E. Altman. Downlink Fluid Model of CDMA Networks. In *Proc. of IEEE Vehicular Technology Conference (VTC Spring)*, pages 2264–2268, May 2005.

[154] X. Shao, J. Yuan, and Y. Shao. Error Performance Analysis of Linear Zero Forcing and MMSE Precoders for MIMO Broadcast Channels. *IET Communications*, 1(5):1067–1074, Oct. 2007.

[155] J. Wang, Z. Liu, Y. Wang, and X. You. Performance of the Zero Forcing Precoding MIMO Broadcast Systems with Channel Estimation Errors. *Springer Journal of Electronics (China)*, 24:490–495, Jul. 2007.

[156] S. Ramanath, M. Debbah, E. Altman, and V. Kumar. Asymptotic Analysis of Precoded Small Cell Networks. *Proc. of IEEE International Conference of Computer (INFOCOM)*, pages 1–8, May 2010.

[157] Y. Xu and T. Le-Nogc. Optimal Power Allocation with Channel Inversion Regularization-Based Precoding for MIMO Broadcast Channels. *EURASIP Journal on Advances in Signal Processing*, 2008:587243, Jan. 2009.

[158] D. Ben Cheikh, J.-M. Kelif, M. Coupechoux, and P. Godlewski. Multicellular Zero Forcing Precoding Performance in Rayleigh and Shadow Fading. In *Proc. of IEEE Vehicular Technology Conference (VTC Spring)*, pages 1–5, May 2011.

[159] J. Panaretos, S. Psarakis, E. Xekalaki, and D. Karlis. The Correlated Gamma-Ratio Distribution in Model Evaluation and Selections. *The Indian Journal of Statistics*, 69(Part 2):221–255, Dec. 2007.

[160] J. Pearson. Computation of hypergeometric functions. Master's thesis, University of Oxford, Sep. 2009.

[161] M. Sawahashi, Y. Kishiyama, A. Morimoto, D. Nishikawa, and M. Tanno. Coordinated Multipoint Transmission/Reception Technique For LTE-Advanced. *IEEE Wireless Communications*, 17(3):26–34, Jun. 2010.

[162] 3GPP TR 36.814. Evolved Universal Terrestrial Radio Access (E-UTRA); Further advancements for E-UTRA physical layer aspects. *Release 9 V9.0.0*, Mar. 2010.

[163] V. Jungnickel, S. Jaeckel, L. Thiele, J. Lei Jiang, U. Kruger, A. Brylka, and C. Von Helmolt. Capacity Measurements in a Cooperative MIMO Network. *IEEE Transactions on Vehicular Techology*, 58(5):2392–2405, Jun. 2009.

[164] P. Marsch, M. Grieger, and G. Fettweis. Large Scale Field Trial Results on Different Uplink Coordinated Multi-Point (CoMP) Concepts in an Urban Environment. In *Proc. of IEEE Wireless Communication and Networking Conference (WCNC)*, pages 1858–1863, Mar. 2011.

[165] H. Zhang, H. Dai, and Q. Zhou. Base Station Cooperation for Multiuser MIMO: Joint Transmission and BS Selection. In *Proc. of Conference on Information Sciences and Systems (CISS)*, pages 1–6, Mar. 2004.

[166] S. Ben Halima, M. Hélard, and D.T. Phan Huy. New Coordination and Resource Allocation Schemes for Uniform Rate in Femtocell Networks. In *Proc. of IEEE Vehicular Technology Conference (VTC Spring)*, pages 1–5, May 2011.

[167] T.K.Y. Lo. Maximum Ratio Transmission. *IEEE Transactions on Communications*, 47(10):1458–1461, Oct. 1999.

[168] D. Ben Cheikh, J.-M. Kelif, M. Coupechoux, and P. Godlewski. Analytical Joint Processing Multi-Point Cooperation Performance in Rayleigh Fading. *IEEE Wireless Communications Letters, accepted for publication*, 2012.

[169] E. Bjornson, R. Zakhour, D. Gesbert, and B. Ottersten. Cooperative Multicell Precoding: Rate Region Characterization and Distributed Strategies With Instantaneous and Statistical CSI. *IEEE Transactions on Wireless Communications*, 58(8):4298–4310, Aug. 2010.

[170] A. Tolli, H. Pennanen, and P. Komulainen. On the Value of Coherent and Coordinated Multi-cell Transmission. In *Proc. of IEEE International Communication Conference (ICC)*, pages 1–5, Jun. 2009.

[171] `http://mathworld.wolfram.com/ConfluentHypergeometricFunctionoftheSecondKind.html`.

[172] D. Ben Cheikh, J.-M. Kelif, M. Coupechoux, and P. Godlewski. Dynamic System Performance of SISO, MISO and MIMO Alamouti Schemes. In *Proc. of IEEE Sarnoff Symposium*, pages 1–5, May 2011.

[173] *Wimax Forum*. WiMax System Evaluation Methodology. V2.1, Jul. 2008.

[174] C. Wengerter, J. Ohlhorst, and A.G.E.V Elbwart. Fairness and Throughput Analysis for Generalized Proportional Fair Frequency Scheduling in OFDMA. In *Proc. of IEEE Vehicular Technology Conference (VTC Spring)*, May 2005.

[175] S. Schwartz and Y.S. Yeh. On the Distribution Function and Moments of Power Sums with Log-normal Components. *Bell System Technical Journal*, 61(7):1441–1462, Sep. 1982.

[176] N.C. Beaulieu, A.A. Abu-Dayya, and P.J. McLane. Comparison of Methods of Computing Lognormal Sum Distributions and Outages for Digital Wireless Applications. In *Proc. of International Conference on Communications (ICC)*, May 1994.

[177] J.-M. Kélif, M. Coupechoux, and Ph. Godlewski. A Fluid Model for Performance Analysis in Cellular Networks. *EURASIP Journal on Wireless Communications and Networking*, 2010:435189, Aug. 2010.